THE OPTICAL PUMPING OF FLUIDS USING COAXIAL FLASHTUBES

by

CONSTANTINOS RAPTIS

Thesis submitted for the
Degree of Doctor of Philosophy
at the University of London
May 1978

TO MY PARENTS

ABSTRACT

A study of the performance of high energy coaxial flashtube systems designed for pumping fluid laser media is presented. The properties of such systems are described and construction details of the flashtubes studied are given.

Temporal and spectral characteristics of the optical output from the flashtubes have been measured at various values of system parameters. Optimum system parameters for high luminous efficiency, uniform discharge pattern and long life of the flashtubes have been obtained.

The effects of radio-frequency preionisation on the optical output, discharge pattern and overall performance of coaxial flashtubes have been investigated.

The use of these coaxial flashtubes as potential pump sources for organic dye and iodine photodissociation lasers is considered. Efficient laser output from atomic iodine is reported.

ACKNOWLEDGEMENTS

I remain deeply indebted to my supervisor, the late Dr. V.I. Little, whose guidance and assistance were invaluable during the major part of my course and whose presence on both professional and personal grounds is greatly missed.

I should like to thank Professor D.W.O. Heddle, who took over the supervision of my research, for his support and interest in the progress of my studies and career.

I am grateful to Dr. S. Majumdar for his help and advice in numerous topics during my course. I wish to thank all the Technicians in the Physics Department, Royal Holloway College, for their willing assistance and advice in practical matters.

I am also grateful to Dr. T.A. King and Dr. H.J. Baker for the facilities offered during experiments on the iodine laser at the Physics Department of Manchester University.

I should like to thank Eileen, whose encouragement, understanding and help have been of great value to me.

Finally, I owe my deepest thanks and appreciation to my parents, without whose moral support and financial assistance this work would not have been possible.

CONTENTS

		Page
	CHAPTER 1	
	INTRODUCTION	1
	CHAPTER 2	
	OPTICALLY PUMPED FLUID LASER SYSTEMS	8
2.1	HISTORICAL INTRODUCTION	8
2.2	ORGANIC DYE LASERS	12
	2.2.1 Absorption and emission of organic dye solutions	12
	2.2.2 Flashtube pumping considerations	20
2.3	PRINCIPLES OF IODINE PHOTODISSOCIATION LASER OPERATION	21
	2.3.1 Photodissociation of alkyl-iodides and emission from atomic iodine	21
	2.3.2 Secondary processes in the photodissociation of alkyl-iodides	25
	2.3.3 Effects of secondary processes on the laser output	32
	2.3.4 Pumping requirements	34
	CHAPTER 3	
	CHARACTERISTICS AND OPERATION OF FLASHTUBE SYSTEMS	35
3.1	GENERAL FEATURES	35
3.2	EXCITATION AND IONISATION OF RARE GASES BY ATOMIC COLLISIONS	39
3.3	HIGH CURRENT, PULSED ELECTRICAL GAS DISCHARGES	45
3.4	RADIATIVE PROCESSES IN RARE GAS DISCHARGES	56
3.5	FLASHTUBE CIRCUIT ANALYSIS	62
3.6	FLASHTUBE GEOMETRY AND PUMPING CONFIGURATIONS. COAXIAL FLASHTUBES	71
3.7	TRIGGERING OF FLASHTUBES	77

Page

CHAPTER 4

THE DESIGN AND TECHNOLOGY OF APPARATUS USED IN THE EXPERIMENTS 80

4.1 DESCRIPTION OF THE COAXIAL FLASHTUBES 80

4.2 THE 5-STAGE MARX GENERATOR 92

4.3 THE RADIO-FREQUENCY PREIONISATION DEVICE 99

4.4 OTHER EXPERIMENTAL DETAILS 103

CHAPTER 5

EXPERIMENTAL STUDIES OF THE COAXIAL FLASHTUBE PUMPING SYSTEMS 107

5.1 ELECTRICAL CHARACTERISTICS OF THE DISCHARGE CIRCUIT 107

5.2 TEMPORAL MEASUREMENTS OF THE OPTICAL OUTPUT FROM THE FLASHTUBES 113

5.2.1 Output optical power profiles at various E/p values 113

5.2.2 Effects of the non-uniform (localised) type of discharge upon the quality of the optical output 129

5.3 SPECTRAL CHARACTERISTICS OF THE FLASHTUBE SYSTEMS 131

5.3.1 Experimental study of the fluorescent output from flashtube excited dye solutions as a means of estimating the spectral response of the flashtube 131

5.3.2 Near UV and visible emission spectrum of a Xenon filled coaxial flashtube 145

5.4 OPTIMISATION OF THE OPTICAL OUTPUT FROM THE FLASHTUBES AND CONCLUDING REMARKS 147

CHAPTER 6

THE EFFECTS OF RADIO-FREQUENCY PREIONISATION ON THE FLASHTUBE PERFORMANCE 151

6.1 INTRODUCTION - THE SIGNIFICANCE OF PREIONISATION IN A HIGH CURRENT PULSED DISCHARGE. PREIONISATION METHODS 151

6.2 OUTLINE OF AC HIGH-FREQUENCY BREAKDOWN OF GASES 154

6.3 EXPERIMENTAL ARRANGEMENTS 156

Page

6.4 EXPERIMENTAL STUDY OF THE PERFORMANCE OF A COAXIAL FLASHTUBE SUBJECTED TO RADIO-FREQUENCY PREIONISATION 161

6.4.1 Enhancement of the optical output 161

6.4.2 Dependence of the enhancement on the delay between main and preionisation pulses 166

6.4.3 Other observations 167

6.5 COMMENTS 167

CHAPTER 7

OUTPUT MEASUREMENTS FROM A COAXIAL FLASHTUBE PUMPED IODINE PHOTODISSOCIATION LASER 169

7.1 EXPERIMENTAL DETAILS 169

7.2 RESULTS AND DISCUSSION 170

7.3 FURTHER ANALYSIS ON THE DEPOPULATION OF THE UPPER LASER LEVEL DUE TO RECOMBINATION AND DEACTIVATION OF ATOMIC IODINE IN THE PRESENCE OF MOLECULAR IODINE 175

CONCLUSIONS 182

REFERENCES 186

CHAPTER 1

INTRODUCTION

The various types of light sources have been excellent appliances in a variety of research fields for several decades. Numerous atomic and molecular spectra of substances have been obtained and a variety of physical phenomena such as optical absorption, photodissociation, emission, scattering etc. have been studied by using the appropriate optical radiation for each application.

The discovery of the laser by Maiman[1] in 1960 - pumped, notably, by a pulsed light source - underlined the importance of light sources in the new field. There was a demand for intense, long life, reliable light sources in order to pump several potential laser materials. Earlier, in their theoretical investigation, Schawlow and Townes[2] had remarked that stimulated emission from strongly fluorescent materials is feasible in the optical region, providing that the material sustains a high degree of excitation so that population inversion occurs between the upper and lower energy levels of the particular optical transition. This theory was justified by Maiman's experiments in which a ruby (Al_2O_3 doped with Cr^{3+}) rod was illuminated by an intense flashtube. From then on, research on intense light sources has been advanced and several optical pumping systems have been designed in order to suit the properties of various laser materials.

Depending on the form of operation, lasers are distinguished in continuous and pulsed systems; therefore, the pumping source should operate accordingly. The theory and the properties of the laser-amplifier or oscillator, continuous or pulsed, can be found in any textbook on Laser Physics (see Bibliography) or in Yariv's[3] review paper. Continuous

lasers or laser amplifiers are of no interest in the present work. The attention is focused on pulsed, flashtube pumped laser oscillators.

Apart from the optical pumping methods, energy can be supplied to substances by other procedures. For example in gases, the most effective and economic method is by discharging electrical energy through the gas, in which case excitation of atoms or molecules takes place as a result of collisions between particles. The first gas-discharge laser (He-Ne mixture) was constructed by Javan[4], shortly after the ruby laser was discovered by Maiman[1]. Another pumping method, employed in semiconductor lasers, is by injecting direct electric current[5].

Compared to other methods, optical pumping methods appear to be uneconomic since the introduction of pump energy to the laser material is indirect; in other words, excitation of the material follows the conversion of a proportion of the input electrical energy supplied to the light source into radiant energy. During these stages a substantial part of the original input energy is lost. In contrast, in gas-discharge lasers the application of the pump energy is direct. Nevertheless, optical pumping systems are very important because they represent the only possibility of introducing sufficient energy into substances like dielectric crystals, organic solutions etc; the active medium (Cr^{3+} in the case of ruby, or dye molecules in the case of organic solutions) of such laser substances possesses a broad-band resonance absorption spectrum which makes flashtubes and other broad-band light sources such as incandescent lamps, high pressure mercury lamps, xenon arc lamps etc. suitable pumps for these systems. In atomic gases and vapours, optical pumping is limited because of the narrow band electronic transitions, in which case the pump source must supply light whose frequency is quite close to the frequency of pump transition in the gas. Such coincidences between emission frequencies of light sources and absorption frequencies of different

materials are rare; the combination of a He lamp and caesium vapour[6] is probably the sole example of a laser operating on these lines.

In molecular gases and vapours, however, optical pumping with a broad-band light source is feasible because excitation of a molecule to a given electronic level is possible for a range of photon energies[7]. This difference between atomic and molecular absorption exists because in molecules an electronic state consists of several vibrational-rotational states. Photodissociation of molecules can be considered as a particular case of photoexcitation, since one deals with transitions from the ground state to defined dissociative states.

Pulsed laser operation is obtained when laser materials are pumped in single pulses by flashtubes. These devices are quartz (rarely pyrex) enclosures of certain shape and length, filled with a rare gas. Flashtubes convert the electrical energy stored in a capacitor into radiant energy following an electrical discharge through the gas. The light output from flashtubes is distributed in the near UV, visible and near infrared regions of the spectrum, notably between 2000Å and 2.5μ. Light below 2000Å and over 2.5μ is absorbed by the quartz walls of the flashtube. The present study deals only with the optical output from flashtubes in the near UV and visible regions (2000Å - 7000Å). By altering certain flashtube parameters one can obtain enhanced light output in the spectral band which the laser material absorbs; this feature is discussed in Section 3.4.

Flashtube pumping has proved a very effective method of producing population inversion in several materials because such sources provide pump energy at high rates. The flashtube and laser material are contained in a pumping arrangement which concentrates the light to the material. Various pumping arrangements are discussed in Section 3.6. So far, three

types of flashtubes have been used as pumps for laser materials: the helical, the linear and the coaxial type. They are distinguished by their characteristic geometry.

The requirements placed on an optical pumping system for pulsed laser operation are listed in the following paragraphs:

a) High Efficiency

A flashtube must supply the maximum possible light output in the spectral region which the laser material absorbs.

b) Low Distortion of the Resonator

Distortion arises by irregular and non-uniform absorption of the pump light in the cross section of the laser material. The quality of the laser output is poor when the laser material is illuminated in a non-uniform fashion; moreover, in the case of a three-level system, the efficiency of the laser output will decrease if parts of the material remain unpumped or insufficiently pumped; this happens because in these systems there is an overlap between absorption and emission spectra. On the other hand, light from a flashtube outside the resonance pump band of the material may affect the actual resonator; illumination by such light may lead to the heating of the material or to undesirable excitation of the active atoms or molecules to higher energy levels.

c) Long Life

The number of flashes before a flashtube breaks[8], depends on the magnitude of the input electrical power at which the flashtube is operated. The maximum input power a flashtube can withstand without any sign of damage increases with increasing discharge volume of the flashtube. The cause of such destruction is the pressure exerted on the walls by the shock-wave front (see Section 3.3). When a flashtube system is designed, attention should be paid in making it resistive to shock-waves (see

Section 4.1) so that it can be operated at higher input powers.

Depending on the laser material to be pumped, additional requirements may be placed on a flashtube system. Two classes of laser materials have been studied in this work, both in the fluid phase:

a) Organic dye solutions and

b) Photodissociative alkyl-iodide vapours.

Additional requirements from flashtube systems designed to pump these classes of laser materials are listed in sub-sections 2.2.2 and 2.3.4.

The efficiency of a laser system depends also on the effectiveness of the coupling configuration between the pump source and the laser material. The ideal case would be to concentrate the entire radiant energy onto the laser material. There is a limiting condition[9] though concerning the energy density attained in the volume of the material. According to the laws of Thermodynamics (Liouville's theorem), the energy density in the absorber, with the same refractive index for both light source and absorber, can be at most equal to that of the light source. This limitation leads to the conclusion[9] that a transformation of the energy density near the ratio 1:1 can be accomplished best if the light source and the laser material have the same shape and size.

The main objectives of the present work are:

a) The design and construction of kilojoule (input electrical energy) coaxial flashtube systems which can be used as pump sources for organic dye and iodine photodissociation lasers.

b) The optimisation of flashtube parameters for: annular discharges in the flashtubes, intense and efficient optical outputs in the near UV and visible spectral regions, and reliable operation of the flashtubes.

c) The investigation into the effects of radio-frequency preionisation

on the temporal and spectral characteristics of the optical output from such flashtubes and on the flashtube performance.

d) The analysis of the conditions leading to a high luminous efficiency of the flashtubes and to an effective pumping of the laser materials.

e) The study of the fluorescent and lasing outputs from various dye solutions and atomic iodine respectively, pumped by these flashtubes.

In view of the above, an outline of the main characteristics of optically pumped fluid lasers - with emphasis on the dye and iodine photodissociation lasers - is presented in Chapter 2. The attention is focused on: the conditions necessary for effective optical excitation of the laser material, the attainment of population inversion and the subsequent laser action.

In Chapter 3, flashtube characteristics and operation are reviewed. In order to understand better the various radiative processes in a flashtube, some elements from the electrical gas discharge theory are presented. Similarly, in order to interpret the temporal characteristics of a flashtube, an analysis is given in which the flashtube is regarded as an element in the external circuit. Various pumping arrangements are also described.

In Chapter 4, four high energy coaxial flashtubes which were specially constructed for this work are described. In the same Chapter, a Marx-generator which provided high power electrical pulses (peak powers up to 500 MWatts) to the flashtubes is also described along with other system details.

The performances of these flashtubes, filled mainly with xenon but occasionally with other rare gases, are presented in Chapter 5; both temporal and spectral characteristics are given.

In Chapter 6, the use of preionisation as an effective means of improving the optical output and the performance of flashtubes is discussed. A radio-frequency preionising device - employed for the first time successfully in a flashtube system - is described. Analysis and interpretation of the results are also made.

In Chapter 7, the use of one of these flashtubes to pump 1 - C_3F_7I vapour and the measurements of the resulting iodine laser output are presented. An analysis concerning the effects of recombination and deactivation of atomic iodine upon the laser output is also carried out.

CHAPTER 2

OPTICALLY PUMPED FLUID LASER SYSTEMS

2.1 HISTORICAL INTRODUCTION

Following the discovery of the solid-state and the gas- discharge lasers, several scientists concentrated their efforts on the search for liquid laser materials. Compared to solids, liquids (and gases) appeared to be advantageous as laser materials. In dielectric crystals, inhomogeneities and crystal imperfections impair coherent amplification; in addition the crystals must be cut and polished accurately, and often attention must be paid to the orientation of the crystal axes. Liquids (and gases) are completely free from these problems. The problem of cooling the system is solved by circulating the liquid.

The initial results were not encouraging and there was a general feeling that laser action in liquids was unlikely because of the high deflection losses[10] inside the laser cavity which arose from the variation of the refractive index of the material with the penetration depth of the pumping radiation; this variation is due to heating by the pumping radiation.

The first liquid laser was reported in 1963 by Lempicki and Samelson[11]. The laser material was a solution of trivalent Europium in an organic chelate and it was highly viscous. The system was operated at 77°K. Later, laser action from such chelates was achieved at room temperature, but the output was much inferior to solid-state and gas-discharge lasers. The inferior performance of chelate lasers was due to the intense absorption of the pumping radiation by the chelate; as a result of the intense absorption, the penetration depth of the pumping radiation was limited to a few microns. The somewhat discouraging results from chelate lasers caused a temporary slow down in liquid laser research.

The interest in liquid lasers was revived in 1966 when, at about the same time, two new types of liquid lasers were discovered:[12,13]

a) The organic liquid laser based on solutions of organic dyes in mainly alcoholic solvents and

b) The inorganic liquid laser based on solutions of rare earth ions.

Laser action from a dye was reported in March 1966 by Sorokin and Lankard[12]; a solution of chloro-aluminium Phthalocyanine in ethyl-alcohol was pumped with a Q-switched ruby laser, which provides intense pumping radiation in a sufficiently short time before the fast radiation less relaxation to the triplet-state becomes effective. Strictly speaking, this dye is an organometallic compound, for its central metal atom is directly bonded to an organic ring-type molecule. Nevertheless, spectroscopic evidence clearly indicated that the stimulated emission originated from the organic part of the molecule. At about the same time Schäfer and his co-workers[14] in Germany, while studying saturation characteristics of dyes of the cyanine series with the use of giant-pulse ruby laser and, unaware of Sorokin and Lankard's work, obtained, as a by-result, laser action from these dyes. In the following year, 1967, Sorokin and Lankard[15] reported laser action from several dyes excited by a specially made coaxial flashtube. Later on in 1967 Schmidt and Schäfer[16], using a low-inductance capacitor to drive a commercial linear xenon flashtube, achieved similar results.

In the same year, another important advance was made when Soffer and McFarland[17] replaced one of the mirrors in a Rhodamine 6G laser system with a diffraction grating. This alteration introduced an effective spectral narrowing in the system from 60 to 0.6Å and a continuous tuning range of 450Å. Continuous wave (CW) operation of dye lasers was achieved by Peterson and co-workers[18] in 1970. They used an argon-ion laser to

pump a solution of Rhodamine 6G in water containing a deaggregating agent. This agent decreases the steady-state population of the triplet state, thus reducing the triplet-triplet absorption.

Since the time of the first reported organic dye laser[12], laser outputs from a large number of dyes have been reported. Dye laser wavelengths cover today the whole visible spectrum with extensions in the near-ultraviolet and infrared.

The first inorganic liquid laser was discovered by Heller[13], shortly after the dye laser was reported by Sorokin and Lankard[12]. The inorganic active medium was trivalent Neodymium dissolved in selenium oxychloride (N^{3+}: $SeOCl_2$). It was already known that Neodymium ions display laser action in crystals[19] and in glasses[20]. But all early attempts to achieve laser action from neodymium ions in solutions had been unsuccessful due to the fast radiationless relaxation which the active ions undergo in solvents containing the hydroxyl group.

Of the two types of liquid lasers, the organic dye laser proved to be more useful in applications and easier to handle. The fact that the variety of highly fluorescent dyes can give coherent, monochromatic and tunable laser output at any wavelength from 3400 to 11000 Å has made the dye laser a unique tool for the spectroscopist. Dyes are relatively cheap and their solutions are easy to make. In contrast, precautions must be taken in the handling of neodymium solutions because the solvents employed are explosive and corrosive materials. Although high powers can be achieved with neodymium liquid lasers, the laser output is of poor quality. Generally, the power and quality of the laser output from liquid neodymium are far inferior to those of the laser output from N^{3+} in crystals or glasses. In recent years, energy outputs from dye laser-oscillators up to 400 Joules have been reported[21]; high power output, which was the main advantage of inorganic liquid lasers, was thus achieved

with organic dye lasers also.

As was mentioned in the previous Chapter, the sole example of an atomic gaseous laser pumped by a light source is the caesium vapour laser[6]. In the same Chapter, it was shown that molecular gaseous compounds are more effective absorbers[7] of radiant energy because of their broad-band resonance transitions; such absorption may result in transitions to dissociative states of the molecule, if the exciting radiation is appropriately selected. If a product of such photodissociation is mainly populated in an excited state, then laser output may be achieved at the frequency of the resonant transition to the ground state providing that the system is placed in a cavity. This is the principle of operation of the photodissociation laser.

The first such laser was reported by Kasper and Pimentel[22] in 1964; laser action was observed during the flash photolysis of both gaseous CH_3I (methyl-iodide) and gaseous CF_3I (trifluoro-methyl-iodide). The products of photodissociation of these molecules are atomic iodine and alkyl radicals. The stimulated emission is due to the $^2P_{1/2} \rightarrow {}^2P_{3/2}$ transition of atomic iodine. In the following years, laser action from atomic iodine (due to the same transition) was observed in photodissociation processes of higher members of the alkyl-iodide and perfluorinated alkyl-iodide families[23,24]. The most efficient iodine laser outputs were observed in photodissociations of CF_3I[24, 25] and 1 - C_3F_7[24] (1 - heptafluoropropyl-iodide); iodine laser outputs up to 65 joules were reported by De Maria and Ultee[25] in 1966. In the late 60's and early 70's groups in Germany[26] and the Soviet Union[27] set up high power oscillator-amplifier iodine laser systems, capable of giving output powers up to 100 GWatts.

Laser emission during the photodissociation of any member of the alkyl and perfluorinated alkyl-iodine families, in their gaseous phase,

is known today by the general term: Atomic iodine photodissociation laser.

Other optically pumped molecular photodissociation lasers include those reported by Pollack[28] in 1966 on vibrational-rotational transitions of NO and CN by photodissociation of NOCl and C_2N_2 respectively. Recently, several laser lines have been observed[29] from optically pumped molecular iodine vapour; it must be pointed out that the laser emission in these systems is due to molecular iodine transitions.

2.2 ORGANIC DYE LASERS

2.2.1 Absorption and Emission of Organic Dye Solutions

Up until the end of the nineteenth century a dye was defined as an organic substance of intense colour which could be imparted more or less permanently to other materials. A substance of similar chemical structure but without colour was not considered as a dye. Today, however, the term dye refers to organic materials containing certain chemical constituents and with certain spectroscopic properties; materials which are now called dyes have broad absorption and emission spectra in the ultraviolet, visible or near infrared.

Of the many dyes known, only a fraction fluoresce in solutions and it is among these that lasing dyes are found. It is the chemical structure, together with the way the dye interacts with the solvent, that determines the spectroscopic properties of such solutions. The most strongly fluorescent dyes belong to the ozazole, xanthene, anthracene, coumarin, acridine, phthalocyanine and polymethine families. A family of dyes is a group of substances having similar chemical structure and therefore some common spectral properties. In a family of dyes, one member differs from another in the nature and number of the substitutional groups attached to a basic organic molecule which characterises the family. Further

discussion on the dye chemistry would be beyond the scope of this work. Details concerning the chemical structure of dyes and its effect on the absorption and emission spectra can be found in review articles by Schäfer[30] and by Bass et al[31].

The absorption and fluorescence bands, the widths, and the strength of the spectral processes vary for different dyes, or for a particular dye in different solvents. But, qualitatively, most dye solutions have the following spectral properties which are similar in many respects to those of Rhodamine B, whose absorption and fluorescence spectra obtained by Weber and Bass[32] are given in Figure 2.1.

a) The principal absorption and emission bands are generally wide (typical width values are 350 - 400 Å). Other weaker absorption bands may be found in the direction of the shorter wavelengths from the principal absorption.

b) The fluorescence peak occurs at longer wavelengths than the principal absorption peak. This is called the Stokes shift of fluorescence. However, the principal absorption band may overlap the fluorescence band. It can be said that the fluorescence spectrum is a mirror image of the absorption spectrum.

c) Typical fluorescence lifetimes are $\sim 5 \times 10^{-9}$ secs.

d) Dye molecules in an excited state may absorb light, thus resulting in transitions to higher states. In this way, a triplet-triplet absorption band may overlap the fluorescence band and in doing so substantially reduce the fluorescence and laser outputs.

In Figure 2.1, curve S illustrates the spectral variation of the molar extinction coefficient ε_S for the principal (singlet) absorption, while curve T shows the spectral variation of the molar extinction coefficient ε_T for triplet-triplet absorption.

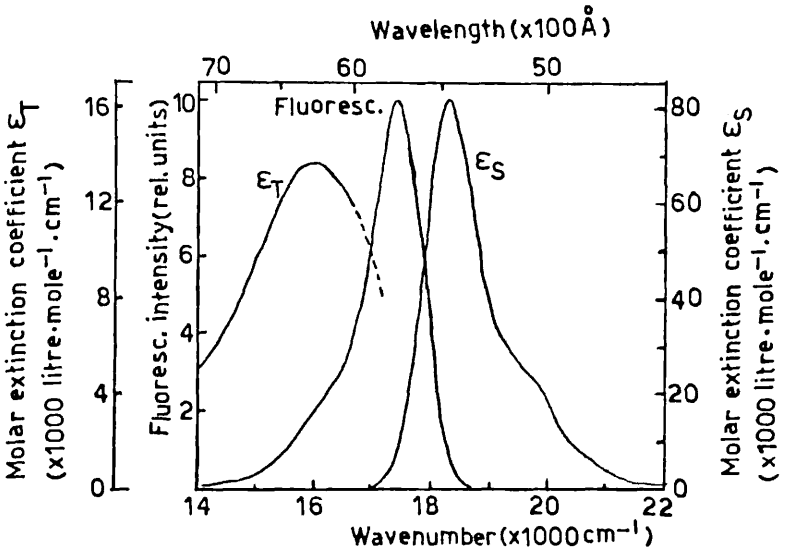

Fig. 2.1: Singlet absorption and fluorescence spectra of Rhodamine B in methanol (5×10^{-5} M), and triplet absorption spectrum for Rhodamine B in polymethylmethacrylate(32). The subscripts S and T denote singlet and triplet absorption, respectively.

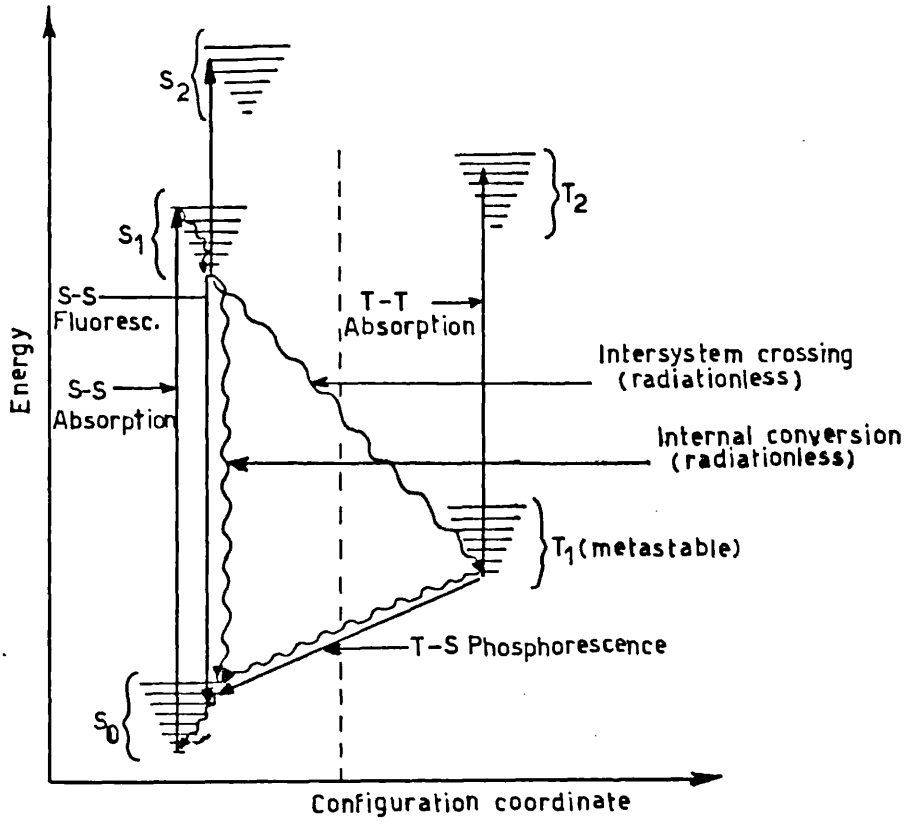

Fig. 2.2: Schematic energy diagram for a dye molecule(32)

In contrast to atomic or simple molecular gas lasers and solid-state lasers, an accurate picture of the energy levels of a dye in solution cannot be obtained at the present time. This is because dyes have complex molecules which are composed of many atoms and therefore the energy of such a molecule depends on a number of configurational coordinates; in addition, the number of possible states, involving the various permitted combinations of electronic, vibrational and rotational motions, is extremely large. However, for the sake of obtaining a schematic diagram of energy levels, it is assumed that the configuration of a state of a dye molecule can be described by only one coordinate. In real terms, only in diatomic molecules can a state be described by one configurational coordinate (the interatomic distance). This conventional picture (Figure 2.2) to describe a complex organic dye molecule was first introduced by Jablonski[33] in 1935 and has been widely used ever since.

In Figure 2.2 the symbols S and T represent singlet and triplet states respectively,and for clarity, the origin of the configuration coordinate for the triplet states has been shifted to the position of the dashed line. Each group S or T consists of states having the same electronic motion but different vibrational or rotational motions. It must be pointed out that the coordinate corresponding to minimum energy is different for each group of states. Radiative transitions resulting in absorption and emission are indicated by solid lines, while radiationless transitions are indicated by wavy lines.

The separation of different electronic states is about 10,000 to 20,000 cm^{-1} while the separation of vibrational states of a particular electronic state is of the order of 1000 cm^{-1}; for the same vibrational state, the separation of different rotational states is of the order of 1 to 10 cm^{-1}. At room temperature, there are very few dye molecules which have energy more than 200 cm^{-1} above the minimum energy of the ground group

of states S_o. The absorption of light by a dye molecule is an electronic process which takes place very rapidly, before any changes in the configuration of the molecule come into effect. For this reason, optical transitions from the low states of S_o to the excited group S_1 will not change the configuration coordinate of the molecule (Frank-Condon principle[34]). Therefore, in such transitions, the upper states of S_1 will be populated, and this process is indicated in Figure 2.2 by a vertical arrow from S_o to S_1. Following the absorption of light, a dye molecule may reemit the absorbed radiant energy, but a more likely process is radiationless thermal relaxation to the lower states of S_1. This process is very fast, having a lifetime of about 10^{-11} to 10^{-12} secs.[35]

A molecule in the lower states of S_1 can sustain a radiative transition to S_o by emitting a photon. This process is referred to as fluorescence. Typical fluorescence lifetime values for most of the lasing dyes are about 5×10^{-9} secs. From the discussion in the previous paragraph, it is apparent why the fluorescence is shifted towards the direction of the long wavelengths from the absorption (Figure 2.2). The ratio of the number of emitted photons to the number of absorbed pump photons is called the fluorescent quantum efficiency and can be close to unity for some dye solutions (Rhodamine 6G in Ethanol or Methanol). Note in the diagram of Figure 2.2 that the radiative transitions from S_1 to S_o terminate at the upper states of S_o. Eventually, a molecule returns to the original low-lying states of S_o following thermal relaxations.

Apart from the radiative transitions to the ground state S_o, molecules in the excited S_1 state can make other transitions which antagonise with fluorescence and consequently with lasing. Optical absorption by such molecules at the same frequencies as the fluorescence can result in transitions to higher-lying singlet electronic states. Radiationless transitions between S_1 and S_o can also take place, thus reducing the

fluorescent quantum efficiency. Finally, radiationless transitions to a triplet metastable state T_1 can also occur. When O_2 is added to the solution, the rate of such intersystem crossing increases [30,31]. The lifetime of the metastable T_1 state is typically 10^{-3} secs, but in a solution rich in O_2 it can be as short as 10^{-7} secs [31, 36]. Transitions from T_1 to S_o can be either radiative or thermal. The radiative transition is a slow process and is referred to as phosphorescence.

The energy level diagram (Figure 2.2) shows that the absorption-emission cycle of a dye molecule involves effectively four states (four level laser system), which indicates that the inversion required for laser action should be small. Nevertheless, for a number of reasons discussed below and in the following sub-section, even small inversions are not easy to achieve.

Intersystem transitions from S_1 to T_1 are generally undesirable in dye laser systems because they reduce the population of the upper level, thus reducing the population inversion. On the other hand, by populating the metastable state T_1, the chances of a triplet-triplet absorption are enhanced. If this absorption is at the same frequencies as the fluorescence, it can quench or even prevent laser action.

The spectral properties of a dye depend also on the type of solvent used. In this aspect, the position and the structure of the absorption and emission spectra, the spontaneous emission lifetime, and the fluorescent quantum efficiency of a dye vary from one solvent to the other. The spectra of dyes dissolved in cyclohexane are generally more structured than when dissolved in methanol or ethanol. Similarly, Rhodamine B in water has a quantum efficiency of 25% and a spontaneous emission lifetime of 0.94×10^{-9} secs [37]; but in a methanol solution these characteristics are 62% and 2×10^{-9} secs [32] respectively. Laser

output is obtained from both solutions, although their lasing efficiencies may be different.

Some spectral characteristics of dyes are also influenced by the concentration of dye molecules. Concentrations higher than 10^{-2}M result in large absorptive losses due to the overlap between absorption and emission spectra (Figure 2.1). In addition, if the concentration is high, the penetration depth of such a solution by the pumping radiation may be short compared to the radius of the cylindrical column of the active solution; due to this high peripheral absorption, the central parts of the column will remain unpumped. Another advantage obtained by using low concentrations is that the chance for dye molecules coming together in pairs is reduced. These molecular pairs (dimers) reduce the effective number of molecules available for lasing and may absorb at the fluorescence frequencies.

The spectral properties of some dye solutions depend also on the pH of the solution. As an example, it has been found[32,38] that the most efficient laser output from 7-hydroxycoumarin is obtained when this dye is in a water solution of pH 9.

Chemical and photochemical (especially when flashtube pumping is employed) instability is a problem with dyes which otherwise display several advantages for laser operation. However, xanthene dyes can be pumped with very intense flashtubes (without any UV filtering) and show no significant sign of decomposition. Solutions of Rhodamine 6G can be used for up to 100 operating hours.

Because of the broad fluorescence spectrum of dye solutions, such systems may exhibit gain over a wide spectral region. The gain of dye lasers depends[31] on:

a) the level populations, which vary with time during flashtube

pumping.

b) the frequency, as determined by the emission and absorption profiles and

c) other parameters such as temperature, concentration and length of the active medium.

Analysis of dye laser action involving both spectral and temporal considerations has been elaborated by several authors [31, 32, 38, 39, 40, 41]. These studies include treatments such as the frequency dependence of the gain, the effects of the intersystem crossing and the triplet losses, and the influence of the pumping rates upon the efficiency of the laser output.

Weber and Bass[32] considered a simplified dye laser model consisting of three groups of energy levels: the ground S_o, the excited singlet S_1 and the triplet T_1 (Figure 2.2). This is effectively a three-level system and the rate equations are:

$$\frac{dN_s}{dt} = -\frac{1}{\tau_s} N_s + P(t)\, N_o \qquad (2.1a)$$

$$\frac{dN_T}{dt} = -\frac{1}{\tau_T} N_T + K_{sT}\, N_s \qquad (2.1b)$$

$$\frac{dN_o}{dt} = P(t) N_o + \left(\frac{1}{\tau_s} - K_{sT}\right) N_s + \frac{1}{\tau_T} N_T \qquad (2.1c)$$

where τ_s and τ_T are the singlet and triplet state lifetimes, P(t) is the optical pumping rate, and K_{sT} is the intersystem crossing rate. Computer solutions of the above equations have been obtained [32, 41] for various lifetimes and optical pulses.

2.2.2. Flashtube Pumping Considerations

As was mentioned in Section 2.1, laser action from dye solutions was achieved first[12, 14] by using Q-switched lasers as pump sources. The short, intense optical pulses from Q-switched lasers provided the high pumping rates required to overcome the depopulation of the excited S_1 state due to the fast, spontaneous radiative decay to the ground S_o state and to the fast radiationless relaxation to the triplet T_1 state.

Shortly after the laser pumped dye laser was discovered[12, 14], Sorokin and Lankard[15] obtained dye laser action using a specially constructed, fast coaxial flashtube. Based on their studies of such coaxial flashtubes, Sorokin et al[39] suggested that in order to achieve laser action from solutions of xanthene dyes, the optical pulse from the flashtube should rise in a few tenths of a microsecond and have an overall width of $\sim$ 1μsec. However, in the following years, efficient laser outputs were achieved[21, 36, 42] from dye solutions pumped by larger flashtubes of longer optical pulses but capable of dissipating higher input electrical energies. This indicated that the important characteristic of a flashtube system for dye lasing was the optical pumping rate provided by the flashtube, rather than the risetime or the width of the pulse. Therefore, in order to achieve and maintain laser action from such solutions, the optical pumping rates provided by the flashtube should be high enough to overcome the depopulation of the upper level and to compensate the resonator losses.

For dyes in which triplet-triplet absorption at the fluorescence frequencies is significant, the pumping rate must be also sufficient to achieve threshold before this loss predominates.

One limitation of flashtube pumping of dyes compared with the laser pumping is that only a small percentage of the flashtube radiation lies

within the pump band of the dye. Assuming that a xenon filled flashtube resembles a blackbody radiator, Furumoto and Ceccon[43] estimated that only about 2% of the radiation from a 50 joule (input electrical energy) discharge lies within the pump band of Rhodamine 6G. Consequently, in order to obtain high pumping rates in the particular spectral band, flashtubes are often pushed to the limit of input electrical power that they can withstand without sustaining permanent damage.

In order to increase the amount of pumping radiation within the absorption band of a dye without increasing the input electrical energy in the flashtube, it has been suggested[31] that an auxiliary dye might be used; this dye, usually referred to as "light converter", is chosen so that its absorption band is not the same as that of the lasing dye, but has a high fluorescent quantum efficiency in the spectral region where the lasing dye absorbs. Working on these lines, Drake et al[44] improved the flashtube pumping efficiency of dye-doped polymer laser systems.

2.3 PRINCIPLES OF IODINE PHOTODISSOCIATION LASER OPERATION

2.3.1. Photodissociation of Alkyl-iodides and Emission from Atomic Iodine

The generation of stimulated emission from atomic iodine is one of the several processes involved in the photodissociation of alkyl-iodides and perfluorinated alkyl-iodides. These processes involve:

a) Interactions of light with particles, such as absorption, dissociation, emission etc. which are directly responsible for the laser action. For convenience, let us call these processes primary and the processes mentioned in the next paragraph secondary.

b) Reactions between atoms, molecules and radicals which may influence the laser output. Recombination of atoms into molecules and deactivation of excited species are typical examples of such processes.

As far back as 1938, Porret and Goodeve[45] showed that photodissociation of CH_3I gives atomic iodine in both the ground $^2P_{3/2}$ state and the excited $^2P_{1/2}$ metastable state. The curves in Figure 2.3, obtained by these researchers, show the measured extinction coefficient for CH_3I as a function of the energy of the incident photons. Curve I represents the total extinction coefficient. Curve A corresponds to the dissociation process:

$$CH_3I + h\nu \ (\lambda < 3500 \text{ Å}) \rightarrow CH_3 + I(^2P_{1/2}) \qquad (2.2)$$

while curve B corresponds to the dissociation process:

$$CH_3I + h\nu \ (\lambda < 4800 \text{ Å}) \rightarrow CH_3 + I(^2P_{3/2}) \qquad (2.2a)$$

The dissociation limits of processes (2.2) and (2.2a) are 3500 and 4800 Å respectively. Figure 2.3 shows that for wavelengths of the incident light longer than 3000 Å, photolysis of CH_3I gives mainly $^2P_{3/2}$ iodine atoms, while for wavelengths shorter than 3000 Å the production of excited $^2P_{1/2}$ atoms becomes very efficient. But the extinction coefficient for process (2.2) averaged in the spectral region between 2200 Å to 3000 Å is much greater than the extinction coefficient for process (2.2a) in any spectral region. Hence, when a vapour sample of CH_3I is illuminated by radiation of, more or less, even spectral distribution in the near UV, the produced iodine atoms will be in a condition of population inversion, irrespective of the absolute intensity of the incident radiation. This feature explains the low threshold of iodine lasers.

Transitions from the excited $^2P_{1/2}$ to the ground $^2P_{3/2}$ state is forbidden in electric dipole radiation, but is allowed in magnetic dipole radiation. Such a transition results in the emission of a photon at 1.31524μ

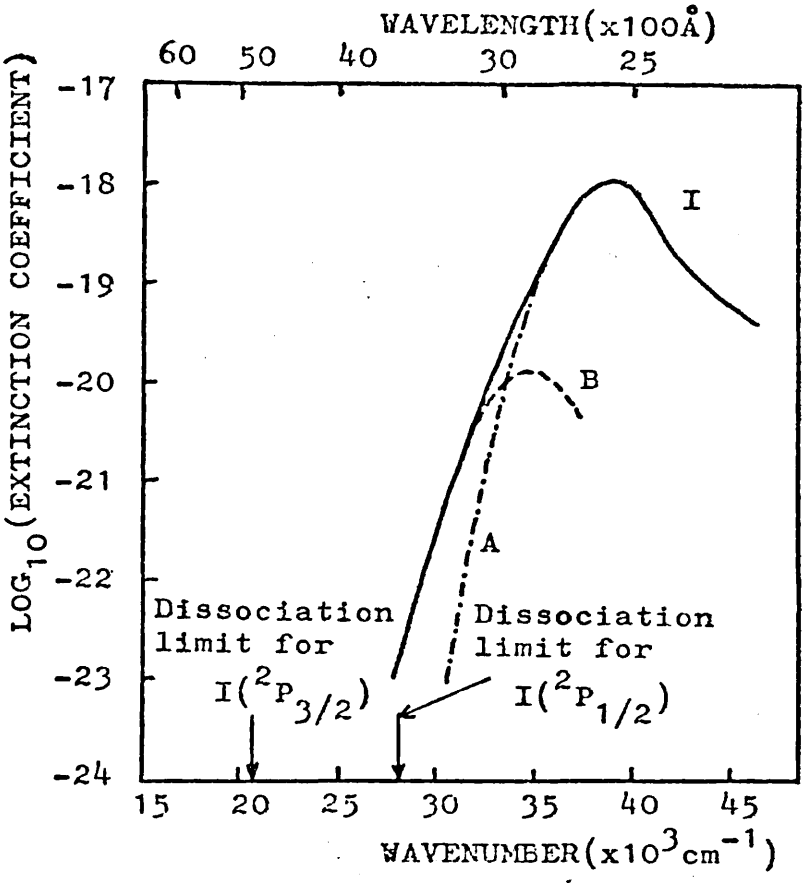

Fig. 2.3 : Extinction coefficients for the photodissociation of CH_3I. Curve I corresponds to the total extinction coefficient. A corresponds to dissociation of CH_3I into $CH_3+I(^2P_{1/2})$ and B to dissociation of CH_3I into $CH_3+I(^2P_{3/2})$(45).

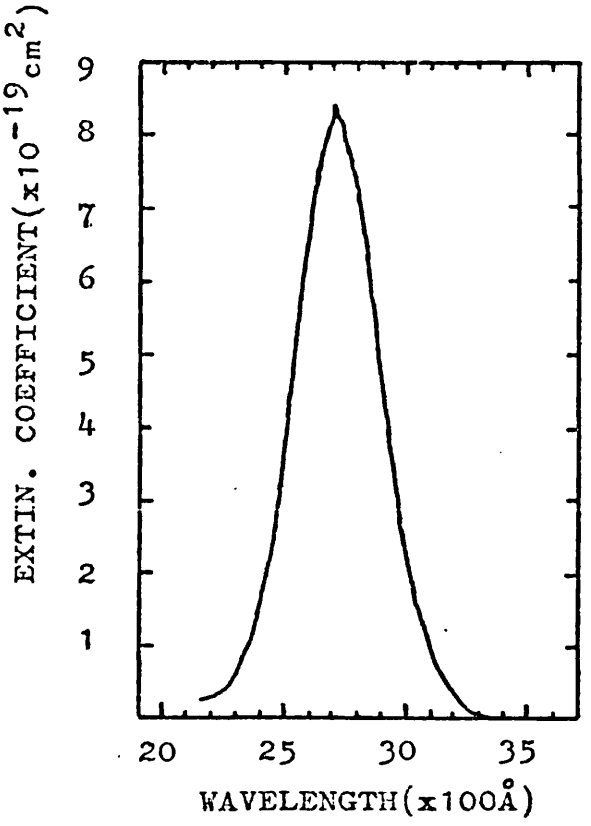

Fig. 2.4 : Extinction coefficient of $1\text{-}C_3F_7I$ in the spectral region appropriate to producing excited atomic iodine(48).

$$I(^2P_{1/2}) \xrightarrow{\text{spontaneous emission}} I(^2P_{3/2}) + h\nu_o(\lambda_o = 1.31524\mu) \qquad (2.3)$$

which is followed by stimulated emission and generation of laser oscillations if the active medium is in a cavity:

$$I(^2P_{1/2}) + h\nu_o \xrightarrow{\text{stimulated emission}} I(^2P_{3/2}) + 2h\nu_o \qquad (2.3a)$$

The spontaneous emission lifetime of the metastable $^2P_{1/2}$ state is of the order of 0.1 sec[46]; this means that the light output from an iodine laser is practically free of fluorescence noise.

Photodissociation of higher members of the alkyl or fluoroalkyl-iodide families gives similar products e.g. alkyl or fluoroalkyl radicals and atomic iodine. But the absorption band and the extinction coefficient may vary from one member to the other. The quantum efficiency of iodine atoms in the $^2P_{1/2}$ state is defined[47] as the ratio of the number of iodine atoms produced in the excited $^2P_{1/2}$ state to the total number of iodine atoms produced from the photodissociation, and it is averaged over the spectrum of the light source. If the light source and the alkyl (or fluoroalkyl) iodide compound are chosen appropriately, the quantum efficiency of the iodine atoms in the $^2P_{1/2}$ state will be very close to unity and virtually the atomic iodine produced will be in a condition of complete population inversion. This implies that the gain of such a laser system will be extremely high. Molecules of CF_3I or $1 - C_3F_7I$ are the most suitable compounds for efficient laser operation. Figure 2.4 shows the absorption spectrum of $1 - C_3F_7I$ obtained by Gusinow[48]; it corresponds to the absorption in the spectral region appropriate to producing excited iodine atoms.

2.3.2 Secondary Processes in the Photodissociation of Alkyl-iodides

If the population of excited iodine atoms was reduced only by the radiative processes (2.3) and (2.3a), then in view of the long spontaneous emission lifetime of the excited state, a laser system working on these lines would be ideal. In reality, however, this is not the case. Quenching of the upper laser level takes place as a result of recombination processes of iodine atoms into iodine molecules and deactivation collisions of excited iodine atoms with molecules.

The recombination of atomic iodine is a third-order reaction because it takes place in the presence of a "third body" whose nature and concentration affects the rate of the process. The overall reaction may be written:

$$I + I + M \rightarrow I_2 + M \qquad (2.4)$$

and the corresponding rate equation is:

$$-\frac{d(I)}{dt} = K_1(I)^2(M) \qquad (2.4a)$$

where I represents atomic iodine in either the excited $^2P_{1/2}$ or the ground $^2P_{3/2}$ state, M is the third body, K_1 is the rate constant of the process, and the figures in the round brackets indicate concentrations of the various compounds. Measurements[46, 49] of rate constants for the recombination of iodine atoms in the presence of various gases or vapours have revealed that the most effective third body is molecular iodine and that the rate constants for the states $^2P_{1/2}$ and $^2P_{3/2}$ are the same [46]. It was found [46, 49] that at room temperature, when $M \equiv I_2$ K_1 is $\sim 5 \times 10^{-30} cm^6.sec^{-1}$, while in the case that Argon acts as third body K_1 is $\sim 8 \times 10^{-33} cm^6.sec^{-1}$.

Depopulation of the upper laser level occurs also as a result of two body processes in which the excited iodine atoms undergo de-excitations

to the ground state; such de-excitations are more frequent in the case of collisions with iodine molecules:

$$I(^2P_{1/2}) + I_2 \rightarrow I(^2P_{3/2}) + I_2 \qquad (2.5)$$

The rate at which excited atomic iodine is lost through such collisions is given by:

$$-\frac{d(I^*)}{dt} = K_2(I^*)(I_2) \qquad (2.5a)$$

where I^* represents atomic iodine in the excited state and K_2 is the rate constant of the process. According to Donovan and Husain[50] the rate constant of process (2.5) at room temperature is 5×10^{-12} $cm^3.sec^{-1}$.

As is well known, the half-time of a reaction represents a measure of the speed with which the particular reaction takes place. Consequently, in order to find out which of the two processes (2.4) and (2.5) is more effective in depopulating the upper laser level, the half-times of these processes are calculated from the solutions of differential equations (2.4a) and (2.5a). In both cases it is assumed that the concentration of molecular iodine does not vary substantially with time. In this way, the recombination half-time is found

$$T_r = \frac{1}{K_1(I_o)(I_2)} \qquad (2.6)$$

and the de-excitation half-time

$$T_d = \frac{\ell n 2}{K_2(I_2)} \qquad (2.7)$$

where (I_o) is the original concentration of atomic iodine and (I_2) is the concentration of molecular iodine. These relations show that the recombination half-time depends on the concentration of atomic iodine,

while the de-excitation half-time is independent of the concentration of atomic iodine in the excited state. Given that in a flash photodissociation of an alkyl-iodide the concentration of atomic iodine produced varies with time, it becomes evident from equation (2.6) that the speed with which recombination takes place varies in a similar fashion. Therefore, the depopulation of the upper laser level due to recombination becomes significant only at the later stages of the light pulse, when a substantial percentage of the alkyl-iodide sample has sustained photodissociation.

In contrast, the depopulation of the upper laser level due to de-excitation collisions with iodine molecules is effective at any stage and, providing that the concentration of molecular iodine remains constant, the speed of such a process is the same throughout the duration of the light pulse. A simple numerical example relevant to the conditions encountered in atomic iodine photodissociation lasers is given below. A sample of CH_3I at 100 Torr in the presence of molecular iodine at 10 Torr is pumped by an intense, fast light pulse. It is assumed that at a certain moment after the initiation of the flash process, the partial pressure of atomic iodine produced is 10 Torr. The concentrations of atomic and molecular iodine, corresponding to the above pressures for room temperature, are inserted into equations (2.6) and (2.7); the recombination and de-excitation half-times are then estimated equal to 1.83×10^{-6} secs and 4.2×10^{-7} secs. respectively. These figures prove that, even for such high concentration of atomic iodine, de-excitation is more than four times faster than recombination. Since the usual operating pressure of alkyl-iodides for efficient atomic iodine laser output is ~ 100[24] Torr, it becomes obvious from the above that only for very high percentage photodissociations (70% - 80%) will the depopulation rate of the upper level due to recombination match the rate of de-excitation.

Equations (2.6) and (2.7) were derived on the assumption that the concentration of I_2 does not vary during the flash procedure. A more representative analysis of processes (2.4) and (2.5) can be carried out by taking into account the cumulative variation of molecular iodine concentration. Such an analysis has been elaborated by the author of this work and is presented in Section 7.3. In this sub-section the results of the analysis are discussed in brief. The following expression was derived for the recombination half-time:

$$T_r = \frac{2}{K_1(I_o)\left[(I_o) + 2(I_2)\right]} + \frac{2\ell n\left[2 + \frac{(I_o)}{2(I_2)}\right]}{K_1\left[(I_o) + 2(I_2)\right]^2} \qquad (2.8)$$

where (I_o) and (I_2) represent the concentrations of atomic and molecular iodine respectively at $t = 0$ and they are measured in number of particles per cm^3. When (I_2) is comparable to or higher than (I_o), half-time values obtained from equation (2.6) are close to those obtained from equation (2.8) and therefore the former equation can be used; but, when $(I_2) << (I_o)$ the values obtained from these equations differ substantially. For example, for $P_{I_o} = 10$ Torr and $P_{I_2} = 10$ Torr, the half-time values obtained from equations (2.6) and (2.8) are 1.83×10^{-6} secs and 1.6×10^{-6} secs, respectively, whereas for $P_{I_o} = 10$ Torr and $P_{I_2} = 0.1$ Torr the respective times are 1.83×10^{-4} secs and 1.76×10^{-5} secs.

The recombination half-time of an atomic iodine sample, free of molecular iodine at $t = 0$, can be obtained from equation (2.8) if (I_2) is assumed extremely small. Such conditions are encountered in iodine lasers in which a pure alkyl-iodide vapour sustains photodissociation. Conventionally, the absence of I_2 in the sample can be demonstrated with accuracy by considering $(I_2) = 1$ molecule per cm^3 instead of $(I_2) = 0$.

In this manner the recombination half-time of such a sample is:

$$T_{r}|_{(I_2)=1} = \frac{2}{K_1(I_o)^2}\left[1 + \ell n \frac{(I_o)}{2}\right] \qquad (2.9)$$

From equation (2.9) it is estimated that a sample of atomic iodine at 10 Torr and free of I_2 will have a recombination half-time equal to 1.5×10^{-4} secs.

The depopulation of the excited $^2P_{1/2}$ state (process (2.5)) in the presence of I_2 of increasing concentration has also been studied in the analysis mentioned above (see Section 7.3). It was found with good approximation that, for values of (I_2) comparable to or higher than (I_o), the population of $^2P_{1/2}$ iodine atoms decays in an exponential form given by:

$$(I^*) = (I^*_o)\left[1 + At\right]^B e^{-Ct} \qquad (2.10)$$

whereas for values of (I_2) much smaller than (I_o), the decay is of the form:

$$(I^*) = (I^*_o)\left[\frac{(I_o) + 2(I_2)}{(I_o) + 2(I_2)e^{Dt}}\right]^B \qquad (2.11)$$

where

$$A = K_1(I_o)\left[(I_o) + 2(I_2)\right] \qquad (2.12a)$$

$$B = \frac{K_2}{2K_1\left[(I_o) + 2(I_2)\right]} \qquad (2.12b)$$

$$C = \frac{K_2 [(I_o) + 2(I_2)]}{2} \qquad (2.12c)$$

$$D = K_1 [(I_o) + 2(I_2)]^2 \qquad (2.12d)$$

In the first case, the de-excitation half-time can be estimated from the relation;

$$(1 + At)^B e^{-Ct} = \tfrac{1}{2} \qquad (2.13)$$

if the known values of parameters A, B and C are inserted into this relation, and then various values of t are tried until equation (2.13) is satisfied. In this way, a de-excitation half-time of 3.8×10^{-7} secs. is obtained from equation (2.13) for a sample of atomic iodine at 10 Torr initial pressure in the presence of I_2 at 10 Torr; the half-time obtained from equation (2.7) for the same concentration of I_2 is 4.2×10^{-7} secs. It is apparent, as in the case of recombination, that for $(I_2) \sim (I_o)$ or $(I_2) > (I_o)$ equation (2.7) gives very good approximations and therefore it can be employed to describe the speed of process (2.5).

In the case where $(I_2) \ll (I_o)$, an analytical expression of the de-excitation half-time can be derived from equation (2.11):

$$T_d \big|_{(I_2) \ll (I_o)} = \frac{1}{D} \ell n \frac{(I_o) + 2(I_2) - (I_o)[0.5]^{1/B}}{2(I_2)[0.5]^{1/B}} \qquad (2.14)$$

Note that, in equation (2.14) T_d is independent of the concentration of atomic iodine in the excited $^2P_{1/2}$ state, but unlike in equation (2.7), it depends on the total concentration of atomic iodine in all possible

states. As an example, a sample of atomic iodine at 10 Torr in the presence of I_2 at 0.1 Torr is considered. From equation (2.14), T_d is estimated equal to 1.04×10^{-5} secs., while from equation (2.7) $T_d = 4.2 \times 10^{-5}$ secs. Consequently, in such cases, equation (2.14) should be preferred.

The de-excitation half-time for an atomic iodine sample free of I_2 at $t = 0$ is derived from equation (2.14) by inserting the value $(I_2) = 1$ molecule per cm^3:

$$T_{d|(I_2)=1} = \frac{1}{K_1(I_o)^2} \ln \frac{(I_o)\left[1 - [0.5]^{\frac{2K_1(I_o)}{K_2}}\right]}{2[0.5]^{\frac{2K_1(I_o)}{K_2}}} \qquad (2.15)$$

For $P_{I_o} = 10$ Torr, a de-excitation half-time of 7.2×10^{-5} secs is estimated from equation (2.15).

The lengthy treatment of recombination and de-excitation of atomic iodine given in this section was considered necessary in order to avoid possible confusion about the half-times of these processes. In fact, some researchers on iodine lasers have mentioned that the half-time of atomic iodine recombination is of the order of 100μsecs., without specifying the concentrations of the sample constituents.

Deactivation of excited iodine atoms can also take place in collisions with undissociated alkyl-iodide molecules:

$$I(^2P_{1/2}) + CH_3I \rightarrow I(^2P_{3/2}) + CH_3I \qquad (2.16)$$

or

$$I(^2P_{1/2}) + CH_3I \rightarrow I_2 + CH_3 \qquad (2.16a)$$

Rate constants of the order of 10^{-16} cm^3. sec^{-1} for the combined action of processes (2.16) and (2.16a) have been reported[51], which indicate that such deactivation processes are very slow.

Finally, in contrast to the recombination of atomic iodine, the recombination of free radicals produced from the photodissociation of alkyl-iodides is a second order process:

$$CH_3 + CH_3 \rightarrow C_2H_6 \qquad (2.17)$$

Known rate constants[52] show that these radicals are consumed rapidly.

2.3.3. Effects of Secondary Processes on the Laser Output

It has been well known since the original works on iodine photodissociation lasers[22, 23], that the laser output efficiency drops dramatically when the alkyl-iodide sample is exposed to a second flash; in certain cases no laser emission is obtained at all. This event cannot be explained only on the grounds of reduced concentration of the alkyl-iodide vapour, because it was observed[23] that, following a mere 3% photodissociation of pure CF_3I at 100 Torr during the first flash, the laser output in the second flash was unusually low. It is apparent that radiationless processes like recombination and de-excitation cause a fast, continuous depopulation of the excited $^2P_{1/2}$ state, so that the population inversion of the active medium does not take on high values above threshold or, even, threshold is not reached at all. As was shown in the previous sub-section, the fast catalytic action of I_2 speeds up the recombination and de-excitation processes and therefore its presence in the second, third etc. flash explains the substantial reduction of laser efficiency. Consequently, in order to obtain an efficient laser output from the photodissociation of an alkyl-iodide, the laser cell

must be evacuated after each flash and then must be filled with a pure sample for the following flash.

In the two original works[22, 23], it was also observed that, when a sample of pure CF_3 was pumped by a long, high energy optical pulse, an abrupt laser quenching took place prior to the flash termination; in fact, laser emission ceased at 10 - 20 μsecs after the application of the optical pulse. It was then proposed that this quenching was due to an increased effectiveness of deactivation processes (2.16) and (2.16a) at higher temperatures, and, to a lesser extent, to pyroltic decomposition of CF_3I. Pyrolysis of CF_3I gives atomic iodine in the ground state only.

$$CF_3I \xrightarrow{heat} CF_3 + I(^2P_{3/2}) \qquad (2.18)$$

This hypothesis was reinforced by observations of continuous laser emission throughout the optical pulse when low pumping energy was used. Other authors[24, 47], however, consider that the effects of the temperature rise are negligible compared to the effects of processes (2.4) and (2.5) in the presence of I_2. Although the concentration of I_2 is very low during the initial stages of a flash photodissociation of a pure alkyl-iodide vapour, the increasing formation of such molecules gradually speeds up the recombination and deactivation of atomic iodine. The analysis carried out in the previous sub-section (see also Section 7.3), showed that the recombination and deactivation half-times of atomic iodine free of I_2 at the beginning of the processes (equations (2.9) and (2.15)) are of the order of 10^{-4} and 10^{-5} secs. respectively for vapour pressures around 10 Torr. These theoretical data are in fair agreement with the observed[22, 23] laser termination at 10 - 20 μsecs. after the application of the flash; therefore, the suggestion that process (2.4) and to a greater extent process (2.5) are the main causes for the early laser termination appears to be justified.

The problem of the population inversion quenching has been tackled by adding rare gases into the alkyl-iodide vapour. This method was first successfully tried by Kasper and his co-workers[23]. Later Aldridge[53] achieved laser action from the photodissociation of CF_3I and C_3F_7I at high pressures by adding rare gases.

2.3.4. Pumping Requirements

From the survey and analysis carried out so far, there is enough information as to what specific requirements should be met by a flashtube intended to pump iodine photodissociation lasers. Thus, as far as spectral conditions are concerned, the flashtube should be efficient in the near UV region of the spectrum and especially in the region between 2200 Å to 3000 Å, since the photodissociation of alkyl-iodides by radiation of this region results in the plentiful production of $^2P_{1/2}$ iodine atoms.

Because of the quenching of the laser output due to the formed I_2, the flashtube should deliver most of its radiant energy within 15 - 20 μsecs. In fact, the faster the optical pulse from the flashtube, the more efficient is the iodine laser obtained. The maximum efficiency achieved[26] from an iodine laser is 0.5% and it was obtained by using a 1 K joule - 3 μsecs flashtube pulse.

With regard to the pressure of the alkyl-iodide vapour, it has been found[24] that the optimum operating pressure for CF_3I and 1 - C_3F_7I laser systems is ∿ 100 Torr; at pressures higher than 100 Torr saturation is observed[24], while at very high pressures the laser output decreases. Laser action from 1-C_3F_7I at pressures up to 3 atmospheres has been achieved[53] by adding a rare gas. The threshold pressure for most alkyl-iodides is ∿ 0.5 Torr[22, 24]. At vapour pressures below 0.5 Torr, laser action cannot be achieved because the concentration of the atomic iodine produced from the photodissociation does not reach the threshold value.

CHAPTER 3

CHARACTERISTICS AND OPERATION OF FLASHTUBE SYSTEMS

3.1 GENERAL FEATURES

Since the construction of the first flashtube in the early 30's[54], there have been numerous studies and developments in this field because of the increasing need for intense light sources for photographic, spectroscopic, photolytic etc. work. However, the discovery of the laser has placed additional demands on the flashtube performance. The requirements from an optical pumping source for reliable and efficient operation of a pulsed laser system have been mentioned in Chapter 1. Several types of flashtubes have been constructed in the last fifteen years, varying in geometry, volume, gas filling and input electrical energy, in order to meet these demands and to explore potential laser materials.

The various forms of conduction of electricity through gases, or electrical gas discharge as it is better known, are phenomena of complex and often unpredictable nature. Since gases display very low conductivity under usual conditions (atmospheric pressure, moderate electric fields), the stages leading to the establishment of a highly conducting channel, under the application of an external electric field, are very important, especially in the case of transient discharges. These stages constitute what is known as ionisation growth (or current growth), while the attainment of high electron and ion density capable of carrying large amounts of electrical energy across the gap, is known as "breakdown" of gas. Breakdown is detected by the sharp rise of the current. During the current growth stages some electrical energy is spent in order to produce enough charged particles in the gas column.

Once the highly conducting channel has been established, large amounts

of energy can be dissipated in the gas, providing that the external source supplies electrical energy at high rates. This high conductivity of strongly ionised gases constitutes the principle of flashtube operation; electrical energy is stored in a condenser and then is discharged through the gas column of the flashtube in the form of DC or impulse voltage. Therefore, a flashtube discharge can be regarded as a form of electric spark. Since impulse forms of voltage were employed exclusively in this work, the mechanism of breakdown and the various stages of an impulse discharge are examined separately in Section 3.3.

Both temporal and spectral characteristics of the optical output from a flashtube discharge depend on:

a) Several parameters, of which the most important are the wave-form of the applied voltage across the electrode gap, the impedance of the circuit, the magnitude of the input electrical energy, the gas pressure and the distance between the electrodes.

b) The gas type and

c) The effects of independently acting agents such as dopants or other preionising devices.

Because of the transient nature of flashtube discharges, large amounts of electrical energy can be dissipated in the gas during a time interval which is relatively short to allow destruction of the system due to cumulative heating. Nevertheless, if the repetition rate is high, a cooling device is necessary. However, thermal effects in flashtube discharges are much evident in the form of shock-wave damage of the walls (see Sections 3.3 and 4.1).

The input electrical energy is provided by a condenser charged through a resistor to a voltage V, so that the energy stored is:

$$E = \frac{1}{2} CV^2 \qquad (3.1)$$

The energy delivered to the flash tube electrodes is slightly less than that stored in the condenser, as a result of circuit losses. These losses are greater, the higher the operating voltage, because of corona formations along the circuit leads.

A fraction of the input electrical energy is used for the production of electrons and ions in the gas and for their transport to the respective electrodes, while another fraction is converted into radiant energy as a result of excitation, electron-ion recombination, thermal etc. processes in the gas. Finally, some energy escapes from the system through heat conduction, diffusion and collisions of particles with the walls.

According to Meek and Craggs[55], the energy balance equation for a spark channel is

$$IE = S + W + \frac{dU}{dt} \qquad (3.2)$$

where IE represents the input electrical power, S is the radiative term, W is the energy loss per unit time through heat conduction and U is the internal energy of the channel given by:

$$U = \pi R^2 N_e \frac{3}{2} kT_e + \pi R^2 N_e e V_i \qquad (3.3)$$

where the first term gives the kinetic energy of all electrons in the channel ($\frac{3}{2} kT_e$ is the average electron energy, T_e is the electron temperature), and the second term is the energy given up by electrons in ionisations.

As will be seen in section 3.2, in a discharge column, the kinetic energies acquired by electrons travelling in the direction of the field can become very high compared to the kinetic energies of ions in the same column. The average electron energy of a discharge - often referred to as 'electron temperature' - increases with increasing value of the

reduced parameter E/p (the electric field per unit pressure, measured in $V.cm^{-1}\ Torr^{-1}$) which characterises the discharge. In fact, the value of E/p is approximately a measure of the average energy acquired by an electron between two successive collisions (the energy acquired by an electron along a mean free path ℓ_e is $eE\ell_e$, where ℓ_e is always $\propto 1/p$).

Conservation of linear momentum prohibits a free electron from radiating in a flashtube discharge. However, radiation may be emitted when an electron collides with an atom or ion, and the change in kinetic energy is converted into radiant energy (bremsstrahlung radiation), while the presence of the other particle balances the linear momentum of the system. Alternatively, part of the electron energy can be transferred to an atom or ion in various collisional processes. Then, the transferred energy may be emitted in the form of radiant energy. The radiative processes in a flashtube discharge are discussed in Section 3.4.

The conversion of electrical energy into radiant energy is efficient when electrons do not acquire excessive kinetic energies. This is explicable from the fact that the total cross-sections for collisions between electrons and atoms or ions are small when the energy of the impinging electron is high[56] (see also Section 3.2); consequently the energy transfer (elastic or inelastic) from electrons to atoms or ions will not be effective if the frequency of such impacts is not high. In this case, a large proportion of the electron energy will be wasted in collisions with the walls or electrodes. Since the electron temperature increases with increasing value of E/p, it becomes obvious that in order to obtain high luminous efficiency from a flashtube discharge, moderate or low values of E/p should be used.

Breakdown curves of gases[57, 58] (curves illustrating the breakdown voltage V_s versus the reduced parameter pd or the pressure p), exhibit one common feature: as the gas pressure is raised, the value of E/p,

at which breakdown occurs, decreases. Therefore, by using gases at high pressures, the range of operating low values of E/p is extended and consequently the luminous efficiency of the flashtube increases. The same argument applies in the case that the flashtube length is increased. But, gas pressure alterations are much easier compared to electrode distance alterations.

As was shown above, the value of the reduced parameter E/p determines, to a great extent, the luminous efficiency of a flashtube. But, for a given flashtube geometry, optimisation of gas pressure for a range of moderate and low values of E/p is more important. Further evidence supporting this statement is obtained from considerations of energy losses due to collisions of particles with the walls. For a given value of E/p, these collisions are less frequent at high pressures because, as is known, the diffusion coefficient D of neutral and excited atoms, in their own gas, is inversely proportional to the pressure, while the ampipolar diffusion coefficient D_a of electrons and ions was also found to decrease [59, 60] as the pressure is increased. Finally, D_a decreases [60] with increasing atomic or molecular weight.

Generally rare gases and rare gas mixtures display high luminous efficiency, which is explicable on the grounds of their very low breakdown voltages [57, 61]. The low breakdown voltages of rare gases make the use of low values of E/p feasible. The heavy rare gases, i.e. Krypton and Xenon, are the most efficient for flashtube operation because of their low heat conductivity.

3.2 EXCITATION AND IONISATION OF RARE GASES BY ATOMIC COLLISIONS

The primary excitation and ionisation processes in any gas discharge are those involving impact between gas atoms and electrons

$$A + e^- \rightarrow A^* + e^- \quad \text{(Excitation)} \tag{3.4}$$

$$A + e^- \rightarrow A^+ + 2e^- \quad \text{(Ionisation)} \tag{3.5}$$

These processes become possible when the kinetic energy of the impinging electron is at least equal to the first excitation or ionisation potential of the atom. Electrons are capable of acquiring high kinetic energy in the direction field, irrespective of the frequency of elastic collisions (or, in other words, irrespective of the gas pressure). This is explicable on the grounds of the very small fractional loss[58,62,63] of electron energy in elastic collisions with gas atoms. According to Llewellyn-Jones[62] the average fractional loss amounts to:

$$f = 2\frac{m}{M} \tag{3.6}$$

where m and M are the electron and atom mass respectively.

Cravath[63] assumed electrons and gas atoms having Maxwellian distribution of velocities and estimated the average fractional loss equal to

$$f = \frac{8}{3}\frac{mM}{(m+M)^2}\left(1 - \frac{T_g}{T_e}\right) \tag{3.7}$$

where T_g is the gas temperature and T_e the electron temperature. Given that, for transient discharges, thermal equilibrium does not exist between electrons, ions, and neutral atoms (at least during the ionisation growth stages), one can assume that $T_e >> T_g$. Then, equation (3.7) reduces to:

$$f = 2.66\,\frac{m}{M} \tag{3.7a}$$

since $m << M$.

Equations (3.6) and (3.7) indicate that the loss in kinetic energy is even smaller in the case of heavier gas atoms. If numerical values for

Ar, Kr and Xe atoms are substituted in equation (3.7a), the fractional losses of electron energy in elastic collisions are: 3.6×10^{-5}, 1.72×10^{-5} and 1.1×10^{-5} respectively.

Unlike electrons, the heavy positive ions transfer a large proportion of their kinetic energy to the gas atoms in elastic collisions and thus the most of them do not acquire high kinetic energies in the direction of the field capable of exciting and ionising atoms. According to Llewellyn-Jones[62] the average fractional loss of positive ion energy is $\frac{1}{2}$, while from equation (3.7) it is obtained:

$$f = \frac{2}{3}\left(1 - \frac{T_g}{T_i}\right) \qquad (3.8)$$

for positive ions since $m_i \sim M$. T_i is the ion temperature. This fraction is very high, at least during the pre-breakdown stages, when the ion temperature is much higher than that of the neutral atoms.

Cross-sections of collisions between electrons and rare gas atoms were measured by Ramsauer and Kollath[64] at low electron energies (energies below the first excitation potential, so that collisions can be regarded as elastic). Very low values were obtained especially at electron energies around 1 eV. Later, Brode[65] extended these studies to higher electron energies and measured the total collision cross-sections $Q = Q_{el.} + Q_{in.}$ of rare gases up to electron energies of 65 eV. $Q_{el.}$ and $Q_{in.}$ are the elastic and inelastic terms respectively. Brode's result for rare gases, H_2 and N_2, are illustrated in Fig. 3.1.

An electron whose energy E_e is at least equal to the energy difference E_{ex} between two states of an atom can excite the atom in a collision providing that the change of the internal angular momentum of the atom takes on a quantised value[66]. This implies that for $Ee = E_{ex}$, the excitation probability for the particular transition is practically

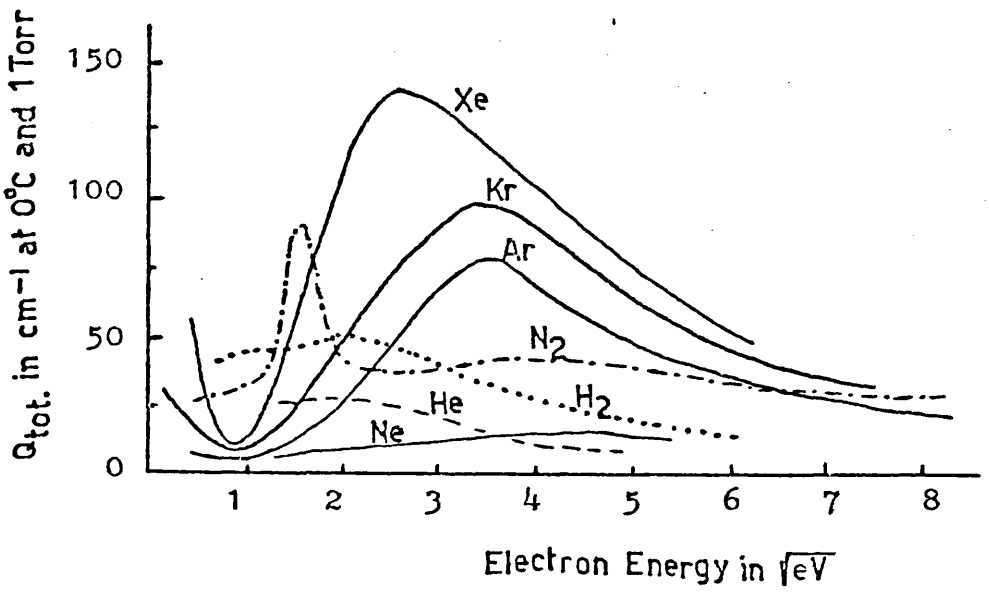

Fig. 3.1: Collision cross-sections of various gas atoms and molecules for electron impact(65).

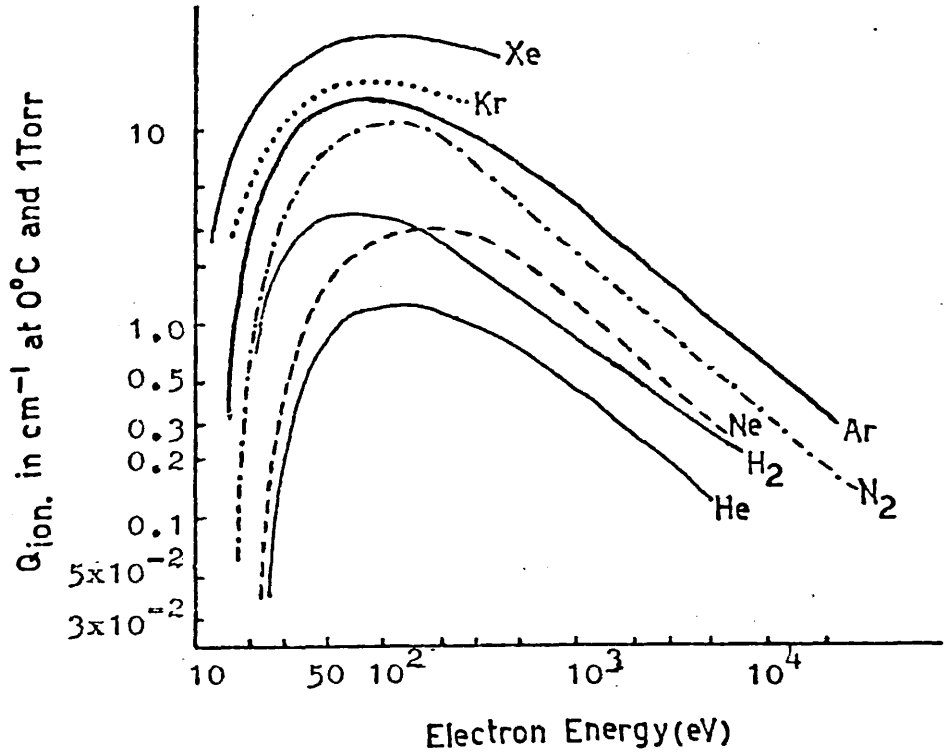

Fig. 3.2: Ionisation cross-sections of various gases for electron impact(75).

zero. As the electron energy increases, the excitation probability increases until for $E_e \sim 1.5 - 2\ E_{ex}$ a maximum is reached for optically allowed transitions[67]. The maximum excitation probabilities for resonant transitions in rare gases[66] are of the order of 10^{-2} or smaller, implying that in 100 collisions or more there will be one excitation to the particular state.

The metastable states of an atom are mainly filled from higher resonant states, although as was found by Corrigan and von Engel[68] in the case of He, the probabilities for transitions from ground to metastable states by electron impact are comparable to those for transitions to resonant states. Evidence that the concentration of metastable atoms is high in rare gas discharges was obtained from the long afterglows observed[69,70] in such discharges. The presence of a large number of metastable atoms explains the very low breakdown voltages of rare gases by means of the two step ionisation:

$$A + e^- \rightarrow A^m + e^- \qquad (3.9)$$

$$A^m + e^- \text{ (or } h\nu) \rightarrow A^+ + 2e^- \qquad (3.9a)$$

In this process, low energy electrons can ionise gas atoms, so relatively low electric fields can cause breakdown. Moreover, excited atoms, whether metastable or not, display very large 'effective radii'[71] in collisions with other particles. For this reason, high excitation and ionisation probabilities should be expected in collisions between metastable atoms and electrons (or photons). Ionisation can also occur when two metastable atoms collide, an effect observed by Biondi[70] in afterglows:

$$A^m + A^m \rightarrow A + A^+ + e^- \qquad (3.10)$$

Ionisation cross-sections of the order of 10^{-14} cm^2 for collision between He metastable atoms have been reported[72].

Another ionisation process, involving metastable atoms in rare gas mixtures, was discovered by Penning, Kruithof and Druyvensteyn[73] and it is known as 'Penning ionisation'. This process involves collisions between metastable atoms of one gas and neutral atoms of the other, the ionisation potential of the latter being lower than the excitation energy of the former:

$$A^m + B \rightarrow A + B^+ + e^- \qquad (3.11)$$

Cross-sections of the order of $10^{-15} cm^2$ were measured[74] for ionisation collisions between He metastables and neutral atoms of other rare gases.

Metastable atoms are deactivated in collisions with the walls or electrodes of the flashtube. This effect is less pronounced at higher pressures due to the lower diffusion coefficient.

An electron of energy E_e can ionise a ground state atom in a collision if $E_e \geq eV_i$, V_i being the first ionisation potential of the atom; if the electron energy is sufficiently high, such impact may result in double or multiple ionisation. However, the single ionisation process dominates over multiple processes. Figure 3.2 shows the total ionisation cross-sections[75] of rare gases, H_2, and N_2 as functions of the electron energy. It can be seen that the ionisation cross-sections take on maximum values for electron energies between 80 and 120eV (i.e. $E_e \sim 5 - 8\ eV_i$). Xenon displays the highest ionisation efficiency for electron impact, due to the high polarisability of its atoms.

Collisions between photons and atoms are different in nature from those between electrons and atoms. A photon can excite a gas atom if its energy (or wavelength) lies within a very narrow energy range corresponding to the width of the resonance line of the atom.

$$A + h\nu \rightarrow A^* \ (h\nu \sim E_{ex}) \qquad (3.12)$$

Absorption cross-sections averaged over the line width can be very large, of the order of 10^{-13} cm^2 [76].

Measurements of photoionisation cross-sections [77] indicate that photons ionise gas atoms with a maximum probability at a certain critical energy which is 0.1 to 1eV above the ionisation energy;

$$A + h\nu \rightarrow A^+ + e^- \ (h\nu \geq eV_i). \qquad (3.13)$$

electrons, on the other hand, require 5 to 8 times the ionisation energy in order to achieve maximum probability. Maximum photoionisation cross-sections up to the order of 10^{-14} cm^2 have been measured for rare gases [77]. Again, as in the case of ionisation by electron impact, the heavier atoms exhibit higher ionisation efficiency than the lighter ones. Because of the relatively high ionisation potentials of these gases, the radiation required lies in the short ultraviolet, below 1000 Å. A photon of energy less than the ionisation energy cannot ionise, unless the atom is already in an excited state. As was mentioned above, photo-excitation and photoionisation cross-sections of excited atoms are expected to be high.

3.3 HIGH CURRENT, PULSED ELECTRICAL GAS DISCHARGES

The various stages in the development of a gas discharge under the application of an impulse voltage are still events not fully understood in a quantitative fashion. Both the pre-breakdown and post-breakdown regimes of such a discharge display a high degree of complexity, especially in the case of high input power and of high pressure. However, the use of sophisticated experimental techniques during the last twenty years enabled several investigators to obtain valuable information

concerning the various stages of current growth and thus give a qualitative explanation of the physical processes involved. Presentation of these techniques would have been beyond the scope of the present study. Haydon's[78] review paper gives a good account of these techniques.

Four main stages can be distinguished in an impulse discharge from the moment the voltage is applied to the moment the current becomes zero- or to the moment the last photons are emitted. Discharge characteristics, such as voltage, current, luminous intensity, vary substantially from one stage to the other.

1. The first stage commences with the arrival of the voltage waveform at the electrodes and terminates with the appearance of a suitably placed initiatory electron - or electrons - at a time t_1 (Figure 3.3) for which the corresponding value of the impulse voltage is $\geq V_s$, V_s being the DC breakdown value of the gap. The time interval t_s which elapses between the above events is referred to as the 'statistical time lag'. From Figure 33, it can be seen that $t_s = t_1 - t_o$.

The initiatory electrons can be provided

a) by natural ionising causes, such as cosmic rays or

b) by artificial external processes, such as irradiation of the cathode with UV light, passage of an electron beam through the gas etc.

Also, it is believed that cold cathodes liberate electrons[79] when the applied field takes on high values.

2. Following the provision of initiatory electrons, the ionisation increases until a highly conducting channel is formed across the gap. Then the voltage which has risen to a value V by that time - stops rising, while the current undergoes a sharp rise. The 'formative time lag' t_f (indicated by the interval $t_2 - t_1$ in Figure 3.3) of a discharge is the time required for the discharge to build up across the gap from

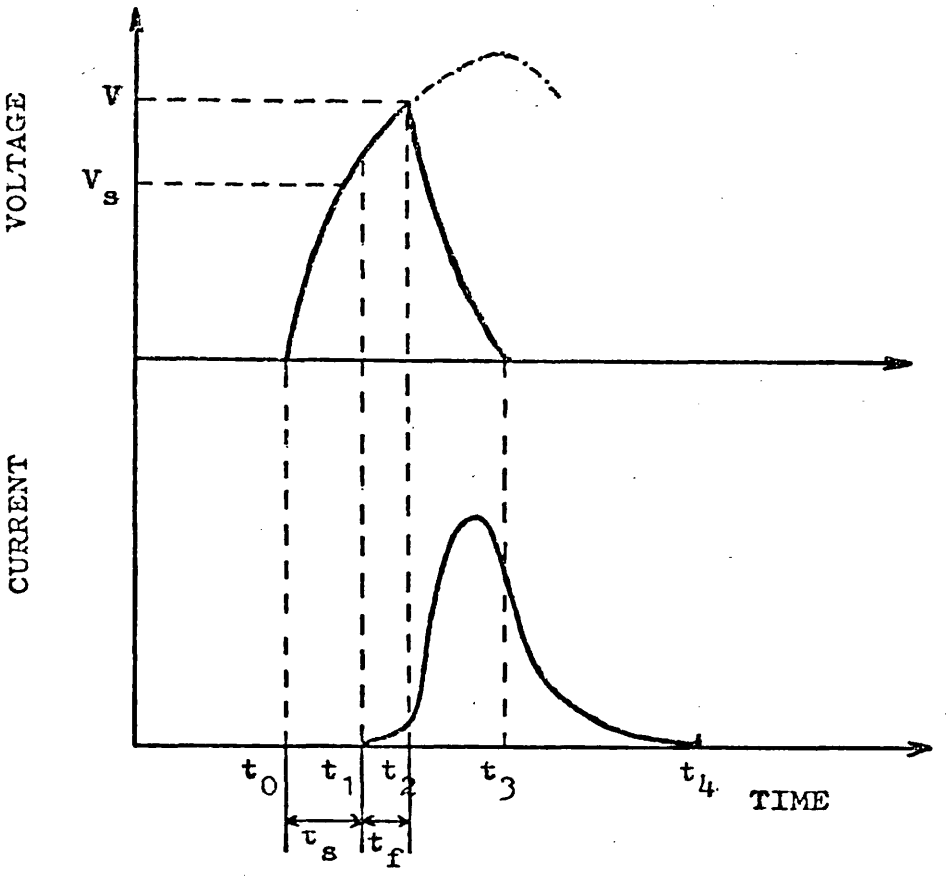

Fig. 3.3: Breakdown under an impulse voltage.

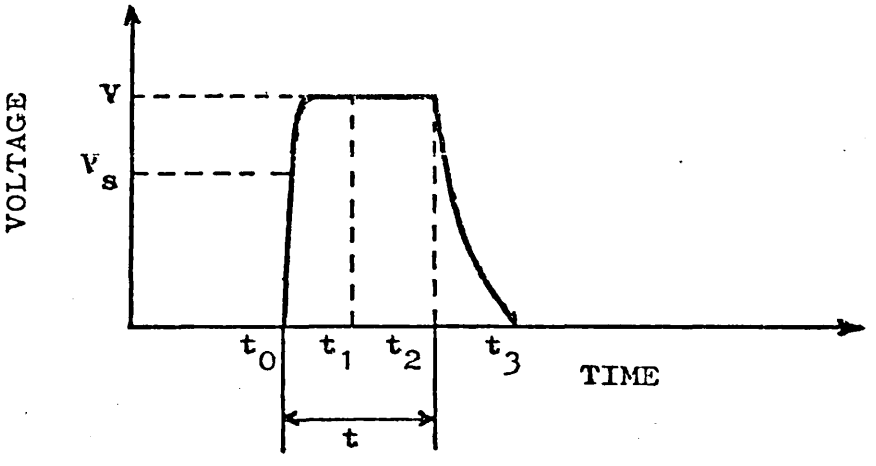

Fig. 3.4: Step-function voltage breakdown.

the instant the first electron appears. There is considerable uncertainty about the beginning of the process, since the definition of the start depends on the sensitivity of the device measuring the current. For this reason, it is easier to measure total time lags $t = t_s + t_f$ than individual ones.

The difference $\Delta V = V - V_s$ is known as the 'overvoltage', while the ratio $\frac{\Delta V}{V_s}$ is the fractional overvoltage. For a given pressure, gap and gas, $\frac{\Delta V}{V_s}$ clearly depends on the rate of growth of the applied voltage; the faster the voltage rises, the higher $\frac{\Delta V}{V_s}$. But, for the same impulse voltage and gas, the higher the pressure or the longer the gap, the lower $\frac{\Delta V}{V_s}$. This is explained on the grounds that V_s increases with increasing value of pd, while ΔV becomes smaller as a consequence of the lower rate of growth of the voltage for points closer to the peak of the pulse.

When the voltage pulse is very fast and the rate which initiatory electrons appear low - as in the case of cosmic ray ionisation - then the voltage may reach its peak value without breakdown occurring. This peak value will remain constant across the electrodes for certain time t (Figure 3.4) until adequate ionisation is produced to achieve breakdown. In this case, the applied voltage pulse can be assumed taking on the form of a step function with the time t equal to the total time lag of the discharge. This kind of event often happens at higher pressures - because, then, V_s is higher - and it is rather undesirable for a flashtube system because of possible energy losses in the circuit.

The rate at which initiatory electrons are provided influence the time lags and the rate of rise of the optical power output. It is obvious that the larger the number of electrons initiating a discharge, the faster breakdown is achieved by means of multiple electron avalanches. As will be seen in Section 3.4 the intensity of the light emitted from a discharge increases with increasing electron density. Therefore, if

initiatory electrons are provided at high rates, then the optical power will increase faster.

The variation of formative time lags with overvoltage has been investigated by Fisher[80] and his co-workers for several gases, both at high and low overvoltages; it was found that the formative time lags become shorter, the higher the overvoltage.

3. In the third stage, the conducting channel expands, the current may increase further - if the external source supplies high rates of electrical energy - and thermal effects are evident in the form of shock-waves; the degree of ionisation of the gas is very high, with a large proportion of atoms having sustained double or multiple ionisation. This stage lasts until the voltage becomes zero at a time t_3 (Figure 3.3). Large amounts of electrical energy can be dissipated by the conducting channel during this stage, providing that the impedance of the circuit is low.

4. When the applied electric field ceases, electrons and ions start becoming slower, so that the probability of electron-ion recombination increases with the time. Recombination and diffusion are the main processes responsible for the decay of electron and ion populations. Eventually, at a time t_4 (Figure 3.3) the current becomes zero and the discharge ceases - at least from the electrical point of view. But, as in the case of rare gas discharges for example, emission of light may continue beyond this time due to delayed de-excitation of metastable atoms.

The development of an impulse discharge, as is given in Figure 3.3, is a simplified picture of the many and complicated stages which may be witnessed in a high current discharge. For example, current oscillations are frequent events. Nevertheless, this picture enables one to reach a

better understanding of the electrical and radiative processes in the gas column.

The growth of the pre-breakdown current and the criterion for breakdown in gas discharges has been the subject of both experimental and theoretical studies for several years by a number of authors [81, 82, 83, 84, 85, 86, 87, 78] in an attempt to establish a satisfactory model of the physical processes involved.

The first theory on the mechanism of ionisation growth and breakdown was proposed by Townsend[81] and it involved primary ionisation in the gas, as a result of electron-atom collisions and secondary electron emission from the cathode due to positive ion bombardment. Later Llewellyn-Jones and Parker[85] - in their studies of breakdown at higher values of pd - included other secondary ionisation processes like electron emission from the cathode caused by impact of photons or excited atoms; their experimental data[85] justified the Townsend theory of ionisation growth and breakdown for static (DC), uniform electric fields and revealed the equation widely accepted today

$$i = i_o \frac{e^{\alpha d}}{1 - \frac{\omega}{\alpha}(e^{\alpha d} - 1)} \qquad (3.14)$$

for the spatial growth of the current, where i_o is the current of the initiatory electrons, d is the gap length, α is Townsend's primary ionisation coefficient representing the number of electrons (or ion pairs) produced by a single electron travelling a distance of 1 cm in the direction of the field, $\frac{\omega}{\alpha}$ is a generalised secondary coefficient representing the number of secondary electrons produced - as a result of one or more secondary mechanisms - per positive ion arriving at the cathode

$$\omega = \beta + \alpha\gamma + \delta + \varepsilon \qquad (3.15)$$

β is the ionisation coefficient for neutral atom-positive ion collisions, and, since this ionisation process is not efficient (see Section 3.2), this term can be neglected; γ is the secondary ionisation coefficient representing the number of electrons emitted from the cathode due to positive ion bombardment; δ and ε are the photoemission and emission coefficients due to incidence of photons and excited atoms on the cathode respectively.

The efficiencies of primary and individual secondary mechanisms depend on the value of E/p. The variation of the reduced parameter α/p with E/p, for rare gases, is shown in the experimental curves obtained by Kruithof[57], Druyvensteyn and Penning[58]. As expected, α/p increases with increasing E/p. It is rather difficult to measure individual secondary ionisation coefficients, because one cannot distinguish easily the mechanism by which electrons escape from the cathode in a gas discharge. Nevertheless, it is expected that the γ mechanism is more effective at high values of E/p, because, for these values, positive ions acquire higher kinetic energy by the time they hit the cathode. On the other hand, the δ and ε mechanisms are expected to be more effective at low values of E/p, because production of photons and excited atoms is high for these conditions. In the above mentioned references (57) and (58), there are curves illustrating the variation of, what the authors called, γ-coefficient with E/p for rare gases. At that time, it was believed that the only significant secondary process at the cathode was the emission of electrons due to positive ion bombardment. It is known now, that those measurements comprise the effects of more than one secondary mechanism and thus an explanation is obtained for the high values of γ at low values of E/p in those curves.

The criterion for breakdown in a uniform static field is obtained from equation (3.14) by equating the denominator to zero:

$$\frac{\omega}{\alpha} \left(e^{\alpha d} - 1\right) = 1 \qquad (3.16)$$

While efforts were made to modify the Townsend theory in order to explain all forms of breakdown in the late 30's, another theory was proposed, first in a qualitative fashion by Loeb[82] and then in an analytical way by Meek[83] and Raether[84] separately. Measurements[88, 89] of the formative time lags of sparks in atmospheric air led the above mentioned authors to the conclusion that none of the secondary mechanisms, described above, make an effective contribution towards breakdown. Time lags of the order of 10^{-7} secswere obtained; it was then argued that, since positive ions could not arrive at the cathode within this time interval, secondary mechanisms can be neglected in pre-breakdown considerations.

As an alternative, the 'streamer' theory of breakdown was proposed, which involved primary ionisation by electrons, photoionisation of the gas and space-charge field effects. The space-charge field is produced by the relatively slow positive ions whose concentration becomes higher in the vicinity of the anode,because ionisations due to primary electron avalanches are more frequent in that area. Apart from the enhancement of the external longitudinal field, this space-charge may produce a strong radial electric field. If the strength of this radial field matches the strength of the external field, then it would give rise to radial electron avalanches starting from photoelectrons produced in the gas around the main avalanche. Then, the discharge looks like a propagating streamer. In this way the time factors would be reduced to transit times of electrons (10^{-7}secsor less) since the time required for photons to travel in the gap is very short. The quantitative analysis of the theory can be found in the original papers by Meek[83] and Raether[84].

The streamer theory is based on some empirical relations and on arbitrary choice of constants, which make its application to gases, other than air, difficult. The streamer theory has been criticised by Hopwood[90]

on the grounds that the ion densities at the head of the main avalanche are calculated on the basis that the primary coefficient α corresponds to the external field E which is assumed constant throughout the avalanche transit. This assumption conflicts with the condition set previously, that there is distortion of the longitudinal field due to the high concentration of positive ions.

The agreement between experimental and theoretical data obtained by Llewellyn-Jones and Parker[85] proved, finally, that secondary processes at the cathode cannot be dismissed. Later, Townsend's theory was modified[91] with the inclusion of photoionisation in the gas, in addition to primary and secondary ionisation. The Townsend theory of ionisation growth is widely accepted today for nearly all conditions. One exception, though is the case of high overvoltages which will be discussed below.

When photoionisation in the gas was proposed - as a process contributing towards the ionisation growth, no explanation was given about the origin of photons capable of ionising. The difficulty arises in the case of pure gas discharges, because in gas mixtures, photoionisation is feasible when the excitation potentials of one gas are higher than the ionisation potential of the other gas. Early speculations[90] that the photoionising radiation comes from the head of the advancing electron avalanche, as a result of radiative electron-ion recombination, were unfounded. Later knowledge of atomic-collision phenomena[71] indicated the importance of excited species in ionising processes in a gas discharge by means of the two step ionisation (see Section 3.2). Therefore, in a pure rare gas discharge, the presence of a substantial population of metastable atoms, whose lifetimes exceed 10^{-3} secs, signifies that photoionisation is strong in these discharges.

The influence of the positive space-charge on the ionisation growth has been studied by von Engel,[92] who concludes that at moderate and lower

values of E/p the external electric field is enhanced and hence space-charges facilitate breakdown; the opposite happens at higher values of E/p.

Equation (3.14), describing the spatial growth in a static field (α and $\frac{\omega}{\alpha}$ constant), is not valid when an impulse electric field is applied. In such a case both ionisation coefficients α and $\frac{\omega}{\alpha}$ vary with the time, and estimation of pre-breakdown currents becomes difficult. The temporal growth of ionisation was studied quantitatively by Davidson[86] and Köhrmann[87] on the basis of Townsend's primary and secondary mechanisms. In addition, the second author took into consideration space-charge effects. The expansion of the conducting channel in the post-breakdown regime is a phenomenon, probably determined by hydrodynamical effects; theories of these later stages were developed by Drabkina[93] and Braginskii[94].

Haydon[78] considers that the significant parameter in an impulse discharge is the total number of electrons (or ion pairs) produced in the gas volume as a result of primary electron avalanches starting from a number n_o of initiatory electrons. When these initiatory electrons have traversed a distance x the total number of electrons is

$$n = n_o e^{\alpha x} \qquad (3.17)$$

This number depends on the gas type and pressure and, since α is a function of the applied field, it increases with increasing overvoltage. It is believed[78, 95] that the critical number of electrons required in the gap to ensure breakdown is of the order of 10^9. In static and slowly varying electric fields (low overvoltages), this critical amplification cannot be achieved by primary avalanches only (as given by equation 3.17) before secondary ionisation processes at the cathode come into effect; hence breakdown is achieved according to the Townsend mechanism.

Critical electron amplification can be achieved before secondary processes become effective by:

a) increasing the initial number of electrons or

b) speeding up the primary ionisation process by applying a high overvoltage; this process explains the short formative time lags and the mid-gap luminocity displayed by highly overvolted impulse discharges. The subsequent development of luminocity - in both anode and cathode directions - in the form of filaments or streamers, suggests that the transition from avalanche to streamer is being controlled by electrons and positive ions produced in primary avalanches. Following the breakdown of the gap, additional streamers appear, emanating from the cathode as a result of secondary effects. The only other process - apart from primary ionisation - which may contribute towards the growth of the pre-breakdown current, in conditions of high overvoltage, is photoionisation of atoms near the avalanche head, because photons move very fast and independently of electric fields.

The expansion of the conducting channel until the discharge fills the available space has been the subject of various propositions. The theory put forward by Haydon[78] and Braginskii[94] is that of hydrodynamical expansion. Once the highly conducting channel is formed, conditions exist in it with electron (or ion) densities $\sim 10^{18} cm^{-3}$ for high gas pressures (200 - 760 Torr) which indicates that the gas in the channel is almost fully ionised. Then, excess energy given to the electrons by the external field will be distributed equally among ionised particles in the channel within a few nanoseconds as a result of the very high elastic collision cross-sections for electron-ion interactions. This process increases the kinetic energy of the ionised particles and the channel becomes 'hot'. As a result of the rapid increase of temperature, the pressure in the channel increases rapidly too, with regard to the

pressure of the gas outside the channel. This pressure difference can become very high, so that the ionised particles of the channel move radially towards the directions of lower pressures. The shock-waves produced by the high pressure front is the cause of destruction of flash-tubes.

Other propositions have been put forward by Furumoto and Ceccon[43] who suggested that photoionisation is the main cause for the discharge expansion. They were led to this conclusion by their studies of discharges in coaxial flashtubes filled with Xenon or Krypton. In view of the fact that photoionisation is a very fast process, there should not be any objections concerning the contribution of this process, providing that photoionisation is effective in the gas involved. The above investigators[43] also suggested that the azimuthal magnetic fields produced in the discharge column may contribute to the expansion of the discharge.

3.4 RADIATIVE PROCESSES IN RARE GAS DISCHARGES

It has been indicated in the previous sections that the passage of electricity through a gas results in the enhancement of the 'gas temperature', following the acceleration of electrons and ions in the direction of the external field and the elastic collisions between electrons, neutral and ionised atoms. When the current densities involved are very large (of the order of 10^4 Amps/cm^2) then the degree of ionisation in the gas becomes very high, to the point of complete ionisation. As is known, the state of a gas column which consists of free electrons and ions is referred to as a 'plasma'.

In a stationary gas discharge, it is assumed that thermal equilibrium exists between all types of particles throughout the discharge column (although there is a question mark for those parts of the column near the walls where the plasma might be 'colder' due to heat conduction).

This means that the kinetic temperatures of electrons, ions and atoms are alike, as must be the temperature characterising the bound-state population densities (Boltzmann distribution) and the temperature characterising the free-state population densities (Saha[96] equation). A uniform plasma like this will emit a continuum of thermal radiation in a similar fashion as a blackbody radiator at the plasma temperature. It has been found[97, 98] that the surface brightness of such a plasma is given by the following equation:

$$B(\lambda,T) = R(\lambda,T)(1 - e^{-a_\lambda \ell}) \qquad (3.18)$$

where $R(\lambda,T)$ is the blackbody radiation function (in $W.cm^{-2}.sr^{-1}\,\text{Å}^{-1}$), while the term $(1 - e^{-a_\lambda \ell})$ describes the emissivity of the plasma, T denotes the electron (or plasma) temperature, a_λ is the absorption coefficient in cm^{-1} and depends on the wavelength, temperature, gas type and pressure. Finally ℓ is the plasma thickness in cm.

Equation (3.18) indicates that the thicker the plasma and the larger the absorption coefficient, the closer the thermal radiation from the plasma comes to that of the ideal blackbody radiator.It has been shown[98] that a_λ increases with increasing pressure and temperature and with decreasing ionisation potential of the gas used. The latter signifies that Xenon should be preferred amongst other rare gases.

It is evident from the foregoing that, if a flashtube was considered emitting like a blackbody, there would not be any difficulty in evaluating and optimising the radiation continuum. In reality, though, this is not the case. There are two main reasons supporting the thesis that flashtubes do not behave like blackbody radiators.

A) As Garbuny[97] remarked, not all radiation continua from a plasma are of thermal origin. In the case of atomic gases, such as rare gases, continuous spectra can be caused by:

a) Radiative recombination processes, which involve free-bound transition of electrons in the field of ions.

$$A^+ + e^- \rightarrow A + h\nu \qquad (3.19)$$

The energy of the resulting photon is equal to the sum of the energy of the bound state plus the kinetic energy of the electron before capture: $h\nu = E_n + \frac{mU^2}{2}$. The last term is not quantised, so a continuous spectrum is obtained.

b) Retardation of electrons in the presence of atoms or ions. This process counts as free-free electron transition in the field of the atom or ion.

$$A + e^-(U_1) \rightarrow A + e^-(U_2) + h\nu \qquad (3.20)$$

or

$$A^+ + e^-(U_1) \rightarrow A^+ + e^-(U_2) + h\nu \qquad (3.20a)$$

where $h\nu$ in both cases is equal to $\frac{1}{2} mU_1^2 - \frac{1}{2} mU_2^2$ $(U_1 > U_2)$.

This kind of continuous radiation is known as 'bremsstrahlung' radiation. In high current density discharges, the free-free process in the field of the ion is predominant compared with that in the field of the atom.

c) Radiative decay of excited, molecular unstable formations[99,100]. This process involves transitions from bound to dissociative molecular states. The excited rare gas molecules (usually referred to as 'excimers') are produced in three body impacts[103]

$$A^* + A + A \rightarrow A_2^* + A \qquad (3.21)$$

where A* represents the excited atom.

Subsequently, the excimers decay to the dissociative ground states

with the emission of radiation.

$$A^*_2 \rightarrow A + A + h\nu \qquad (3.22)$$

B) Because of the transient nature of flashtube discharges, the entire plasma in the flashtube enclosure is not in thermal equilibrium and therefore it does not emit like a blackbody. In the early stages of the discharge the kinetic temperature of electrons is much higher than the temperatures of atoms or ions. During these stages, neither the Boltzmann distribution of bound states, nor the Saha equation giving the population of free states are valid. Eventually, thermal equilibrium is approached through elastic collisions. It can be argued that, until the temperature of atoms or ions in the plasma becomes substantial, the thermal term does not contribute significantly (at least in the optical frequencies which are of most interest in this study) in the overall continuous radiation. Hence, radiation in these stages is the result of two (or three) body interactions, since conservation of linear momentum prevents a free electron from emitting radiation.

It has become apparent in recent years that modelling of radiation continua in rare gases is not possible, at least for the time being; the origin of such continua in the optical region (2000 - 7000 Å) is still controversial.

At this point, it is appropriate to distinguish two classes of gas discharge:

a) at low current densities (of the order of 1 Amp/cm^2 or less) and

b) at high current densities (usually higher than about 10^2 Amps/cm^2).

In the first class the thermal continuum is considered as negligible. According to Prince and Robertson[99], Kenty[101] and Wieme[100] the origin of the continuum is due to transitions from bound to dissociative

molecular states, (process 3.22) while Vasileva et al[102] and Rutscher and Pfau[104] advance the idea of an electron-neutral atom bremsstrahlung process (process 3.20).

In the second class, it is believed[97] that all radiative processes contribute towards the total radiation continuum. The contribution of the thermal term is larger, the higher the current density. But there is certain reservation concerning the effectiveness of the molecular process in view of the fact that production of excimers, as was described above, is not a likely event when the gas is almost fully ionised.

Apart from the continuous radiation, a gas discharge plasma emits a line spectrum superimposed on the continuum. This spectrum is due to bound-bound electron transitions in the field of the neutral or ionised atom and it is characteristic of the gas type. It must be pointed out, that the lines emitted from a plasma have sustained a broadening[105] due to the thermal Doppler effect and to Stark effect resulting from the electric microfields surrounding the emitter (these microfields are produced by space-charge).

The parameters which determine, to a great extent, the radiative properties of a flashtube plasma are the electron (and ion) density and the electron temperature.

The variation of these parameters with time in a flashtube discharge can be anticipated if one examines the various stages of the discharge (see Section 3.3). When the voltage wave-form arrives at the electrodes, it is expected that the electron density would rise from zero to a very high value (once breakdown is achieved). Then, as the electrons begin losing kinetic energy, the probability of electron-ion recombination would increase and therefore their population would fall slightly. Finally, when the external field becomes zero, the electron population is expected

to sustain a rapid decrease. As for the electron temperature, it is expected to rise rapidly with time and then fall, in the same manner, to a value which indicates that thermal equilibrium is being approached. Then the fall would be slow, corresponding to the fall of temperature of a nearly uniform plasma. Experimental data[106] for the case of high pressure (2700 Torr) hydrogen sparks showed that the variation of these parameters with time is similar to that predicted above for flashtube discharges.

The importance of these two parameters in flashtube discharges and their dependence on macroscopic parameters, such as electric field, pressure etc. is discussed below:

A) Recombination and Bremsstrahlung radiation continua.

The intensities of these continua increase with increasing frequency of such impacts; the frequency of impacts, in its turn, is higher, the higher the electron and ion densities. Similarly, the higher the electron temperature, the higher the energy of the resulting photon, which means that the spectrum becomes more efficient in the direction of short wavelengths.

B) Thermal radiation continuum

When the concentration of electrons is large, thermal equilibrium is approached faster because elastic collisions between electrons, atoms and ions become more frequent. The ultimate plasma temperature depends on the product of the electron density and the electron temperature rather than the latter parameter alone. So, the intensity and the 'colour' of the thermal continuum is expected to be a function of the current density, something which has been observed[107]. As the current density is increased, the plasma temperature rises and the flashtube becomes more efficient in the short wavelength region. If one has to choose between high electron density and high electron temperature, it is better to opt

for the former, since at high electron temperatures the collision cross-section becomes extremely small (see Section 3.2) to allow fast establishment of thermal equilibrium. Brown[105] believes that the electron temperature should be less than about 10 eV. In view of the fact that the electron density is proportional to the gas concentration (pressure) and the electron temperature is proportional to the reduced parameter E/p (see Section 3.1), it is advantageous to use high pressures for a range of low or moderate values of E/p. The same conclusion was obtained in Section 3.1.

C) Line Spectrum.

The effects of the electron density and temperature on the line spectrum are similar to the effects on the recombination and bremsstrahlung continua. The frequency of excitation impacts in atoms and ions depends on the number of electrons available. Similarly, more lines will appear in the short wavelength region when the electron temperature is increased.

3.5 FLASHTUBE CIRCUIT ANALYSIS

So far, in this Chapter, analysis of flashtube systems has been made by considering the flashtube in isolation from the external circuit. In doing so, only processes involving the gas and the electrodes were studied. It is apparent, though, that parameters of the external circuit, such as capacitance, inductance etc., influence the optical power output.

In order to investigate the effects of the external circuit, the flashtube is considered as an element in the discharge circuit (Figure 3.5), connected in series with a capacitor C at an initial voltage V_o, and an inductor L. Note that L represents the sum of the external inductance and the self-inductance of the flashtube. It is assumed at

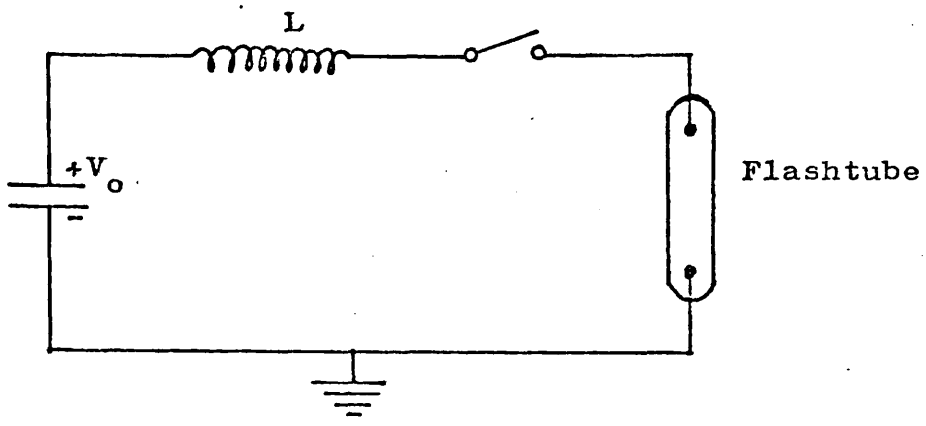

Fig. 3.5 : Single stage flashtube discharge circuit.

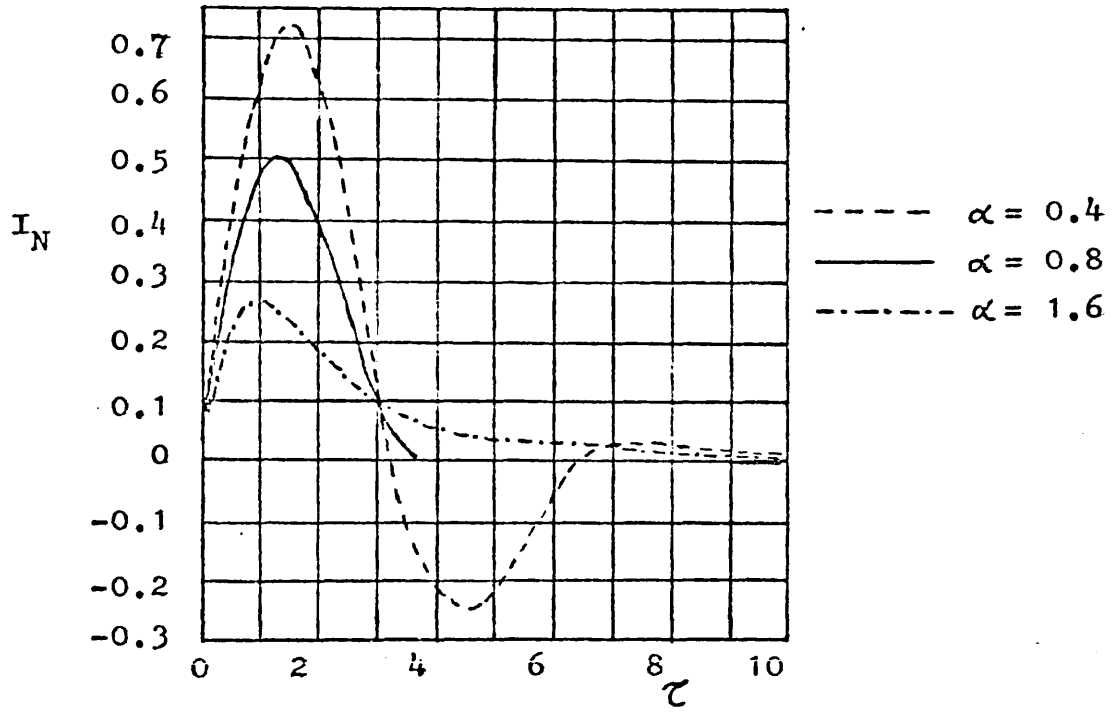

Fig. 3.6 : Solution for normalised current of a single stage flashtube discharge circuit(110).

the moment that there are no external circuit losses due to ohmic resistance.

The analysis of a flashtube circuit would, of course, be easy if the flashtube was behaving like a linear resistor. This, however, is not the case. It has been found[108,109] that the voltage-current characteristics of a flashtube, for the high current region, can be represented by

$$V = \pm K_o |i|^{\frac{1}{2}} \tag{3.23}$$

the sign of V is chosen to be the same as the sign of i. K_o is a constant that depends on flashtube geometry, gas type and pressure. It has been shown[110] that

$$K_o = K \frac{\ell}{d} \tag{3.24}$$

where ℓ and d are the length and the diameter of the discharge column respectively. Then, K is a constant depending on the gas type and pressure. It must be pointed out that equation (3.23) refers to the post-breakdown regime, when the current takes on substantial values.

The non-linear differential equation for the circuit of Figure 3.5 is:

$$L \frac{di}{dt} \pm K_o |i|^{\frac{1}{2}} + \frac{1}{C} \int_o^t i\,dt = V_o \tag{3.25}$$

The solutions of this equation have been obtained by Markiewicz and Emmett[110] with the help of computers, since there is no analytical solution. They introduced the following normalisations in the circuit parameters:

$$Z_o = \left[L/C\right]^{\frac{1}{2}} \quad (3.26a), \qquad i = I_N \frac{V_o}{Z_o} \quad (3.26b)$$

$$\tau = \frac{t}{T} \quad (3.26c), \qquad T = \left[LC\right]^{\frac{1}{2}} \quad (3.26d)$$

$$\alpha = \frac{K_o}{\left[V_o Z_o\right]^{\frac{1}{2}}} \qquad (3.26e), \qquad P = P_N \frac{V_o^2}{Z_o} \qquad (3.26f) \text{ and}$$

$$E = E_N E_o \qquad (3.26g)$$

Then, equation (3.25) becomes

$$\frac{dI_N}{d\tau} \pm \alpha |I_N|^{\frac{1}{2}} + \int_o^\tau I_N d\tau = 1 \qquad (3.27)$$

The physical significance of the normalisation constants can be seen from equations (3.26a) to (3.26g). If the flashtube impedance were zero, then Z_o would be the impedance of the whole discharge circuit and the peak current that would flow is given by the ratio $\frac{V_o}{Z_o}$. So, Z_o and T are the impedance and the natural time constant in the undamped LC circuit. Similarly, the ratio $\frac{V_o^2}{Z_o}$ represents the maximum input power in the undamped LC circuit. $E_o = \frac{1}{2} CV_o^2$ is the energy stored in the capacitor and α is the damping parameter which depends on the initial capacitor voltage.

Computer solutions of equation (3.27) for various values of α are shownin Figure 3.6.

The normalised power and energy dissipated by the flashtube can be found from the following simple calculations:

The power input is

$$P = V_i = K_o |i|^{3/2} \qquad (3.28)$$

and the normalised power is found

$$P_N = \frac{P}{V_o^2/Z_o} = \alpha |I_N|^{3/2} \qquad (3.29)$$

Also, since the energy dissipated in the flashtube is $E = \int_o^t P dt$,

the normalised energy is given by:

$$E_N = 2\alpha \int_0^{\tau} |I_N|^{3/2} \, d\tau \qquad (3.30)$$

Curves showing the variation of P_N and E_N with τ for various values of α are given in Figures 3.7 and 3.8 respectively.

It has been suggested[110] - and later shown[43] - that the optical power output correlates with the power input rather than the current or the energy. In this respect, one can choose the suitable values of parameters involved and thus obtain the desired optical output pulse.

From the solutions of normalised power (Figure 3.7), it can be seen that for a value of $\alpha \sim 0.8$, nearly the whole input power is dissipated in one pulse, the peak power is maximum, and the pulse width at half peak power is ~ 1.9; this value of α corresponds to the critically damped case, while values of $\alpha < 0.8$ or > 0.8 correspond to the underdamped or the overdamped cases respectively.

Later, further analysis of the power dissipated by a flashtube was made by Holzrichter and Schawlow[8] in the following manner:

The first cycle of any curve in Figure 3.7 can be approximated quite well by:

$$P(\tau) = P_N(\alpha) \sin \left[\frac{\tau}{3}\pi\right], \quad \tau \leq 3 \qquad (3.31)$$

This equation can be de-normalised by using equation 3.26f:

$$P(t) = P(\alpha) \frac{V_o^2}{Z_o} \sin \left[\frac{t}{3\left[LC\right]^{\frac{1}{2}}}\pi\right], \quad t \leq 3\left[LC\right]^{\frac{1}{2}} \qquad (3.32)$$

$P(\alpha)$ is defined such that:

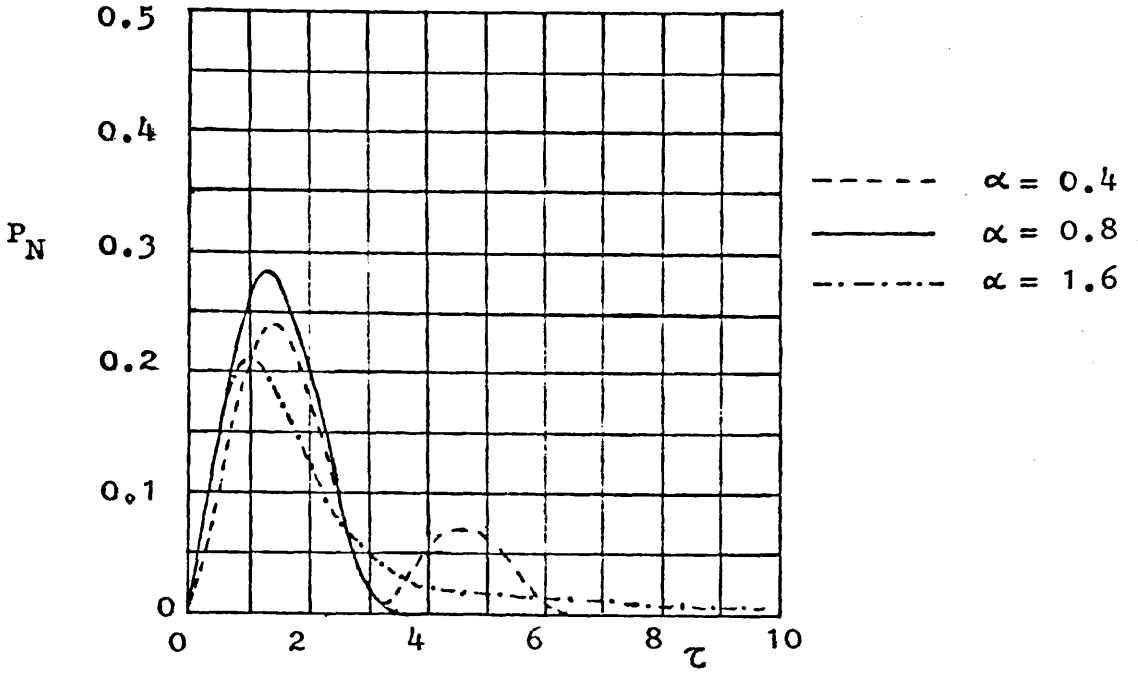

Fig. 3.7 : Solution for normalised power of a single stage flashtube discharge circuit(110).

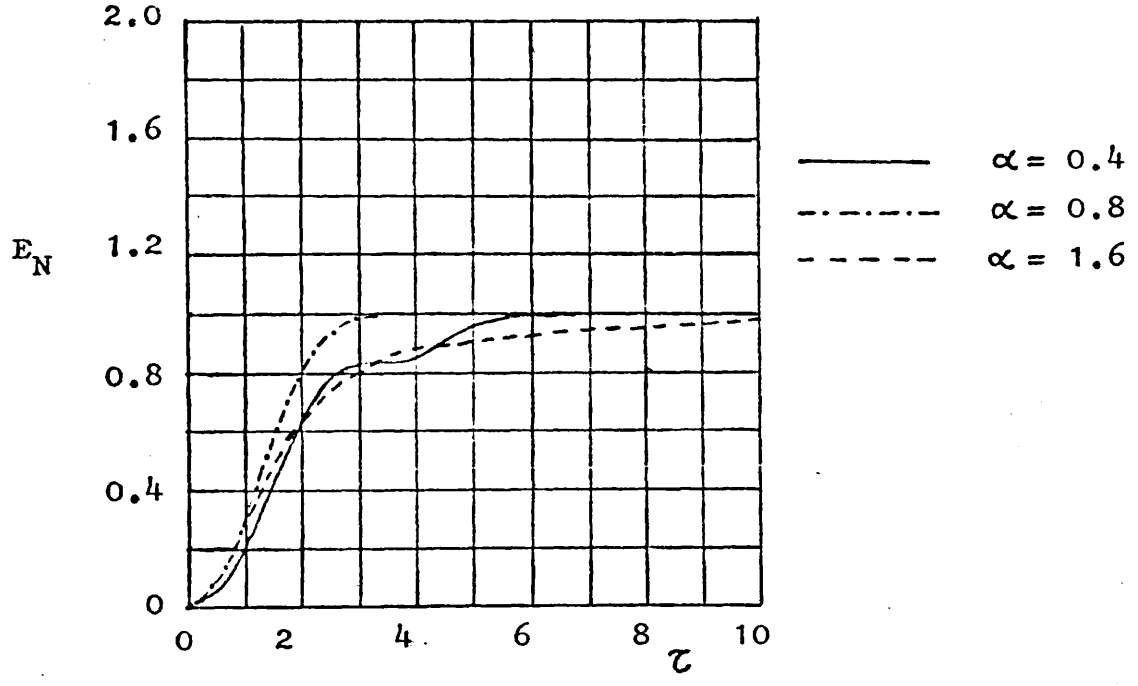

Fig. 3.8 : Solution for normalised energy of a single stage flashtube discharge circuit(110).

$$\int_0^{3[LC]^{\frac{1}{2}}} P(t)dt = \left[E_N(\tau,\alpha)\Big|_{\tau = 3} \right] E_o \qquad (3.33)$$

where $E_N(\tau,\alpha)$ is obtained from Figure 3.8 and is the fraction of the energy transferred to the flashtube at a given time. The average power in the first pulse is found from equation (3.22)

$$P_{av} = 0.638\ P(\alpha)\ \frac{V_o^2}{Z_o} \qquad (3.34)$$

Therefore, in order to maximise this average power (or the peak power), the initial voltage in the capacitor should be as large as possible, while the impedance of the system $Z_o = \left(\frac{L}{C}\right)^{\frac{1}{2}}$ should be as small as possible.

The rate of rise of the input power can be found by differentiating* equation 3.32

$$\frac{dP}{dt} = \frac{\pi}{3}\ P(\alpha)\ \frac{V_o^2}{L}\ \cos\left[\frac{t}{3[LC]^{\frac{1}{2}}}\pi\right] \quad , t < 1.5\ [LC]^{\frac{1}{2}} \qquad (3.35)$$

and for $t = 0^+$ equation (3.35) becomes:

$$\frac{dP}{dt}\Big|_{t = 0^+} = \frac{\pi}{3}\ P(\alpha)\ \frac{V_o^2}{L} \qquad (3.36)$$

Equations (3.35) and (3.36) indicate that in order to obtain maximum rate of rise, V_o should be large and the inductance of the system small. These requirements are often contradictory, because for a given capacitance

---

* For the sake of clarity, the analysis of the rate of power rise is given here in a modified form with regard to the analysis elaborated by Holzrichter and Schawlow[8].

C, an increase of V_o means that the input electrical energy increases; the ability of a flashtube to dissipate energy is proportional to its length, and its self-inductance is also proportional to its length. So, one cannot increase the initial voltage in the capacitor arbitrarily. The problem can be overcome by using lower capacitance, so that an increase of V_o will not be followed by an increase of the input electrical energy.

The advantages of a combination of low capacitance - high initial voltage in the capacitor can be seen from equations 3.26d and 3.34. In the first case, the lower the capacitance, the shorter the time constant of the system. In the second case, an increase of V_o by a factor of 2 and a decrease of C by a factor of 4 will result in the same input energy, but, the average power in the first cycle will increase by a factor of 2. High initial voltages in the capacitor are not always feasible because of corona losses in the circuit and because insulation becomes difficult.

The importance of critical damping, in the case that intense optical output is required, can be seen in equations (3.34), (3.35) and (3.36), where both the average power and the rate of power rise depend on $P(\alpha)$.

Objections concerning the temporal range of validity of equation (3.23) were expressed by Markiewicz and Emmett[110] who reckoned that hysteresis in the V-I characteristic is a problem for short pulses, during which a significant part of the pulse time is spent in the transition of the discharge from a small filament or streamer to a fully expanded channel which fills the discharge column. Hysteresis times of the order of 10^{-5} to 10^{-4} secswere mentioned by these authors; such times are quite long. But one should take into account the fact that these long times were the result of the low initial voltages which were employed in the early and mid 60's. It is known today (see Section 3.3) that high overvoltages speed up

all processes, so that substantially shorter hysteresis times should be expected (see also relevant results in Section 5.1).

Another problem encountered in circuit analysis arises from the fact that the flashtube inductance is not constant during the expansion of the conducting channel. The total inductance of the circuit at a certain time t is $L = L_c + L_f(t)$, where L_c is the inductance of the external circuit (independent of time) and $L_f(t)$ the flashtube inductance which initially is large (due to the small filament size) but it becomes, gradually, lower as the channel expands. If (3.25) is rewritten to show its dependance on the flashtube inductance, it is obtained[110]

$$L_c \frac{di}{dt} + \frac{d\left[L_f(t)i\right]}{dt} \pm K_o|i|^{\frac{1}{2}} + \frac{1}{C}\int_o^t idt = V_o \qquad (3.37)$$

which is expanded to:

$$\left[L_c + L_f(t)\right]\frac{di}{dt} \pm \left[K_o + |i|^{\frac{1}{2}} \frac{dL_f(t)}{dt}\right]|i|^{\frac{1}{2}} + \frac{1}{C}\int_o^t idt = V_o \qquad (3.38)$$

During the channel expansion $\frac{dL_f(t)}{dt}$ is a negative number and therefore, at high currents, the term $|i|^{\frac{1}{2}} \frac{dL_f(t)}{dt}$ can be quite significant. It is then quite usual in high power microsecond systems to observe a negative voltage drop across the flashtube during the first part of the pulse. The importance of low flashtube inductance in short pulse systems becomes evident from the above.

The case in which the ohmic resistance of the external circuit is $\neq 0$ was studied by Holzrichter and Emmett[111]. The equation for that type of circuit is:

$$L \frac{di}{dt} \pm K_o|i|^{\frac{1}{2}} + R_c i + \frac{1}{C}\int_o^t idt = V_o \qquad (3.39)$$

By introducing a further normalisation

$$\beta = \frac{R_c}{Z_o} \tag{3.40}$$

and taking into account the normalisations of equations (3.26a) to (3.26g), one can obtain the normalised form of equation (3.39)

$$\frac{dI_N}{d\tau} + \alpha |I_N|^{\frac{1}{2}} + \beta I_N + \int_0^{\tau} I_N d\tau = 0 \tag{3.41}$$

Computer solutions of equation (3.41) for the critically damped case ($\alpha = 0.8$) have been obtained[111] showing that the pulse width and amplitude are changed only by 5% or less when $\beta \lesssim 0.6$. Hence, by reducing the resistance of the external circuit to a minimum value, the energy losses will be very small and the effects on the pulse shape negligible.

3.6 FLASHTUBE GEOMETRY AND PUMPING CONFIGURATIONS. COAXIAL FLASHTUBES

Before the discovery of the laser, the shape and size of flashtubes were largely determined by the amount of light required for the particular application, but no particular dimension was of substantial significance. Since in laser technology, good flashtube-laser medium coupling is of great importance for efficient pumping, the flashtube geometry became significant. The large radiation density required to produce population inversion means that one has to make maximum use of the available radiation, so that the source is not pushed to the limit. This implies that the exciting radiation should be concentrated onto the laser medium, preferably in a uniform fashion to ensure that all parts of it sustain equal illumination.

Since flashtube pumping is always transverse, with regard to the laser output, the axis of the flashtube should be parallel to the axis of the active material. Also, the length of the flashtube should be at least

equal to that of the active material; the latter is supplied in cylindrical columns.

The three main types of flashtubes - which have been used for pumping laser media - namely, the helical, the linear and the coaxial type owe their name to their characteristic geometrical appearance. The first laser of Maiman[1] involved a helical flashtube surrounding the ruby rod. Although this configuration provides uniform illumination, it is not efficient because large amounts of energy are wasted as a result of the frequent collisions of electrons with the walls in the long helical gas column. Helical flashtube arrangements are no longer in use, and they are mentioned only for historical reasons.

Linear flashtubes have been very effective sources for most of the optically pumped materials. They consist of a straight cylindrical quartz tube with plain or round electrodes sealed in the ends of the tube. Of the various coupling configurations employed so far, that of the elliptical cylinder - first used by Ciftan et al[112] has been very effective in focusing most of the radiation from the flashtube in the active material. In this arrangement, the flashtube is placed in one focal line of the cylinder, while the active material is placed in the other. The inside surface of the clyinder and the end plates are coated with highly reflective material. In order to concentrate a large amount of radiation in a small volume, it is desirable to make the active material thin and the source thick, because its power dissipation capability increases with its size. But, in the elliptical cylinder arrangement, the efficiency of the radiative power transfer is greater in the reverse case. There are two good reasons justifying this: First, if the source is large, rays emanating from the periphery at an angle (see Figure 3.9), will be imperfectly focused or they will not be focused at all in the case of a thin absorber. Second, some rays will be blocked

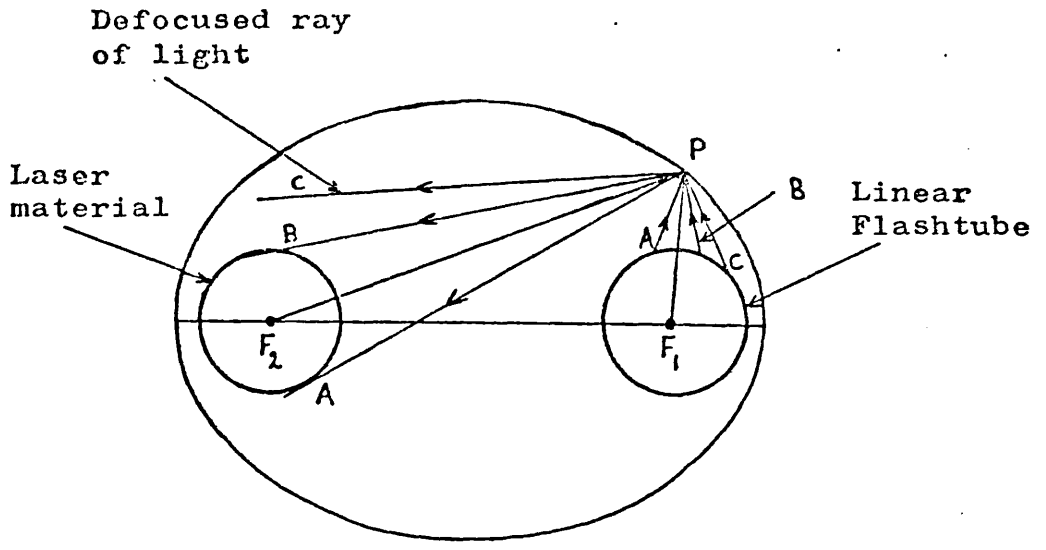

Fig. 3.9 : Cross-sectional schematic diagram of the elliptical cylinder coupling between linear flashtube and laser material.

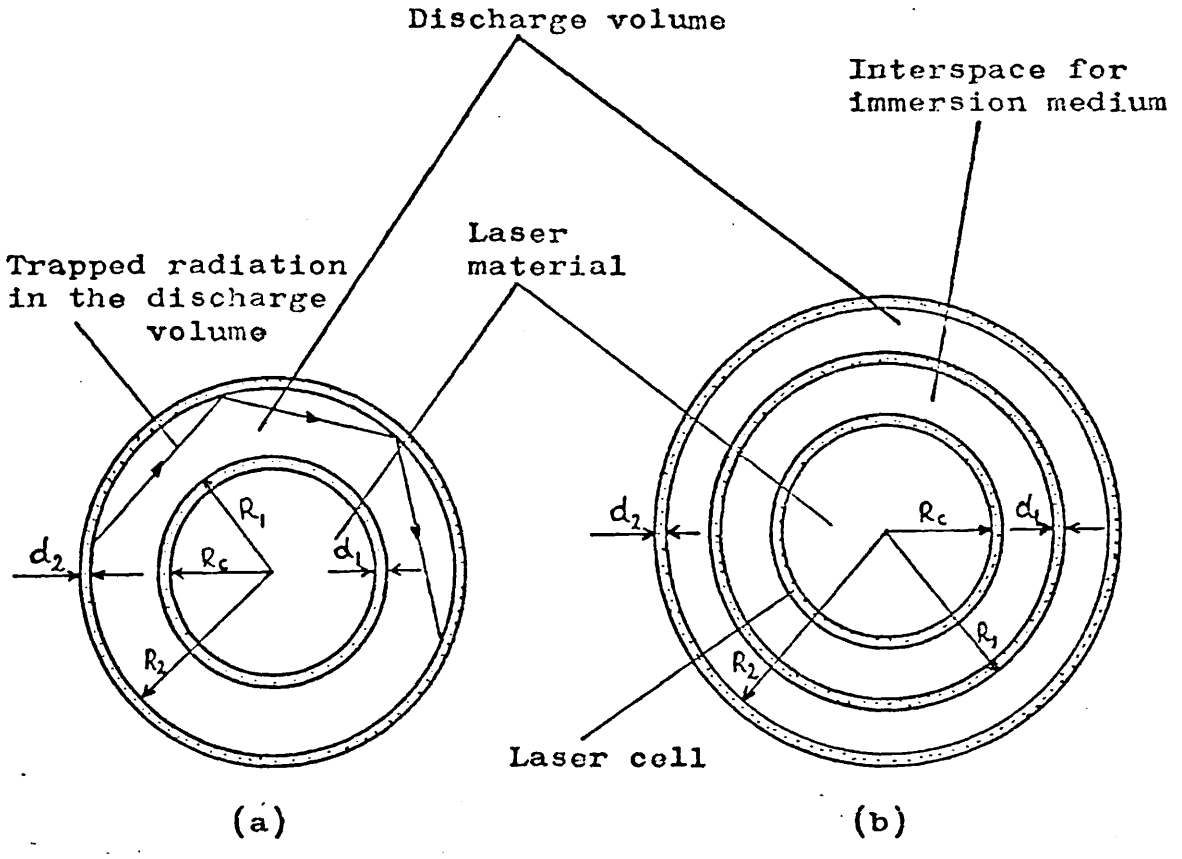

Fig. 3.10 : Coaxial flashtube couplings.

because of shadowing by the light source itself. Efficiencies for elliptical cylinder configurations were calculated by Schuldt and Aagard[1] for various eccentricities and sizes of source and absorber. The exfocal version of the elliptical cylinder - first used by Röss[114] - has also been quite an efficient arrangement.

Although the elliptical cylinder configuration concentrates the light in the laser material, the illumination of the latter is not uniform. But, by combining two or four elliptical cylinders[115, 116] inserted into one another, the laser material in the centre can be pumped simultaneously in a uniform fashion by two or four light sources.

The first coaxial flashtube was constructed by Claesson and Lindqvist[117] in 1957 who were led to the idea by the need for a fast and intense light output in order to study photolysis of various substances whose products or intermediaries have short lifetimes. But the first time a coaxial flashtube arrangement was employed to pump a laser material was in 1963 by Church and his co-workers[118] who achieved laser action from neodymium-glass by using such a flashtube. The obtained laser efficiencies[119] were well above those obtained by linear flashtubes subjected to the same electrical input energy. Wide scale exploitation, though, of the coaxial flashtube properties in the laser field did not come until 1967 when fast pulsed sources of light were needed to pump organic dyes (see Section 2.2). Laser output from these dyes was achieved by Sorokin and his group[15, 39] with the use of a small coaxial flashtube. From then on several groups[21, 43, 120, 121] have reported laser radiation in numerous dyes by employing coaxial flashtube systems.

A coaxial flashtube consists of a) two cylindrical quartz tubes of the same length but of different diameter (Figure 3.10) placed in such a way that their central axes coincide and b) two ring shaped electrodes

which seal the annular space between the tubes; discharge takes place in this space. The active medium either fills the volume of the inner tube (Figure 3.10a) or is inserted centrally inside the flashtube allowing a small gap from the nearest wall (Figure 3.10b). In the first case the medium is usually fluid, so that the inner tube acts as laser cell, while in the second case it can be either a solid rod or fluid filling a separate cell. Let us call, from now on, the first coupling biaxial and the second triaxial. Coating of the outer surface of the flashtube with reflective material enables some radiation, otherwise wasted, to be reflected towards the centre of the flashtube.

Providing that the discharge in a coaxial flashtube is annular, comparison between linear and coaxial flashtubes finds the latter superior in two aspects: uniform pumping of the laser medium and faster pulses for the same electrical input energy. The first aspect is obvious, the second can be explained from the fact that coaxial flashtubes exhibit the lowest self-inductance as a result of symmetrical reductions or cancellations in the elementary azimuthal fields which are created during current changes in individual conducting lines (filaments). It is known from equations (3.35) and (3.36) that the rate of rise of electrical power dissipated in the flashtube is inversely proportional to the inductance of the circuit; so one should expect faster pulses by using coaxial flashtubes. Experimental data[117, 15, 39, 43, 120] have proved that this is true. But, as Furumoto and Ceccon[43] remarked, if the discharge is not annular, but consists of localised filaments, then the pulse will not be very fast and non-uniform pumping of the material will result; in addition localised discharges will cause the premature shattering of the flashtube and thus its lifetime becomes shorter.

It has been found[43] that irrespective of gas type, discharges in coaxial flashtubes tend to become annular when the value of E/p is

increased. But, it has been shown in Section 3.1 that, at higher values of E/p the luminous efficiency of the discharge is lower. Then the choice depends on the particular application, whether one wishes to sacrifice radiative energy in favour of uniform pumping and fast optical pulse or vice versa. By using rare gases, especially Xenon and Krypton[43], annular discharges can be achieved in coaxial flashtubes at values of E/p which are lower than any other gas. This is attributed to the strong photoionisation which is evident in rare gas discharges; even if a localised discharge starts developing along a line, photoionisation can spread the discharge to other parts of the gas column. In fact, photoionisation is probably the dominant mechanism in the discharge expansion (see Section 3.3) in the case of coaxial flashtubes filled with rare gas. This conclusion is reinforced by the fact that the hydrodynamical expansion of the discharge stops when a transversely moving high pressure front meets the wall of the inner tube.

Further comparison between linear and coaxial flashtubes can be made by considering the circuit constant K_o in equation (3.24). Given a linear flashtube of volume $V = \pi R_0^2 \ell$ and a coaxial flashtube of the same volume and length $\left(V = \pi(R_2^2 - R_1^2)\ell\right)$ it is obvious that the sections of the two flashtubes are equal. So, one could define the equivalent diameter of the coaxial flashtube as $R_e = \sqrt{R_2^2 - R_1^2}$ and then from equation (3.24) equal values of K_o are obtained for both flashtubes. In reality though, a coaxial flashtube displays higher 'resistivity' because collisions of particles with the walls are more frequent than collisions in the equivalent linear flashtube. This is explained by the fact that the gap between the walls $R_2 - R_1$ in a coaxial flashtube is smaller than the diameter $2R_0$ of the equivalent linear flashtube.

As a result of its geometry, a fraction of the light emitted from a coaxial flashtube will not reach the active medium, but, following multiple

reflections on the outer wall of the flashtube (see Figure 3.10a) it will be trapped in the discharge column. When the configuration of Figure 3.10b is used, some of the trapped radiation may be regained by filling the interspace between flashtube and laser medium with optically thick immersion liquid (high refractive index) so that rays travelling through it are bent towards the normal. The liquid is chosen so that it does not absorb in the same band as the pumped material.

3.7 TRIGGERING OF FLASHTUBES

The triggering technique determines whether a flashtube will be subject to a DC or an impulse voltage. In the former case the triggering is direct, in the sense that the flashtube and the condenser are in parallel with regard to the charging resistor, so that the flashtube is subjected to a voltage equal to the initial voltage in the condenser (Figure 3.11a). This voltage is below the breakdown voltage of the electrode gap; then a high voltage trigger pulse is employed, by means of an ignition coil wound outside the flashtube wall or of a wire inside the discharge column. Ignition is also achieved by superimposing the trigger pulse on the operating voltage across the electrodes. As a result of the ionisation created, the gas becomes conducting and discharge of the stored energy takes place.

If an impulse voltage is required, then the triggering should be indirect, in which case a thynatron or a pressurised spark gap (Figure 3.11b) is used, the latter being preferred because it can withstand higher electrical energies. In this arrangement the flashtube and the condenser are connected in series, with regard to the charging resistor, so initially there is no voltage across the flashtube. Then, following the breakdown of the spark gap with the use of a trigger pulse the energy from the condenser discharges through the flashtube in the form of an impulse voltage

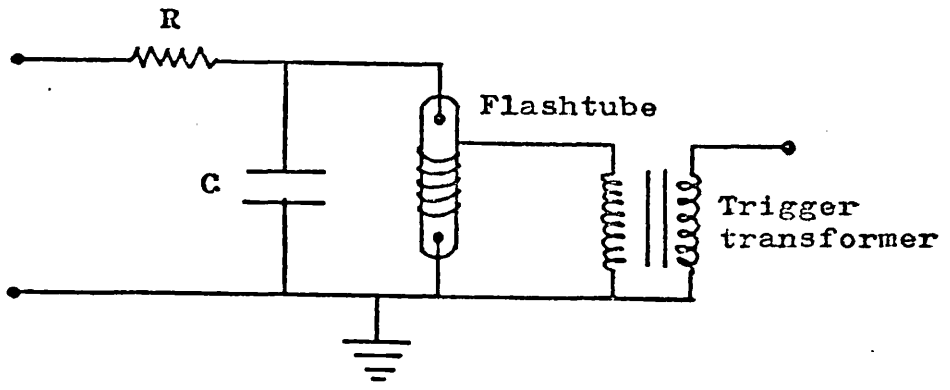

(a)

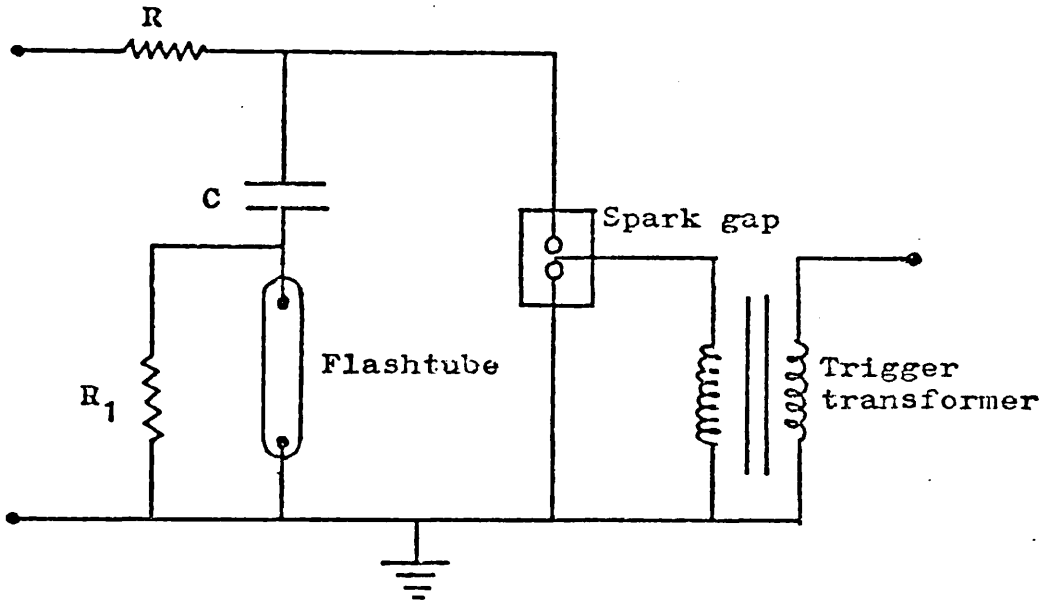

(b)

Fig. 3.11 : Flashtube triggering techniques

whose peak can be much greater than the breakdown voltage of the gap. The advantage of this technique is that it enables the use of high overvoltages which are important when fast optical pulses are needed (see Sections 3.3 and 3.5). In addition, by employing this technique, good synchronisation with other devices is achieved. All the flashtube systems used in this work were triggered through pressurised spark gaps.

CHAPTER 4

THE DESIGN AND TECHNOLOGY OF APPARATUS USED IN THE EXPERIMENTS

4.1 DESCRIPTION OF THE COAXIAL FLASHTUBES

All coaxial flashtubes used in this work were specially constructed during the course of the investigation in order to meet the physical requirements set by the nature of the investigation and to overcome the engineering restrictions which arise when high energy electrical pulses are employed. Four of these flashtubes, varying in discharge volume and method of construction, were studied systematically and their performances are presented in the following Chapters. The dimensions of these flashtubes along with constructional details are given below:

TABLE 4.1

	R_1 (mm)	R_2 (mm)	R_2-R_1 (mm)	d_1 (mm)	d_2 (mm)	ℓ (cm)	V(cc)
MARK 1	15.2	17.5	2.3	2.0	1.5	20	47.2
MARK 2	19.5	23.4	3.9	2.1	2.4	18	94.5
MARK 3	19.4	22.8	3.4	2.1	2.4	18	81.1
MARK 4	8.0	13.5	5.5	1.5	1.5	20	74.2

where R_1 is the outside radius of the inner tube, R_2 is the inside radius of the outer tube, R_2-R_1 is the gap between the tubes, d_1 is the wall thickness of the inner tube, d_2 is the wall thickness of the outer tube, ℓ is the effective length of the flashtube (the distance between the edges

of the two electrodes), and $V = \pi \left[R_2^2 - R_1^2\right] \ell$ is the discharge volume of the flashtube. The symbols representing the cross-sectional dimensions of coaxial flashtubes are illustrated in Figures 3.10a and 3.10b.

The first three flashtubes were designed for triaxial laser coupling, while the last one was designed for biaxial laser coupling (see Section 3.6 for definitions). Figures 4.1 and 4.2 illustrate schematically the triaxial and biaxial types of flashtube used in this work; in the triaxial type, a separate laser cell is housed centrally inside the flashtube and the annular interspace between flashtube and laser cell can be filled with a 'light converter' solution (see sub-section 2.2.2) or an 'immersion' liquid (see Section 3.6). In the biaxial type, the inner tube of the flashtube effectively acts as the laser cell. But in both couplings, provision was made for the circulation of the active medium.

Two different techniques were employed to seal the discharge volume of the flashtubes. The first involved the use of an adhesive, referred to as 'Torr Seal', which was applied between the quartz tubes and the electrodes; good seals were achieved in the flashtubes by applying this technique, but after some time of operation ($\sim 10^3$ flashes), the quality of the flashtube performance showed some deterioration due to the carbon dust produced from the burning of the adhesive and to electrode sputtering; these effects were the results of the high temperatures attained within the discharge volume due to the passage of high currents. Another disadvantage of this sealing technique arises from the fact that the flashtube walls cannot withstand strong shock-wave vibrations at high input electrical powers because of the rigid manner by which the quartz walls are attached to the electrodes. In fact, such premature shock-wave destruction was observed in the form of cracks on both ends of the tubes in two coaxial flashtubes used for preliminary tests; eventually, these cracks led to an early shattering of the flashtubes.

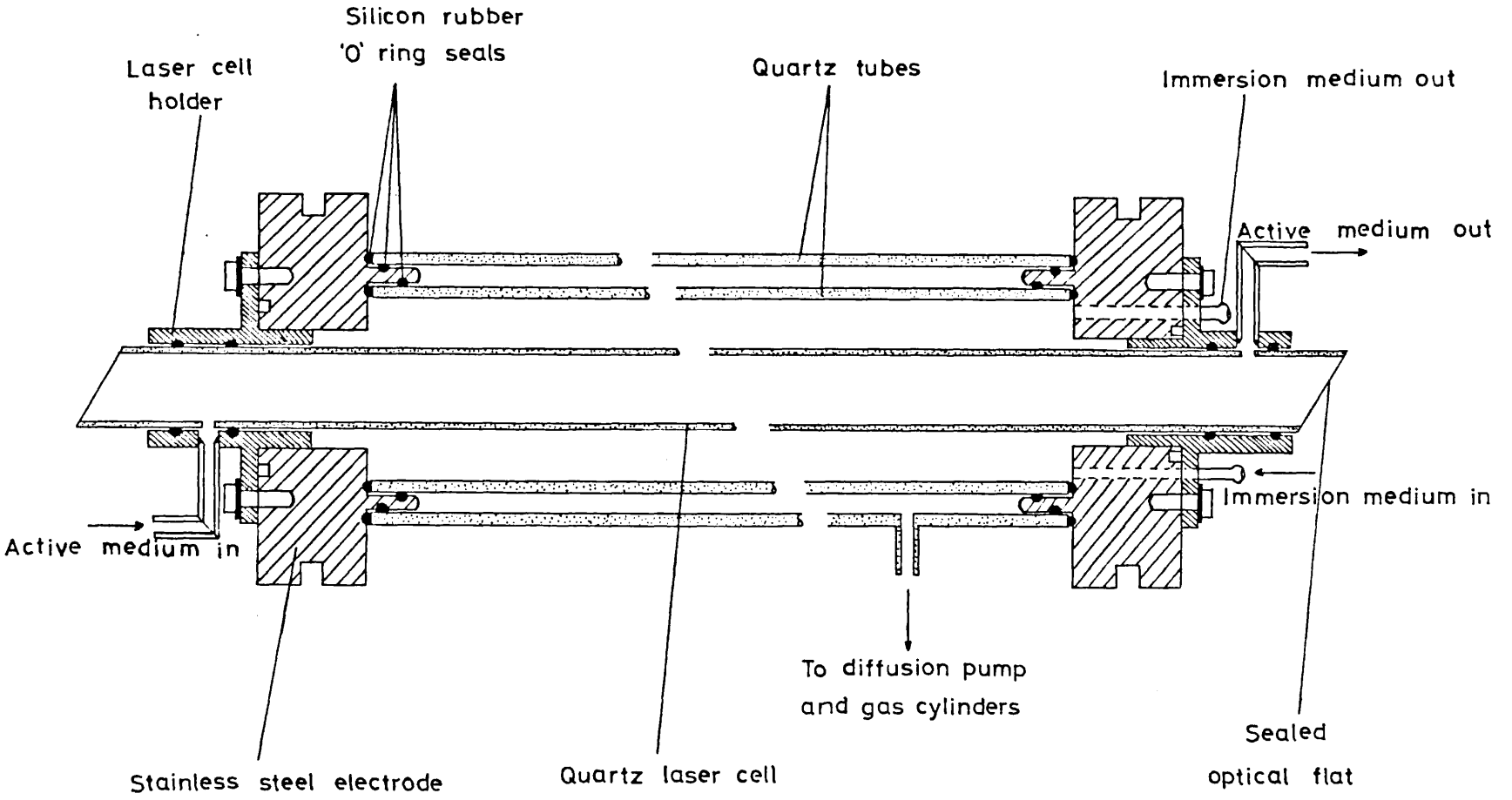

Fig. 4.1 : Schematic diagram of the triaxial type of flashtube.

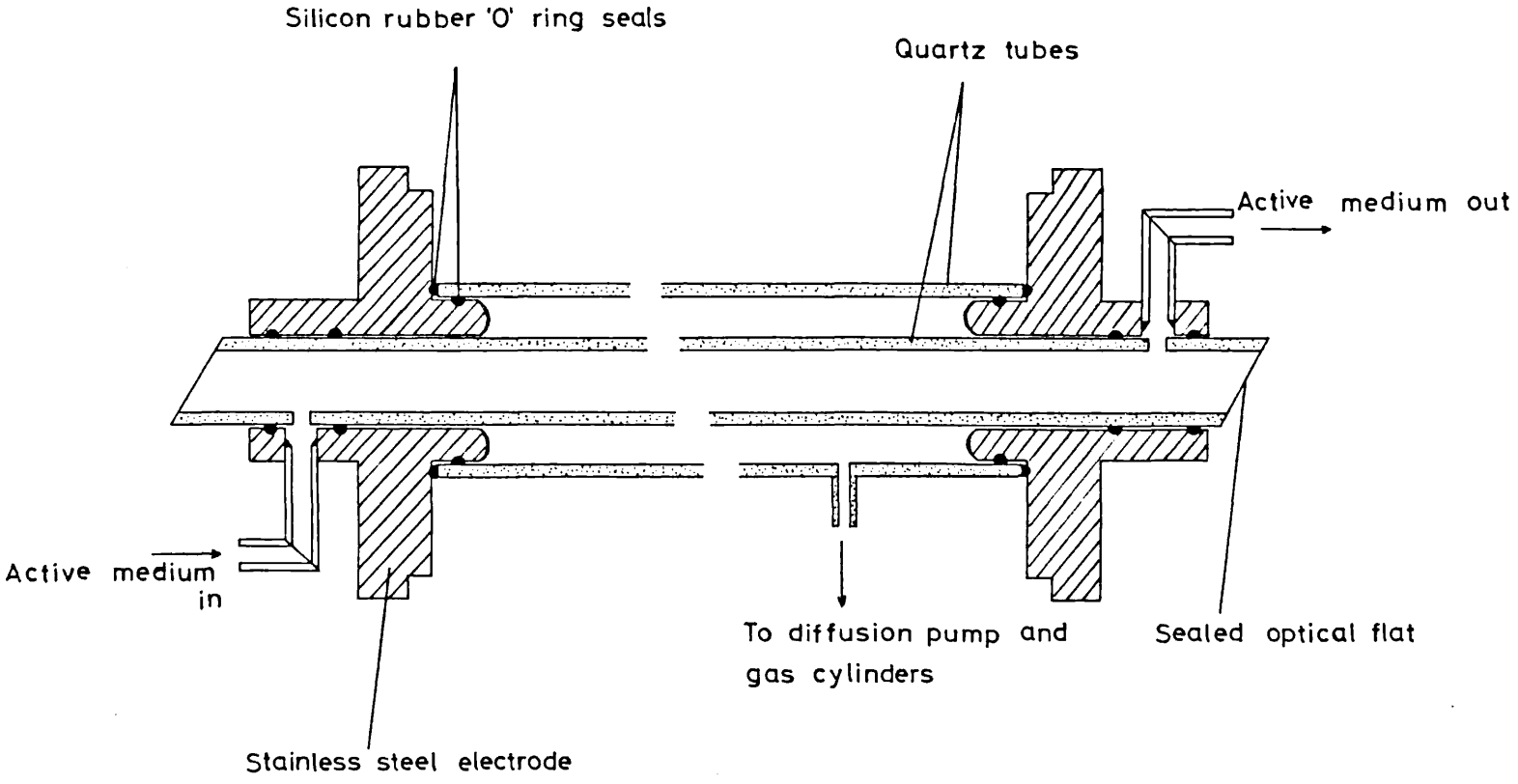

Fig. 4.2 : Schematic diagram of the biaxial type of flashtube.

The construction of MARK 1 and MARK 2 was based on the adhesive sealing technique. Figure 4.3 shows a photograph of MARK 1 after 5×10^3 flashes at an average input electrical energy of about 500 Joules, which corresponds to an average energy density in the flashtube of $\sim$ 10 Joules per cc, if the volume of the flashtube is taken into account. The maximum input electrical energy applied to this flashtube was 850 Joules. Non-uniform electrode sputtering caused a gradual deterioration of the performance of MARK 2, until a stage was reached after 10^3 flashes, in which the discharge became localised in the form of a single bright filament. The effects of the electrode sputtering on the temporal characteristics of the optical output from MARK 2 are presented in Section 5.2.

In order to overcome the limitations of the above sealing technique, a different technique was applied in the later stages of this investigation to seal the discharge volume of the last two flashtubes (MARK 3 and MARK 4) by using viton or silicone rubber 'O' rings, as shown in Figures 4.1 and 4.2. The introduction of this sealing technique made these flashtubes completely demountable, which meant that they could be taken apart and cleaned when electrode sputtering or other contaminations became severe enough to affect the flashtube operation. In addition, the elastic 'O' rings were excellent intermediaries between the quartz tube ends and the electrodes in that they cancelled a fair amount of shock-wave vibrations. As a result, higher input electrical powers could be applied to the flashtubes.

By the time the systematic measurements of this investigation were completed, MARK 3 and MARK 4 had been flashed more than 2×10^4 times each at an average input energy of 900 Joules and 800 Joules respectively, without any obvious sign of damage. By considering their discharge volumes, it is obtained that the average energy densities applied to these flashtubes were about the same - that is, 11 Joules/cc. The maximum input electrical energy applied to MARK 3 was 1500 Joules while that applied to MARK 4 was

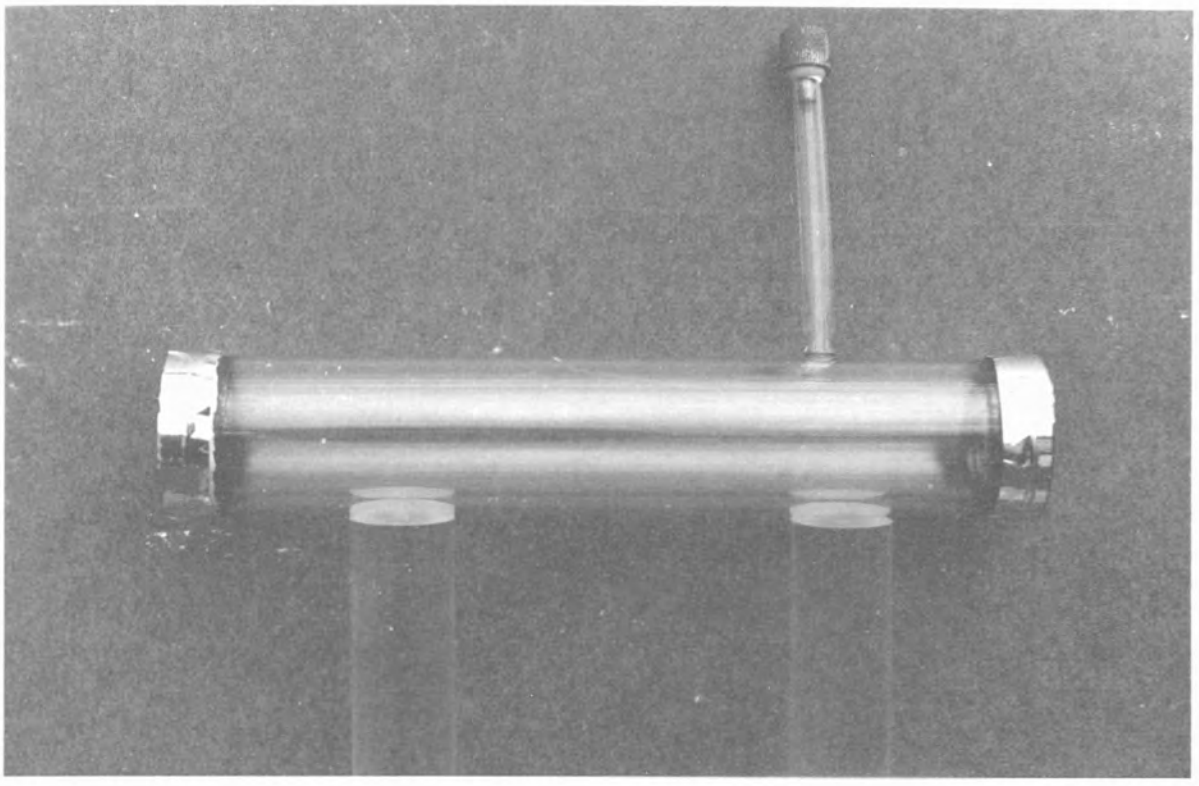

Fig. 4.3

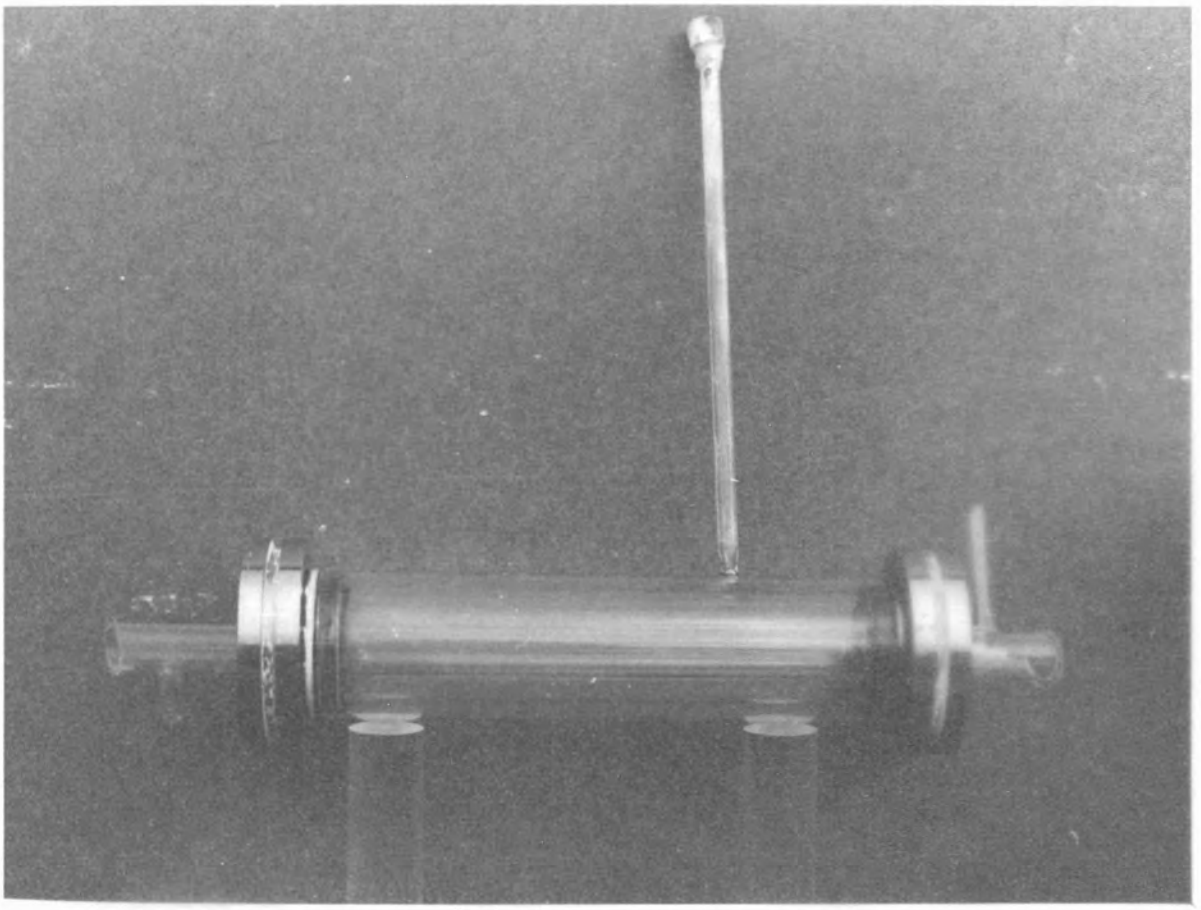

Fig. 4.4

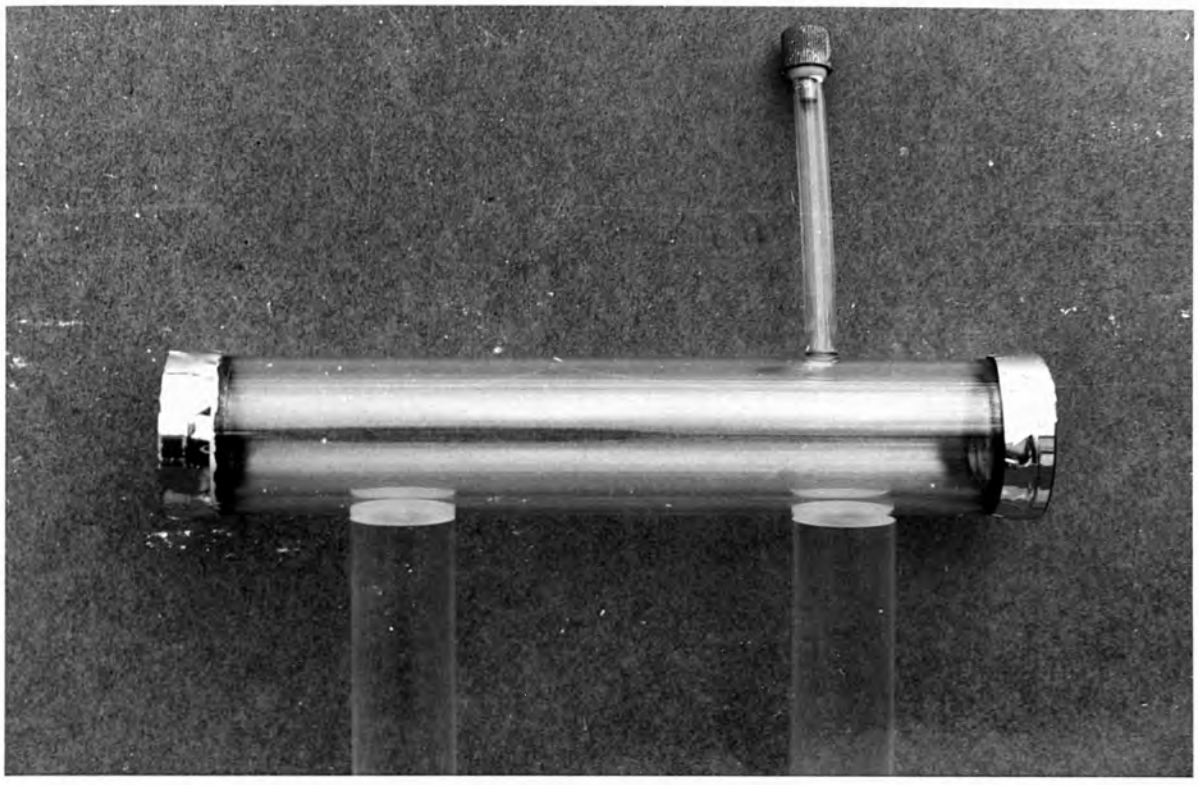

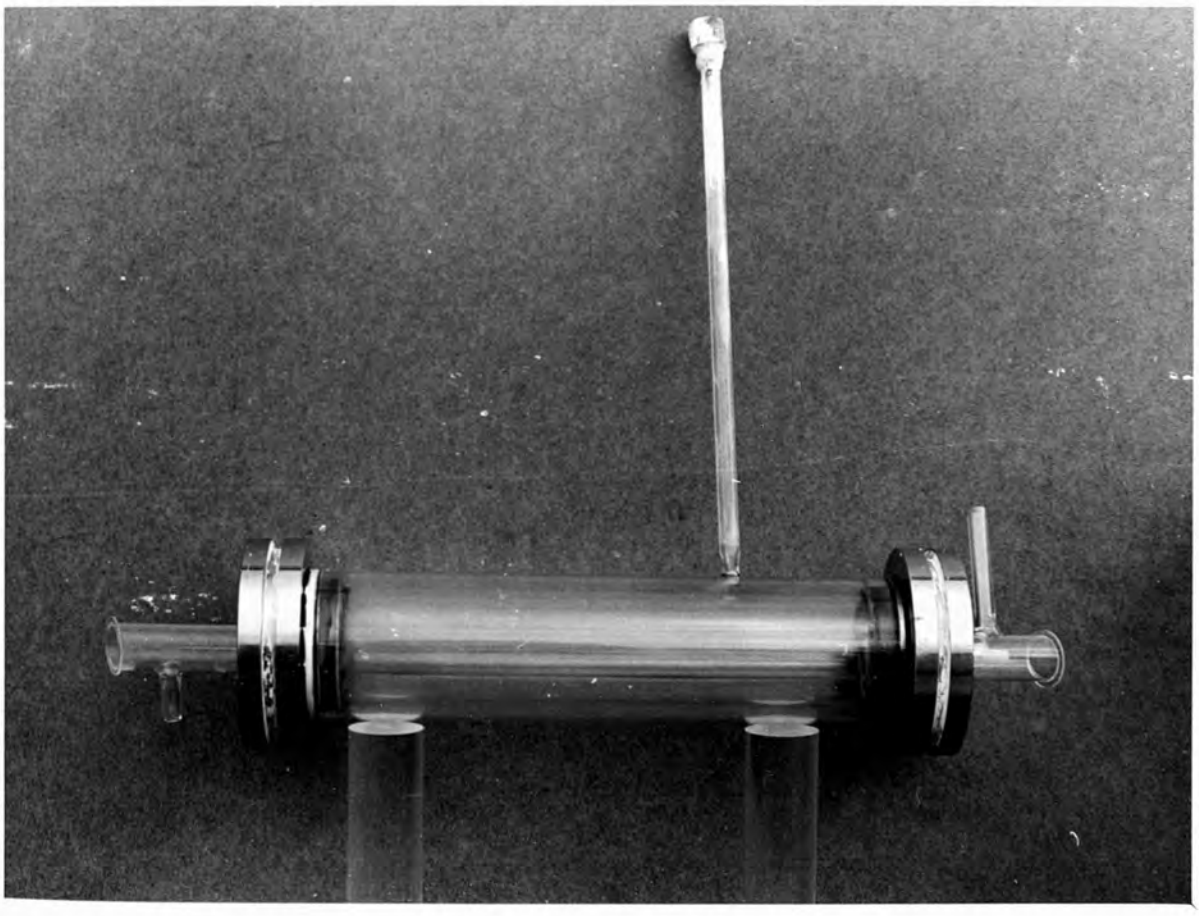

1200 Joules. Following the completion of measurements, and for the purpose of testing their durability, these flashtubes were further operated for up to 10^5 total flashes each at the above mentioned average input energies. Apart from the increased effects of the electrode sputtering, no other damage was observed. From the foregoing it is apparent that the 'O' ring sealing improves the operation and extends the life of flashtubes*. Figure 4.4 shows a photograph of MARK 3 with a laser cell attached inside it. Figures 4.5 and 4.6 show photographs of MARK 4 demounted and assembled respectively.

The electrodes of the flashtubes studied were made of stainless-steel, except those of MARK 1 which were made of brass. It was observed that electrode sputtering was stronger in the case of brass, and for this reason stainless-steel electrodes were adopted. It was also found that when the electrode edges were round rather than flat or sharp, the sputtering was limited. However, when electrodes with sharp edges were employed, breakdown in the flashtube occurred at lower voltages and the system could be operated at higher gas pressures. Given that a negative voltage pulse was applied across the flashtube, this feature is probably due to electron emission from the highly stressed cathode[79]. Such electron emission is stronger in sharp metalic surfaces due to the very high, non-uniform localised fields in the vicinity of such surfaces. MARK 1 had electrodes with sharp edges.

All the flashtubes had a narrow glass tube joint attached on the outside surface for the purpose of evacuating the discharge volume and then filling it with the appropriate gas. This joint interconnected the

---

* MARK 4 was subjected to an r.f. preionising pulse prior to the main electrical pulse for most of its operating time (see Sections 4.3, 6.3 and 6.4)

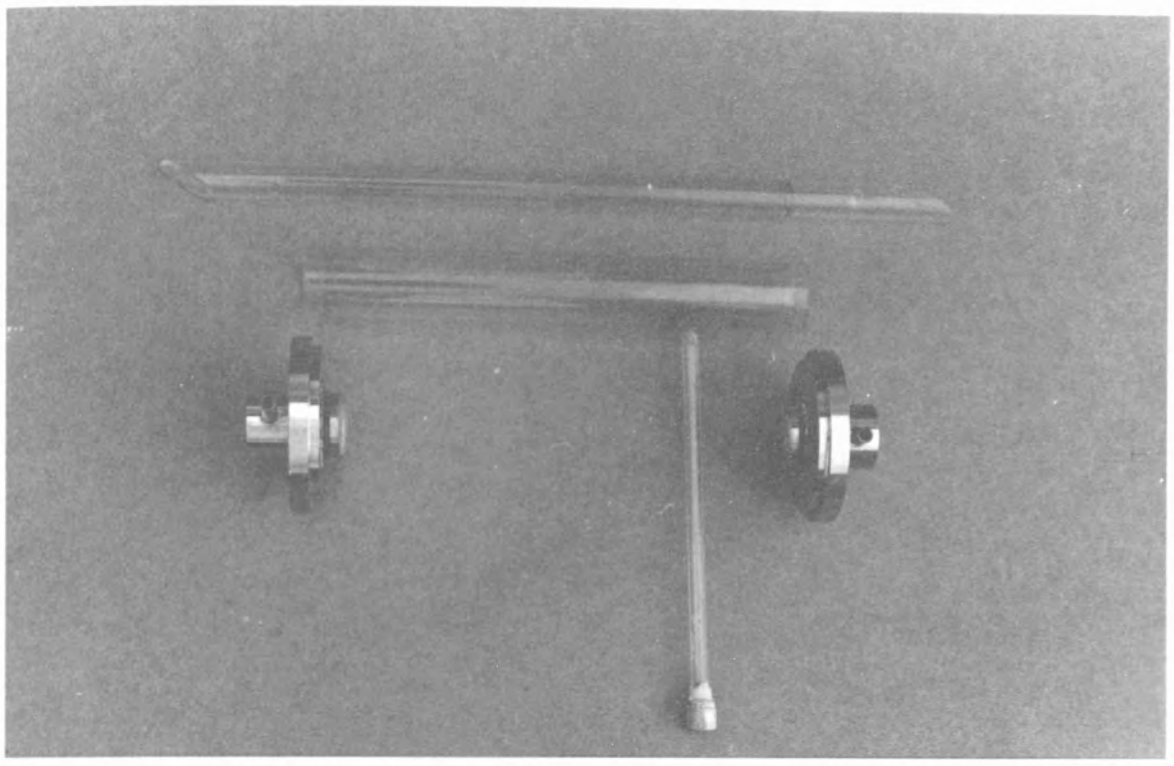

Fig. 4.5

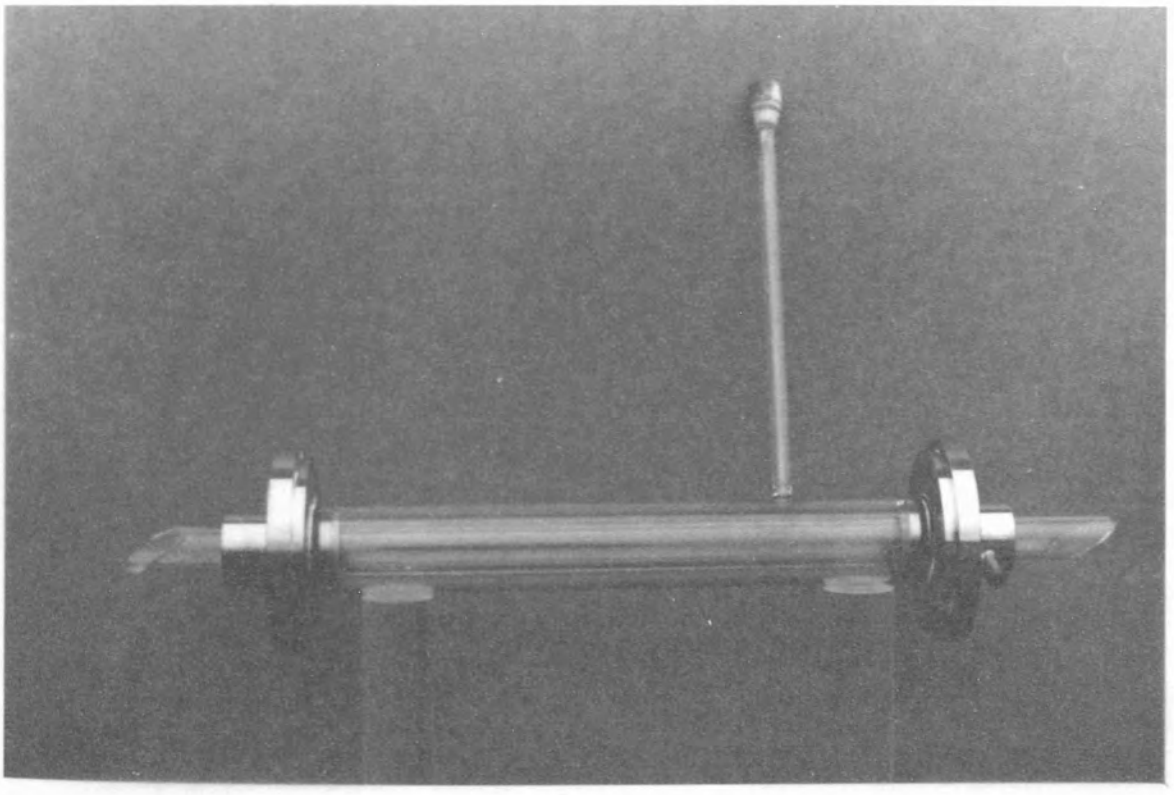

Fig. 4.6

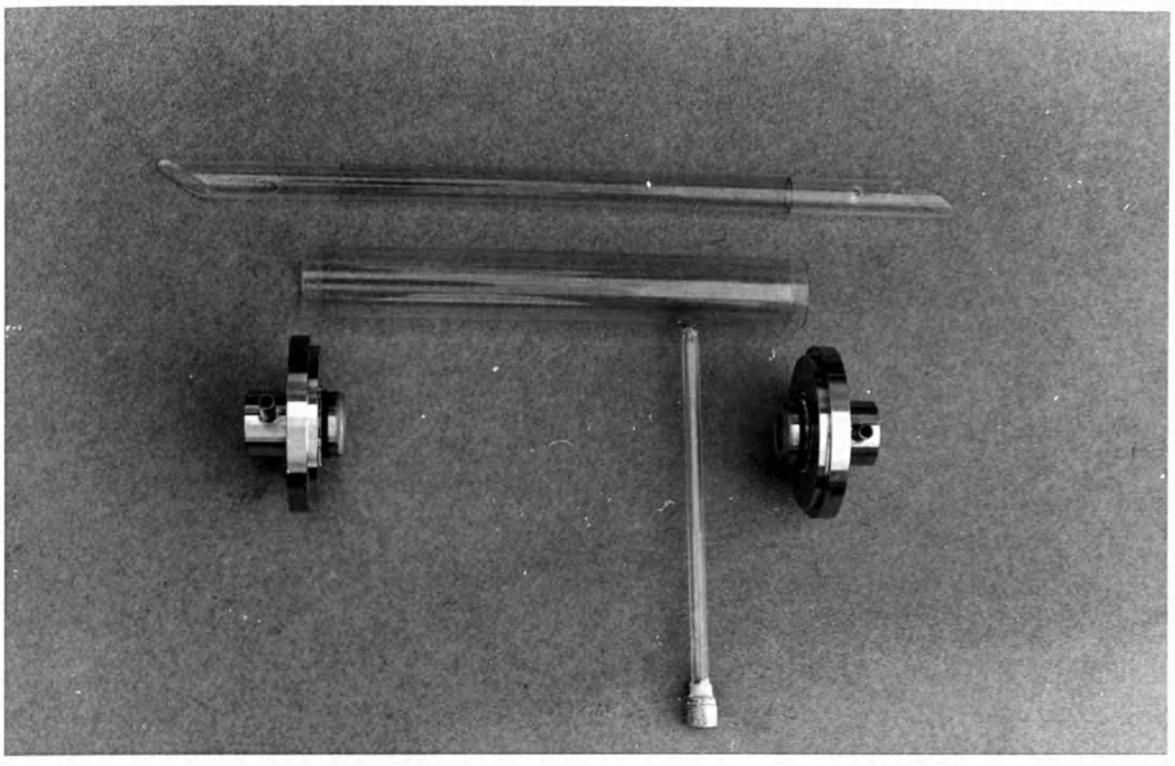

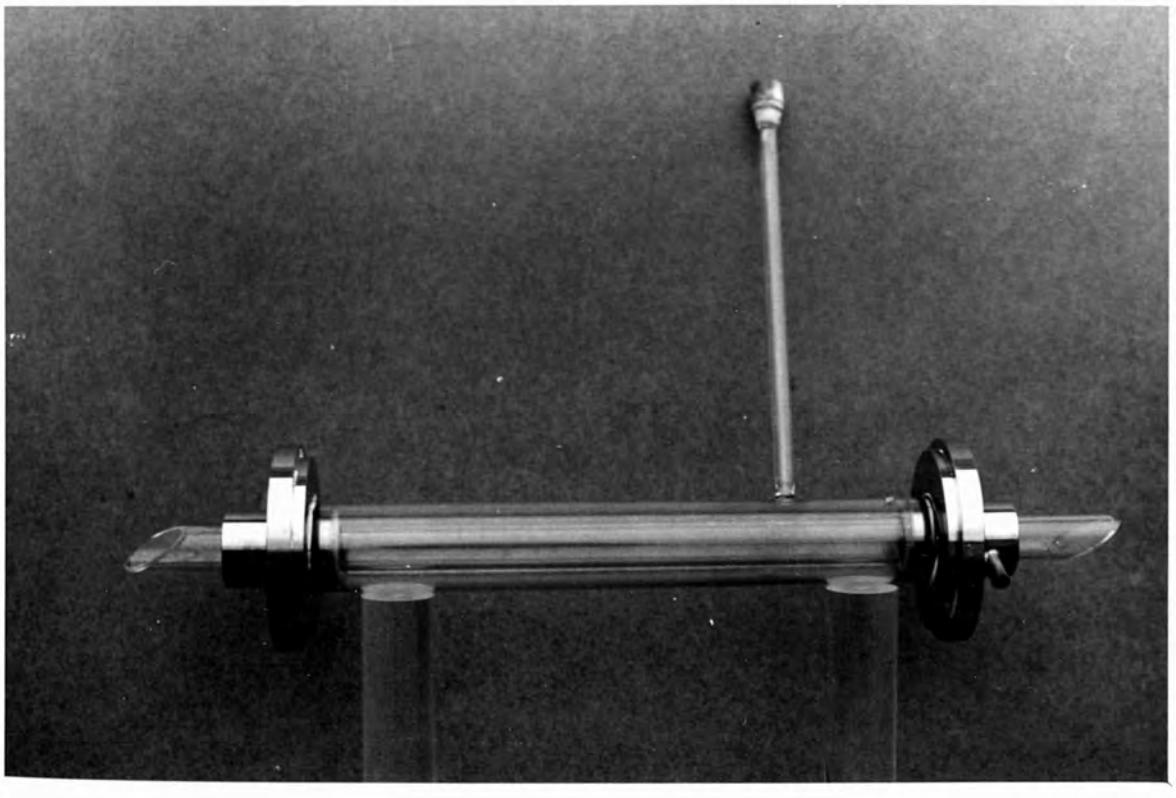

discharge volume with the diffusion pump and the gas cylinder through some vacuum lines made of PTFE or glass tubing. A schematic diagram of the arrangement for pumping out the flashtubes is shown in Figure 4.7. An EDWARDS oil diffusion pump type E02 was employed to evacuate the discharge volume; a vacuum pressure of 10^{-6} Torr was adequate for the experiments carried out. Research grade BOC rare gases, supplied either in glass flasks (760 Torr pressure) or in metalic cylinders (at high pressure) were used to fill the flashtubes. A MATHESON pumpable regulator type 19 and a high accuracy ($\pm$ 2%) GENE VAC gauge type GVG 14 (0 - 760 Torr) were connected to the vacuum lines (Figure 4.7) in order to flow the gas into the discharge volume and measure its pressure respectively. In this way, the gas pressure inside the tube could be varied. Figures 4.8 and 4.9 show photographs of the arrangement for pumping out the flashtubes.

During most of their operating time, the outside surface of the flashtubes (except MARK 2) was coated (just before operation) with EASTMAN white reflectance paint[122]. The paint was applied with a spray unit supplied by the manufacturers. A coat of 1mm thickness was necessary for 99% reflectivity in the spectral region between 2000Å - 7000Å. Photographs of MARK 4 and MARK 3 after painting are shown in Figures 4.10 and 4.11. When the optical output from the flashtube was studied, a narrow strip (1cm) in the middle of the flashtube was left unpainted (Figure 4.10). Apart from the obvious benefit of regaining some of the light travelling towards the outside of the flashtube, the use of reflectors improved the quality of the flashtube performance. It will be seen in Section 5.2 that the improved performance is attributed to further ionisation of the gas caused by the reflected light (photoionisation). It was also observed that the electrode sputtering in painted flashtubes was uniform. In contrast, the effects of non-uniform sputtering were evident after $\sim$ 500 flashes in the walls of MARK 2, which was always operated without any reflector on its outer surface.

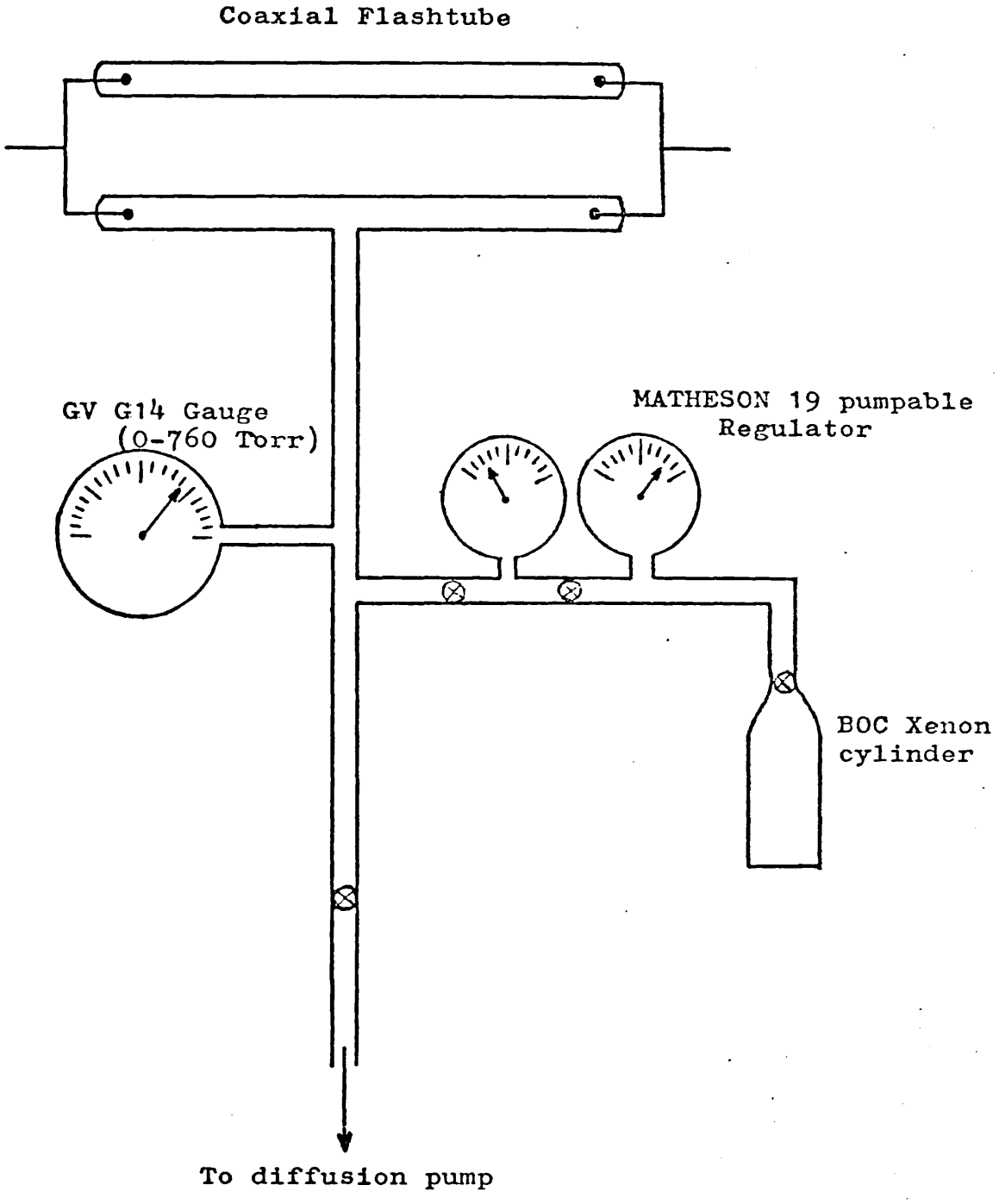

Fig. 4.7 : Schematic diagram of the experimental arrangement for pumping out the flashtubes.

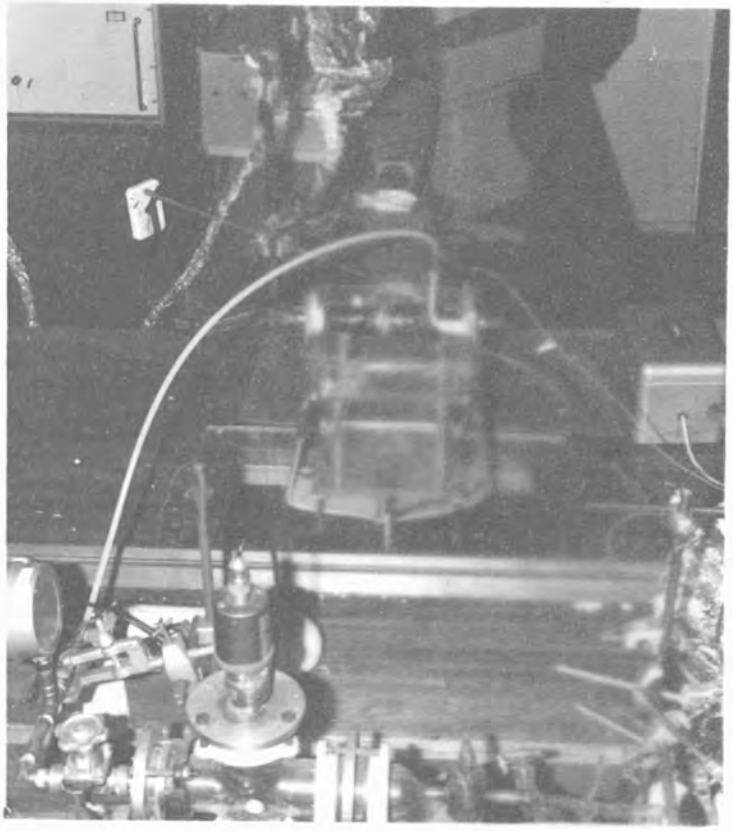

Fig. 4.8

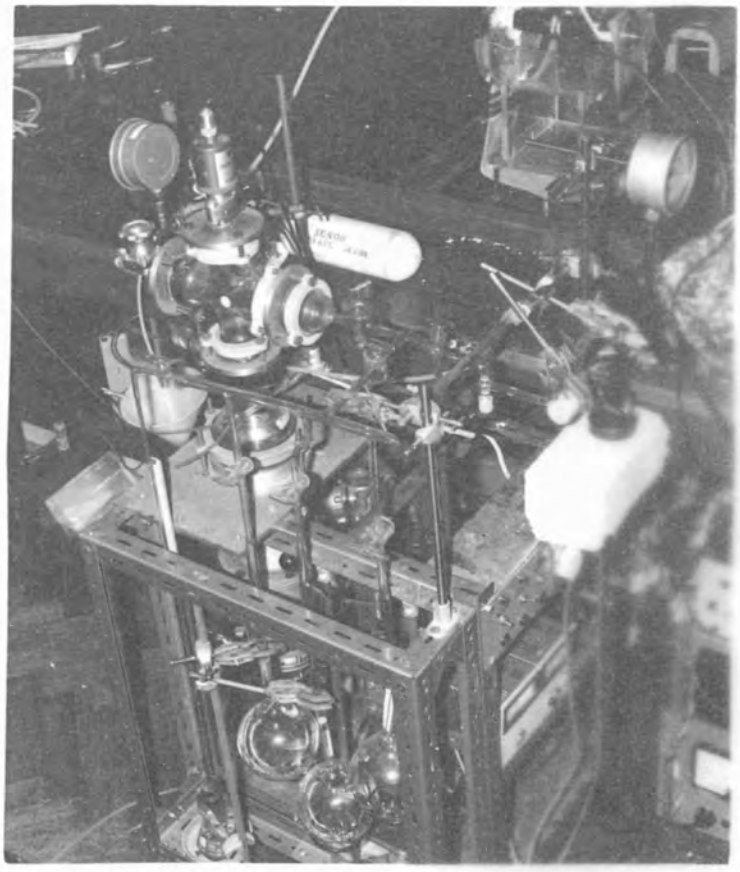

Fig. 4.9

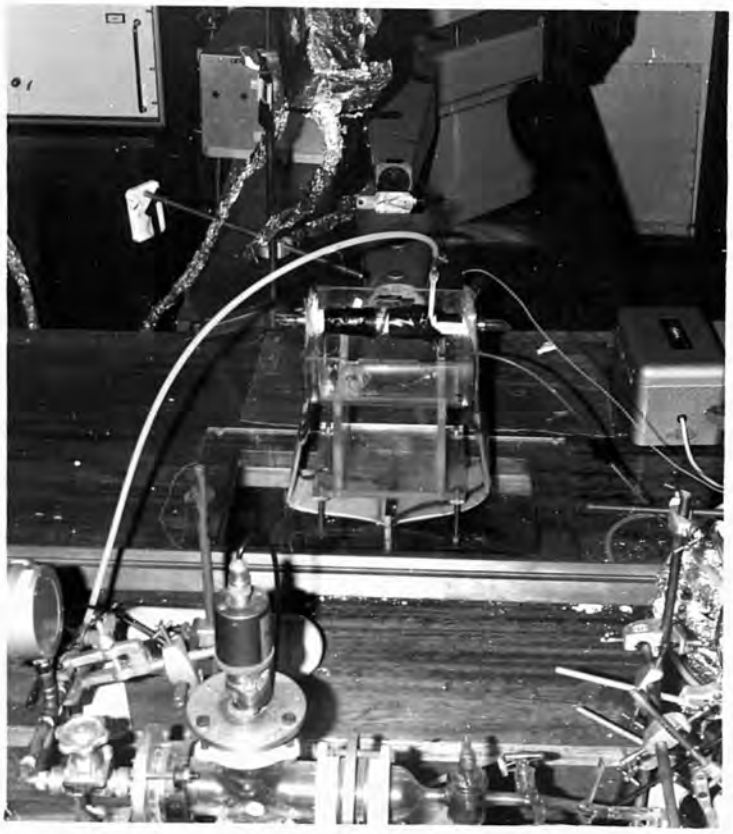

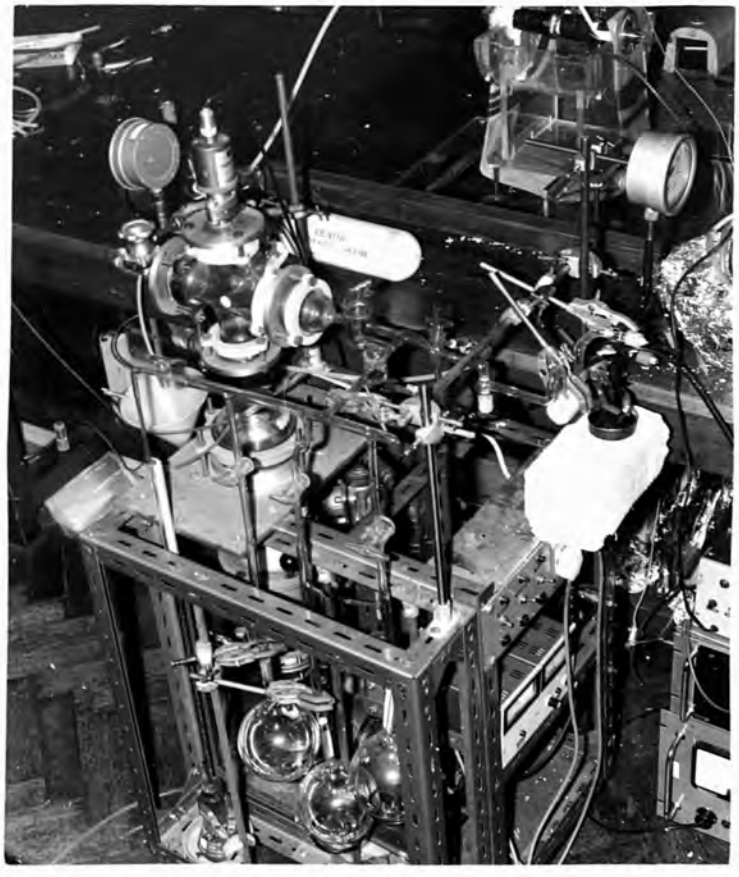

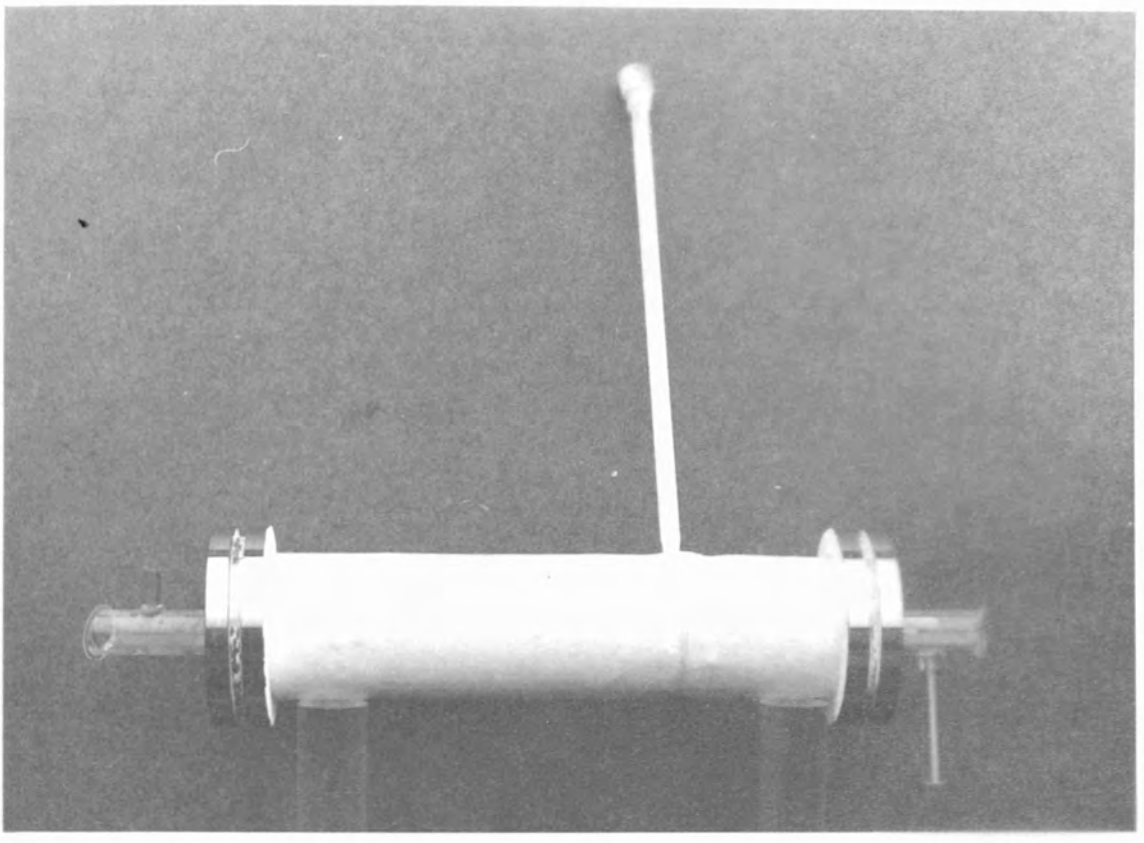

Fig. 4.10

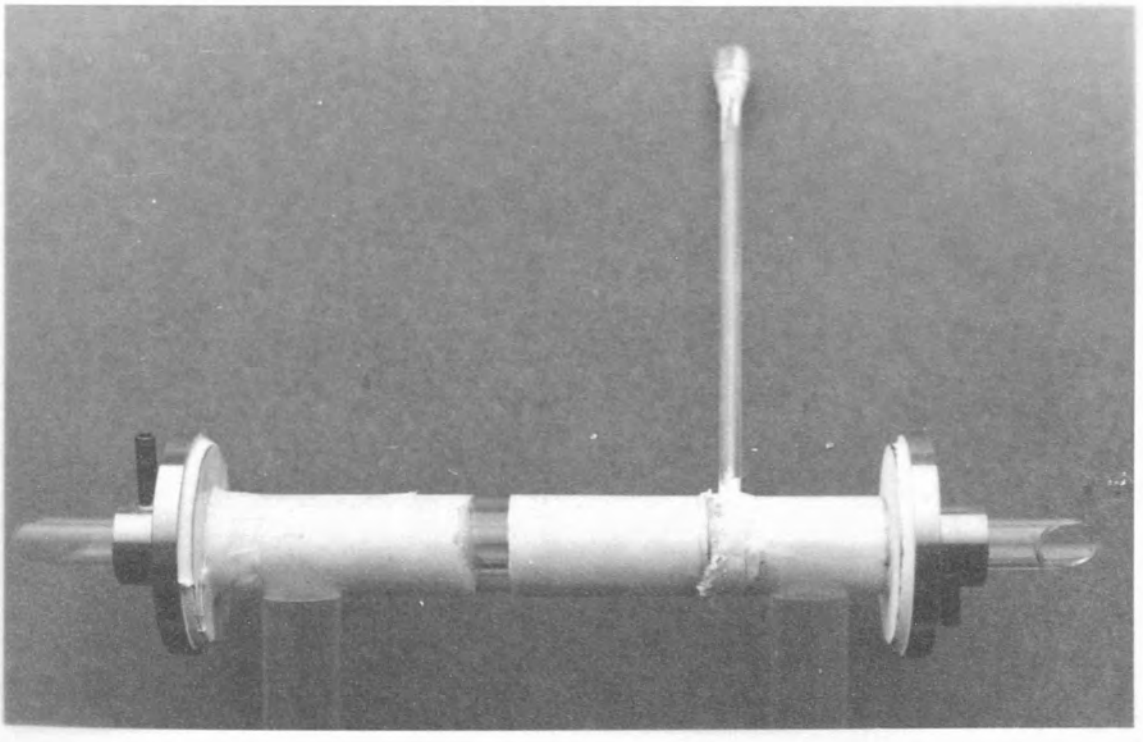

Fig. 4.11

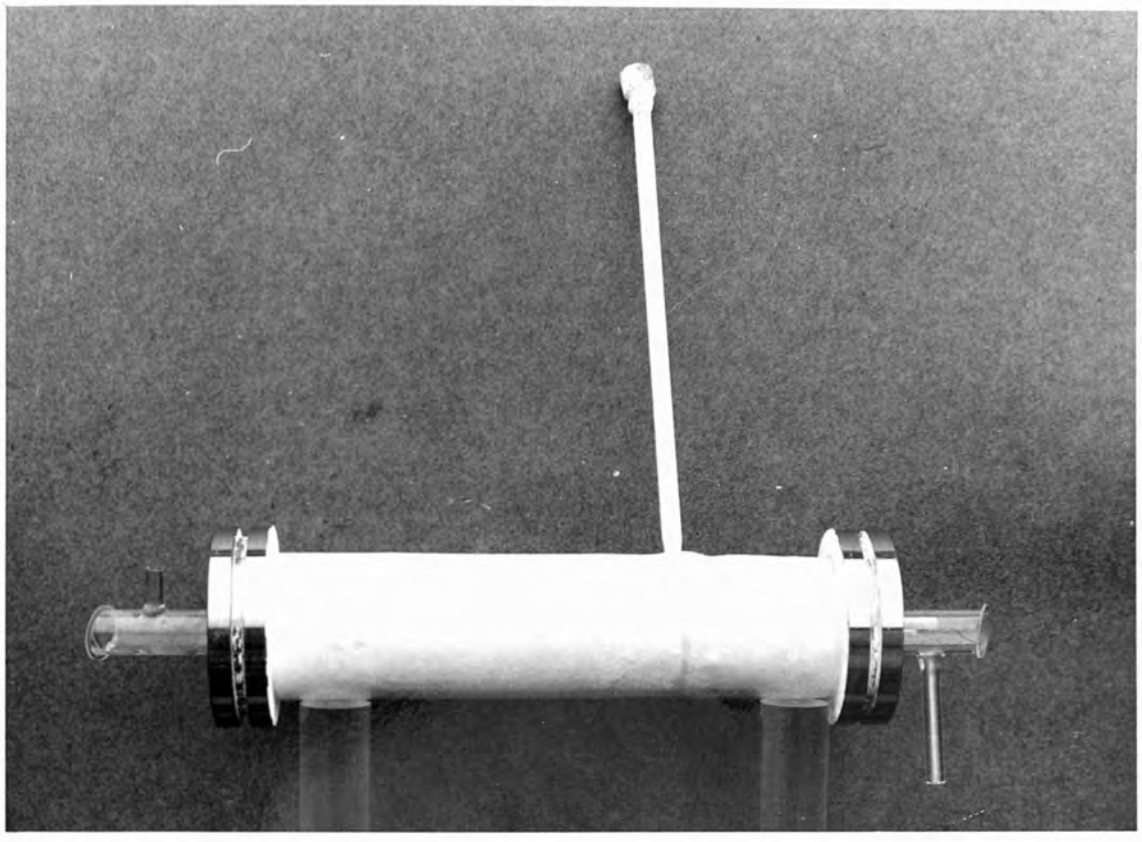

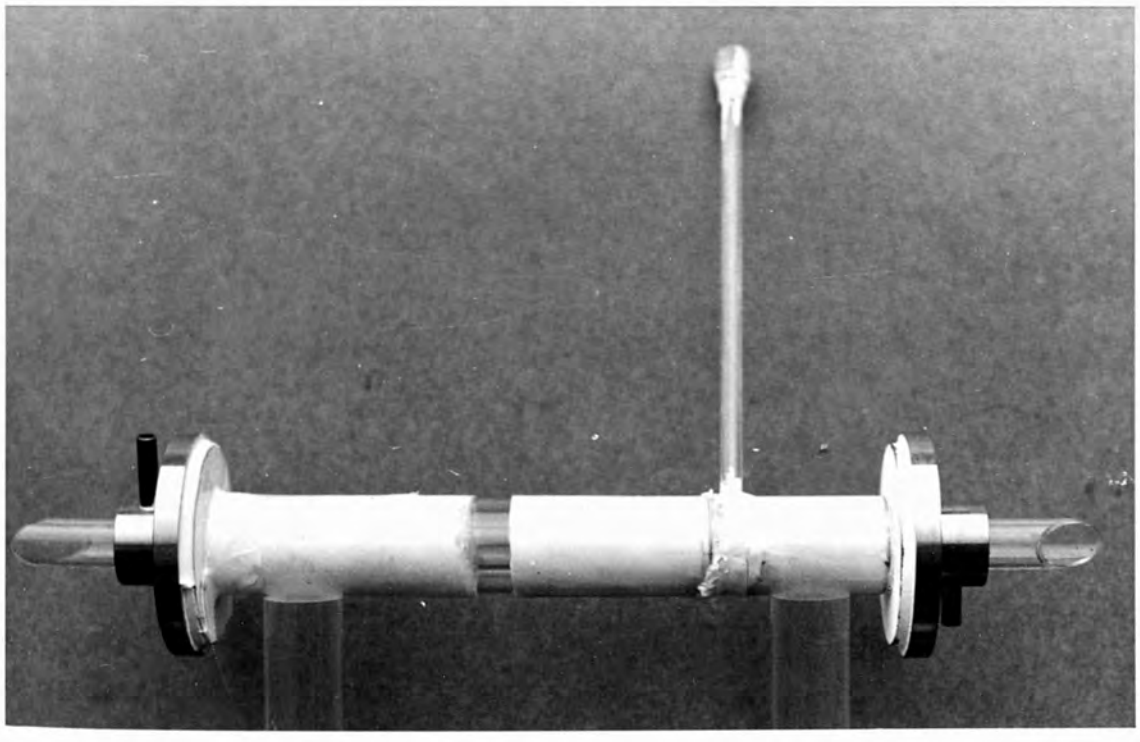

4.2 THE 5-STAGE MARX GENERATOR

In order to provide Kilojoule electrical pulses to the flashtubes, a 5-stage Marx generator was built. This type of generator was chosen for its fast and high voltage pulse characteristics[123, 124]. The discharge circuit of the Marx generator used is shown in Figure 4.12. The system was equipped with five identical medium inductance capacitors (NPL type), each having a capacitance of 2μFar. Each stage could be charged up to 20KV, thus giving up to 2 Kilojoules electrical energy.

As has been shown in Sections 3.3 and 3.5, the application of high overvoltages in flashtube discharges permits a rapid deposition of electrical energy, and the combination of high voltage-low capacitance rather than the opposite should be preferred. It is shown below that the Marx generator possesses such useful properties. The capacitors of such a generator are charged in parallel[123, 124] through high value resistors and they are discharged in series through an equal number of pressurised spark gaps following the ignition of the first spark gap by a trigger pulse.

The mechanism of the consecutive breakdown in the other spark gaps can be visualised with the aid of the discharge circuit diagram (Figure 4.12). Once conduction is established in the first spark gap, conditions of overvolting exist across the electrodes of the second spark gap due to the appearance in the electrode, which was at earth potential before ignition, of a voltage pulse having a peak value equal to that of the DC charging voltage in the capacitors, but of opposite polarity. Given that the other electrode of the spark gap is at a potential equal to the charging voltage, breakdown occurs when the algebraic potential difference across the gap exceeds the DC value for breakdown. The same breakdown mechanism applies for the succeeding spark gaps.

From the above it is apparent that the voltage pulse increases in each

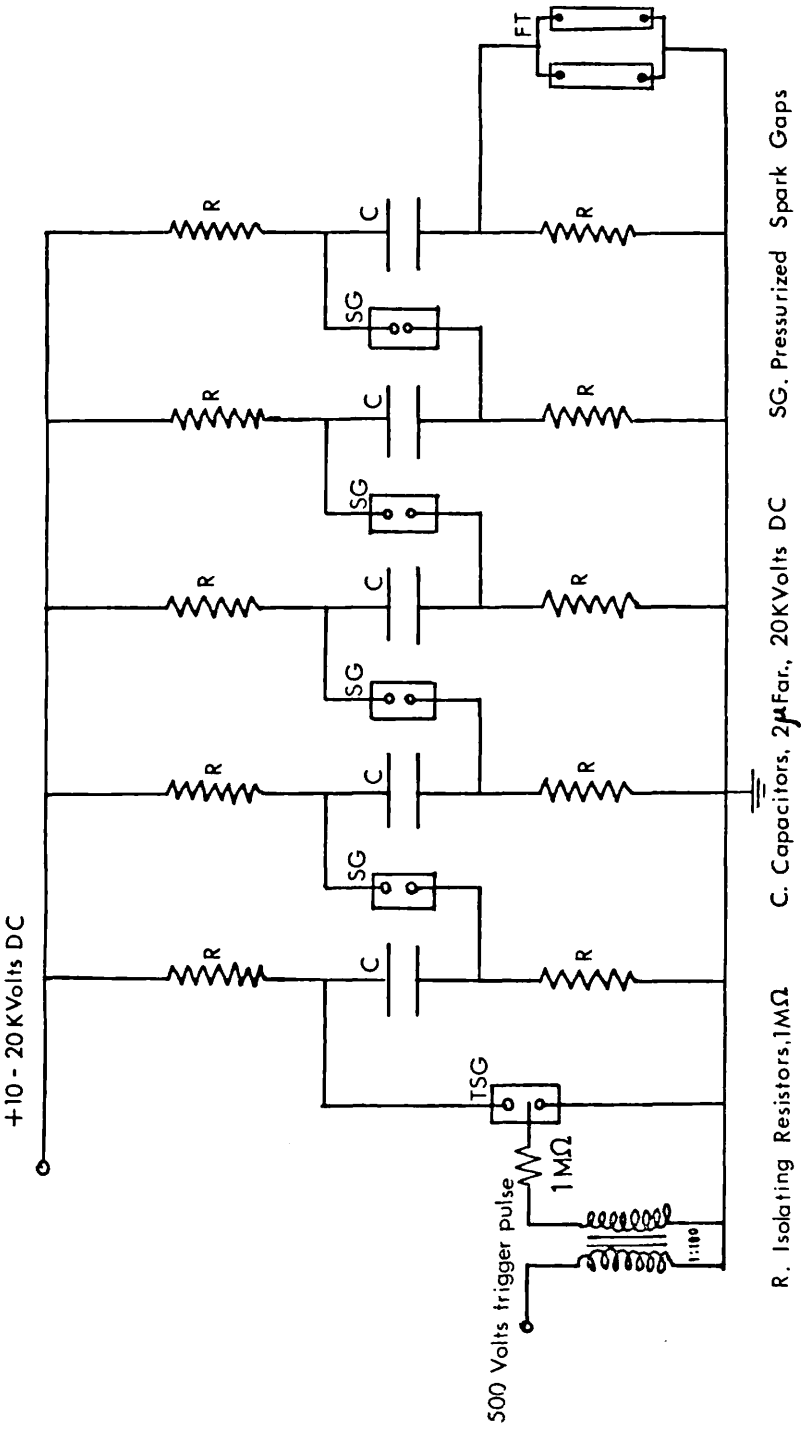

Fig. 4.12 : Circuit diagram of the 5-stage Marx generator.

stage by an amount equal to the charging voltage in the capacitors. Therefore, if the capacitors are charged to a positive voltage +V and an n-stage Marx generator is used, a negative voltage pulse of -nV peak value will be obtained after the n^{th} stage. It seems then that this voltage pulse is generated by a single stage discharge circuit of the type shown in Figure 3.5 or 3.11b, charged to an initial voltage nV and delivering an amount of electrical energy equal to the total energy stored in the n stages of the Marx generator. If the capacitance of each stage in the Marx generator is C, the capacitance of the single stage equivalent circuit is C/n. This relation is derived easily by equating the electrical energy stored in the Marx generator $\left(E_M = \frac{n}{2} CV^2\right)$ to the electrical energy stored in a single stage circuit charged to a voltage nV $\left(E_e = \frac{1}{2} C_e(nV)^2\right)$. From the foregoing, it is implied that a Marx generator discharge system displays those characteristics necessary (high voltage pulse, low inductance) for a fast efficient flashtube operation, without being restricted by the engineering and other practical problems which emerge when a single stage system, having the same characteristics, is used. Some of the problems encountered in the single stage system include the difficulty in achieving proper insulation of the very high initial DC voltage in the capacitor of the system, the provision of a capacitor which could be charged to such very high DC voltages, and the provision of a power supply giving these voltages. In a Marx generator, the charging voltage in the capacitors is substantially reduced, while insulation of the various leads is easier for fast pulsed voltages. As was mentioned earlier, the 2μFar capacitors of the 5-stage Marx generator built during the course of this investigation could be charged only up to 20KV DC; but they could withstand the high voltage pulses generated by the system (up to 100 KV). The capacitance of the equivalent single stage system for this 5-stage Marx generator is found equal to 0.4μFar.

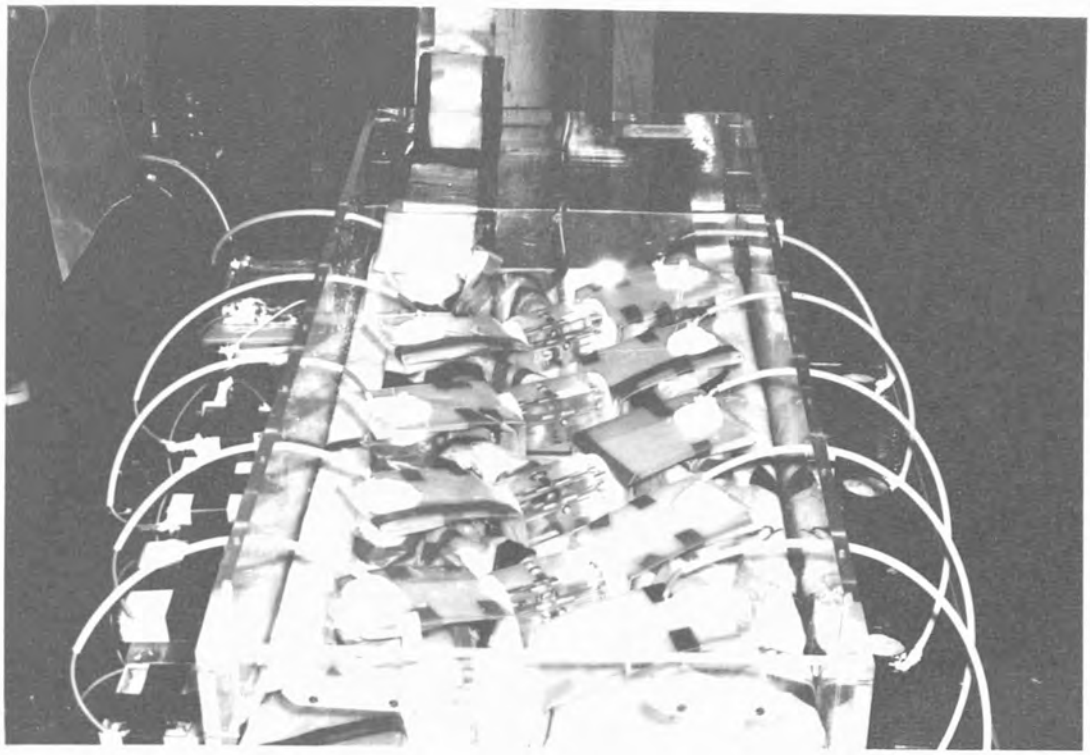

Fig. 4.13

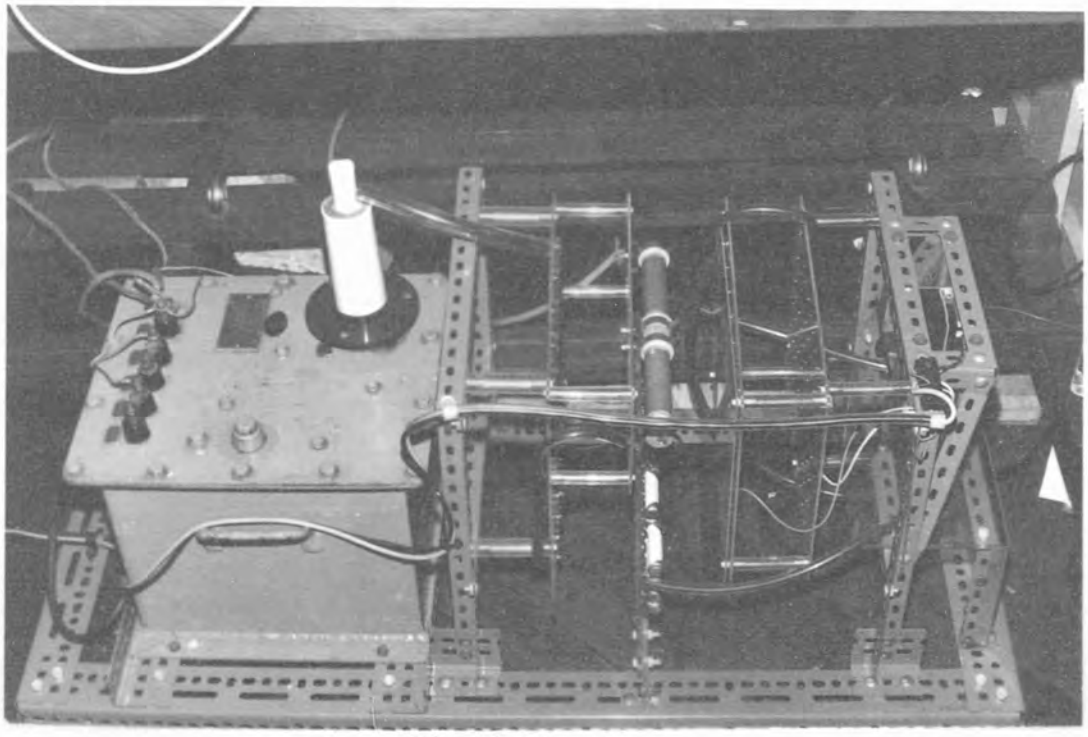

Fig. 4.14

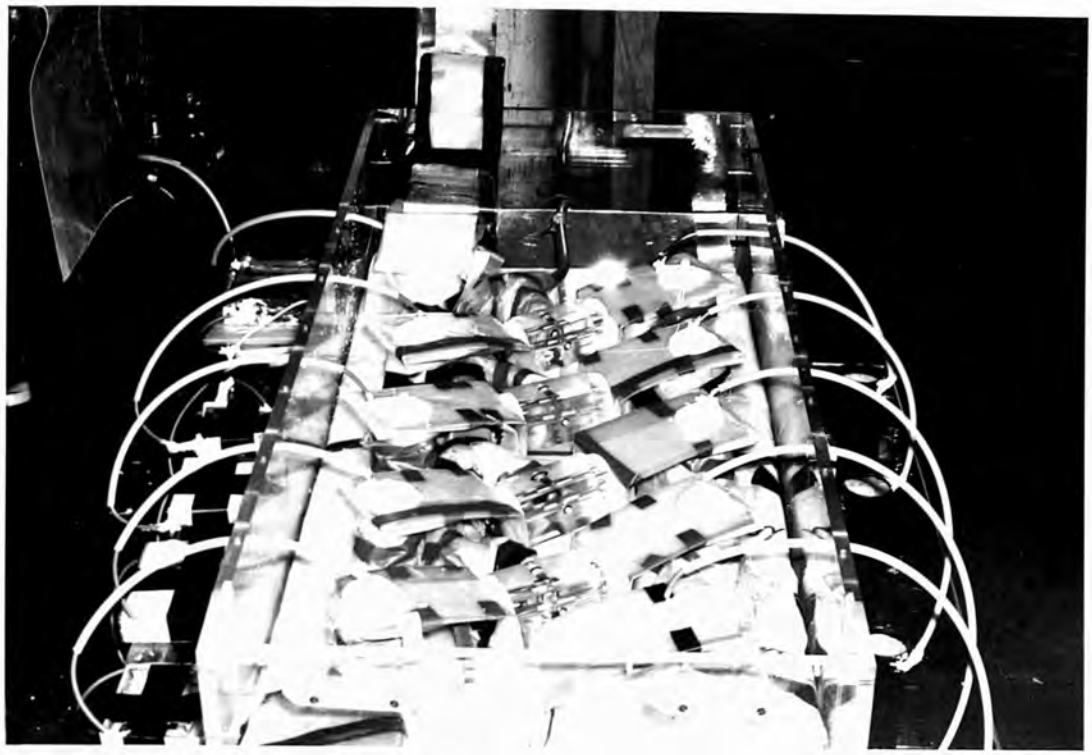

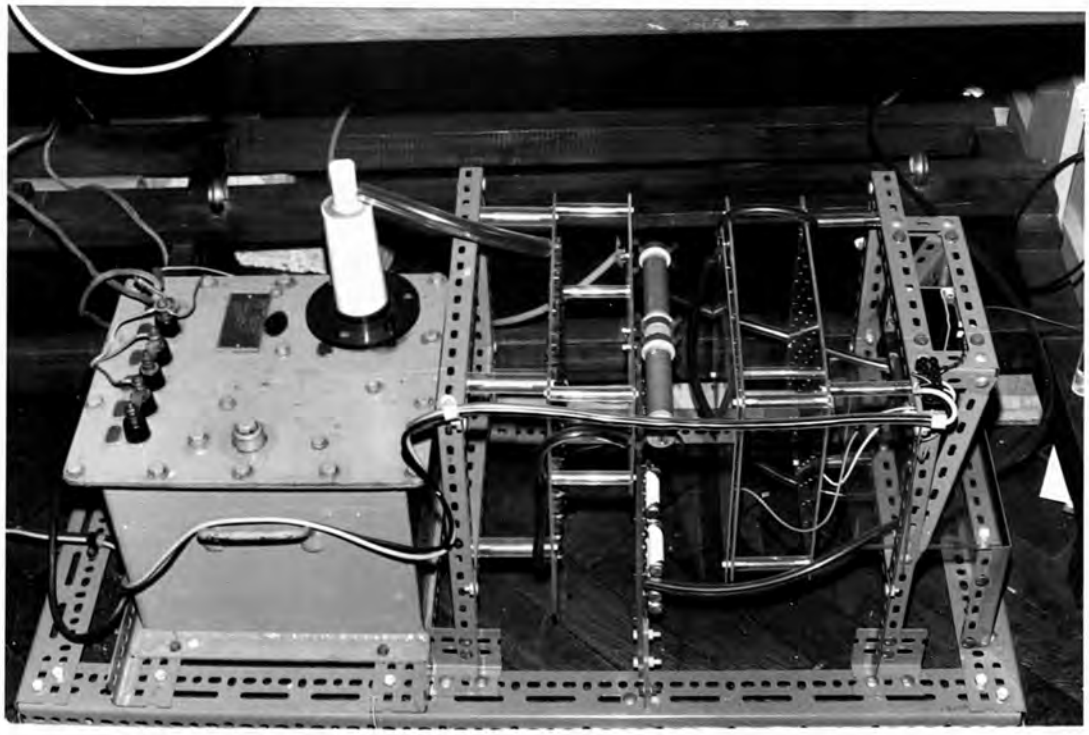

A photograph of the 5-stage Marx generator used is shown in Figure 4.13. Figure 4.14 shows a photograph of the power supply for the generator (this power supply was capable of giving up to 20 mAmps maximum current). The isolating resistors were specially made in order to withstand high electric powers; they consisted of several 2Watt carbon resistors connected in series and insulated inside boxes with silicone rubber or wax. Initially, resistors of high values $\sim$ 1MΩ were used,but later on values $\sim$ 100 KΩ were found to be adequate. All leads for the high current path were copper sheets of 1mm thickness and 10cm width. The edges of these sheets were smoothed and then covered with insulating tape to reduce the high voltage corona losses; the whole sheets were then wrapped in several layers of polythene insulator. All connections between leads and capacitor poles, spark gap electrodes or flashtube electrodes were covered with silicone rubber. This kind of practice was necessitated after repeated breakdowns which occurred outside the normal high current path.

The spark gap enclosures were 5 x 5 x 10cm square blocks made of perspex, with a 1.5cm diameter hole drilled centrally along the larger dimension. Brass electrodes with stainless steel tips were specially made. Figure 4.15 shows a photograph of the first (triggered) spark gap; the other spark gaps were like the first,except that they did not have the trigger pin. High pressure lines connected the spark gaps with a N_2 gas cylinder, and 'O' ring seals were employed. The tungsten trigger pin in the first spark gap was placed close to the earthed electrode in order to avoid premature breakdown from the highly stressed electrode. Figure 4.16 shows a photograph of the spark gap electrodes separately.

When the spark gaps and the flashtube were clean, the system functioned at its best,exhibiting an extremely low jitter ($\sim$ 50nsecs) in delay between the triggering of the system and the output optical pulse. But after $\sim 10^3$ flashes, the spark gap enclosures became dirty due to the carbon

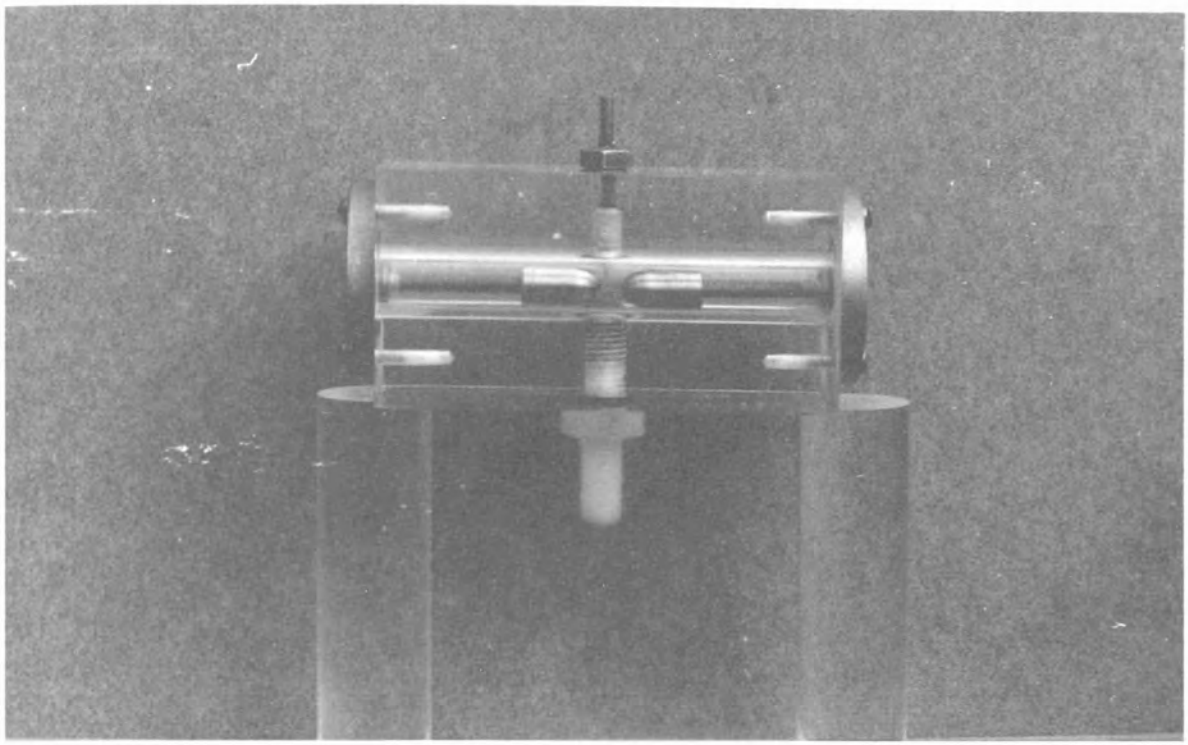

Fig. 4.15

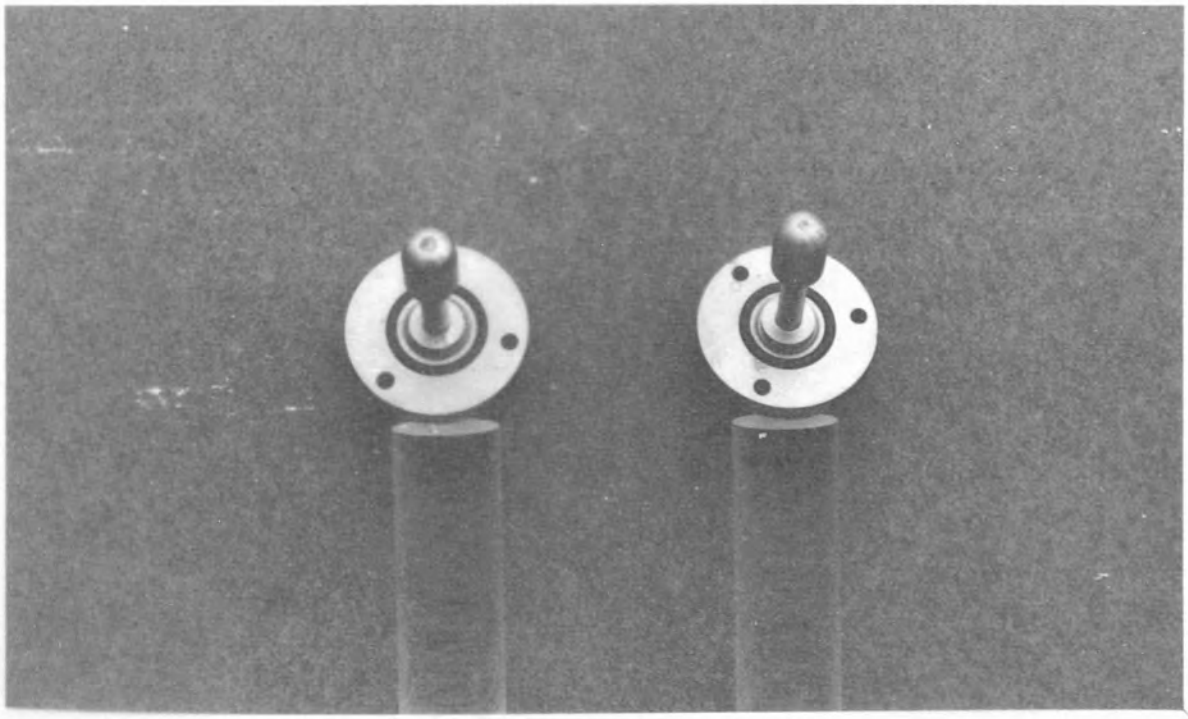

Fig. 4.16

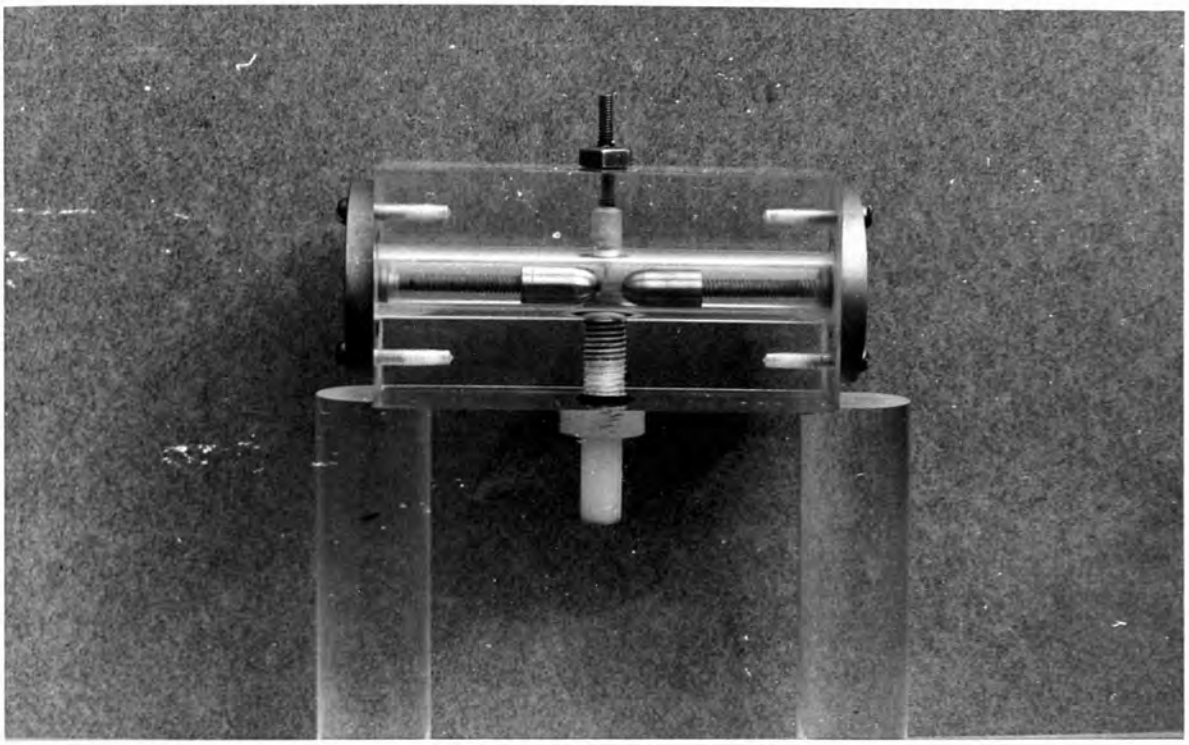

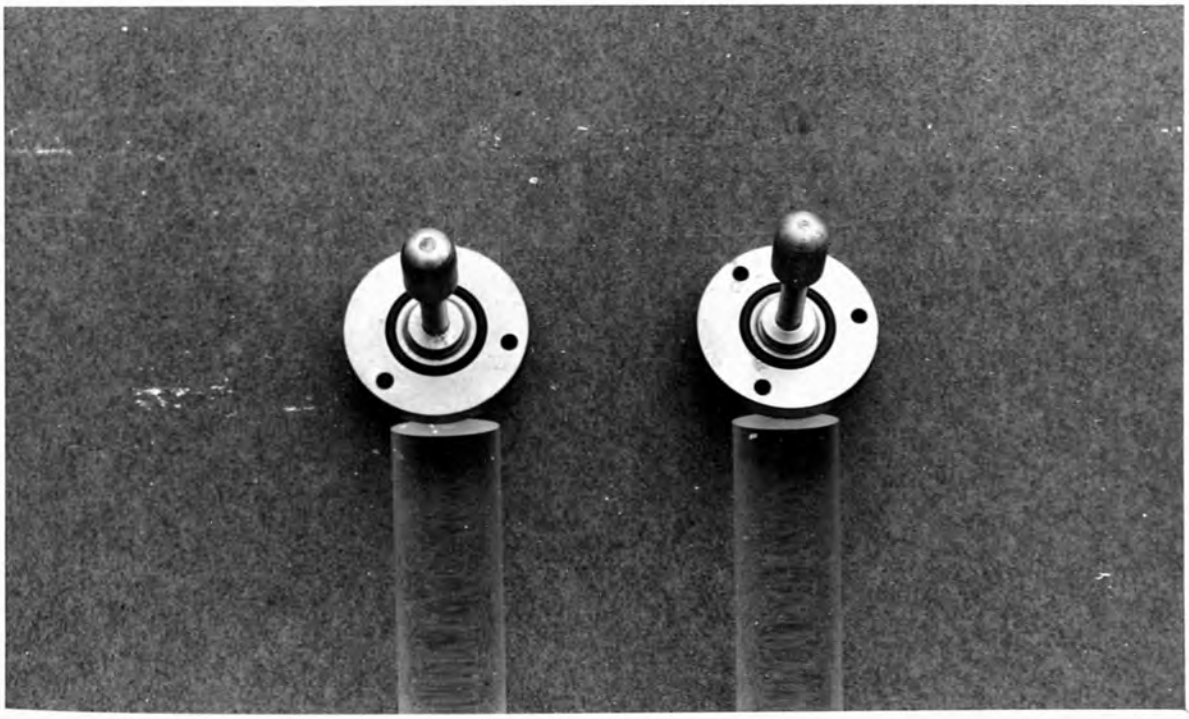

dust produced from the passage of high currents; as a result of this, a gradual deterioration of the performance of the system was observed in the form of high jitter amplitudes. Regular cleaning of the spark gaps was necessary for reliable system operation. The delay between triggering and output optical pulse is the sum of the delay in the external circuit (Marx generator) and the delay in the flashtube.

The delay in the external circuit, for clean spark gaps, varied from one session of experiments to the other, because the distances between the electrodes were different each time the spark gaps were reassembled. A delay of ∿4μsecs was observed in the external discharge circuit during the early stages of an experimental session with MARK 3, whereas a delay of ∿ 18μsecs was observed during the corresponding stages of a session with MARK 4 (see Section 5.1). In the first case, the gaps between the electrodes were very short (∿ 2mm), while in the second they were longer ∿ 5mm); the shorter gap arrangement was abandoned because it was observed that the effects of the carbon formation were evident sooner in the system performance. However, in all sessions, these spark gaps were consistent in displaying a similar low jitter amplitude, providing that they were clean; this consistency was important when the discharge system was to be synchronised with other units. Most of the delay in the external circuit was caused by the first (triggered) spark gap. This is in accordance with the discussion carried out in Section 3.7 in which it was shown that direct triggering (Figure 3.11a) results in a slow breakdown process.

The delay in the flashtube became comparable to that in the external circuit when low overvoltages (or high pressures) were used, or after ∿ 5×10^3 flashes when the effects of the electrode sputtering became severe; in the latter case, the flashtube performance was jittery. Results concerning the time behaviour of the discharge system are given in Section 5.1

The high voltage pulse generated by the system was of negative polarity (positive charging voltage in the capacitors, Figure 4.12) so that discharge in the flashtubes was taking place between a highly stressed cathode and an earthed anode. This arrangement was chosen because it is believed[79] that cold cathodes in strong electric fields emit electrons which facilitate breakdown in the flashtube.

Most of the experimental work of this investigation has been done by using the 5-stage discharge system described above. However, a 3-stage discharge system, equipped with identical capacitors and spark gaps, was built separately and used exclusively in the iodine photodissociation laser experiments.

A 2-stage Marx generator equipped with low inductance capacitors was used by Ewanizky and Wright[120] to drive a coaxial flashtube for pumping dye lasers. Dezenberg et al[125] used an 8-stage Marx generator to excite axially pulsed CO_2 lasers. Finally, a 20-stage, 2MV Marx generator was used to study breakdown in very high pressure spark gaps[126].

4.3 THE RADIO-FREQUENCY PREIONISATION DEVICE

Preionisation of the gas in the flashtubes was provided by a low energy radio frequency pulse which was applied to the flashtubes a few microseconds prior to the arrival of the main pulse from the Marx generator. A simple device providing such pulses was specially built, and its circuit is shown schematically in Figure 4.17 together with the circuit of its trigger unit (right), and the Marx generator circuit (left).

The preionisation device effectively consisted of two parts: the first part was a single stage generator of voltage pulses whose output terminals were connected to the primary terminals of a high voltage transformer (Figure 4.17). In the second part, one terminal of the secondary of the transformer was earthed, while the other was connected to a suitably

with the Dual beam oscilloscope revealed valuable information concerning the time sequence of the various events in the discharge system.

In this experimental session, MARK 4 - coated on the outer surface with EASTMAN white reflectance paint, and filled with Xenon at various pressures - was used. When time delays between the triggering of the system and the various events (arrival of the voltage pulse across the flashtube, breakdown of gas, etc.) were to be observed, the oscilloscope traces were initiated by an attenuated pulse from the master trigger, similar to the pulse triggering the first spark gap of the system; the two pulses were generated simultaneously, and provision was made for them to arrive at the same time at their destinations. Similarly, short and equal lengths of cable were used to transmit the voltage and current signals to the oscilloscope, which ensured that the measured delay between these quantities was accurate.

Figures 5.2a, 5.2b, 5.2c and 5.2d show externally triggered oscilloscope traces of the voltage (upper beam) and current (lower beam; strictly speaking, the signal in the lower beam is that of the induced voltage) taken by the Dual beam oscilloscope. The traces in Figures 5.2a and 5.2b, recorded during the early stages of the session, show a delay between the triggering of the system and the arrival of the voltage pulse across the flashtube of 18 μsecs; this was the delay of the external circuit for the particular spark gap spacings used in this experimental session when the system was clean (see section 4.2). The effects of contaminated spark gaps on the delay of the external circuit are illustrated in the oscillograms of Figures 5.2c and 5.2d which were recorded later on in the same session (after $\sim$ 500 flashes); a delay of $\sim$24 μsecs was observed by that stage, and there were signs suggesting that the spark gaps were becoming jittery.

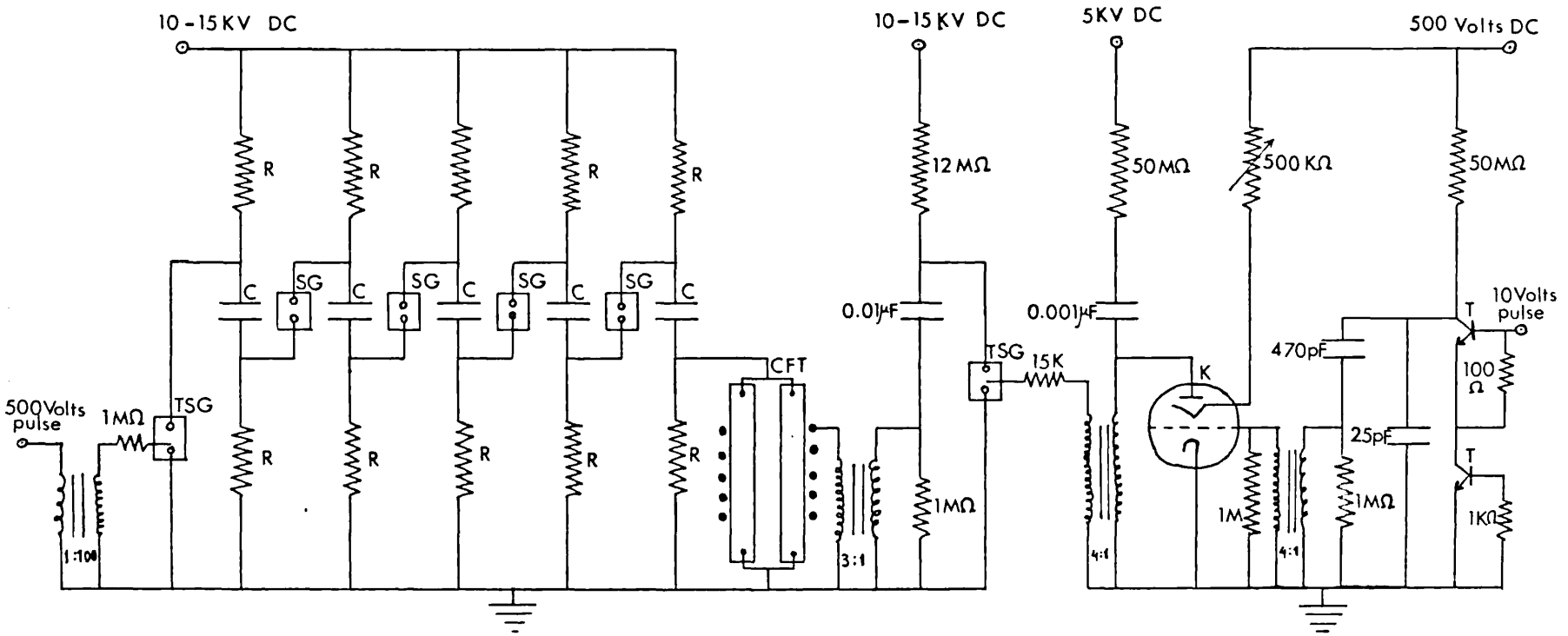

Fig. 4.17 : Circuit diagram of the preionisation device coupled with the Marx generator.

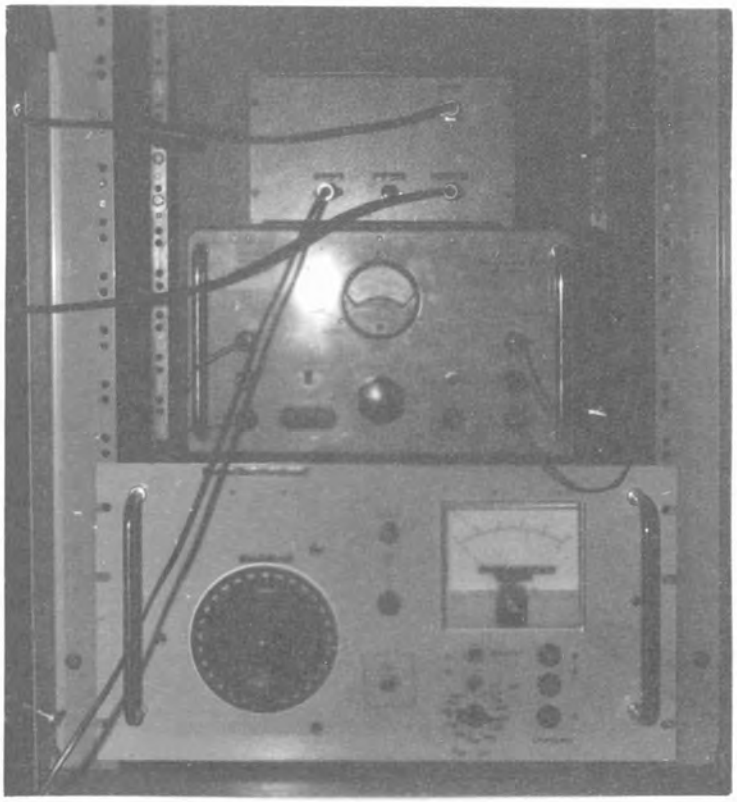

Fig. 4.18

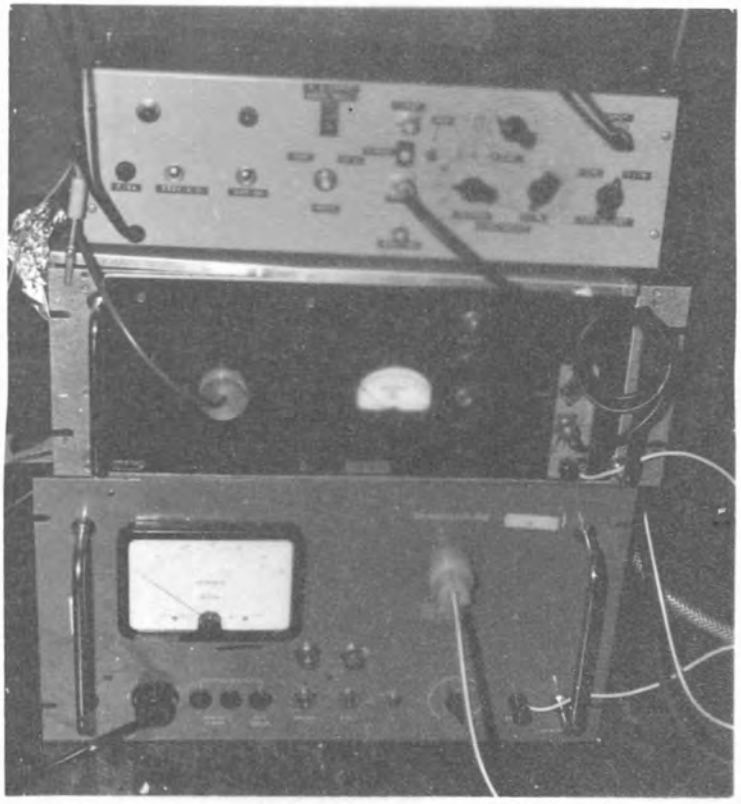

Fig. 4.19

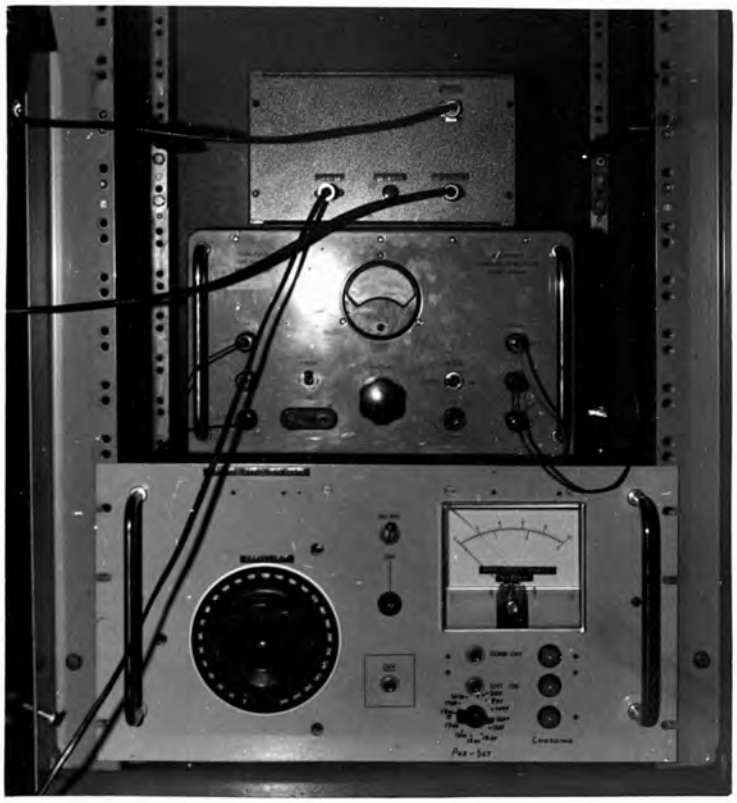

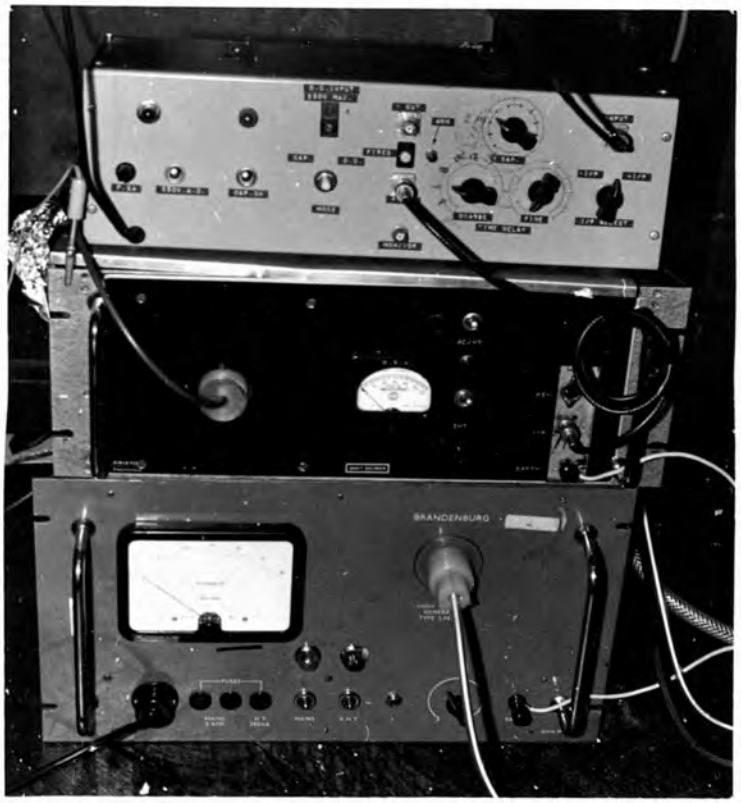
BRANDENBURG

includes the master trigger (the unit which triggers the first spark gap of the Marx generator) with its power supply (top) and the control unit of the system (bottom).

4.4 OTHER EXPERIMENTAL DETAILS

The experimental studies of the light emitted from the flashtube discharges involved temporal and spectral measurements of the output optical power. In the first class of measurements, time resolved profiles of the output optical power were obtained by using photodiodes and oscilloscopes. Two S-20, ITL photodiodes type HD 125 and HD 125 UV were used. The S-20 type of photodiode is sensitive in the near UV and visible spectral regions. The first of these photodiodes had an ordinary window so that only light in the visible region was detected; the other was equipped with a UV transmitting window so that light in both the visible and UV regions could be detected.

During the first stages of this work, the photodiode type HD 125 was used to detect the optical output from MARK 1 and MARK 2. Since optical absorption by the atmospheric air is not substantial in the visible region, the photodiode was placed at a distance of 1.5 - 2 metres from the flashtube and in doing so the interference caused by the electrical noise produced from the flashtube discharge was limited. Later, measurements of the optical output from MARK 3 and MARK 4, carried out with the photodiode type HD 125 UV, included also the near UV spectral region, and because atmospheric air absorbs a fair amount of light in this region, the photodiode had to be placed close to the flashtube (30 - 40cm). In order to reduce the electrical noise picked up by the detecting system and the various leads, the photodiode was mounted inside a metallic box shielded all around with aluminium foil (Figures 4.20 and 4.21). A wire mesh diffuser, mounted in front of the photodiode window, and a 6mm diameter aperture

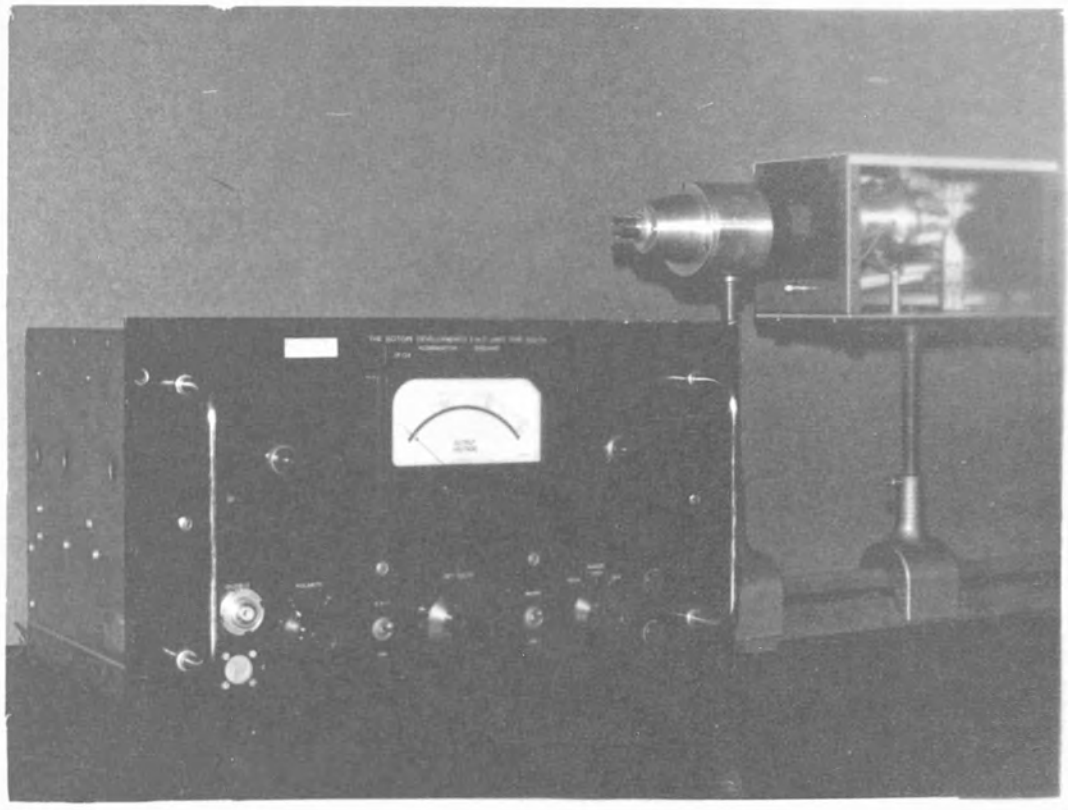

Fig. 4.20

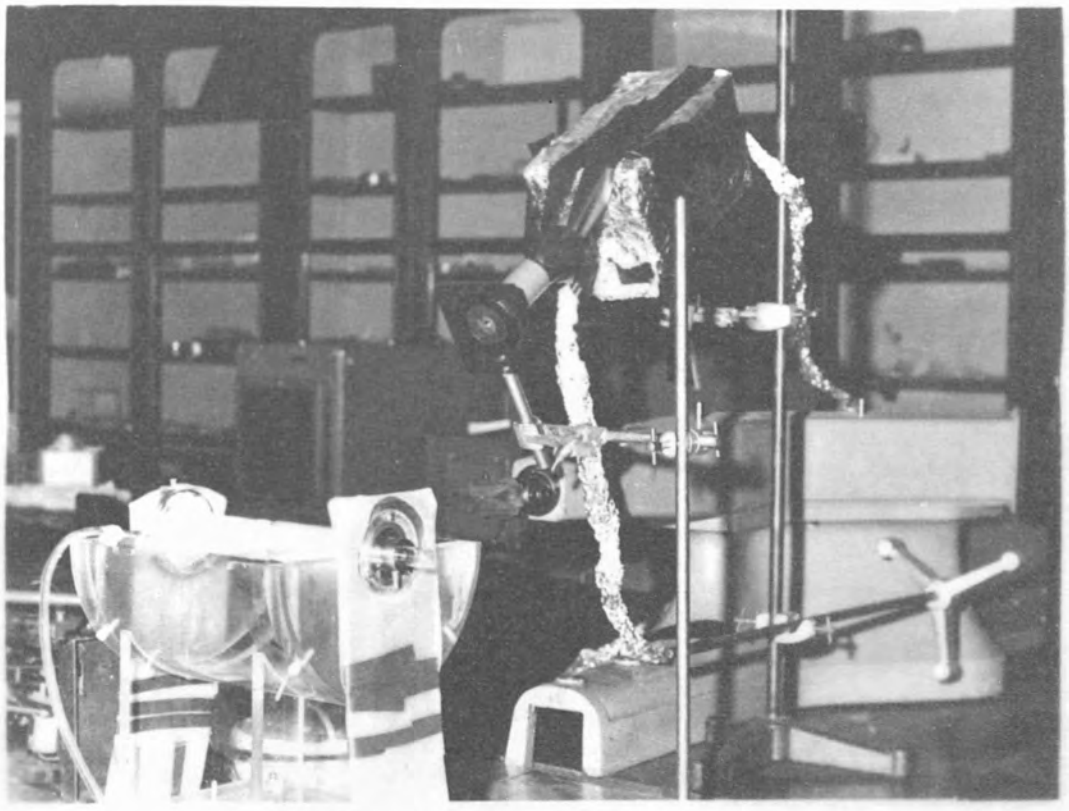

Fig. 4.21

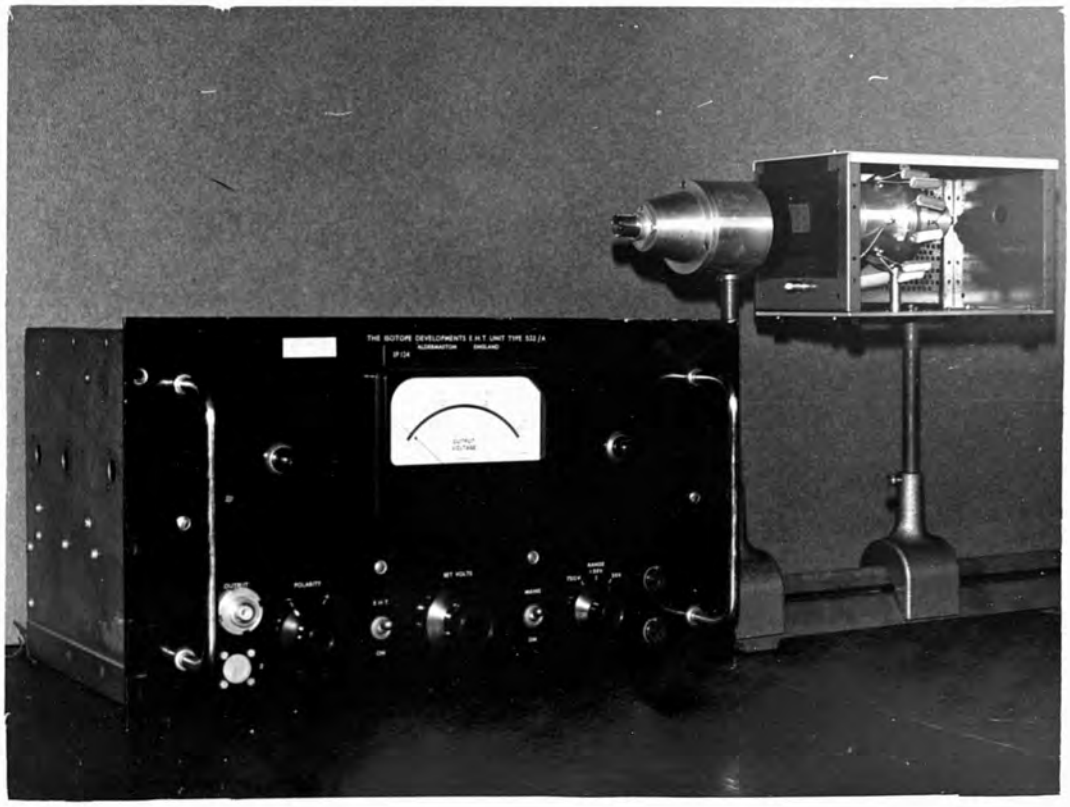
THE ISOTOPE DEVELOPMENTS E.H.T. UNIT TYPE 532/A
KIDDINGTON OXFORD
OUTPUT VOLTAGE
POLARITY
SET VOLTS
RANGE

placed half-way along the optical path from the flashtube reduced the amount of light falling on the photodiode, thus saturation of the latter was avoided. Neutral density filters were also used from time to time. In order to protect the photodiode from any kind of background light (room lights for example), a melanex tube of 30 mm diameter was mounted between the screened box and the aperture, with its axis parallel to the direction of the optical path. Figure 4.20 shows a photograph of the two photodiodes and their power supply.

Similarly, all cables to or from the photodiode were covered with aluminium foil. Other sources of electrical noise were the spark gaps of the Marx generator and the preionisation unit. Such noise was reduced to a few mVolts at the oscilloscope by screening these units with aluminium sheets. TEKTRONIX oscilloscopes type 544, 551 (Dual beam) and 519 were employed to detect the signal from the photodiode. Such signals, showing the variation of optical power with time, were recorded on polaroid photographic paper through a camera mounted in front of the oscilloscope screen.

Spectral measurements were carried out by using a HILGER Quartz Medium Spectrometer. The photograph of Figure 4.21 shows the experimental set up for temporal and spectral detection of the optical output from the flashtubes. Spectra of light from the flashtube discharges were recorded on ILFORD HP3 plates. These plates were analysed with the aid of a JOYCE LOEBL Double beam Microdensitometer; the resulting density traces were rescaled, in order to give relative intensities of incident light on the plates, by taking into account the characteristic curves of these plates (Density versus logarithm of relative Exposure) as provided by the manufacturers[127], and the spectral sensitivity of the plates as measured by Gorokhovskii[128].

The energy of the iodine photodissociation laser pulses was measured with an ITL laser output calorimeter which had an accuracy better than

± 5%. The near field pattern of the laser output was determined from the burnmark induced by the intense laser radiation on a processed unmarked polaroid photographic paper placed outside the cavity and close to the output mirror. The fluorescence energy output from dye solutions was measured with a COMARK (LASER ASSOCIATES) calorimeter type 48, placed at the end of the dye cell.

CHAPTER 5

EXPERIMENTAL STUDIES OF THE COAXIAL FLASHTUBE PUMPING SYSTEMS

5.1 ELECTRICAL CHARACTERISTICS OF THE DISCHARGE CIRCUIT

It has been shown in sections 3.3 and 3.5 that the power of the optical output from a flashtube discharge depends on a number of electrical parameters, such as the voltage waveform applied, the energy of the electrical pulse, the inductance of the circuit, etc. Consequently, the electrical characteristics of the discharge circuit and the time delays between various events, such as the arrival of the voltage pulse across the flashtube electrodes, the breakdown of gas, and the current rise, greatly affect the optical pulse characteristics. For these reasons, one experimental session was devoted to the study of the time behaviour of the voltage and current across the flashtube at various E/P values.

Simultaneous observations of the voltage and current variations with time were possible by using the Dual beam oscilloscope. Unfortunately, the brightness and the speed of the particular oscilloscope used were not good enough to record the rapid changes of these quantities, especially when breakdown in the flashtube occurred. Separate observations of the voltage were also made by using the single beam oscilloscope. It must be pointed out that another problem faced during these experiments with both oscilloscopes was the high level of interference noise which was superimposed on the signal to be detected; this high level noise was due to the closeness of the detecting cables and the flashtube in the experimental arrangement used in these observations (Fig. 5.1)

The experimental arrangement used for the detection of the voltage and current of the discharge system is shown schematically in Fig. 5.1.

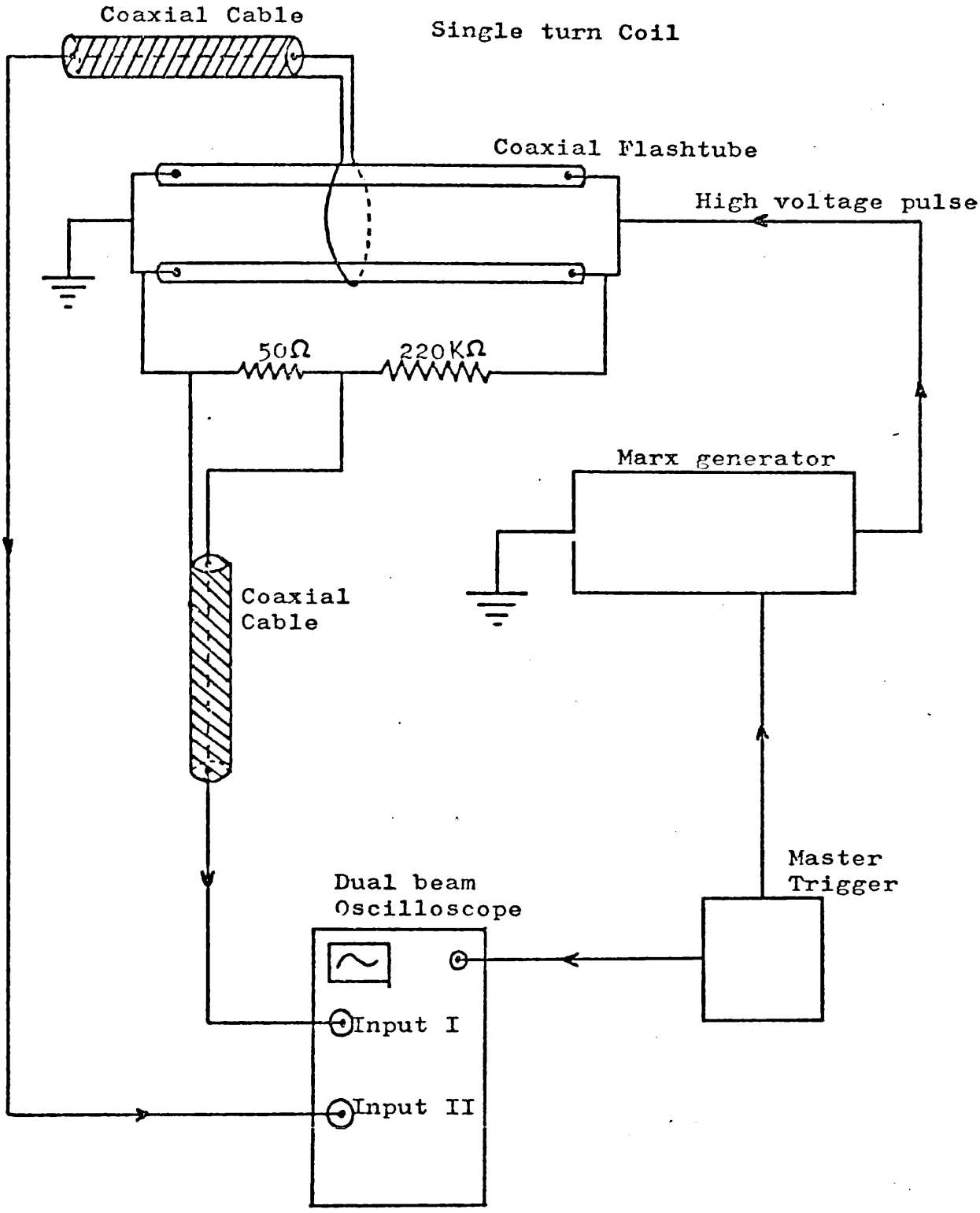

Fig. 5.1 :Schematic diagram of the experimental arrangement for the detection of the voltage and current of the discharge system.

The voltage across the flashtube was measured by using a high voltage divider made up of a 220 KΩ high power resistor connected to the highly stressed electrode, and a 50Ω resistor connected to the earthed electrode and in series with the high value resistor. In this way, the voltage drop across the 50Ω resistor was 1/4400 of the total voltage drop across the flashtube electrodes, and it could be detected by the oscilloscope. For convenience, a 50Ω match at the oscilloscope input terminals was used, instead of the 50Ω resistor.

The passage of electric current in the flashtube was detected by using a coil wound around the outer wall of the flashtube (Fig. 5.1). The variation of electric current flowing in the flashtube results in the appearance of an induced voltage at the ends of the coil. This voltage is given by:

$$V = -M \frac{di}{dt} \qquad (5.1)$$

where M is the mutual inductance between coil and flashtube. It was found that a 40 mm diameter single turn coil, made of copper wire and placed at an angle of $\sim 75^{o}$ with regard to the flashtube axis, was adequate to detect the breakdown of gas. But the observation of the actual induced voltage signal was not possible, at least during the first 2-3 μsecs following the breakdown of gas, partly because of the oscilloscope limitations in recording very fast pulses and - to a greater extent - because of the high level noise picked up by the coil (Fig. 5.2). Several attempts were made to overcome this problem by using the single beam oscilloscope, but there was little evidence of improvement. This meant that a quantitative estimation of the current variation with time from equation (5.1) was not feasible. Nevertheless, the observations made

with the Dual beam oscilloscope revealed valuable information concerning the time sequence of the various events in the discharge system.

In this experimental session, MARK 4 - coated on the outer surface with EASTMAN white reflectance paint, and filled with Xenon at various pressures - was used. When time delays between the triggering of the system and the various events (arrival of the voltage pulse across the flashtube, breakdown of gas, etc.) were to be observed, the oscilloscope traces were initiated by an attenuated pulse from the master trigger, similar to the pulse triggering the first spark gap of the system; the two pulses were generated simultaneously, and provision was made for them to arrive at the same time at their destinations. Similarly, short and equal lengths of cable were used to transmit the voltage and current signals to the oscilloscope, which ensured that the measured delay between these quantities was accurate.

Figures 5.2a, 5.2b, 5.2c and 5.2d show externally triggered oscilloscope traces of the voltage (upper beam) and current (lower beam; strictly speaking, the signal in the lower beam is that of the induced voltage) taken by the Dual beam oscilloscope. The traces in Figures 5.2a and 5.2b, recorded during the early stages of the session, show a delay between the triggering of the system and the arrival of the voltage pulse across the flashtube of 18 μsecs; this was the delay of the external circuit for the particular spark gap spacings used in this experimental session when the system was clean (see section 4.2). The effects of contaminated spark gaps on the delay of the external circuit are illustrated in the oscillograms of Figures 5.2c and 5.2d which were recorded later on in the same session (after $\sim$ 500 flashes); a delay of $\sim$24 μsecs was observed by that stage, and there were signs suggesting that the spark gaps were becoming jittery.

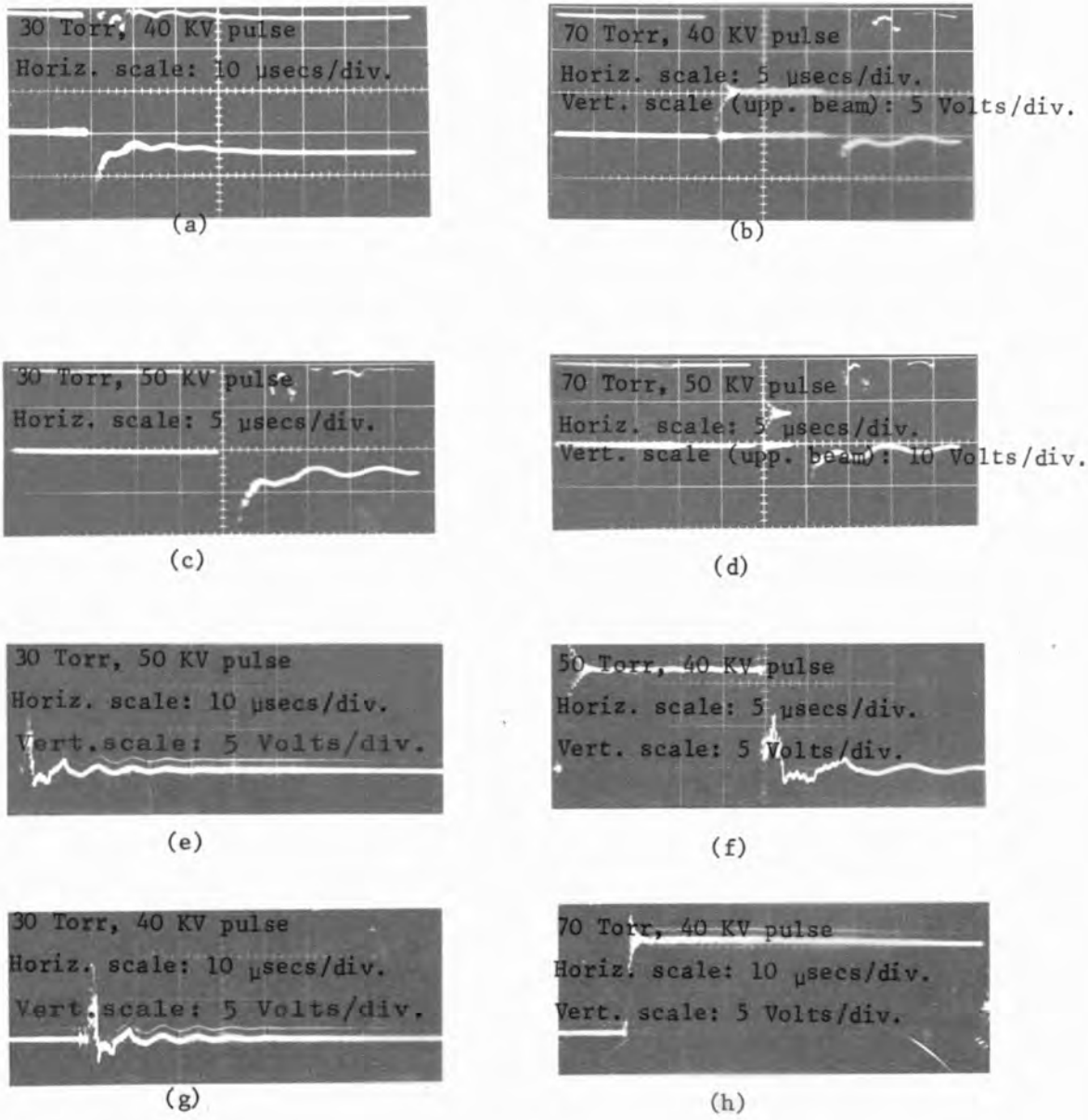

Fig. 5.2: Voltage and current traces of flashtube (MARK 4 filled with Xenon) discharges at various E/p values. In the top four oscillograms, the upper beam represents the voltage and the lower beam the current. The bottom four oscillograms give voltage traces only.

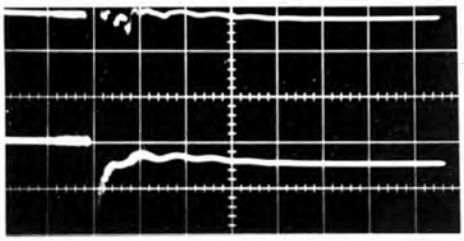

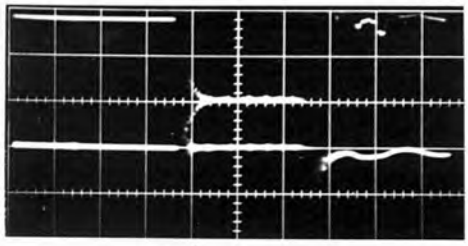

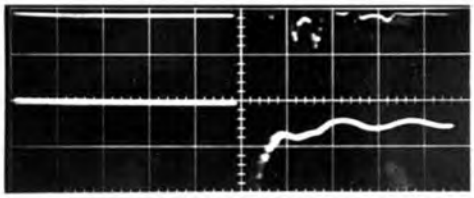

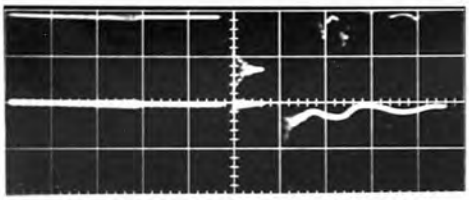

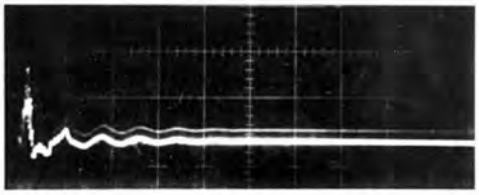

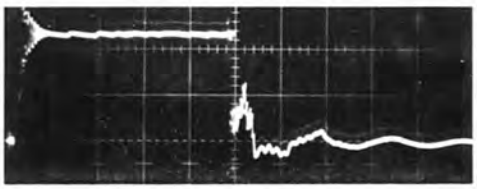

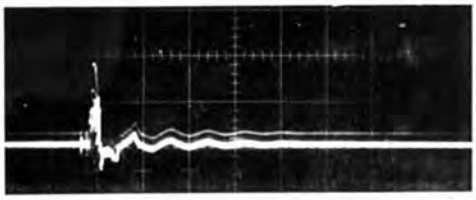

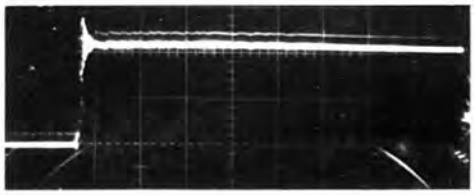

The occurrence of breakdown of gas was indicated by the abrupt discontinuity of the lower beam of the scope; this discontinuity was caused by the sharp rise of current in the flashtube. As was predicted, the time interval between the arrival of the voltage pulse and the breakdown of gas - defined as the total time lag (section 3.3) or hysteresis (section 3.5) - was found to be dependent on the overvoltage. Since, for a given voltage pulse profile, the overvoltage is proportional to the peak value of the voltage pulse and inversely proportional to the gas pressure and the distance between the electrodes, the peak E/p value of a flashtube discharge can be considered as a measure of the overvoltage. The oscillograms 5.2a, 5.2b, 5.2c and 5.2d correspond to discharges of peak E/p value of 66.6, 28.4, 83.3 and 35 Volts/cm.Torr respectively; the respective total time lags of these discharges are $\sim$1, 14, 0.5 and 5 μsecs. It is apparent that the higher the overvoltage is, the faster are the discharge processes leading to breakdown. At low overvoltages (oscillograms 5.2b and 5.2d), the incoming voltage pulse reaches its peak value and remains constant for some time, until breakdown occurs; thus it appears that the voltage pulse takes on the form of a step function. It was mentioned in section 3.3 that this feature is undesirable in flashtube discharges because of the increased energy losses in the circuit. This was confirmed from simultaneous observations of the optical output from the flashtube with another oscilloscope. Both the luminous efficiency and the peak output power were reduced when the total time lag was very long (>10 μsecs).

Further information concerning the electrical characteristics of the system was obtained by observing the voltage separately with the single beam oscilloscope. The traces of Figures 5.2e and 5.2f - triggered

internally by the detected signal - show the voltage variation across the flashtube for identical input electrical pulses (40 KV peak voltage value, 320 Joules energy) and at gas pressures in the flashtube of 30 and 50 Torr, respectively. In the first case, breakdown occurs when the voltage pulse reaches a value of ∿30 KV; in contrast, at the higher pressure, breakdown occurs long after the voltage pulse reaches its peak value. The effects of the degree of overvolting on the discharge speed are again evident. The traces of Figures 5.2g and 5.2h - triggered externally by the master trigger, give the voltage variation across the flashtube for the same input electrical pulses as the traces of Figures 5.2e and 5.2f, and at gas pressures of 30 and 70 Torr, respectively. It can be seen that at 70 Torr, breakdown has not occurred during the first 85 μsecs after the arrival of the electrical pulse. From all these traces, it is observed that the incoming electrical pulse rises rapidly in 1-1.5 μsecs.

5.2 TEMPORAL MEASUREMENTS OF THE OPTICAL OUTPUT FROM THE FLASHTUBES

5.2.1 Output optical power profiles at various E/p values

The temporal measurements and the consequent analysis of the optical output from the flashtubes are presented in a chronological order (with regard to the course of the investigation) in this sub-section. Typical oscillograms, showing the variation of the output optical power with time, have been analysed; in this way the dependence of the temporal characteristics of the optical output on the discharge parameters has been established.

The six oscillograms of Fig. 5.3 show early recordings of the optical output from MARK 1 filled with atmospheric air at various pressures. An

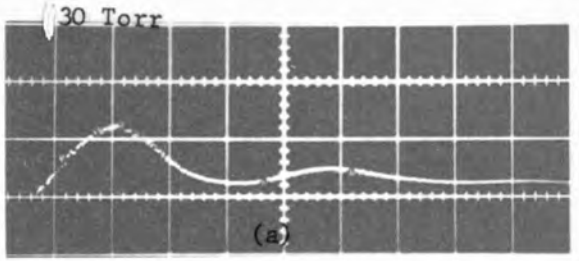

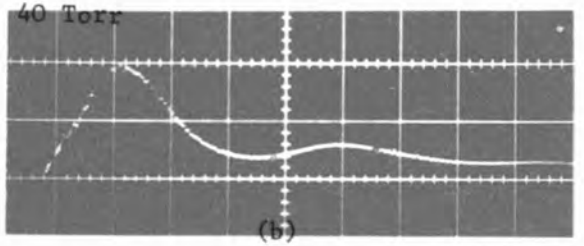

Fig. 5.3 Optical output profiles from MARK 1 at various pressures (atm. air)
57.5 KV pulse
Horiz. scale: 1 μsec/div.
Vert. scale: 2 Volts/div.

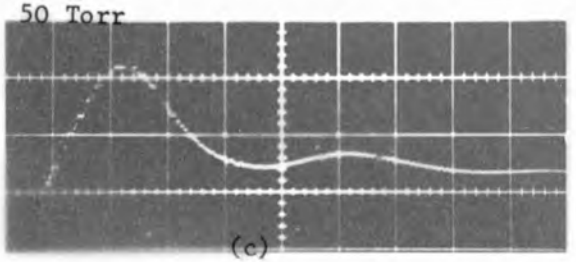

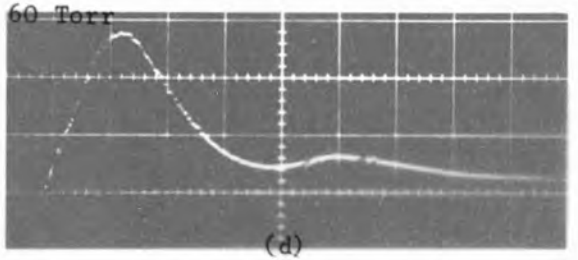

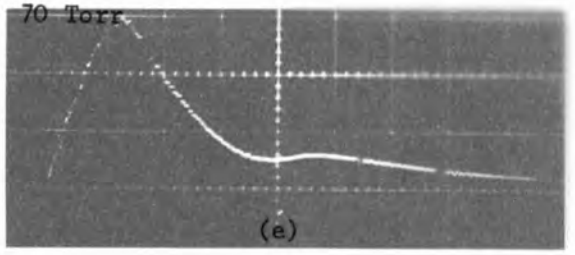

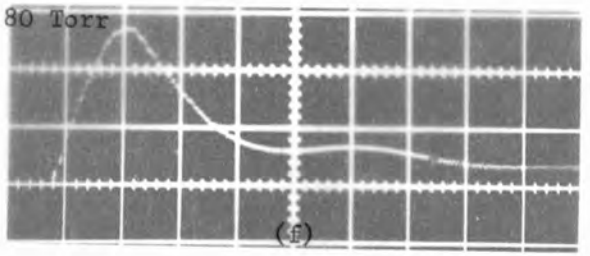

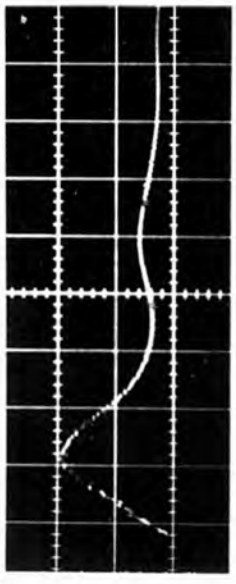

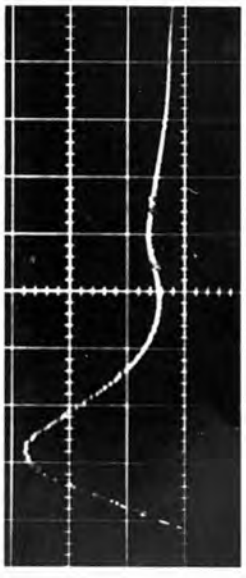

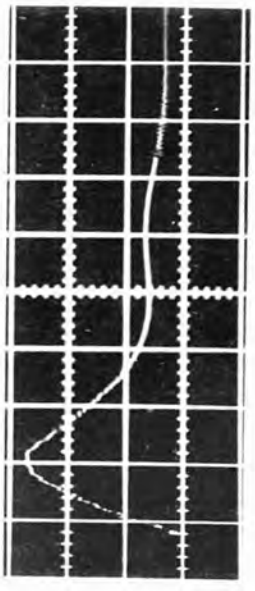

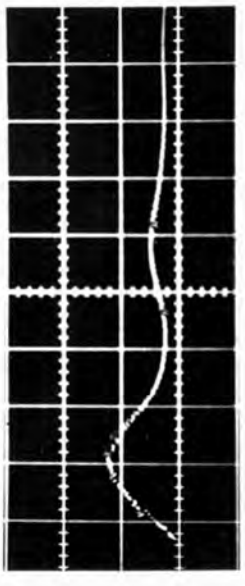

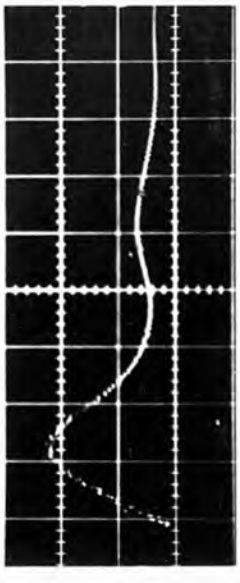

input electrical pulse of 57.5 KV peak voltage value and of 660 Joules energy was applied to the flashtube. The flashtube was not painted with the reflective material, and so light from all parts of the discharge column reached the photodiode, which was ∿1.5 metre away from the flashtube; the photodiode window did not transmit UV light, which meant that only light in the visible region was detected.

The area of oscillogram under the optical pulse represents the relative radiant energy of the particular flash. It can be observed that this area becomes larger as the gas pressure is increased. Therefore, these oscillograms confirm the theory that the luminous efficiency of a flashtube discharge increases with increasing gas pressure in the flashtube (see section 3.1). Similarly, the oscillograms of Fig. 5.3 show that the relative peak optical power first increases as the pressure is increased up to 70 Torr, and then decreases (Fig. 5.3f). Further oscilloscope observations of the optical output from flashes at pressures above 80 Torr showed a continuous deterioration of the peak optical power, without any significant change of the overall radiant energy.

Direct visual observations of flashtube discharges, made through highly absorbent glasses, revealed that at high E/p values (∿100 Volts/cm. Torr*) the luminocity of the discharges was more or less even around the annular discharge section of the flashtube, while at low E/P values (< 40 Volts/cm.Torr) the luminocity varied around this section. At E/p values around 30 Volts/cm.Torr, localised discharges were observed along a small part of the discharge volume, which meant that the energy density

---

*All numerical values of the reduced parameter E/p, mentioned in the experimental chapters, refer to peak values.

in this part became extremely high. These observations are in agreement with the view put forward by Furumoto and Ceccon[43], that the discharge of a coaxial flashtube tends to become more uniform as the E/p value is increased (section 3.6). In Fig. 5.4, the two photographs a and b show the overall luminous pattern of the discharge column of MARK 1 when flashed at E/p values of 100 Volts/cm.Torr (60 KV peak voltage, 30 Torr pressure) and 35 Volts/cm.Torr (60 KV peak voltage, 85 Torr pressure), respectively. Neutral density filters were placed in front of the camera, so that the intensity of the transmitted light from the flashtube was attenuated by a factor of $\sim$30. It is apparent from these photographs that, as the E/p value is decreased, a transition takes place from a diffuse and virtually uniform discharge to a localised, non-uniform discharge.

The graphs of Fig. 5.5 give various temporal characteristics of the optical output from MARK 1 as functions of the gas pressure. It can be seen that, in addition to the relative peak power, the rise time of the pulse increases with increasing pressure also. But, as has been mentioned in the previous chapters, for flashtubes designed to pump pulsed lasers the important characteristic of an optical pulse is the rate at which radiant energy is emitted, rather than the rise time or any other characteristic time interval (such as the half-width) of the pulse. The relative mean powers, over the characteristic time intervals indicated in the graphs, have also been plotted as functions of the gas pressure. These mean powers represent measures of the average rate at which radiant energy is emitted over the respective time intervals and, like the peak power, they increase with increasing pressure. However, their rate of increase is not as high as that of the peak power, because the characteristic time intervals, over which these powers are averaged, become longer

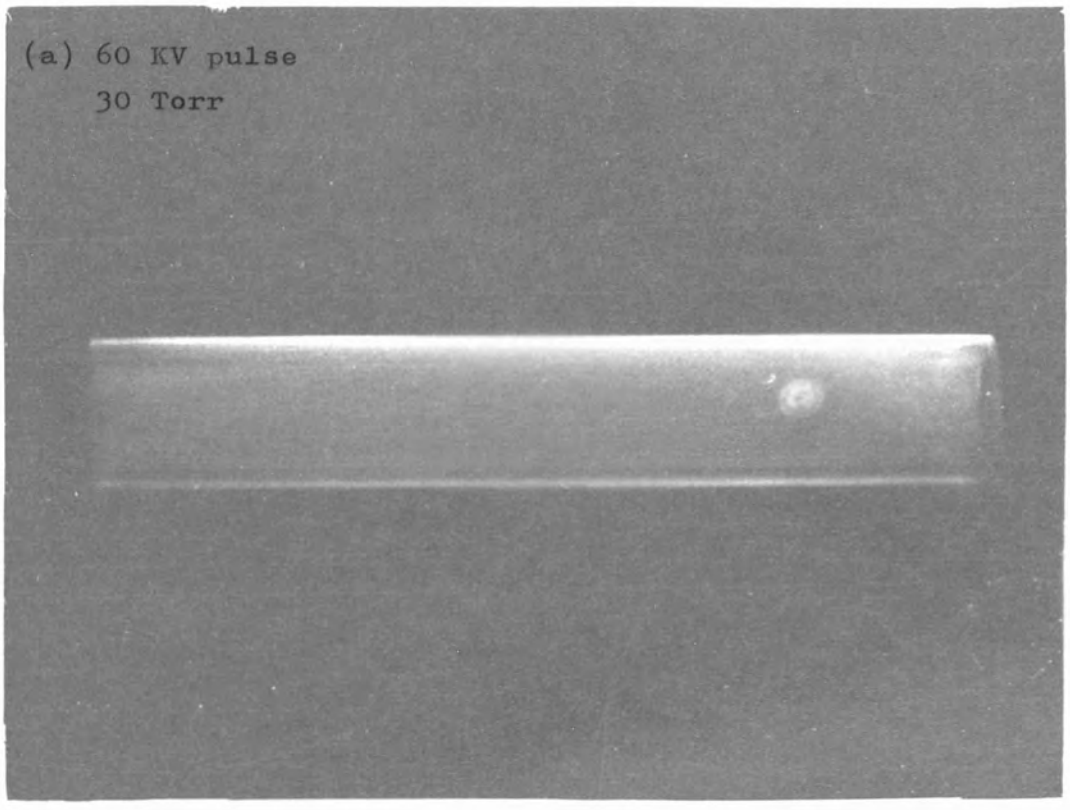

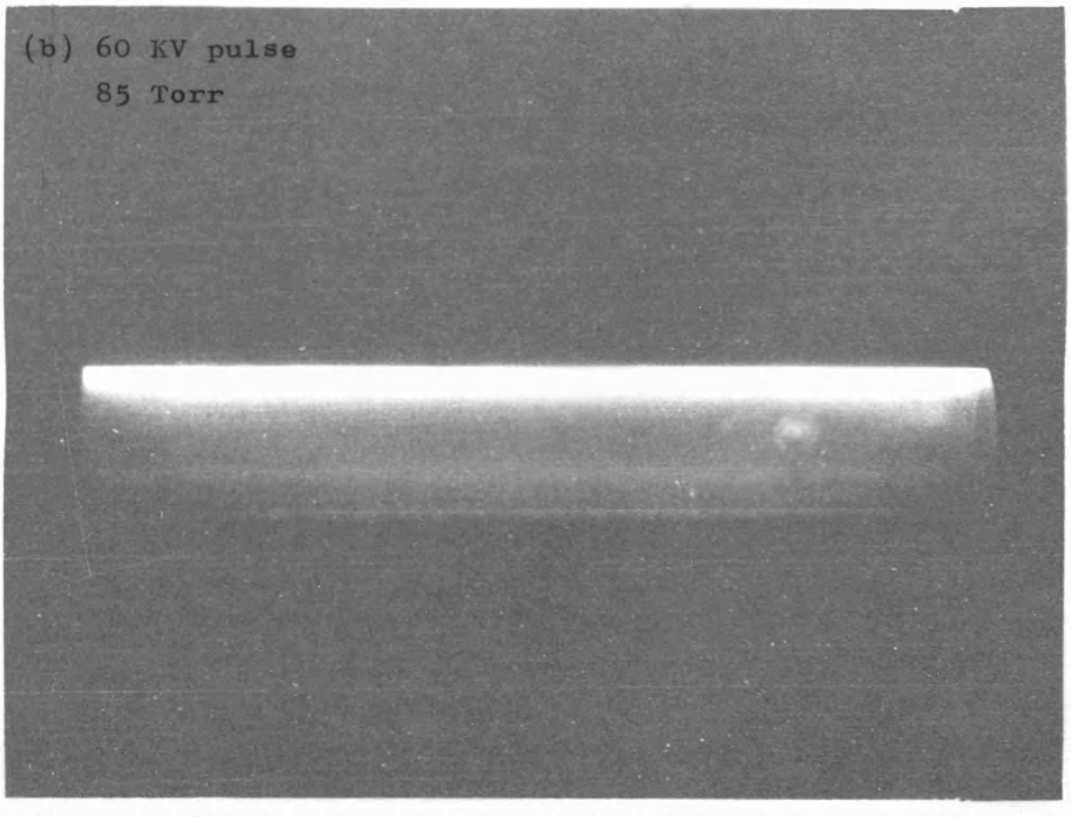

Fig.5.4: Discharge luminocity pattern in MARK 1 (filled with atm.air) for two different E/p values.

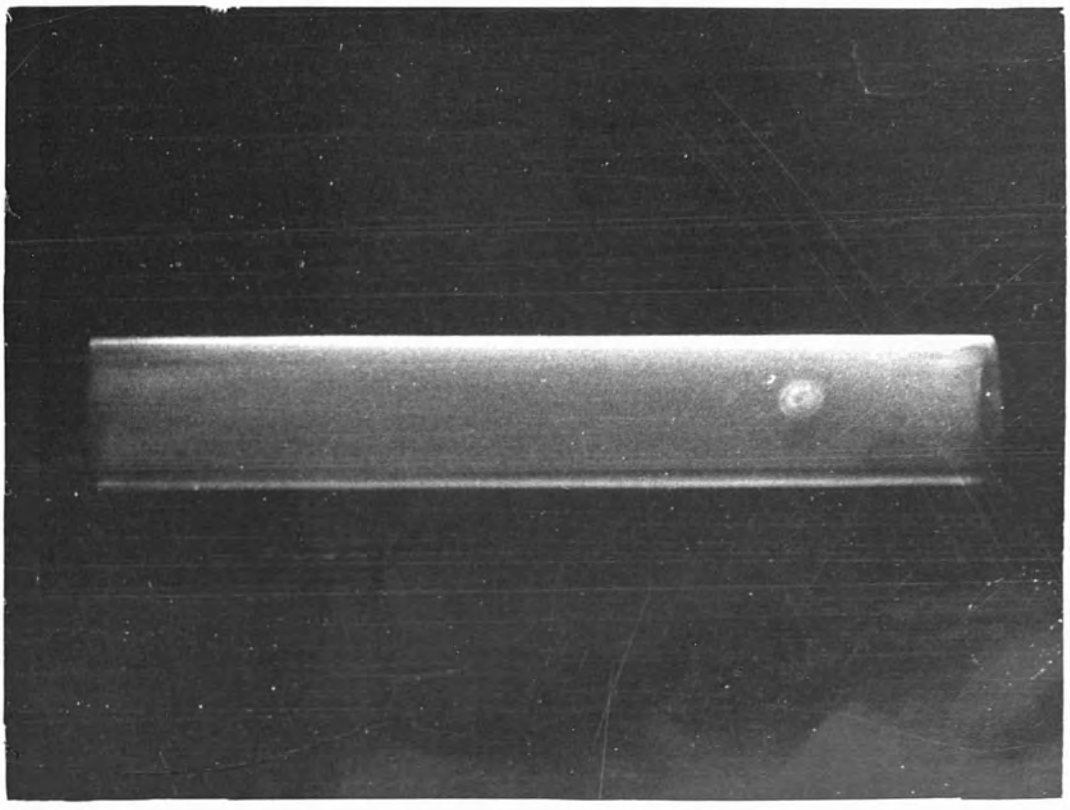

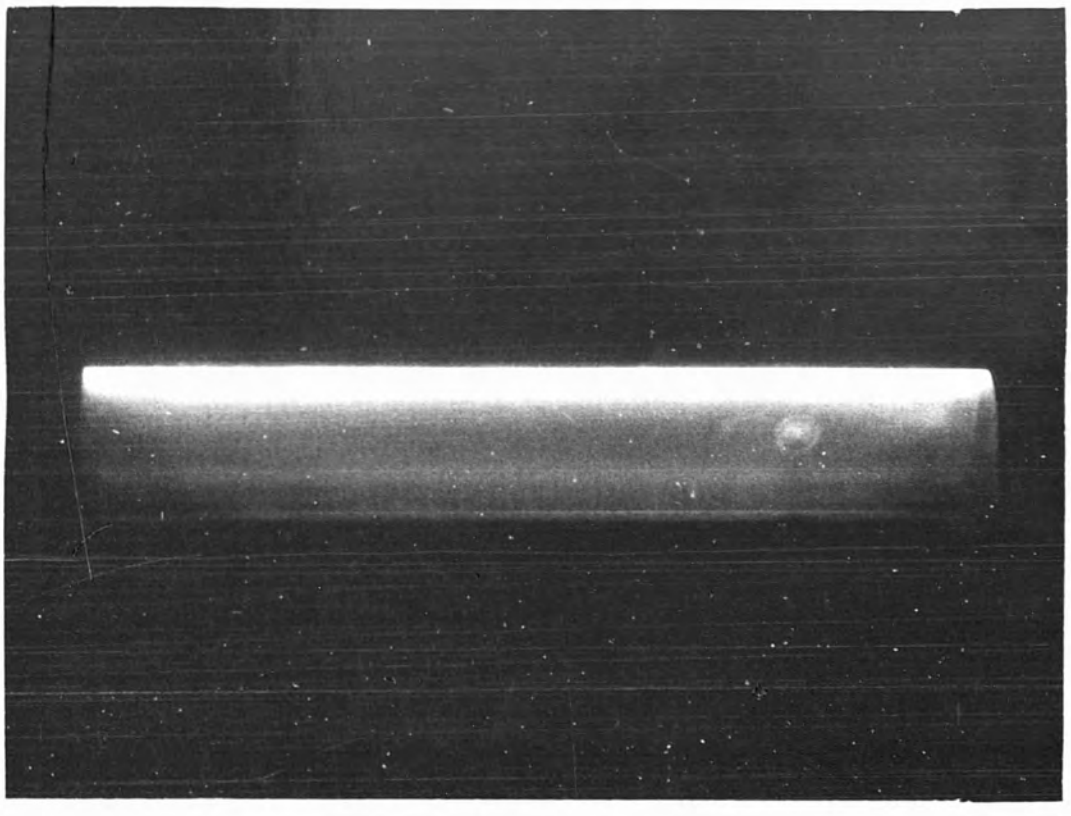

TEMPORAL CHARACTERISTICS OF THE OPTICAL OUTPUT(VISIBLE) FROM A 47cc UNCOATED COAXIAL FLASHTUBE AS FUNCTIONS OF PRESSURE

(660 Joules Input Electrical Energy)

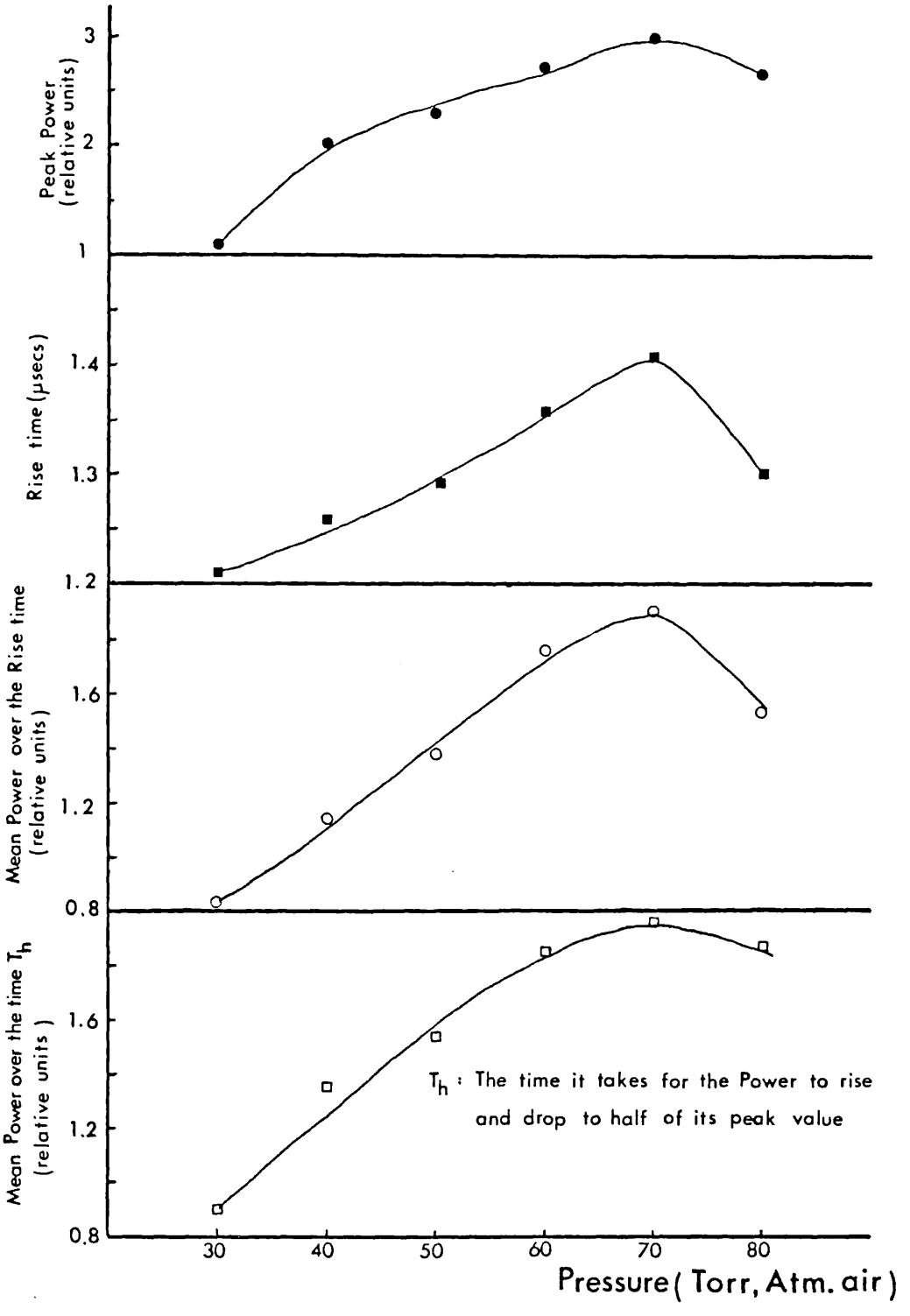

Fig. 5.5

as the pressure is increased. The half-width of the pulses varies from 1.6 μsecs (lower pressures) to 2.2 μsecs (higher pressures).

The graphs of Fig. 5.5 indicate that the best optical output, with regard to the criteria mentioned in the previous paragraph, corresponds to a pressure of ∿70 Torr or, if the strength of the electrical pulse is taken into account, to an E/p value of ∿40 Volts/cm.Torr; at this E/p value, the time-resolved optical output (Fig. 5.3e) consists of virtually a single pulse. In this experimental session, MARK 1 was not flashed many times at pressures higher than 80 Torr in order to avoid its premature shattering or any other damage. At a later stage of the course (pumping of iodine photodissociation laser), this flashtube - filled with Xenon - was flashed at E/p values as low as 10 Volts/cm.Torr and at pressures up to 210 Torr; but, during that stage, the flashtube was coated with the reflective material and was subjected to preionisation.

MARK 2 was always operated without any reflecting coat on its outer surface. The study of the optical output from MARK 2 - filled with atmospheric air - produced results similar to those of MARK 1. The gradual deterioration of the optical output from this flashtube with increasing number of flashes is discussed in the following sub-section.

The oscillograms of Fig. 5.6 give the time-resolved optical output from MARK 3 at various gas pressures. In this experimental session, the flashtube was filled with pure Xenon but, again, no reflectors were used on the outer surface of the flashtube. From this session onwards, the photodiode with the UV transmitting window was used. In order to reduce UV absorption by the atmospheric air, the photodiode was placed at a short distance from the flashtube (∿40 cm).

The first five traces of Fig. 5.6 correspond to an input electrical pulse of 42.5 KV peak voltage (or an energy of 360 Joules), while the

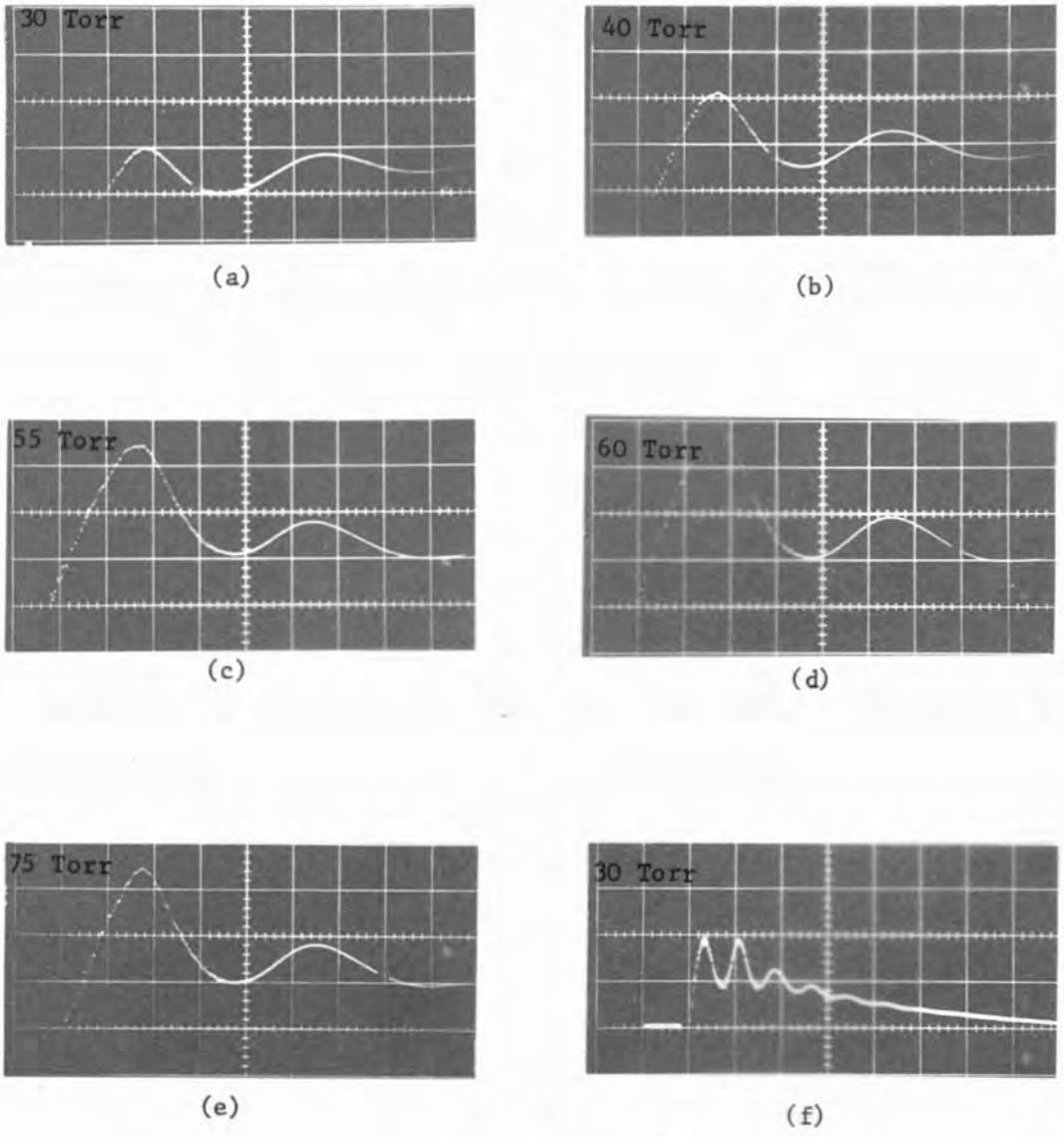

Fig. 5.6: Optical output profiles from MARK 3 at various pressures (Xenon).
First five traces: 42.5 KV pulse
Horiz. scale: 1 μsec/div.
Vert. scale: 0.1 Volt/div.

Last trace: 50 KV pulse
Horiz. scale: 5 μsecs/div.
Vert. scale: 0.1 Volt/div.

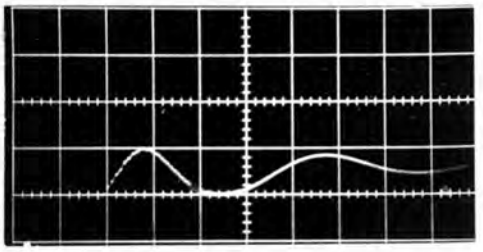

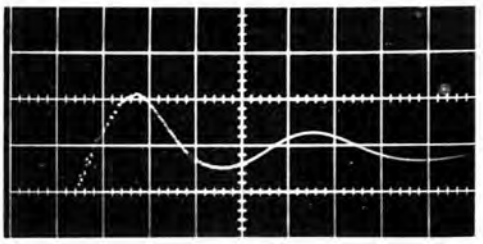

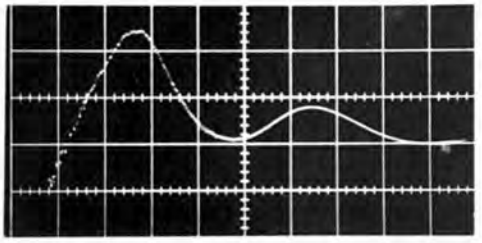

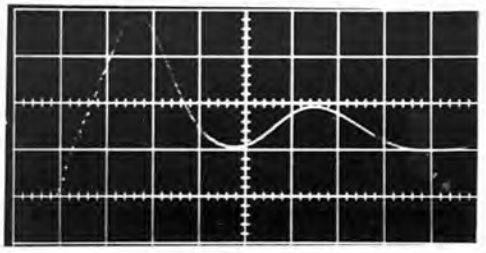

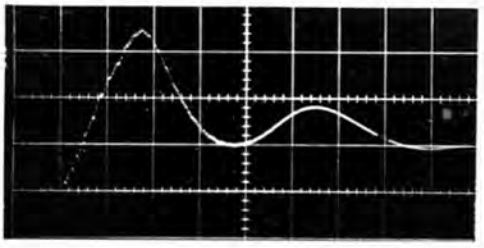

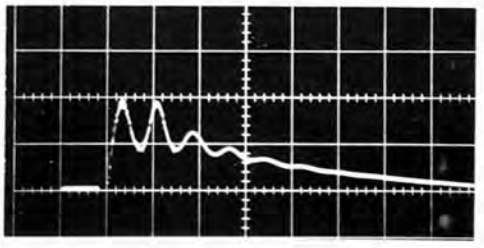

last trace - which was initiated externally - corresponds to a pulse of 50 KV peak voltage (500 Joules). Fig. 5.7 shows graphs of the temporal characteristics of the optical output from MARK 3 as functions of the gas pressure. Although these results display several similarities with those from MARK 1, the use of Xenon resulted in some differences in the shape of the output optical power, as the traces of Fig. 5.6 indicate. Thus the radiant energy is emitted in more than one pulse and the overall emission lasts longer. However, as the gas pressure is increased, the rate of increase of the first peak becomes far greater than the rates of increase of the second, third, etc. peaks. From the graphs of Fig. 5.7, it is concluded that the peak power of the optical output becomes maximum at an E/p value $\sim$35 Volts/cm.Torr. The last oscillogram of Fig. 5.6 shows that the delay between the triggering of the system and the optical output is $\sim$4 μsecs; given that this oscillogram was recorded in the early stages of the experimental session (when the system was clean), it is concluded that the delay of the external circuit was less than 4 μsecs for this particular session.

In the next experimental session, the optical output from MARK 4 was studied. After $\sim$300 flashes, a 1 mm thickness coat of EASTMAN white reflectance paint was applied to the outer surface of the flashtube, leaving only a strip 1 cm wide uncovered in the middle, so that the optical output could be detected. Previously, before the coat was applied, the optical output of the flashtube was detected through the same central area by covering all but the 1 cm wide strip with several layers of black cloth. In this way, comparison between the output optical powers from the uncoated and coated flashtube arrangements could be made.

The oscillograms of Figures 5.8, 5.9 and 5.10 illustrate power profiles of the optical output from MARK 4 (coated) at various gas pressures

TEMPORAL CHARACTERISTICS OF THE OPTICAL OUTPUT(VISIBLE+NEAR U.V.) FROM AN 81cc UNCOATED COAXIAL FLASHTUBE AS FUNCTIONS OF PRESSURE

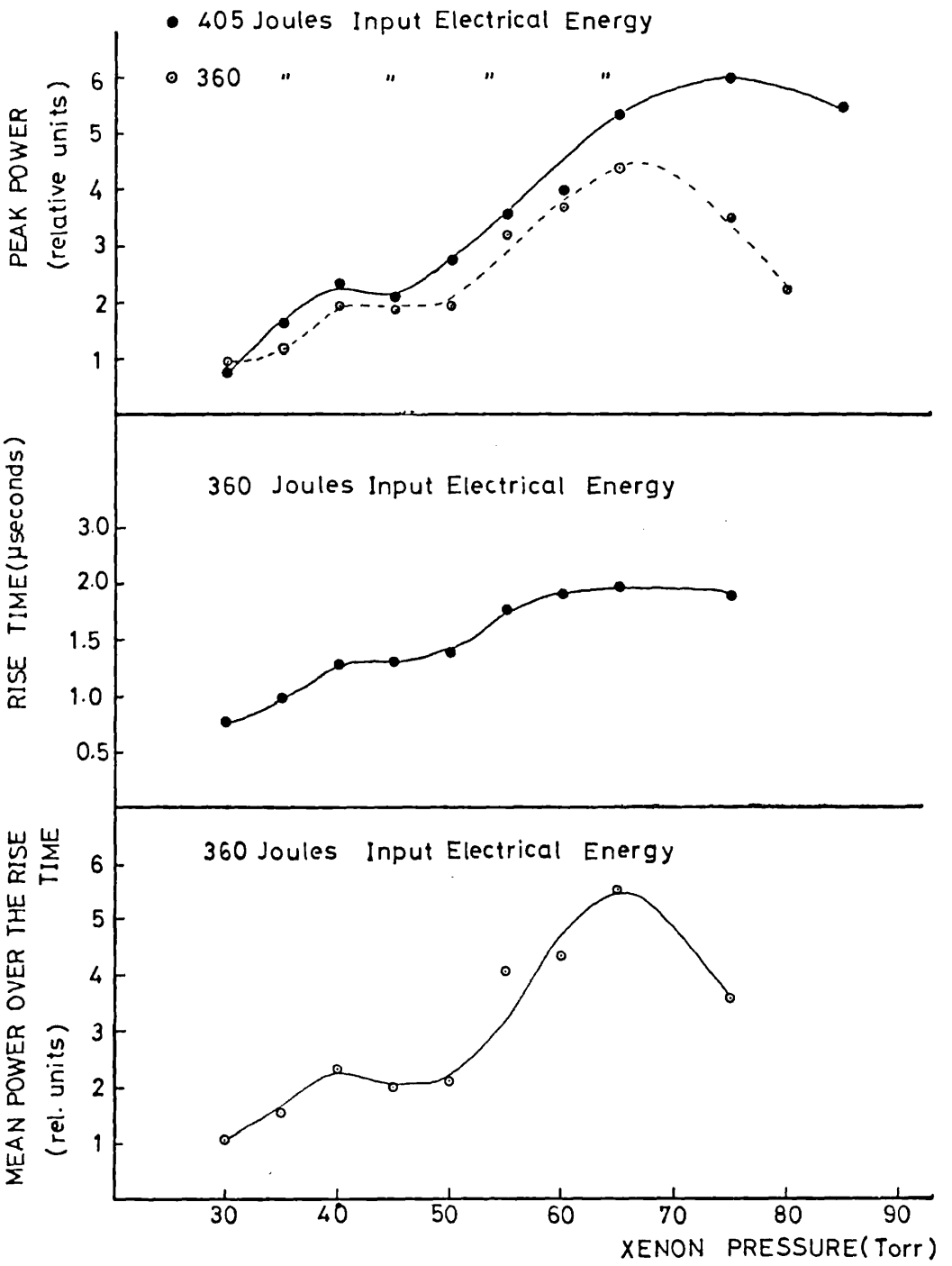

Fig. 5.7

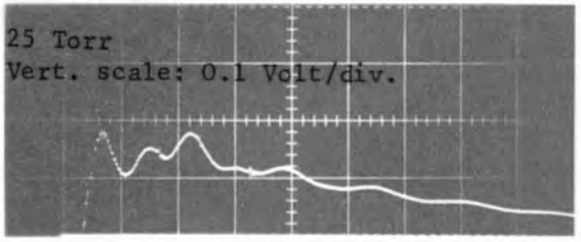

(a)

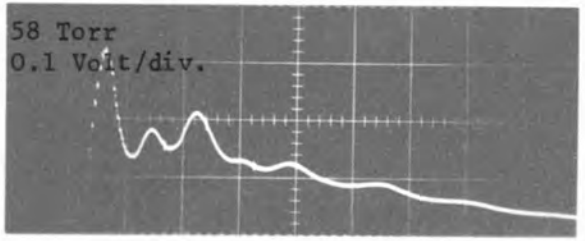

(b)

Fig. 5.8: Optical output profiles from MARK 4 at various pressures (Xenon).
Early results.
50 KV pulse.
Horiz. scale: 5 μsecs/div.

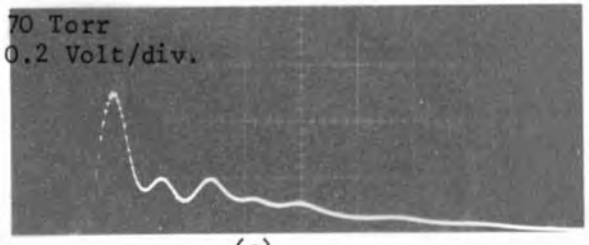

(c)

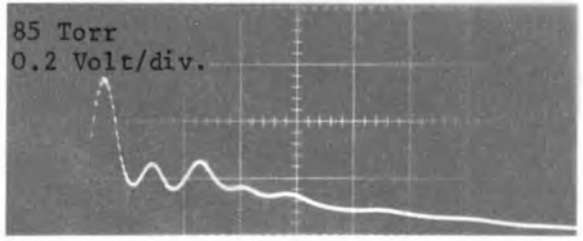

(d)

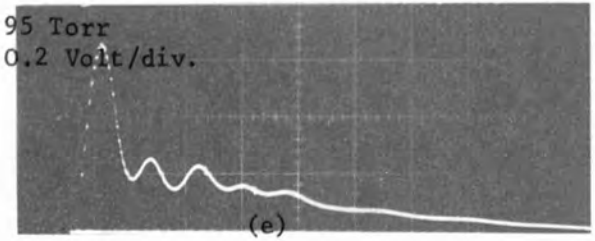

(e)

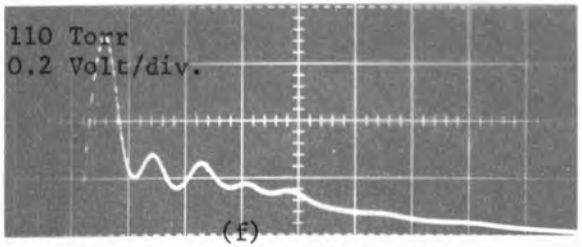

(f)


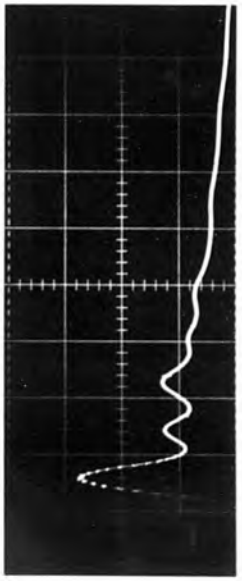
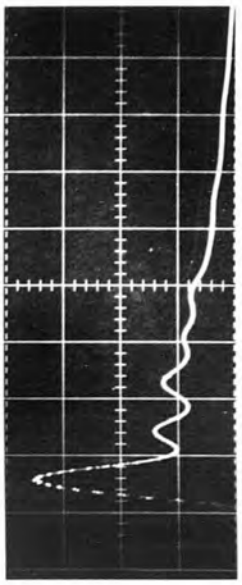
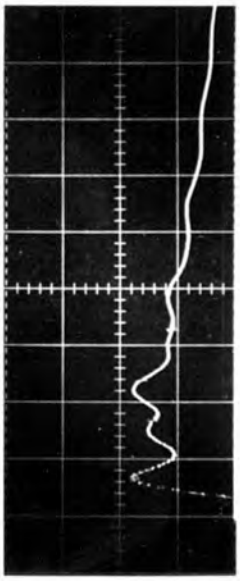

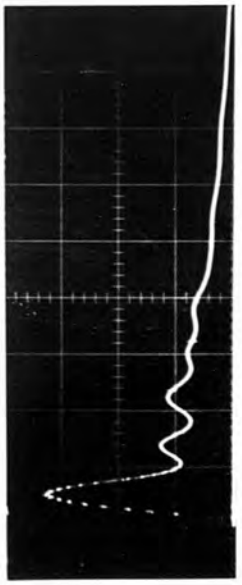

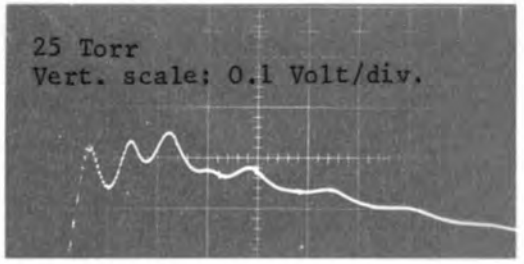

(a)

(b)

Fig. 5.9: Optical output profiles from MARK 4 at various pressures (Xenon).
Early results.
60 KV pulse.
Horiz. scale: 5 μsecs/div.

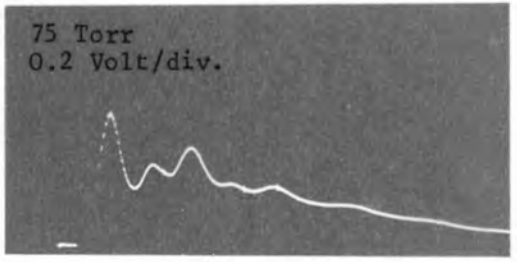

(c)

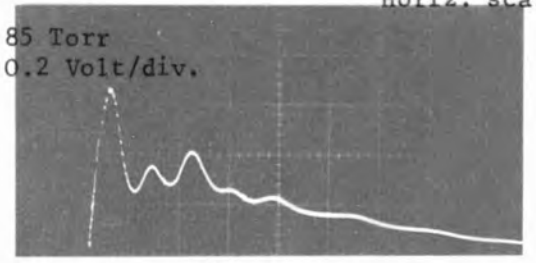

(d)

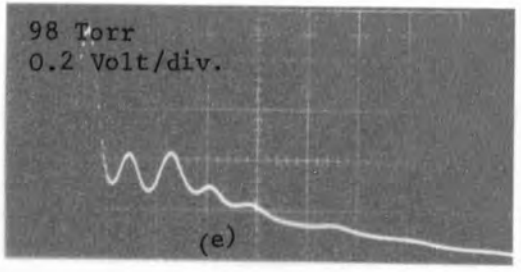

(e)

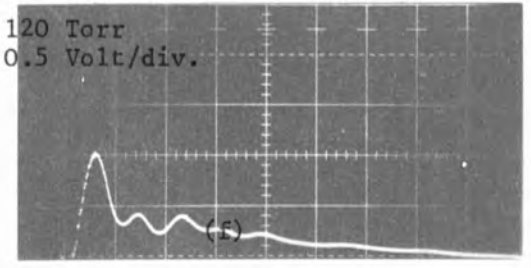

(f)


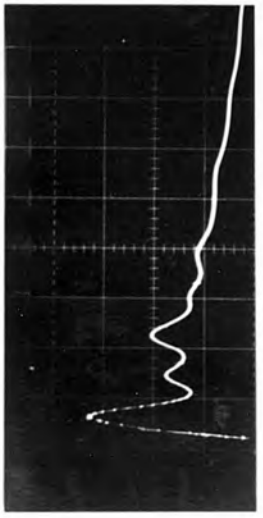
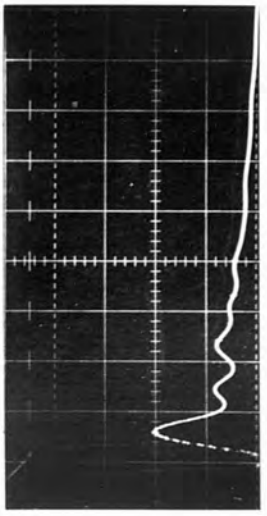
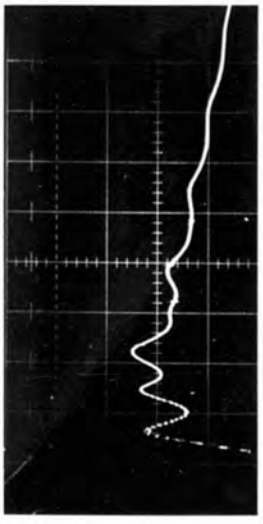

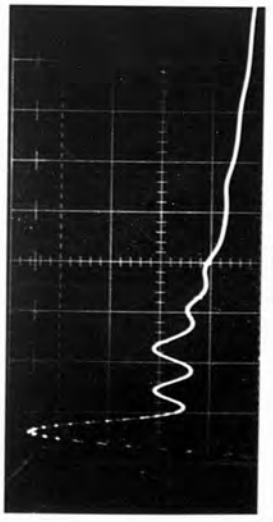

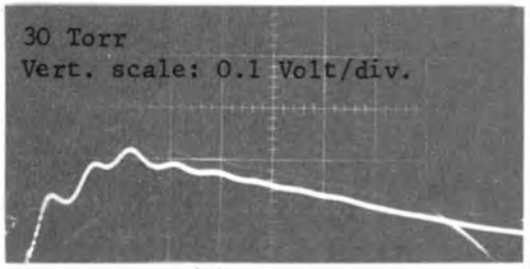

(a)

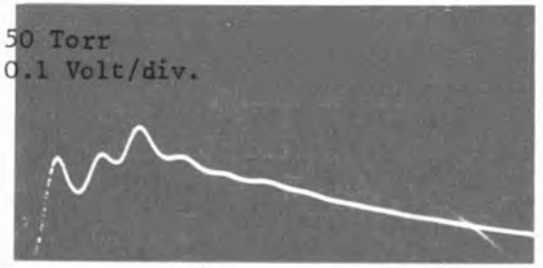

(b)

Fig. 5.10: Optical output profiles from MARK 4 at various pressures (Xenon).
Late results.
60 KV pulse.
Horiz. scale: 5 μsecs/div.

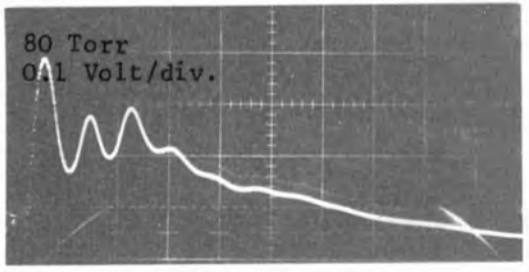

(c)

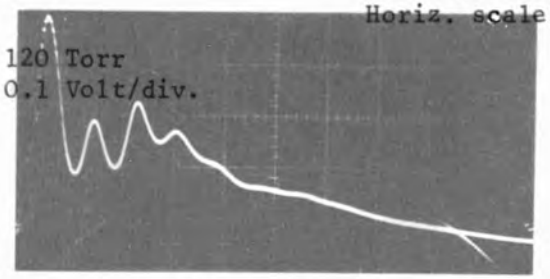

(d)

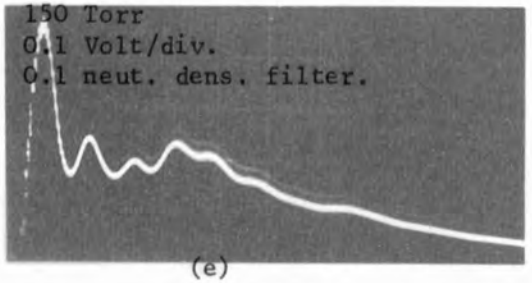

(e)

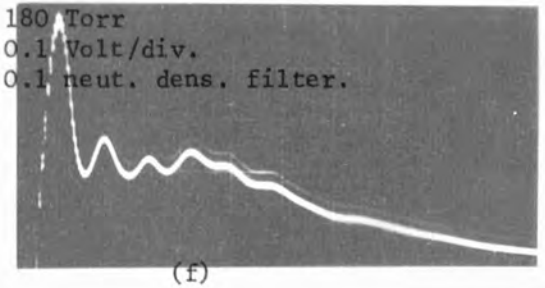

(f)

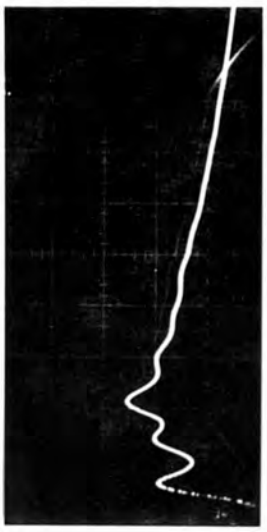
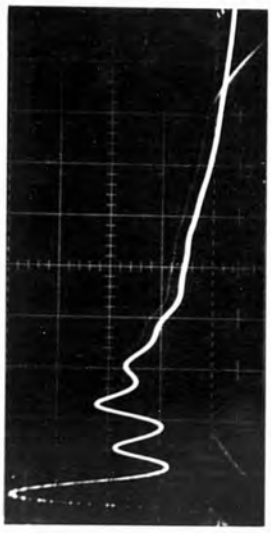

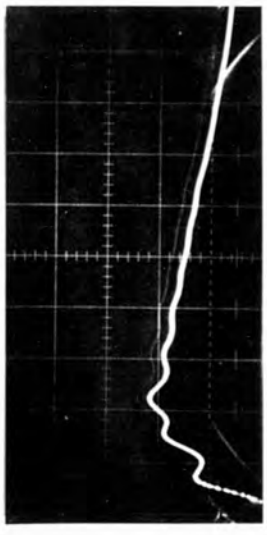
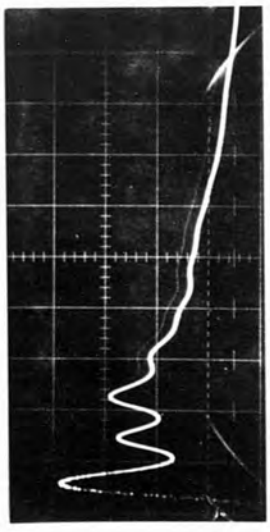


up to 180 Torr; the traces of Fig. 5.8 correspond to an input electrical pulse of 50 KV peak voltage (500 Joules energy), while the traces of Figures 5.9 and 5.10 correspond to a pulse of 60 KV peak voltage (720 Joules). For the first time in the course of this investigation it was possible to fire a flashtube at pressures higher than 80 Torr, without any sign of deterioration in the flashtube performance and - more importantly - without any sign of destruction. In fact, the flashtube performance improved in terms of its optical output; as Figures 5.8, 5.9 and 5.10 show, the luminous efficiency and peak power increase as the pressure is increased up to 180 Torr.

As was mentioned above, the traces of Figures 5.9 and 5.10 correspond to the same input electrical pulses. But it is apparent that certain quantitative and qualitative differences exist between the two sets of results. These differences are observed when comparison of the optical output profiles of flashes at the same E/p value is made, and they are due to the fact that the traces of Fig. 5.9 (and those of Fig. 5.8) are the results of an early session (when the flashtube was clean), while the traces of Fig. 5.10 refer to a later session (after $\sim 1.5 \times 10^4$ flashes). In the later session, observations of the voltage across the electrodes of the flashtube revealed a long delay between the arrival of the voltage pulse and breakdown, and a high jitter amplitude in this delay. These features explain the deteriorated quality of the optical output in Fig. 5.10. However, one common feature of the traces of Figures 5.8, 5.9 and 5.10 - irrespective of the stage of the experimental session at which they were recorded - is that the optical output improves with increasing pressure.

The top graph of Fig. 5.11 shows the pressure dependence of the relative peak power of the optical output from MARK 4, for both the uncoated and coated versions, and for two input electrical energies; the

TEMPORAL CHARACTERISTICS OF THE OPTICAL OUTPUT(VISIBLE + NEAR U.V.)
FROM A 74 cc COAXIAL FLASHTUBE AS FUNCTIONS OF PRESSURE

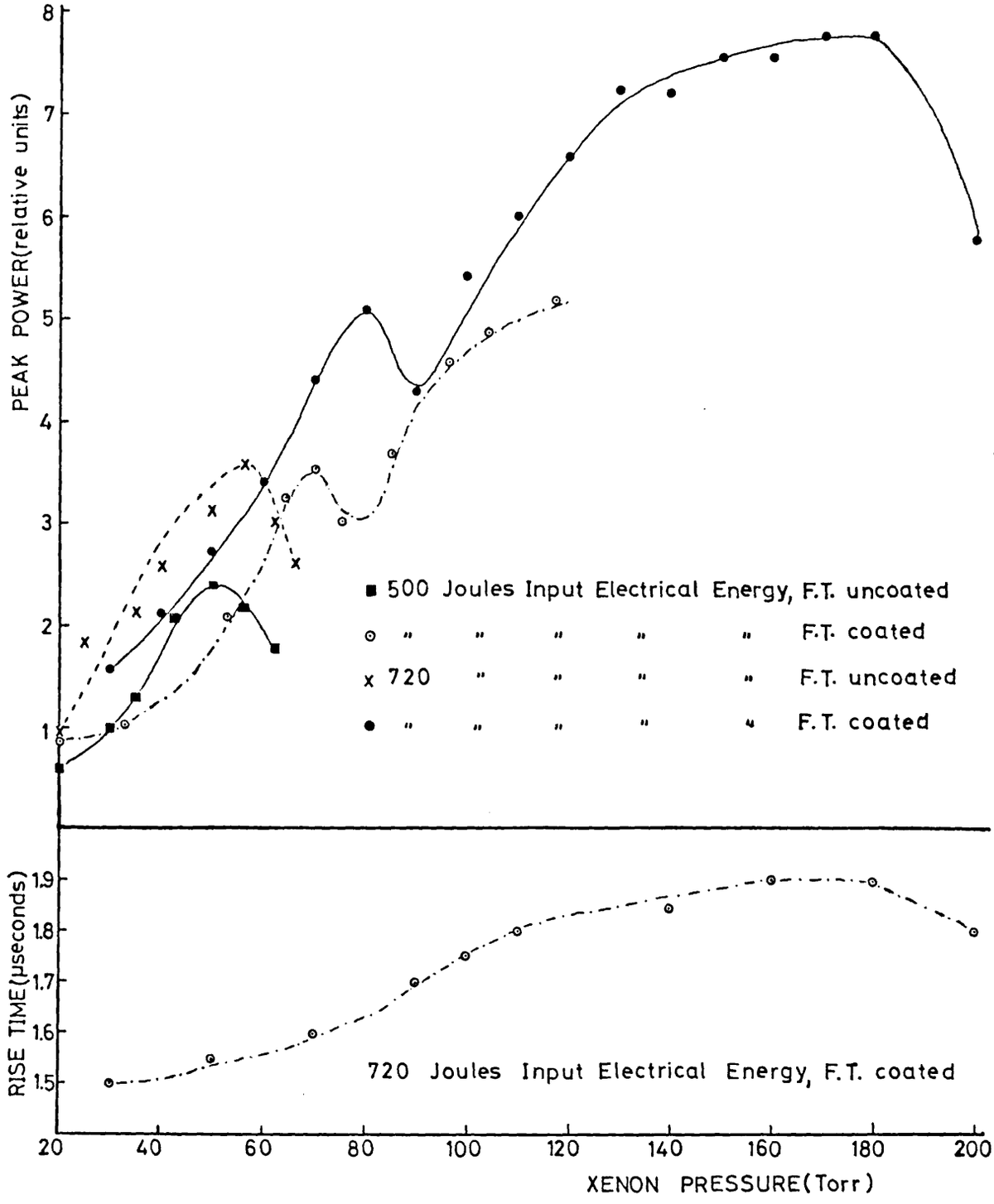

Fig. 5.11

bottom graph of Fig. 5.11 shows the variation of the rise time of the optical output with the gas pressure for the coated version at an input electrical energy of 720 Joules (no substantial variation of the rise time was observed when the flashtube was uncoated or subjected to different input electrical energies). It must be pointed out that in these graphs, the values of the relative peak power and the rise time correspond to the first pulse of the output profiles; in addition, the peak power curves for the coated version represent mean values which are obtained by taking into account results from both the early and late experimental sessions.

The peak optical power from MARK4, when no reflectors on its outer surface are used, becomes maximum at an E/p value ∿50 Volts/cm.Torr, whereas, when the flashtube is coated with the reflective material, the peak power becomes maximum at an E/p ∿17 Volts/cm.Torr. For E/p values below 17 Volts/cm.Torr (gas pressures > 180 Torr) a substantial drop in the peak power was observed. The apparent ability to operate the discharge system at high pressures (low E/p values) when reflectors are employed, together with the subsequent enhancement of the luminous efficiency of the flashes, are features attributed to further ionisation of the gas caused by the reflected light. Therefore, the results from MARK 4 appear to justify the theory stating that photoionisation contributes substantially towards breakdown in rare gas discharges (see sections 3.2 and 3.3). Moreover, the continuous increase of the peak power with increasing pressure, in the range between 80 to 180 Torr, indicates that, for pressures within this range, the discharges in the coated MARK 4 are uniform (observations of flashes from the uncoated MARK 4 proved that the discharges at pressures within this range are localised); these uniform discharges at high pressures can be explained on the grounds of

the strong photoionisation produced by the light reflected on the outer wall of the flashtube. Thus, it appears that there is ample evidence supporting the suggestion made by Furumoto and Ceccon[43] that photoionisation is the dominant mechanism in the discharge expansion in the case of coaxial flashtubes filled with rare gas (see sections 3.3 and 3.6).

5.2.2 Effects of the non-uniform (localised) type of discharge upon the quality of the optical output

The analysis of the experimental results carried out in the previous sub-section has demonstrated that the peak power of the optical output from coaxial flashtubes sustains a substantial decrease in the case of non-uniform discharges; as has been indicated in section 3.5, this decrease is explicable on the grounds of the higher flashtube inductance in such discharges. It has been shown that non-uniform discharges occur at high pressures (> 80 Torr) when the flashtube is uncoated.

As was mentioned in section 4.1, non-uniform discharges in uncoated coaxial flashtubes may also be evident at low pressures after a number of flashes, if the electrode sputtering is uneven around the flashtube walls. The gradual deterioration of the optical output from MARK 2 with increasing number of flashes is illustrated in the four oscillograms of Fig. 5.12. These oscillograms - taken with the 519 TEKTRONIX oscilloscope - correspond to flashes at the same input electrical energy (500 Joules) and the same pressure (40 Torr atmospheric air). The flashtube was operated without reflectors throughout the experimental session. The top trace of Fig. 5.12 was recorded at the beginning of the session when the flashtube was clean. The other traces, from top to bottom, were recorded after ∿400, 700 and 1000 flashes, respectively. The effects of the non-uniform discharges on

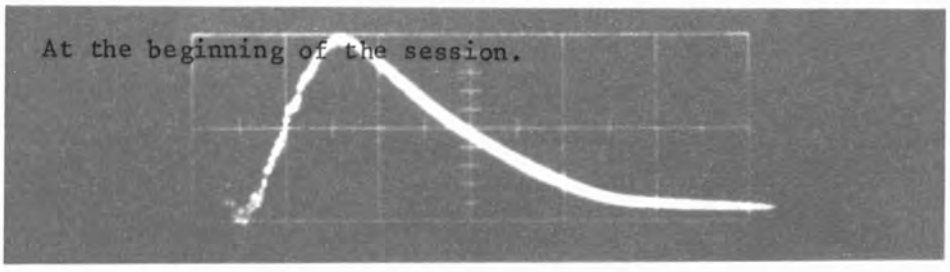

(a)

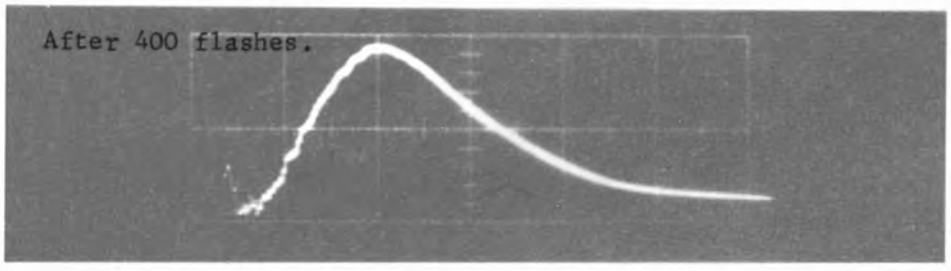

(b)

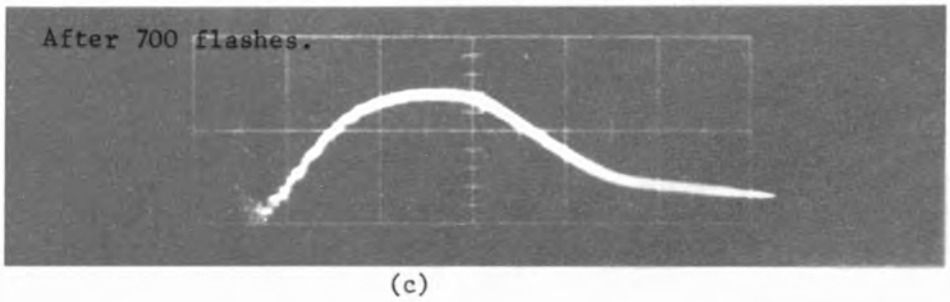

(c)

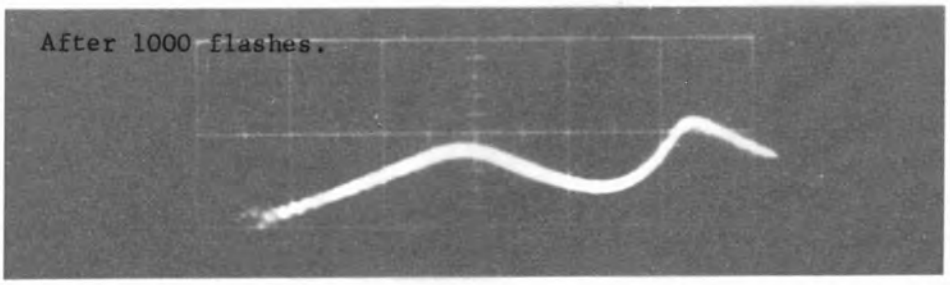

(d)

Fig. 5.12: The effects of non-uniform discharges on the quality of the optical output from a coaxial flashtube.
Optical output profiles from MARK 2 at various stages of the experimental session.
40 Torr atm.air. 50 KV pulse.
Horiz. scale: 1 μsec/div.

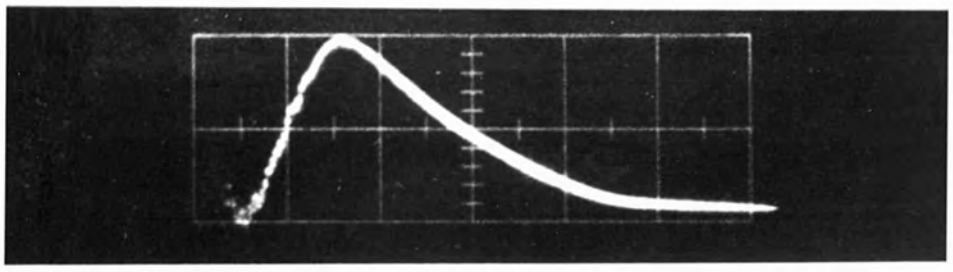

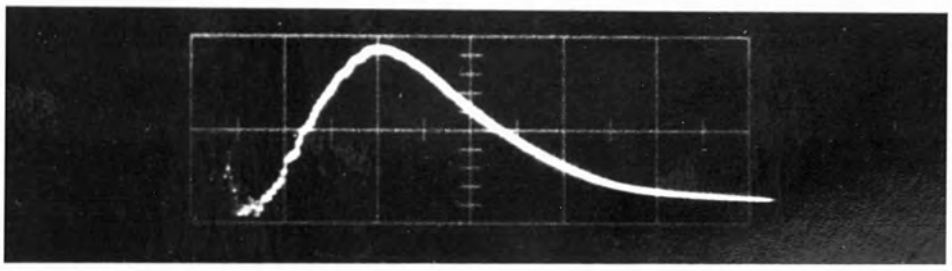

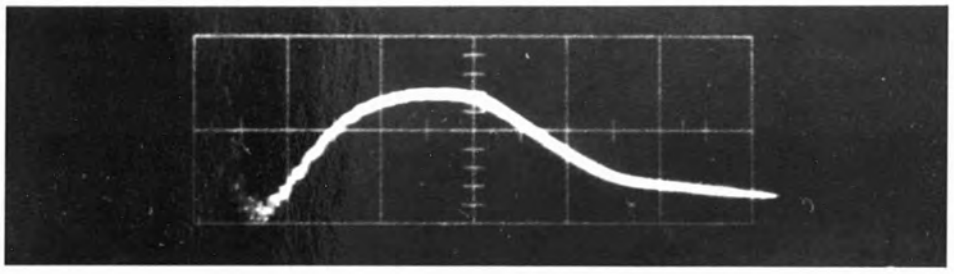

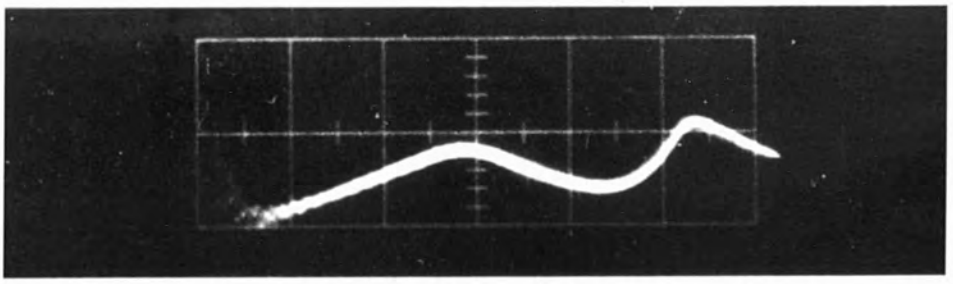

the peak power and the rise time of the optical output are evident. Visual observations of flashes by the end of the session revealed that the discharge consisted of virtually a single bright spark channel on one side of the annular section of the flashtube; it was found that the accumulation of metal - ejected from the electrodes - on the flashtube walls was most dense on this side of the section.

5.3 SPECTRAL CHARACTERISTICS OF THE FLASHTUBE SYSTEMS

5.3.1 Experimental study of the fluorescent output from flashtube excited dye solutions as a means of estimating the spectral response of the flashtube

The study of fluorescent outputs from dye solutions can offer useful information about the flashtube light lying within the principal absorption band of each solution, providing that the properties of the dyes used are well known.

Such a study usually consists of two parts. In the first part, the fluorescent output profiles are observed and recorded through the detecting apparatus (photodiode, oscilloscope); each of these profiles also represents the pulse shape of the exciting flashtube light for the particular spectral region (absorption band of the dye). In the second part, energy measurements of fluorescent outputs are taken by a calorimeter placed at a fixed distance from the dye cell; if the absorption and emission properties of the dyes involved are taken into account, these measurements can lead to the estimation of the spectral response (strength of the flashtube for each spectral region).

In order to compare the fluorescence results from various dye solutions, dyes having absorption curves of similar width and shape should be chosen; moreover, for convenience, dye solutions of equal optical density over

their absorption bands should be used, thus ensuring that the fraction of the incident light absorbed by the active medium is the same for all solutions. As is known, the optical density of a solution is defined as the dimensionless quantity $M\varepsilon x$ in the absorption expression

$$I/I_o = 10^{-M\varepsilon x} \qquad (5.2)$$

where I/I_o is the transmittance for an incident monochromatic beam of light after traversing a thickness x (cm) of solution, M is the concentration of the solution (in mole.litre^{-1}) and ε is the molar extinction coefficient; this coefficient depends on the wavelength of the incident light and varies from one dye to the other.

In experiments involving optical excitation of dye solutions, their optical density should be such that (a) the whole volume of the active medium is sufficiently irradiated and (b) most of the incident pump radiation is absorbed by the solution.

All conditions mentioned so far, together with the dimensions of the dye cell and the magnitude of the molar extinction coefficient of the dyes, averaged over their absorption bands, determine the concentrations of the dye solutions to be used. A cylindrical cell of 0.65 cm inside radius was used to contain the dye solutions. Table 5.1 gives details about the dye solutions used in this experimental session. Of the four dyes used, two belong to the Xanthene family and have their principal absorption band in the visible, while the other two are members of the Coumarin family and have their principal absorption band in the near UV. Coumarin 1 and Coumarin 4 are the adopted conventional names for 7-Diethylamino-4-methylcoumarin and 7-hydroxy -4-methylcoumarin, respectively. On the whole, the concentrations of these solutions were determined in order to satisfy the conditions mentioned above. Because

TABLE 5.1

Dye	Solvent	Molar Concentration	Principal Absorption band (Å)	Absorption λ_{max} (Å)	Fluoresc. λ_{max} (Å)	Fluoresc. quantum efficiency	References
Rhodamine 6G	Ethanol	2×10^{-5}	4600-5600	5300	5550	84%	15, 32, 36, 38, 39, 129
2',7' Dichloro-Fluorescein	Methanol	5×10^{-5}	4250-5400	5100	5300	~70%	38, 39, 130
Coumarin 1	Ethanol	10^{-4}	3000-4000	3650	4470	-	129, 130,131
Coumarin 4	Basic Distil. water	1.5×10^{-4} (plus 4×10^{-4} of NaOH)	3250-4100	3700	4450	65%	39, 129, 130 131, 132

Rhodamine 6G and 2', 7' Dichloro-Fluorescein on the one hand, and Coumarin 1 and Coumarin 4 on the other, absorb at about the same wavelengths, it can be said that in effect the fluorescence output measurements can reveal information about the spectral response of the flashtube in two wide spectral regions (blue-green and near UV).

When comparison of the fluorescence results from various dye solutions is made in order to find the relative amount of pump light absorbed in each spectral region, the fluorescence quantum efficiency of the dye solutions should be taken into account. In table 5.1 there is a separate column giving the quantum efficiencies of the solutions; these quantum efficiencies were measured by Snavely and Peterson[38] (Rhodamine 6G in Ethanol) and Snavely et al[132] (Coumarin 4 in basic water). There is no first hand data available for the quantum efficiencies of 2', 7' Dichloro-Fluorescein and Coumarin 1. However, as Sorokin et al[39] indicate, the dye 2',7' Dichloro-Fluorescein is much like Sodium-Fluorescein, whose quantum efficiency has been found[38] ~70%. Generally, dyes of the Coumarin family display lower quantum efficiencies in solutions than dyes of the Xanthene family.

At this stage it is appropriate to point out that the study of the fluorescence output from dyes gives only approximate estimations of the spectral response of a flashtube. This is the case because, apart from their principal absorption band, dyes absorb in other spectral regions towards the direction of the shorter wavelengths. In addition, when the profile of the pump light varies, the degree at which the fluorescence output from dyes changes may be different from one dye to the other; this can be explained by the fact that the rates of time-dependent processes, such as inter-system crossing, phosphorescence, etc (see section 2.2), vary from one dye to the other. However, these fluorescence experiments served another purpose in the present work - namely, the investigation of the

optimum conditions (optimisation of flashtube parameters such as gas pressure and E/p value) under which such a coaxial flashtube system could be used as a potential pump source for dye lasers.

In the last month of the course, when proper dielectric mirrors were obtained, attempts were made to achieve laser action from a solution of Rhodamine 6G pumped by MARK 3, but with limited success. A narrowing of the fluorescent output beam was observed a few times on a screen placed ∿1 metre from the output mirror, but even this pattern was not consistent, due to the lack of a device to circulate the dye solution, and therefore no useful measurements could be taken.

Throughout this experimental session, the coated version of MARK 3 was employed. (As a point of information, all results from now on involve coaxial flashtubes coated on their outer surface with EASTMAN reflectance paint.) In addition to Xenon and atmospheric air used so far, other rare gases - namely Krypton and Argon - were tried in the flashtube.

In the first part of this session, intensity profiles of the fluorescent output from dye solutions were detected by using the S-20 photodiode and the single beam oscilloscope. Figures 5.13 and 5.14 illustrate such fluorescent intensity profiles from a 2×10^{-5} M solution of Rhodamine 6G in Ethanol for Krypton, Argon, Xenon and atmospheric air flashtube fillings, at various pressures. Since the photodiode was always at a fixed distance from the flashtube, these oscillograms give the relative strength of the fluorescent outputs.

The graphs of Fig. 5.15 show the dependence of the peak intensity of the fluorescent output on the gas pressure and type. It is apparent that the rate at which radiant energy is emitted from the flashtube in the blue-green spectral region is greatest when the flashtube is filled with Xenon. The peak intensity of the fluorescent output - and therefore the peak power of the pump light in this spectral region - becomes maximum at

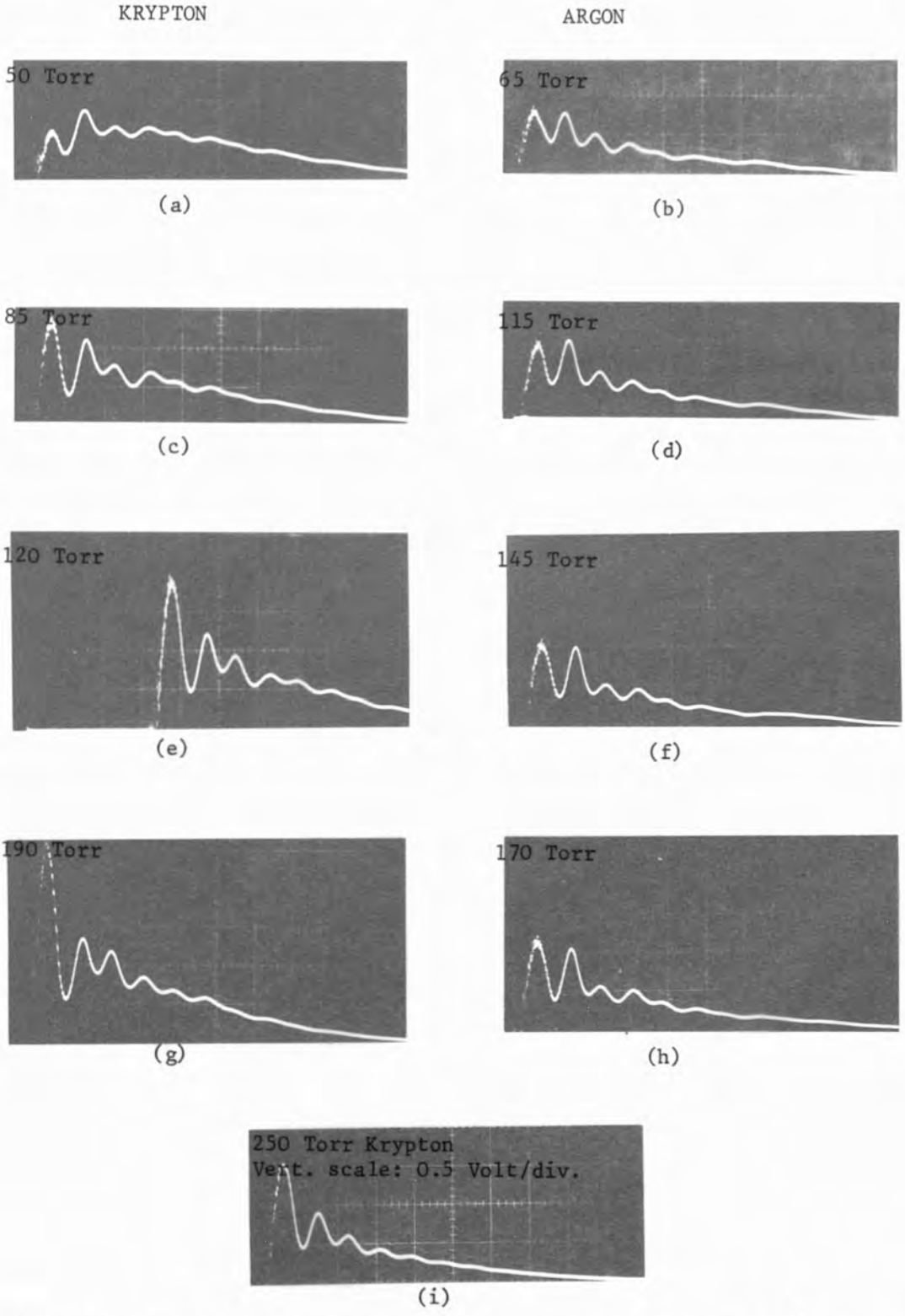

Fig. 5.13: Fluorescent output intensity profiles from a 2 x 10^{-5}M solution of Rhodamine 6G in Ethanol pumped by MARK 3.
Left column: Krypton in flashtube. Right column: Argon in flashtube.
720 Joules inp.Elec. Energy (60 KV pulse)
Horiz. scale: 5 μsecs/div.
Vert. scale (except bottom trace): 0.2 Volt/div.

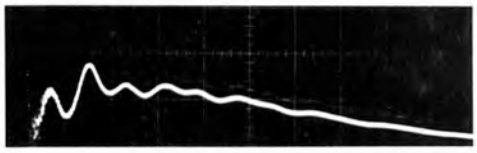

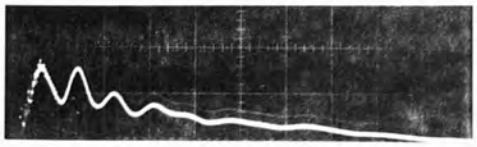

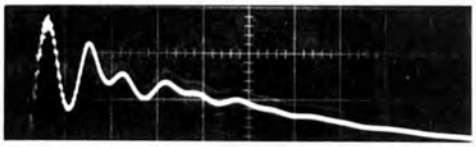

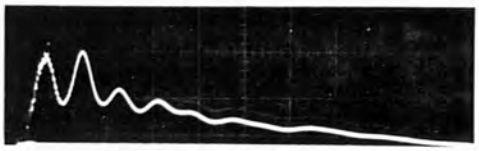

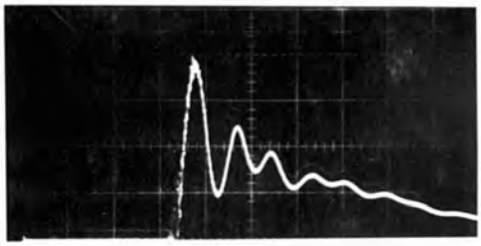

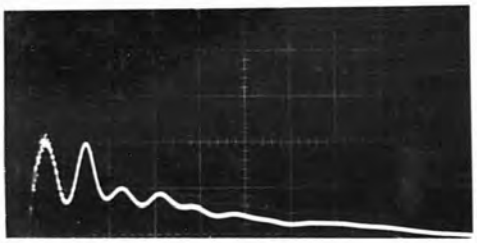

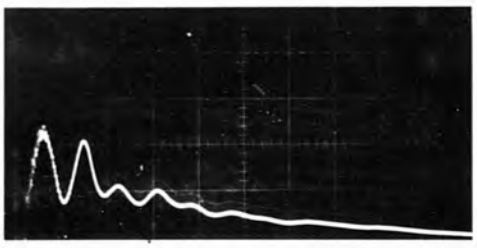

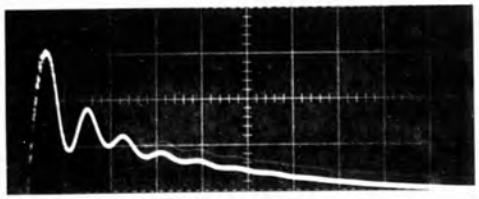

XENON

ATM. AIR

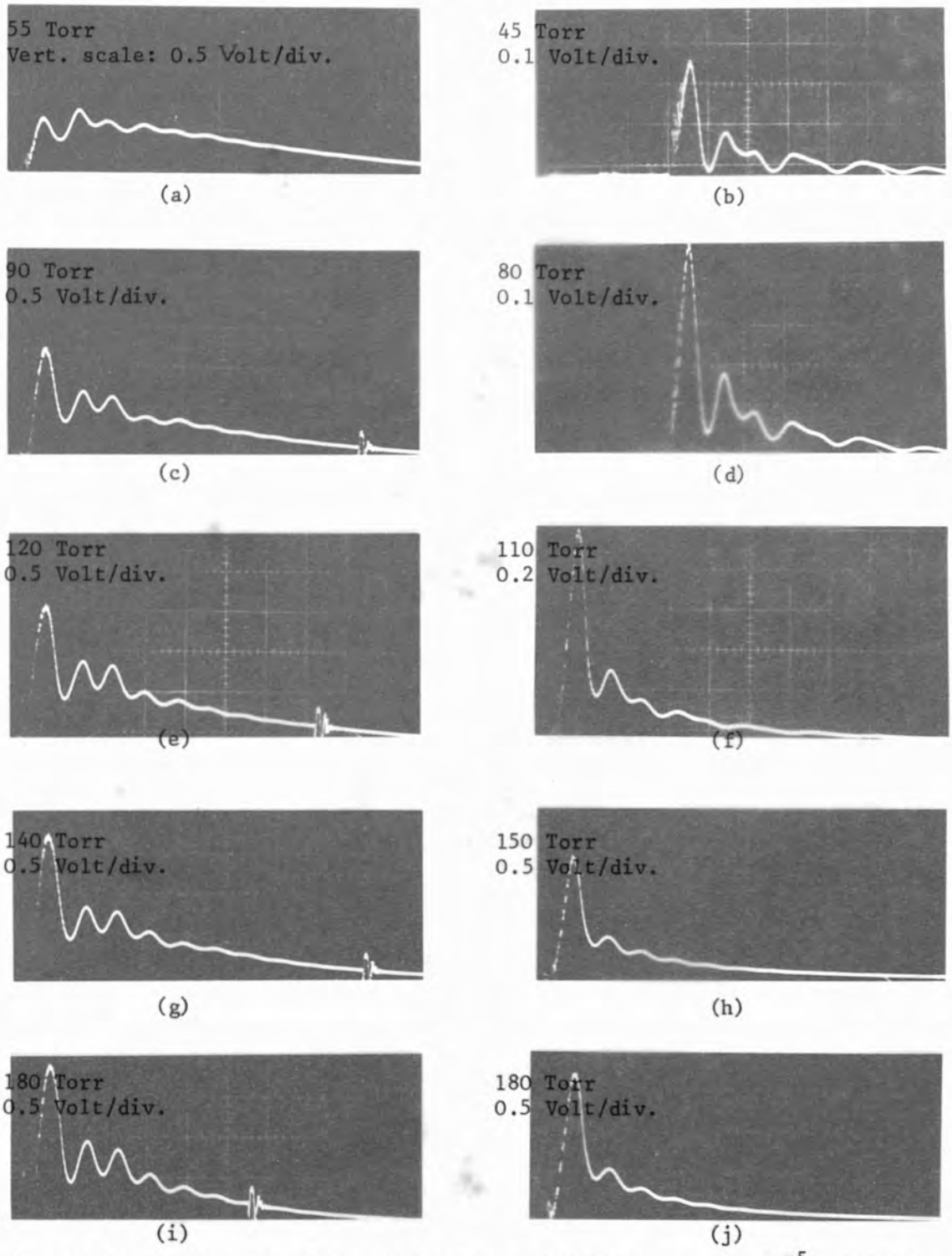

Fig. 5.14: Fluorescent output intensity profiles from a 2 x 10^{-5} M solution of Rhodamine 6G in Ethanol pumped by MARK 3.
Left column: Xenon in flashtube. Right column: Atm. air in flashtube.
720 Joules inp. Elect. Energy (60 KV pulse)
Horiz. scale: 5 μsecs/div.

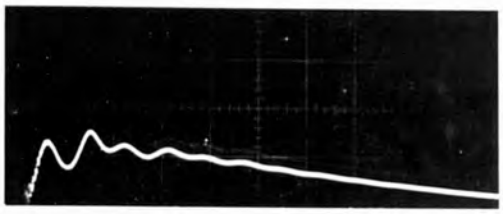
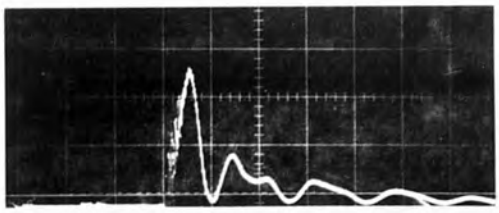
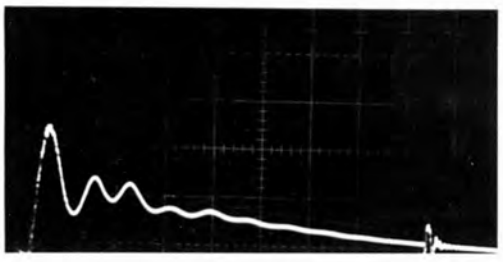
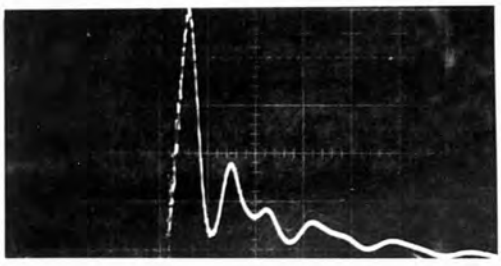
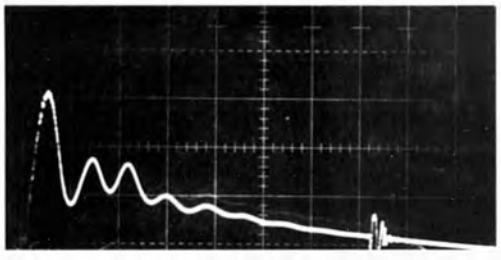
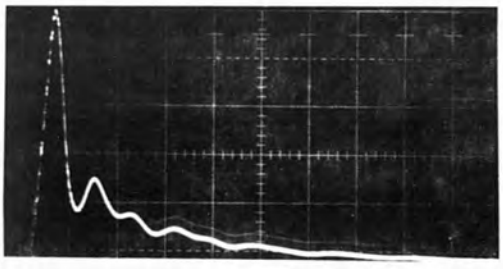
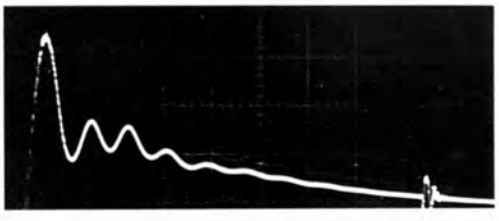
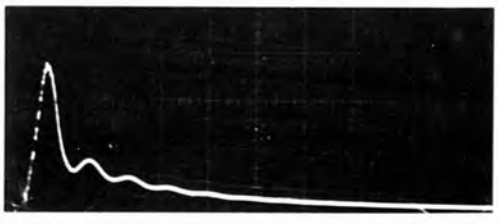
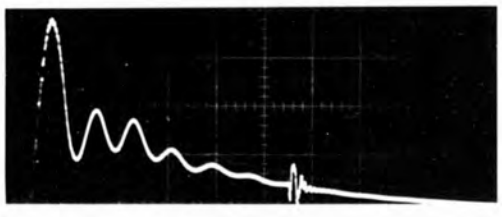


a pressure ∿170 Torr (or at an E/p value ∿20 Volts/cm.Torr).

Looking at the oscillograms of Figures 5.9 and 5.10 on the one hand, and those of Figure 5.14 (left column) on the other, one finds that the shape of the output optical pulse from a coaxial flashtube in the spectral region from 4600Å to 5600Å is virtually the same as the shape of the overall optical pulse from 2000Å to 7000Å. Moreover, comparison of the graphs of Figures 5.11 and 5.15 (in the case of Xenon) indicates that the variation with gas pressure of the peak powers of the partial and overall optical outputs from a coaxial flashtube is practically the same.

In another experiment, oscilloscope observations of the fluorescent output from a 1.5×10^{-4} M solution of Coumarin 4 in basic water were made; the solution was pumped by MARK 3, again filled with Xenon. It was found that the shape and variation (with time) of the optical output from the flashtube in the spectral region from 3250Å to 4100Å resembled the shape and variation of the overall optical output. However, the peak power of the pulse in the near UV region was found greater than the peak power in the blue-green region; as will be seen below (Fig. 5.16) this feature is due to the higher spectral (luminous) efficiency displayed by the flashtube in the near UV region.

From Figure 5.15 it is observed that, with atmospheric air in the flashtube, the output optical pulse of the discharges is fairly fast; but a more detailed study of the relevant oscillograms (right hand side of Fig. 5.14) indicates that the overall luminous efficiency of such discharges is low (this is confirmed from energy measurements of the fluorescent output; see Fig. 5.18).

It was found that when the flashtube was filled with Krypton, the shock-wave noise was substantially reduced compared to the noise produced in other gas discharges (the sharpest shock-wave noise was produced when the

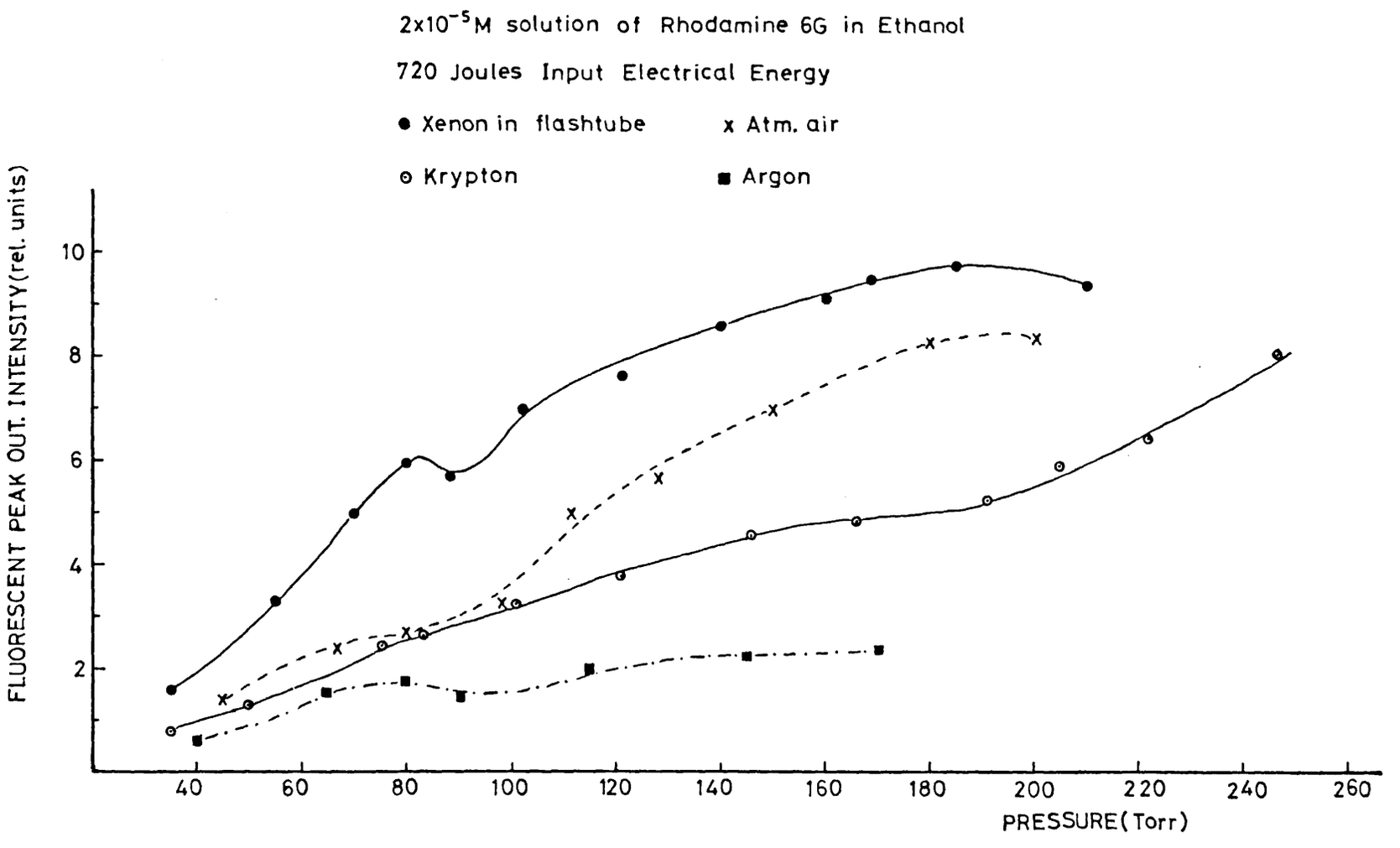
2x10⁻⁵M solution of Rhodamine 6G in Ethanol
720 Joules Input Electrical Energy
● Xenon in flashtube
x Atm. air
⊙ Krypton
■ Argon
FLUORESCENT PEAK OUT. INTENSITY(rel. units)
10
8
6
4
2
40
60
80
100
120
140
160
180
200
220
240
260
PRESSURE(Torr)

Fig.5.15

flashtube was filled with atmospheric air). Because of this feature, it was possible to operate the Krypton filled flashtube at higher pressures (lower E/p values). Figure 5.15 indicates that the relative peak power of the optical output of Krypton discharges takes on high values for pressures >180 Torr and that it increases at a fairly high rate with increasing pressure; in fact, for pressures ~250 Torr (E/p values ~ 12 Volts/cm.Torr), the peak optical power of Krypton discharges matches that of Xenon discharges. As can be seen from the oscillograms of Fig. 5.13 (right column) and the bottom graph of Fig. 5.15, the peak power and the overall quality of the optical output from Argon discharges are far inferior to those from discharges in the other gases used.

During the second part of this experimental session, relative energy measurements of fluorescent outputs from the dye solutions listed in Table 5.1 were made by placing the calorimeter at a fixed position close to the end of the dye cell. These fluorescent energy outputs represent measures of the proportion of flashtube radiant energy emitted in the absorption bands of the various dyes or, in other words, the luminous efficiency of the flashtube in these bands.

The graphs of Fig. 5.16 show the variation of the fluorescent energy output with gas pressure in the flashtube and for four different solutions. All these graphs correspond to the same input electrical energy in the flashtube and therefore, for a fixed gas pressure, to the same optical output from the flashtube. It is evident that at higher gas pressures (>60 Torr), the fluorescent energy output from Rhodamine 6G is higher than the corresponding outputs from the other dyes. In fact, for pressures higher than ~50 Torr, the fluorescent energy output from Rhodamine 6G is, on average, about 12% stronger than the fluorescent energy output from

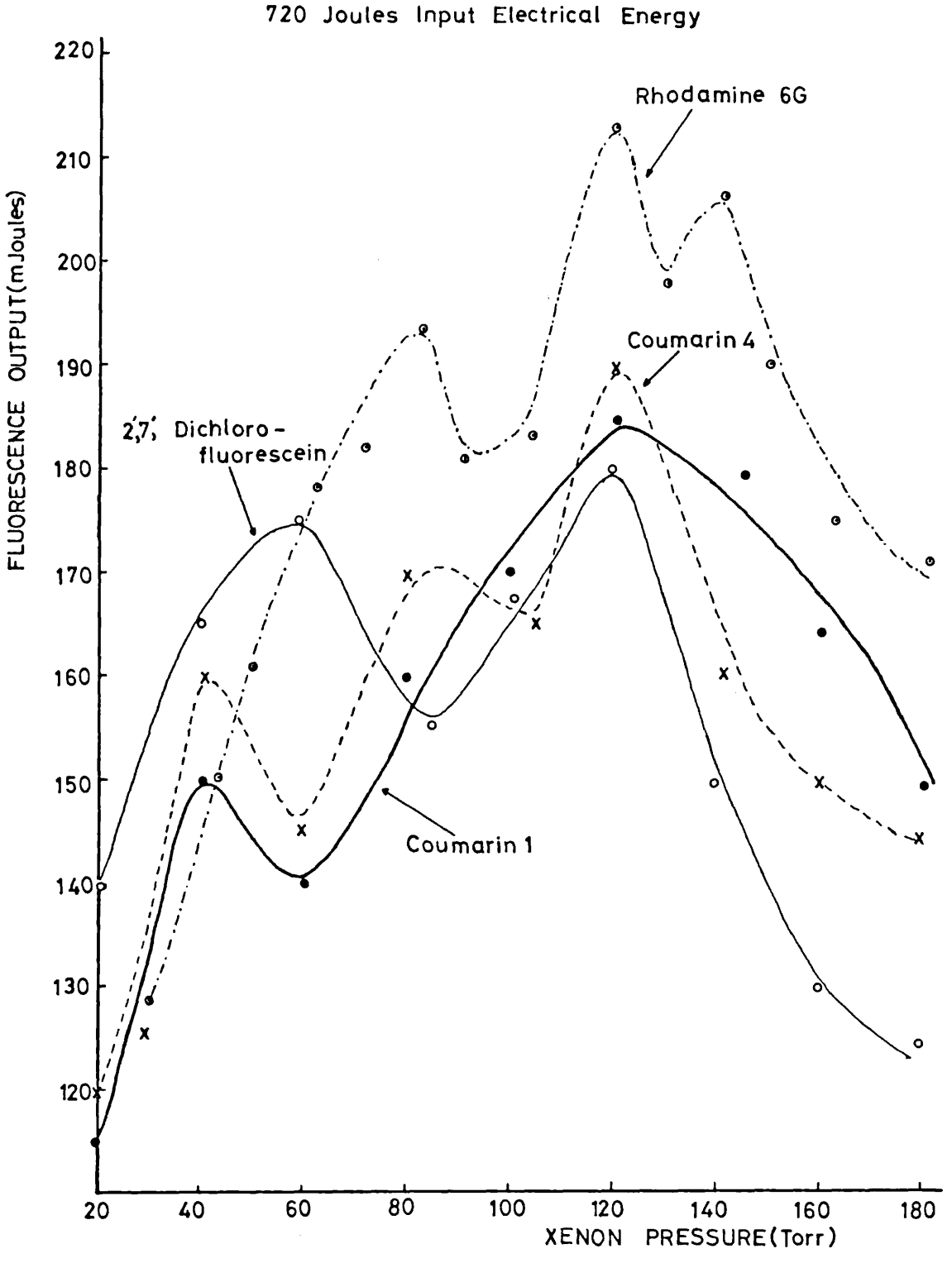
720 Joules Input Electrical Energy
FLUORESCENCE OUTPUT(mJoules)
220
210
200
190
180
170
160
150
140
130
120
Rhodamine 6G
Coumarin 4
2,7, Dichloro-
fluorescein
Coumarin 1
20
40
60
80
100
120
140
160
180
XENON PRESSURE(Torr)

Fig. 5.16

Coumarin 4. However, in order to compare the relative radiant energy outputs from the flashtube in the two spectral regions, one must take into account the fluorescence quantum efficiencies of the dyes involved (see Table 5.1). Normalisation of the fluorescent outputs from the two dyes shows that, at higher gas pressures, the average radiant energy emitted from the flashtube in the near UV spectral region (3250$\mathring{A}$ - 4100$\mathring{A}$) is ∿15% higher than that emitted in the blue-green region (4600$\mathring{A}$ - 5600$\mathring{A}$). Such normalisation is achieved by multiplying the fluorescent energy output from Coumarin 4 by a factor equal to the ratio of the fluorescence quantum efficiencies of the dyes: $\frac{84}{65} \simeq 1.3$.

If the same analysis is made for the fluorescent energy outputs from the two dyes (Rhodamine 6G and Coumarin 4) for pressures in the flashtube <50 Torr (Fig. 5.16), it is obtained that the ratio of flashtube radiation in the near UV region to that in the blue-green region increases with decreasing pressure. It is found that, on average, the radiant energy emitted in the near UV region is ∿40% higher than that emitted in the blue-green region. This feature is the result of the increased electron temperatures of the discharges when the E/p value is increased; it has been shown in section 3.4 that the higher the electron temperature, the more efficient the flashtube spectrum becomes towards the direction of the shorter wavelengths.

The graphs of Figure 5.17 give the variation of the fluorescent energy output from Rhodamine 6G with gas pressure in the flashtube and for three different input electrical energies. Note that in both Figures 5.16 and 5.17 the fluorescent energy outputs from dye solutions become maximum for an E/p value in the flashtube ∿28 Volts/cm.Torr.

Finally, Fig. 5.18 shows graphs of the fluorescent energy output from Rhodamine 6G plotted against the gas pressure in the flashtube for the four types of gas used in this work. It is evident that Xenon filled

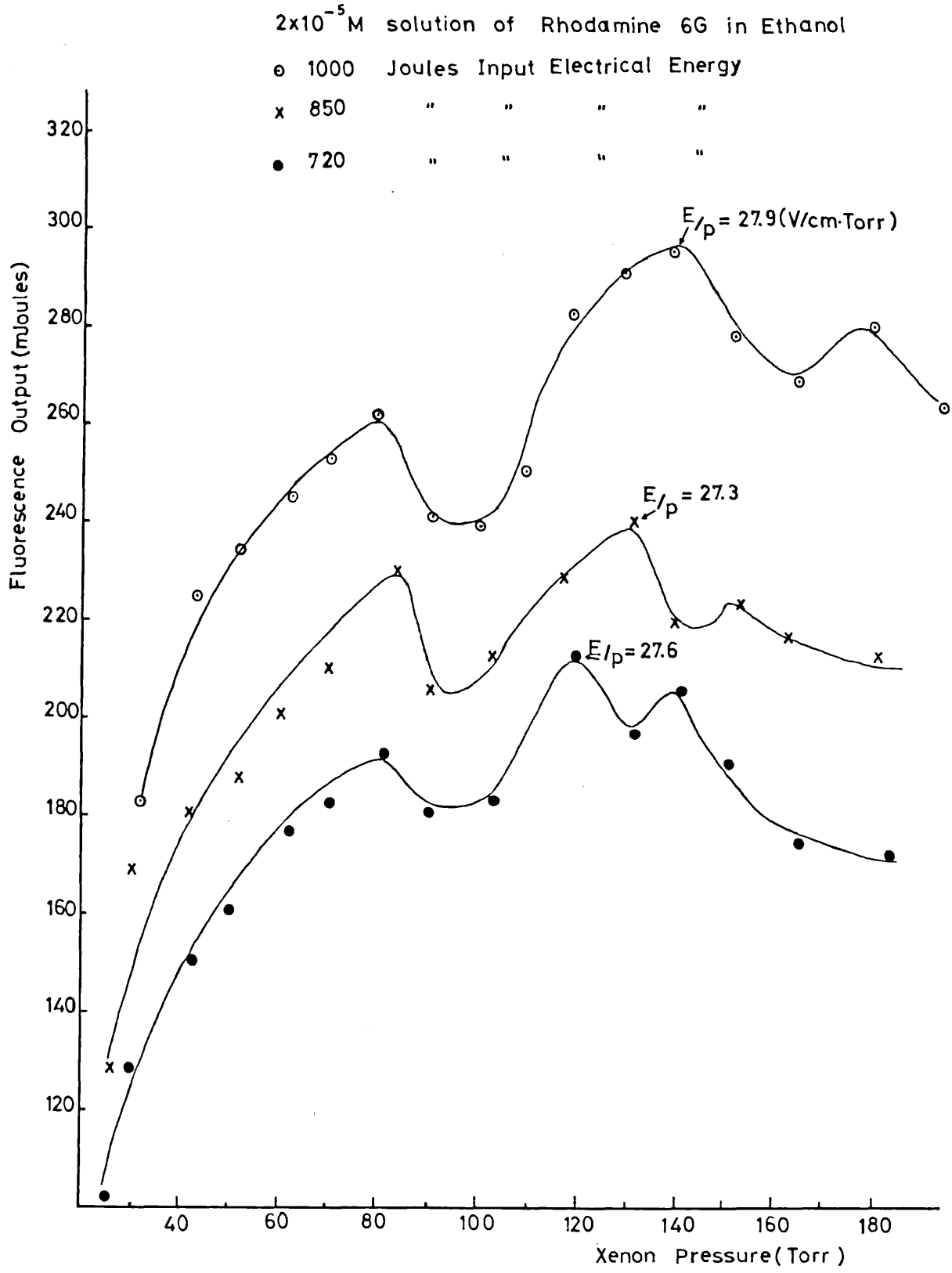
2x10⁻⁵M solution of Rhodamine 6G in Ethanol
⊙ 1000 Joules Input Electrical Energy
x 850 " " " "
● 720 " " " "
E/p = 27.9(V/cm·Torr)
E/p = 27.3
E/p = 27.6
Fluorescence Output (mJoules)
320
300
280
260
240
220
200
180
160
140
120
40
60
80
100
120
140
160
180
Xenon Pressure(Torr)

Fig. 5.17

$2x10^{-5}M$ solution of Rhodamine 6G in Ethanol

720 Joules Input Electrical Energy

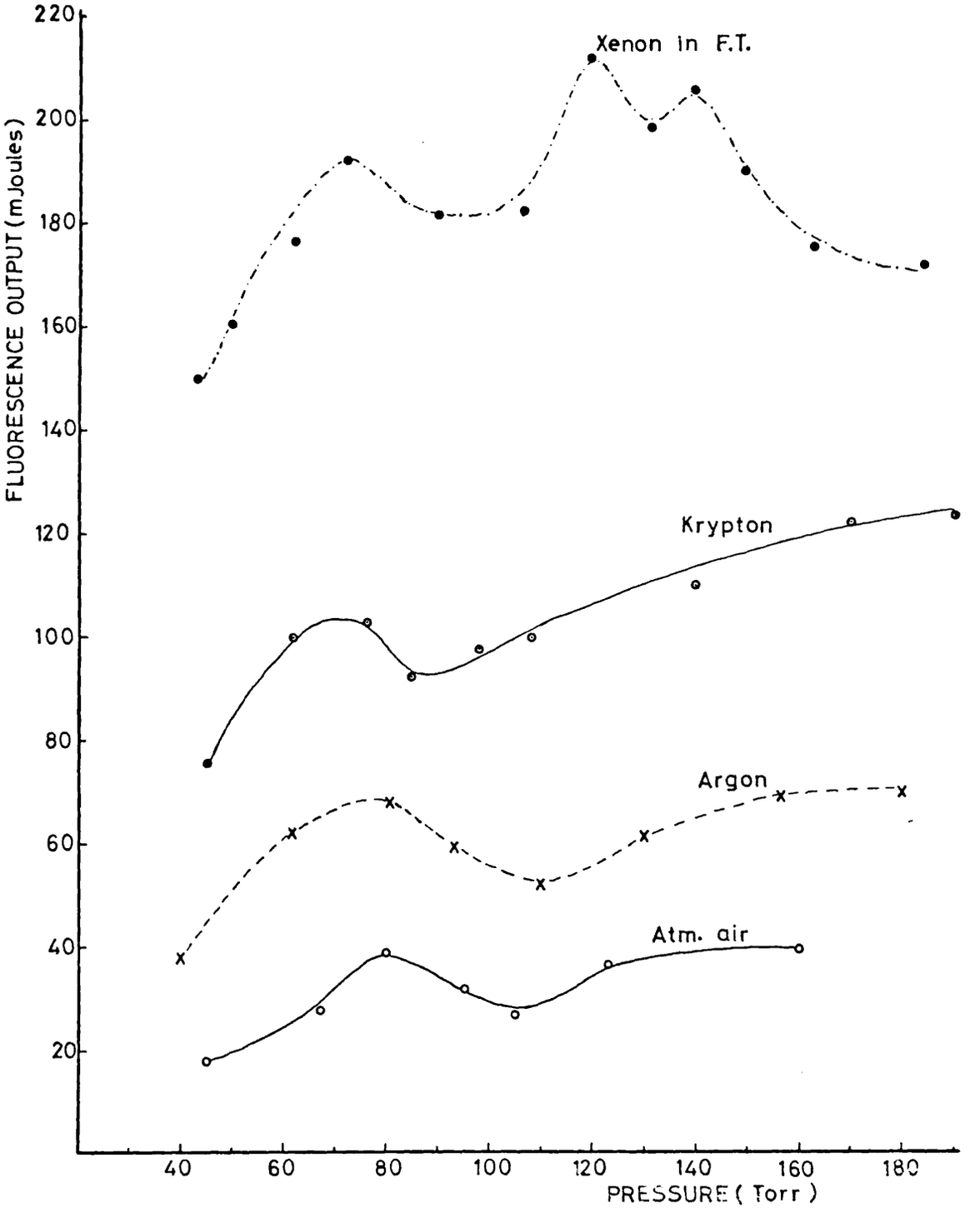

Fig. 5.18

flashtubes display the highest luminous efficiency in the visible spectral region.

5.3.2 Near UV and visible emission spectrum of a Xenon filled coaxial flashtube

The spectral distribution of the optical output from MARK 4 in the near UV and visible regions was measured by a quartz medium spectrometer (such a spectrometer has quite good resolution in the near UV, but it does not resolve properly line spectra in the visible). Emission spectra of several flashtube discharges were recorded on HP3 Panchromatic plates (see section 4.4) whose spectral sensitivity extends from 2300Å - 6500Å.

Fig. 5.19 shows the emission spectrum of MARK 4 filled with Xenon at two different E/p values, but at the same input electrical energy. The two traces of Fig. 5.19 correspond to recordings made on the same plate and give the relative intensity of flashtube light as a function of the wavelength. The strong lines observed in the UV are attributed[133,134] to optical transitions of singly and doubly ionised Xenon atoms whose population is large in such high current density discharges (see sections 3.3 and 3.4).

From Fig. 5.19 it is observed that both the continuum and the line spectrum of the flashtube are more intense in the case of the lower E/p value, thus confirming the theory that the luminous efficiency of a discharge increases when the E/p value is decreased. It is also observed that the fractional increase of the continuum becomes higher towards the direction of the longer wavelengths. Therefore, it is concluded, once again, that the reduced parameter E/p of a discharge determines, to a great extent, the intensity and the 'colour' of the optical output.

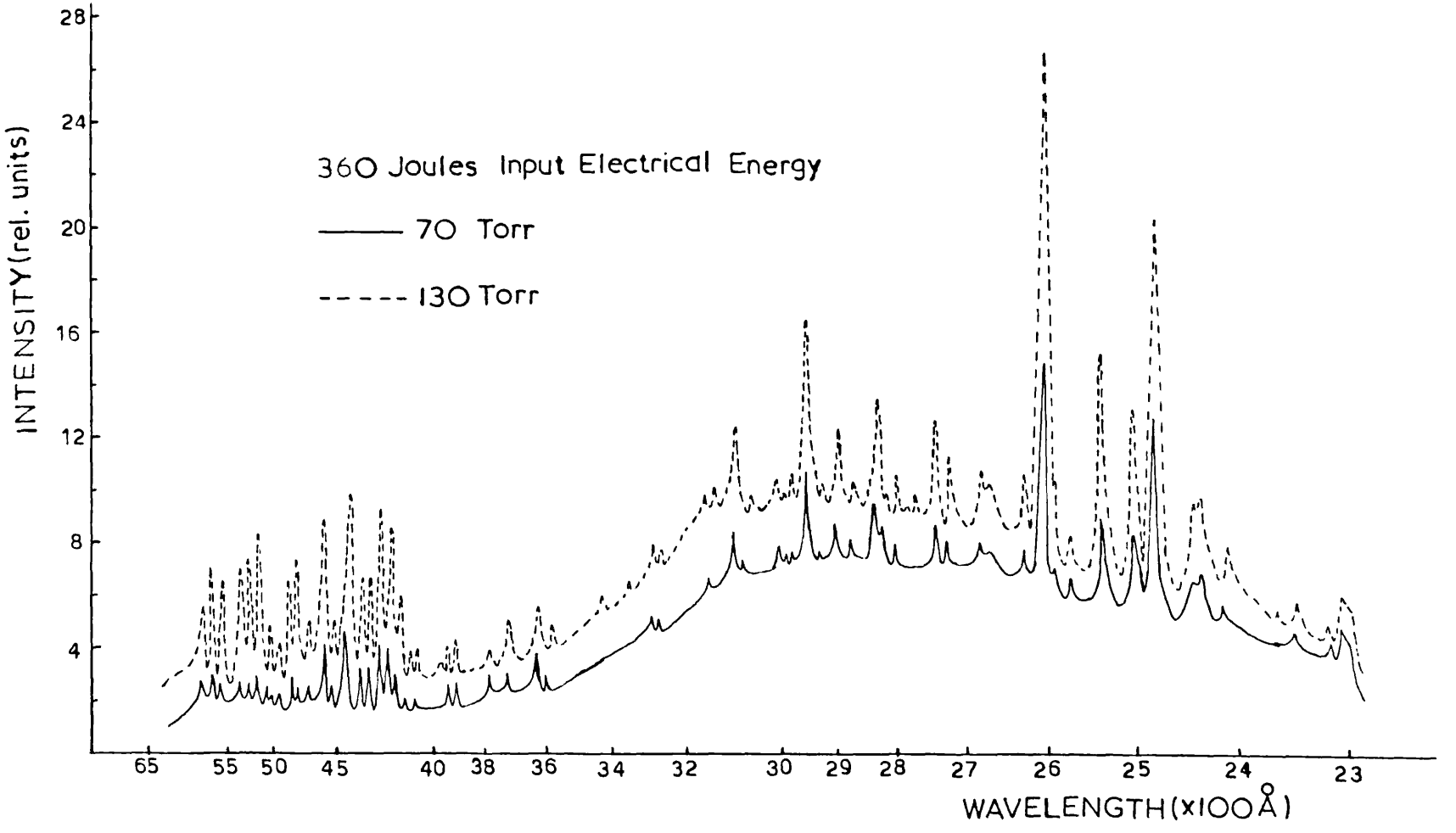

Fig. 5.19: Emission spectrum of a Xenon filled coaxial flashtube

5.4 OPTIMISATION OF THE OPTICAL OUTPUT FROM THE FLASHTUBES AND CONCLUDING REMARKS

In this chapter, it has been established in a conclusive way that the discharge pattern of a coaxial flashtube greatly affects the quality of the optical output. It has been shown that fast optical pulses are obtained in the case of uniform discharges. When the flashtubes are operated without reflectors on their outer surface, it has been found that uniform discharges are feasible for E/p values higher than 40 Volts/cm.Torr. However, the introduction of reflectors has resulted in the attainment of fast optical pulses for E/p values as low as 17 Volts/cm.Torr; such fast optical pulses provide evidence that the corresponding discharges are uniform. Besides the improvement of the flashtube performance, it has been shown that the use of reflectors extends the life of the flashtubes.

The study of the overall optical output from MARK 4 (filled with Xenon) between 2000$\mathring{A}$ and 7000$\mathring{A}$ has revealed that high luminous efficiencies are achieved for a range of low E/p values between 30 Volts/cm.Torr and 17 Volts/cm.Torr, which correspond to pressures between 100 Torr and 180 Torr. On the other hand, the rate at which radiant energy is emitted from MARK 4 in the first cycle of the optical pulse (Figures 5.8, 5.9 and 5.10) becomes high for E/p values around 20 Volts/cm.Torr; in fact, operation of this flashtube system at E/p values around 20 Volts/cm.Torr would provide the high pumping rates required for laser excitation of organic dye solutions and iodide photodissociative vapours. Therefore, if this flashtube is filled with Xenon at an optimum pressure of 150 Torr and then sealed permanently, it can be employed as a pump source for such laser materials at input electrical energies in the range between 500 Joules and 1000 Joules. At input electrical energies higher than

1000 Joules, the energy density in the flashtube becomes high, so that successive flashes at such input energies may result in the early destruction of the flashtube.

As is shown in Figures 5.16 and 5.17, high fluorescent outputs from dye solutions are attained when MARK 3 (filled with Xenon) is flashed at E/p values between 32 Volts/cm.Torr and 20 Volts/cm.Torr. Because of its larger discharge volume (compared to the volume of MARK 4), this flashtube can withstand higher input electrical energies. It is found then, that for a range of input energies between 700 Joules and 1200 Joules, MARK 3 will provide pump light at high rates if it is permanently filled with Xenon at $\sim$165 Torr, or with Krypton at $\sim$250 Torr.

The study of fluorescent outputs from dye solutions offered some information about the spectral response of the flashtubes, but for reasons explained in sub-section 5.3.1, a complete picture giving the variation of the optical output with time for narrower spectral regions could not be obtained. Time-resolved spectral measurements with the use of a monochromator will reveal further information concerning the spectral behaviour of the flashtubes.

The fraction of flashtube radiation between 2000$\mathring{A}$ and 2.5μ (the range in which quartz transmits) reaching the active medium in a pumping arrangement depends on the geometry and type of the coupling used. It is obvious that biaxial couplings are more efficient than triaxial ones (see sections 3.6 and 4.1). A general expression has been derived[135] which gives the coupling efficiency of coaxial flashtube pumping arrangements as a function of the geometrical parameters. A shortened version of this expression giving very good approximations is presented below.

$$f = \frac{R_c\left[(R_1 + R_2)^2 - 4R_c^2\right]^{\frac{1}{2}}}{\pi\ell(R_1 + R_2)} \left[\frac{2\ell}{R_1 + R_2} I + J\right] \qquad (5.3)$$

where

$$I = \arctan\left(\frac{\ell}{R_1 + R_2}\right) + \arctan\left(\frac{2\ell}{R_1 + R_2}\right) \tag{5.4}$$

$$J = \ln \frac{(R_1 + R_2)^3}{[(R_1 + R_2)^2 + \ell^2][(R_1 + R_2)^2 + 4\ell^2]^{\frac{1}{2}}} \tag{5.5}$$

and R_c is the inside radius of the laser cell (or the inside radius of the inner tube in the case of biaxial couplings) effectively representing the radius of the cylindrical column of the active medium. The above expression was derived on the following assumptions: (a) all points in the discharge column of the flashtube emit according to Lampert's law; (b) the outer wall of the flashtube displays 100% reflectivity; (c) all incident radiation on the laser cell is transmitted; (d) there is no re-absorption by the plasma in the discharge column; (e) there are no absorptive losses in the interspace between flashtube and laser cell.

From equation (5.3) the coupling efficiencies of the various pumping systems used in this work can be estimated. In this way, it is found that the triaxial system used to excite dye solutions - consisting of MARK 3 and the 0.65 cm inside radius laser cell - has a coupling efficiency of only 20.5%; similarly, it is obtained that the coupling efficiency of the biaxial system of MARK 4 is 40%. It is evident that, even in biaxial systems, most of the flashtube radiation is trapped in the discharge volume or in the interspace between flashtube and laser cell.

As a final remark, it must be pointed out that these flashtube systems (including the Marx generator) are better suited to pump iodine photo-dissociation lasers, rather than dye lasers. This conclusion has been reached by studying the emission spectra of the flashtubes. It is apparent

from Fig. 5.19 that the emission spectrum of MARK 4 is most efficient in the region between 2300Å to 3100Å where alkyl and fluoroalkyl-iodides absorb.

The higher efficiency in the UV region displayed by these flashtube systems is explained on the grounds of the high current densities (see section 3.4) attained in the flashtubes as a result of the fast and strong electrical pulses provided by the Marx generator.

CHAPTER 6

THE EFFECTS OF RADIO-FREQUENCY PREIONISATION ON THE FLASHTUBE PERFORMANCE

6.1 INTRODUCTION - THE SIGNIFICANCE OF PREIONISATION IN A HIGH CURRENT PULSED DISCHARGE. PREIONISATION METHODS.

It has been shown in section 3.3 that the rate at which initiatory electrons are provided in an impulse, high current density discharge influences the speed of the electrical processes (ionisation growth, breakdown, etc.). Later in the same section, it was indicated that critical electron amplification for breakdown can be achieved by primary electron avalanches alone (before secondary ionisation processes at the cathode come into effect), if the number of initial electrons in the discharge column is substantially increased. Generally, in an electrical gas discharge, the provision of a large number of initiatory electrons by external sources, other than the natural (cosmic rays), just before the application of the electric field which causes the complete breakdown of the gas, is known as preionisation of the gas. By external source is understood any device providing (directly or indirectly) electrons in the discharge column, other than the main discharge circuit.

Since in high current density discharges, the intensity of the emitted light depends largely on the electron density (see section 3.4), it should be expected that preionisation of the gas will cause an increase in the rate at which the intensity rises; in other words, a faster output optical pulse should be anticipated when preionisation is provided.

In the case of coaxial flashtubes, it should be expected that provision of a large number of initiatory electrons, in an even manner over the

annular discharge column, will be an important factor (especially at low E/p values), in achieving uniform discharges.

The preionisation method depends on the nature of the discharge involved and on practical matters which emerge from the variety of discharge arrangements. Preionisation can be achieved by introducing external electrons in the form of a high energy electron beam[136,137] or by producing electrons in the discharge column; in the latter case, the origin of the initiatory electrons is either the cathode or the gas itself. It has been mentioned in section 3.3 that initiatory electrons are produced by irradiating the cathode or the gas with UV light. Preionisation of the gas by UV radiation was successfully applied in CO_2 discharge lasers[138]. However, the electron beam and the UV irradiation methods are not practical or efficient in flashtube systems.

In the years following the discovery of the laser, preionisation in flashtubes was provided by a low energy electrical pulse applied to the flashtube electrodes prior to the main pulse. Improved optical output from double-pulsed linear flashtubes was reported in 1963 by Emmett and Schawlow[139]; the first pulse of their system was much slower than the second (main), but produced enough preionisation to prevent the shattering of the flashtube when high input electrical energies were used. Soon after Emmett and Schawlow's publication, Gandy et al[140] observed enhanced UV radiation from double pulsed flashtubes. Recently, Ornstein and Derr[141] reported enhanced output optical power from pre-pulsed linear flashtubes.

All preionisation methods in flashtubes mentioned so far involve the use of a low energy, high voltage pre-pulse applied between the flashtube electrodes; this means that in such an arrangement, the preionising and main discharge circuits are closely coupled, so that the pre-pulse may induce a premature triggering of the main circuit[141], thus destroying

the synchronisation between the two pulses.

Since in coaxial flashtubes one aim of preionisation is to provide initiatory electrons evenly distributed over the discharge volume, it appears that the application of pre-pulse methods to high energy, high voltage coaxial flashtube systems, like the systems used in this work, is impractical. In fact, in order to improve substantially the discharge pattern of such flashtube systems, the preionising voltage pulse should be higher than the main discharge pulse. In this case, one can imagine the practical problems arising from the close coupling of the two high voltage discharge circuits.

It is evident from the above that the method of providing preionisation in such coaxial flashtube systems should not involve the flashtube electrodes. The only alternative of providing preionisation by a discharge is to apply an AC Voltage through a coil wound around the flashtube. When the frequency and the amplitude of the oscillation are appropriately chosen, the application of such a Voltage will result in an electrodeless (inductive) discharge. Due to the method of application, it should be expected that the pattern of the resulting discharge will be uniform over the flashtube volume.

In an experiment reported by Papayoanou and Buser[142], an electrodeless coaxial flashtube was subjected to two successive low frequency (5×10^5 KHz and 10^5 KHz in order of application) Voltage pulses through separate coils made of metallic sheets; the first pulse - applied through a single turn coil - was of low energy and its purpose was to preionise the gas, while the second pulse - applied through a two turn coil - delivered high electrical energies. However, it was found that the optical output from such an arrangement was not as efficient as that from double-pulsed flashtubes.

In a recent publication[143], enhanced optical output from high energy coaxial flashtubes was reported by using a low energy, high amplitude radio-frequency preionising pulse applied over a large part of the discharge volume through a 15-20 turns coil. It was the first time radio-frequency preionisation was used successfully in a flashtube. A detailed presentation of the results of that work[143], together with additional results obtained afterwards, is given in section 6.4. It must be pointed out that earlier on, radio-frequency preionisation had been used[144] successfully to produce uniform discharges at high pressures in transverse CO_2 lasers; but on this occasion the preionising pulse was applied between the cathode and a grid placed near the cathode of the discharge gap.

Radio-frequency preionisation, when exercised through an inductive coil, suits ideally the coaxial flashtube geometry. In contrast, this method is not applicable in linear flashtube pumping systems; this is because in such an arrangement a fair amount of pump light is blocked by the coil around the flashtube.

6.2 OUTLINE OF AC HIGH-FREQUENCY BREAKDOWN OF GASES

Ionisation and breakdown in a gas subjected to AC electric fields differ in several respects from ionisation in steady (DC) fields. First, because of the periodical change of the field direction, the charged particles may not reach the walls or electrodes of the discharge column; with losses due to collisions with the walls or electrodes reduced, ionisation growth and breakdown of the gas can be achieved by applying quite low fields. In these circumstances secondary processes at the

electrodes do not constitute an important condition for breakdown as they do in DC discharges. Another difference between DC and AC discharges is that the latter can be produced in insulating vessels as a result of the inductive action of alternating electric fields applied through coils wrapped around the discharge vessels.

The breakdown voltage of a gaseous column (defined as the amplitude of the voltage oscillation required to break down the gas), depends, like the breakdown voltage for DC fields, on the gas pressure p and therefore on the mean free path of electrons in the gas ℓ_e. An additional parameter which influences the breakdown voltage in such discharges is the frequency of the oscillating field. The breakdown voltage of a gas for AC fields at a frequency $\sim$50 Hz is almost the same[145] as that for DC conditions. But, if the frequency is raised to a value at which positive ions have insufficient time to traverse the column in half a cycle, a positive space charge is gradually built up leading to field distortion and breakdown of the gas at values below the DC value. At much higher frequencies, the breakdown voltage is further lowered as a result of the amplitude of electron oscillations becoming comparable with the length of the gaseous column, so that cumulative ionisation can be produced by the original electrons traversing many times this length in the direction of the field. In this case the breakdown is independent of secondary mechanisms at the electrode (if electrodes are used) and the losses due to collisions with the electrodes or the walls are reduced.

When the amplitude of electron oscillations becomes comparable to the mean free path of electrons in the gas and the field strength is such that the average electron energy at the end of a mean free path is just above the ionisation potential of the gas (condition for maximum ionisation probability, see Fig. 3.2), then the production of electrons in the gas is most efficient, and breakdown occurs at lower voltage values. The amplitude of electron oscillations in the direction of a sinusoidal field is

proportional[146] to E/ν^2 where E and ν are the amplitude and the frequency of field oscillation.

From the above it is concluded that strong preionisation in a flash-tube can be achieved by applying relatively low (compared to DC or pulsed voltages) AC voltages, providing that the frequency of the oscillation is high enough.

6.3 EXPERIMENTAL ARRANGEMENTS

The device used to generate the radio-frequency preionising pulses has been described in section 4.3. In the present section the experimental arrangements for synchronisation between the main and preionising pulses and for measuring the optical output from a coaxial flashtube subjected to such preionisation is described.

Figure 6.1a shows a schematic diagram of the experimental set up used to obtain various delays between main and preionising pulses. When the main discharge circuit (Marx generator) displayed a low jitter amplitude (clean spark gaps), the required delay between the two pulses was achieved by using a variable delay unit along the triggering line of the preioniser (procedure $1 \rightarrow 2 \rightarrow 3 \rightarrow 4$ in the diagram of Fig. 6.1a).

The time interval which elapses between the initiation of the master trigger (push button) and the AC breakdown by the preionising pulse was measured from observations of externally triggered oscilloscope traces of the current oscillation in the flashtube which follows the AC breakdown of the gas. For clarity, let us call this time interval the 'preionisation delay'. The current oscillation was detected through a single turn coil placed near the flashtube. It must be pointed out that only the preionisation discharge circuit was fired during these observations. The traces of

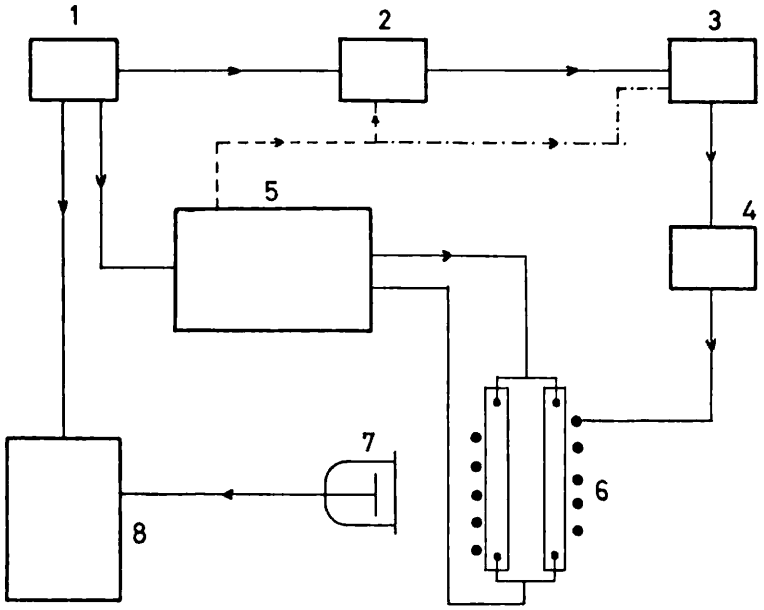

1. Master Trigger 2. Variable Delay Unit 3. Preioniser Trigger

4. Preioniser 5. Marx Generator 6. Coaxial Flashtube

7. S-20 Photodiode 8. Oscilloscope

(a)

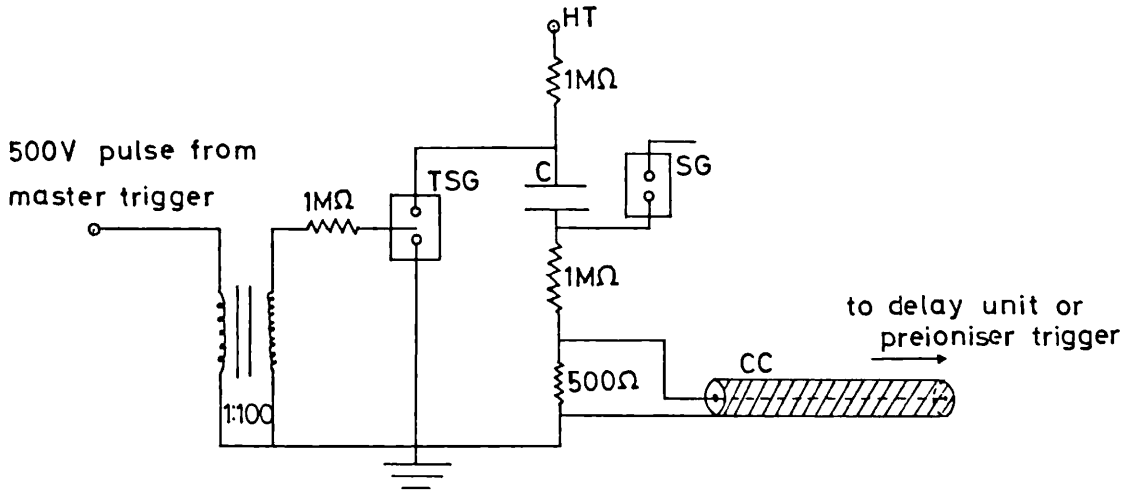

TSG: Triggered & Pressurised Spark Gap, C: 2μF, 20 KV

SG: Pressurised Spark Gap, CC: Coaxial Cable

(b)

Fig. 6.1 : Triggering processes for the synchronisation between main and preionisation pulses.

Figures 6.2a and 6.2b show the current oscillation for two different input electrical energies in the preioniser. As is expected, the preionisation delay is shorter for the higher input electrical energy, but the variation is relatively small around the value of 1 μsec.

In order to study the effects of preionisation for a number of different delays between main and preionising pulses, spark gaps with relatively long distances between their electrodes (see sections 4.2 and 5.1) were used, so that a long time interval (> 10 μsecs) between the triggering of the Marx generator and the arrival of the main pulse across the flashtube was obtained. Let us call this time interval the 'main pulse delay'. At the beginning of the session, the main pulse delay was ∿12 μsecs (Figures 6.2c and 6.2d), but later on it was increased to ∿20 μsecs by increasing the distance between the spark gap electrodes in the main discharge circuit. Consequently, in view of the measured preionisation delay, the delay between the preionising and main pulses could take on any value in the range between zero and ∿19 μsecs.

When, after a number of flashes, the spark gaps became jittery, the triggering arrangement described in the preceding paragraphs was unsuitable for synchronising the two pulses. Since most of the main pulse delay and jitter were caused by the first (triggered) spark gap of the Marx generator, it was thought that good synchronisation would be obtained if the preioniser was triggered by a signal generated from the circuit of the first spark gap at the moment breakdown occurred in that spark gap. Such a signal was attained across a 500 Ω in series with the high value isolating resistor, as is shown in the schematic diagram of Fig. 6.1b. Depending on the circumstances, the delay unit could be omitted (procedure 1 → 5 → 3 → 4 in the diagram of Fig. 6.1a), or included in the triggering arrangement

(procedure 1 → 5 → 2 → 3 → 4). Because of the nature of this triggering arrangement, the flashtube performance could be studied only for short delays between the preionising and main pulses, namely ∿1 μsec.

In this experimental session MARK 4 filled with Xenon was used. From Figures 6.2a and 6.2b the duration and frequency of the preionising pulse are found equal to ∿6 μsecs and 10 MHz, respectively.

The oscillograms of Figures 6.2c and 6.2d were recorded during the initial stages of the experimental session, while the oscillogram of Fig. 6.2e corresponds to a later stage when the spacing of the spark gap electrodes was increased. Figure 6.2c shows an externally triggered trace of the optical output from the flashtube without preionisation. It is observed from this trace that the emission of light starts after ∿12 μsecs from the moment the system is triggered; in view of the fact that hysteresis in the V-I characteristic of the flashtube is very short (∿0.5 μsecs) when the flashtube is clean and operated at high E/p values (see section 5.1), this time interval can be regarded as the main pulse delay.

Figure 6.2d shows an externally triggered trace of the optical output with preionisation. The triggering procedure 1 → 2 → 3 → 4 in the diagram of Figure 6.1a was followed for the initiation of the preioniser. In the same trace, the current oscillation in the flashtube caused by the action of the radio-frequency preionising pulse is recorded about 1.5 μsecs prior to the application of the main pulse. On this occasion, the current oscillation was picked up by the cable transmitting the optical output signal from the photodiode to the oscilloscope, so that the two signals are superimposed on the same trace. In this way, by making one observation, it was possible to measure both the optical output from the flashtube and the delay between preionising and main pulses.

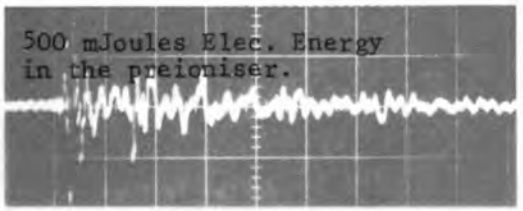

(a)

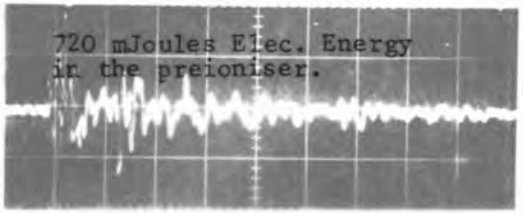

(b)

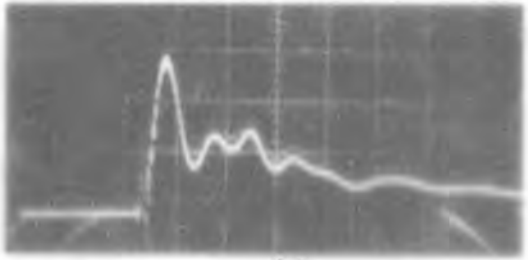

(c)

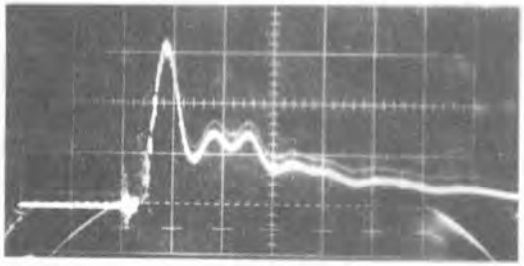

(d)

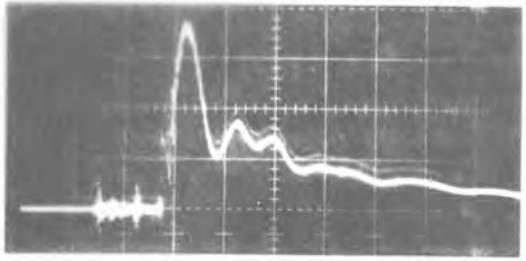

(e)

Fig. 6.2

(a) and (b): Externally triggered traces of the current oscillation in the discharge column of MARK 4, following the breakdown of gas (Xenon at 40 Torr) by the preionising pulse.
Horiz. scale: 1 μsec/div.

(c), (d) and (e): Externally triggered power profiles of the optical output from MARK 4 without preionisation (c), and with preionisation for two different delays between preionising and main pulse (d) and (e); the preionising pulse is indicated by the current oscillation recorded in the same trace and prior to the main pulse.
60 KV main pulse (720 Joules Elec. Energy)
36 KV preion. pulse (720 mJoules Elec. Energy)
50 Torr Xenon in the flashtube.
Horiz. scale: 5 μsecs/div.
Vert. scale: 0.5 Volt/div.

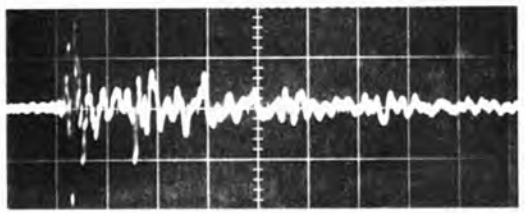

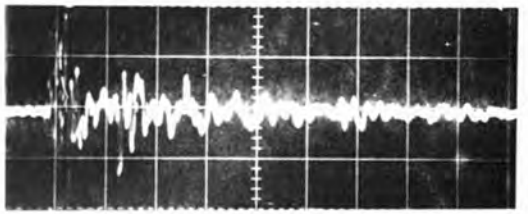

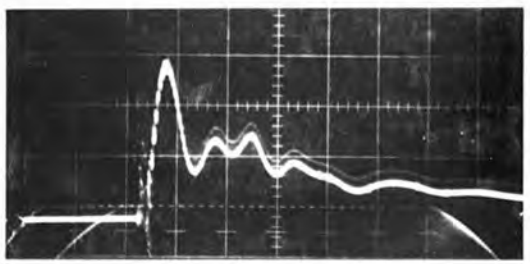

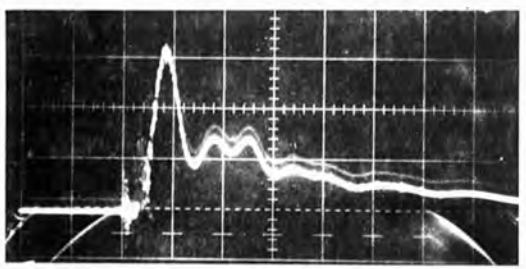

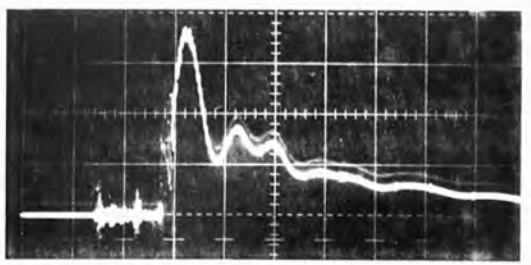

Figure 6.2e shows another externally triggered trace of the optical output with preionisation. But this time, the arrival of the preionising pulse at the flashtube precedes that of the main pulse by ∿7 μsecs. As a matter of fact, this particular trace indicates that a second preionising pulse has been generated by the preioniser about 4 μsecs after the generation of the first pulse.

6.4 EXPERIMENTAL STUDY OF THE PERFORMANCE OF A COAXIAL FLASHTUBE SUBJECTED TO RADIO-FREQUENCY PREIONISATION

6.4.1 Enhancement of the optical output

If comparison between the optical output profiles shown in Figures 6.2c and 6.2e is made, one finds that the peak power of the output in Figure 6.2e is ∿15% higher than that in Figure 6.2c. This observation indicates that the application of pulsed, radio-frequency preionisation to a coaxial flashtube may result in the enhancement of the optical output.

Following the preliminary experiments and tests described in the previous section, a systematic study of the effects of radio-frequency preionisation on the optical output from the flashtube and, generally, on the flashtube performance was carried out for various gas pressures and delays between the preionising and main pulses. The electrical energy of the preionising pulse was the same throughout the session, namely 720 mJoules and the triggering procedure $1 \rightarrow 2 \rightarrow 3 \rightarrow 4$ in the diagram of Figure 6.1a was followed.

Figure 6.3a shows two oscilloscope traces of the optical output from flashes at the same gas pressure and main pulse strength in the flashtube; but in the case of the more intense signal, a radio frequency pulse was applied to the flashtube 5 μsecs before the arrival of the main pulse. It is apparent that both the peak power and luminous efficiency of the optical

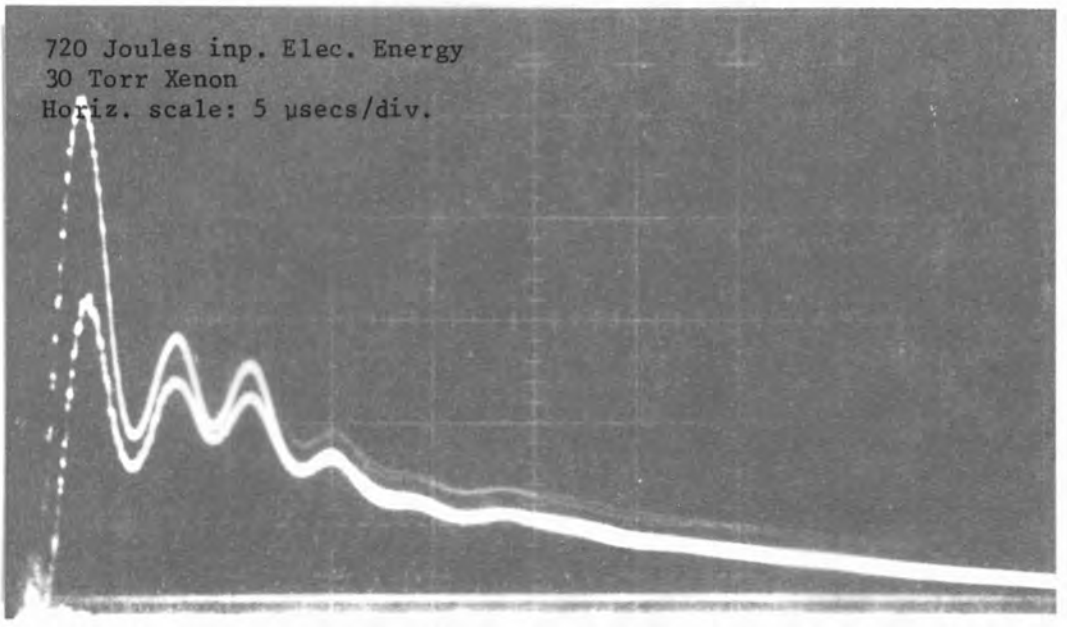

(a) Optical output without preionisation (smaller signal) and with preionisation (larger signal).

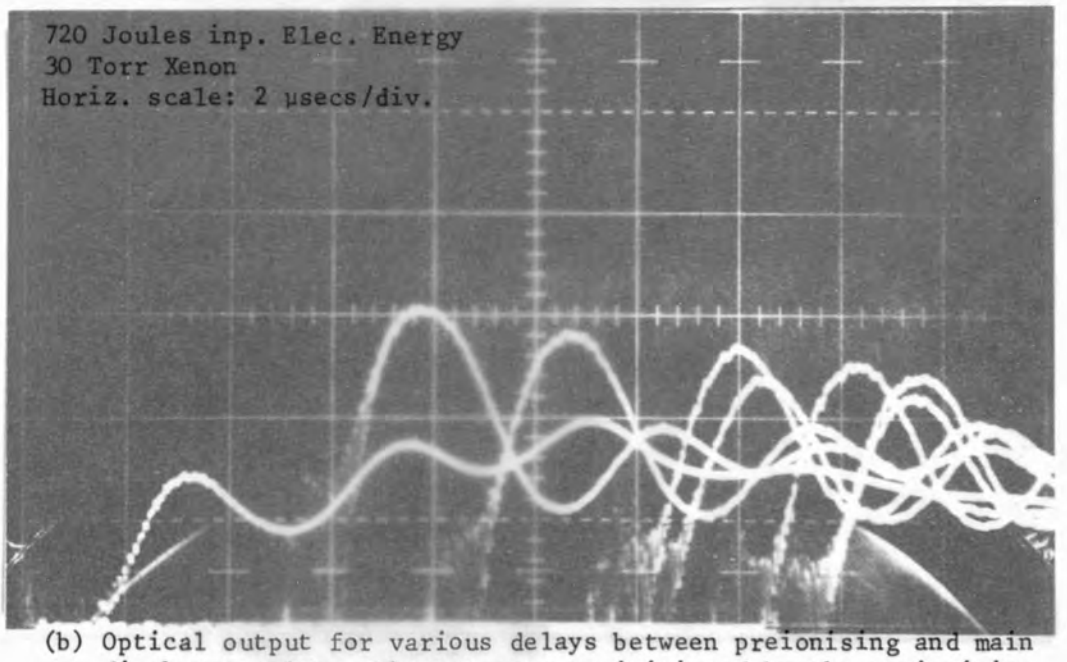

(b) Optical output for various delays between preionising and main discharge pulse; the traces were initiated by the preionising pulse, except for the one on the extreme left (without preionisation) which was initiated internally by the oscilloscope.

Fig. 6.3: Enhancement of the output optical power from MARK 4 with preionisation.

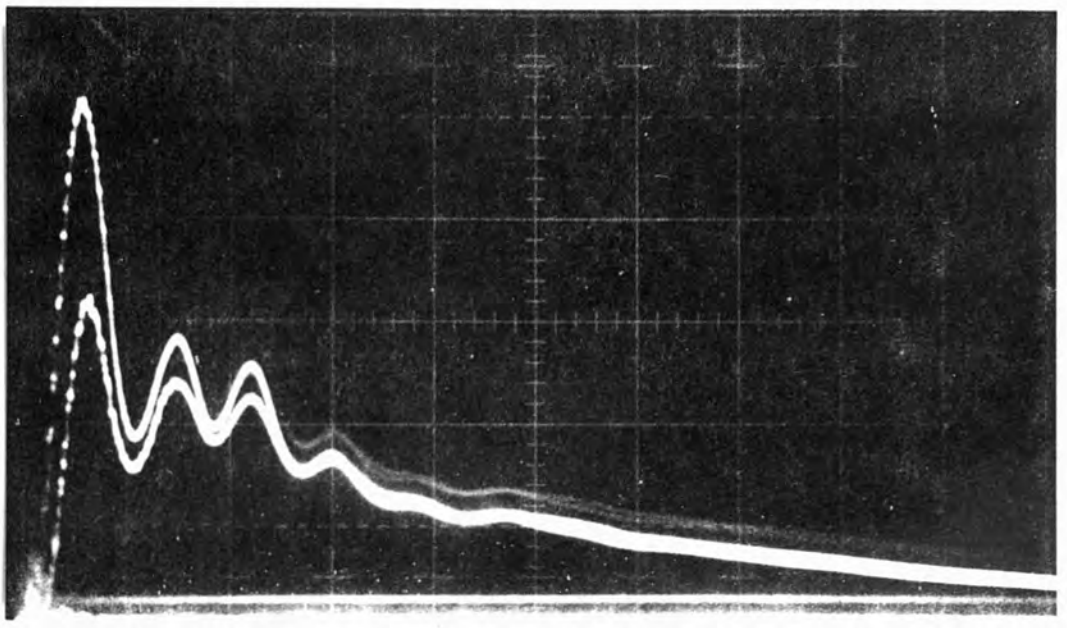

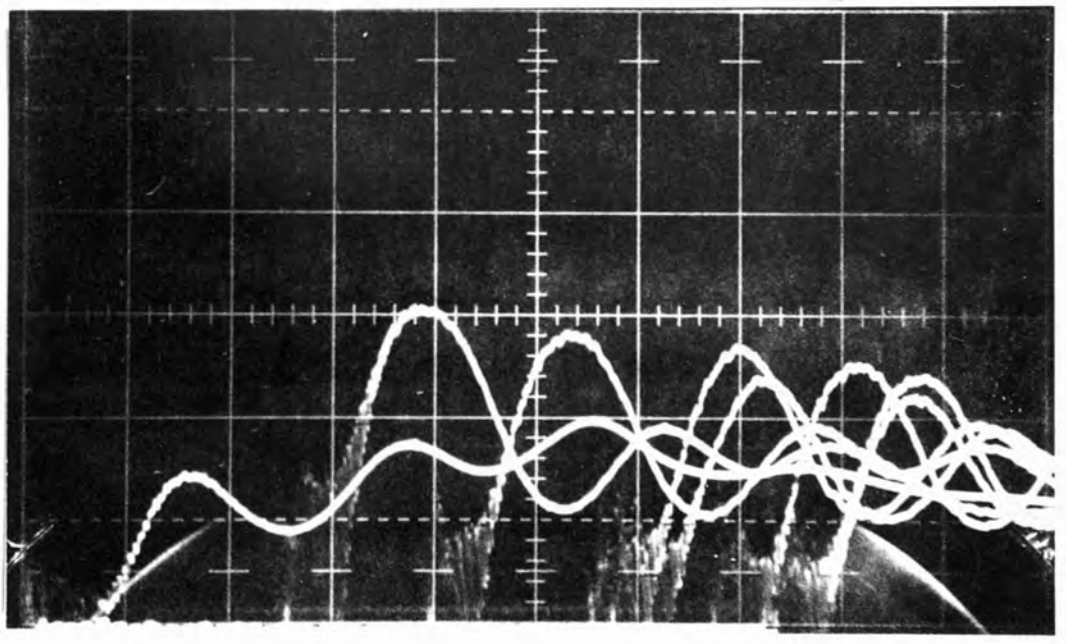

output are higher when the flashtube is subjected to such preionisation; in fact, the peak power increases by a factor of 2. It is reminded that the traces of Figure 6.3a correspond to discharges at 30 Torr pressure in the flashtube. Experiments carried out at higher pressures have showed that the enhancement of the peak power with preionisation is not as high as that at 30. The graphs of Figure 6.4a give the variation with gas pressure of the peak power of the optical output with and without preionisation. In addition, these graphs give the dependence of the peak power enhancement (defined as the ratio of the peak power with preionisation to the peak power without preionisation) on the gas pressure up to 100 Torr. It is noticed that the enhancement decreases with increasing gas pressures. No significant increase of the peak power, due to preionisation, was observed when the pressure in the flashtube was increased above 100 Torr.

Spectrograms of the flashtube light (in the near UV and visible regions) revealed that the enhancement of the optical output with preionisation was effectively due to the emission of a more intense line spectrum; no significant change in the continuous spectrum was observed. Figure 6.5 shows the emission spectrum of the flashtube with and without preionisation; the pressure in the flashtube was 30 Torr and the delay between preionising and main pulses was $\sim$6 μsecs. A consistent increase of the intensity of spectral lines is noticed throughout the spectrum.

Parallel consideration of the temporal and spectral measurements of the optical output from the flashtube with preionisation can lead to some significant conclusions concerning the nature of radiation emitted from pulsed, high current density, rare gas discharges. From the observed enhancement of output optical power in the early parts of the pulse (Fig. 6.3a) and the spectral enhancement (Fig. 6.5), it is conclusively implied that the

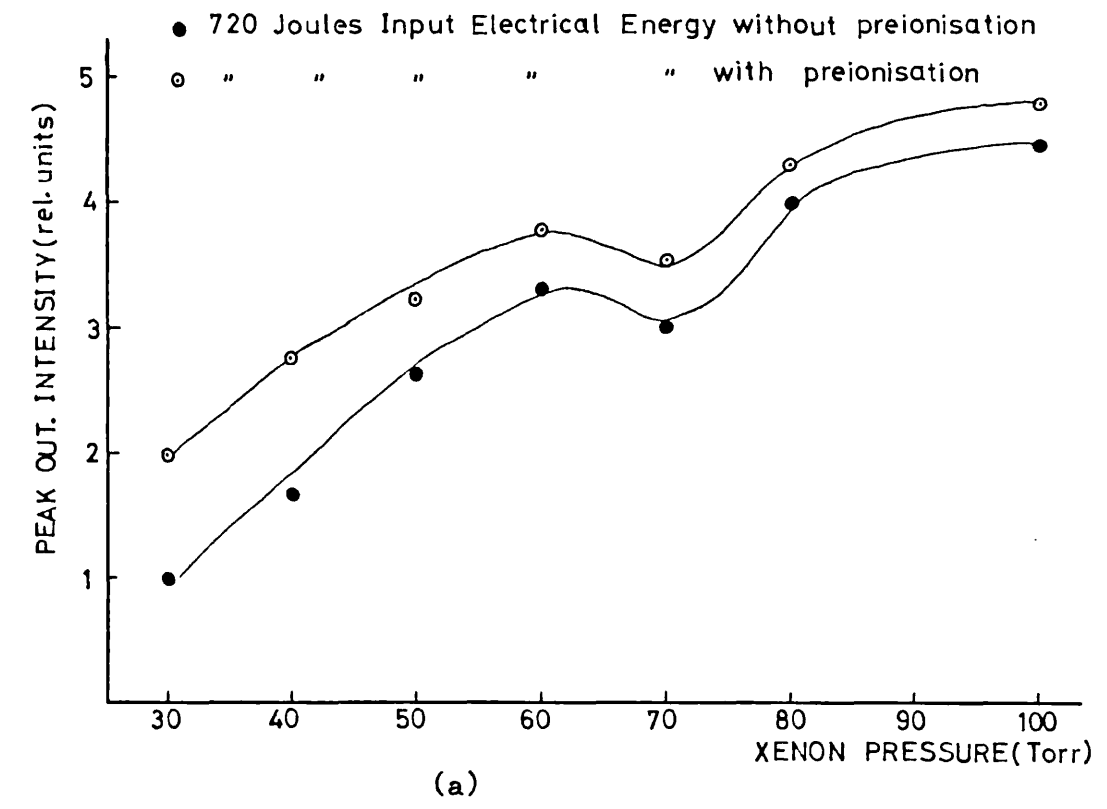

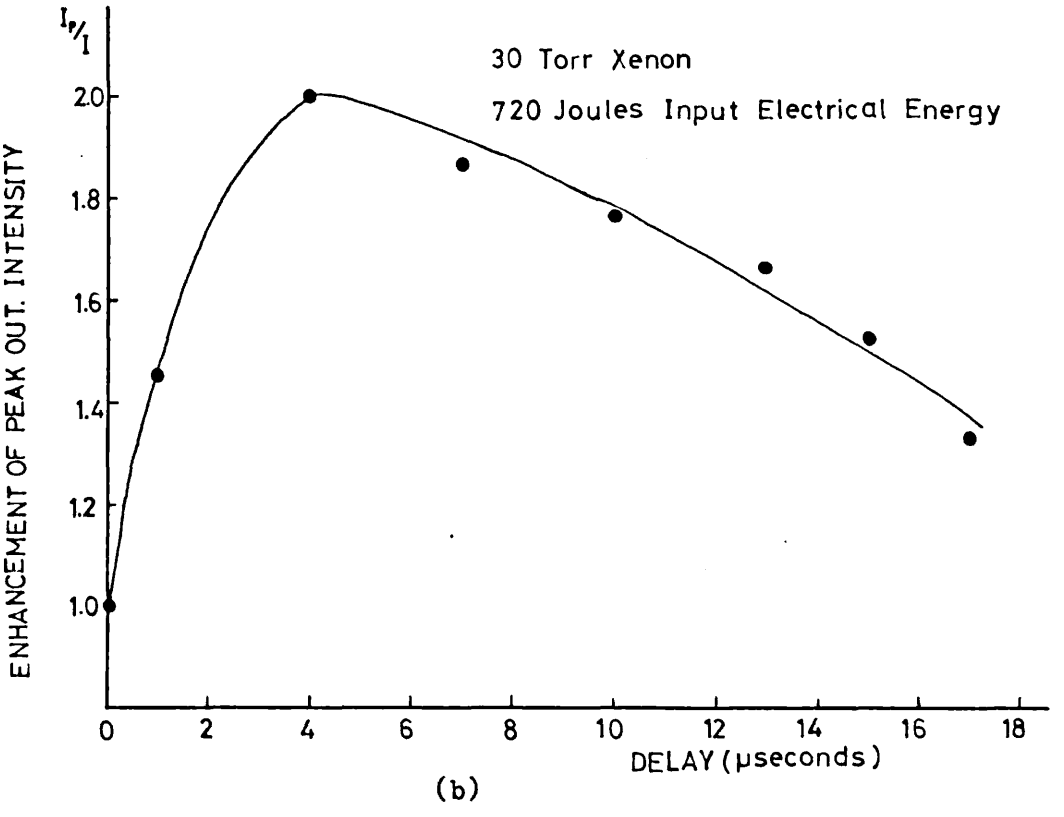

Fig. 6.4 : Characteristics of the optical output from a 74cc Xenon filled coaxial flashtube subjected to radio-frequency preionisation.

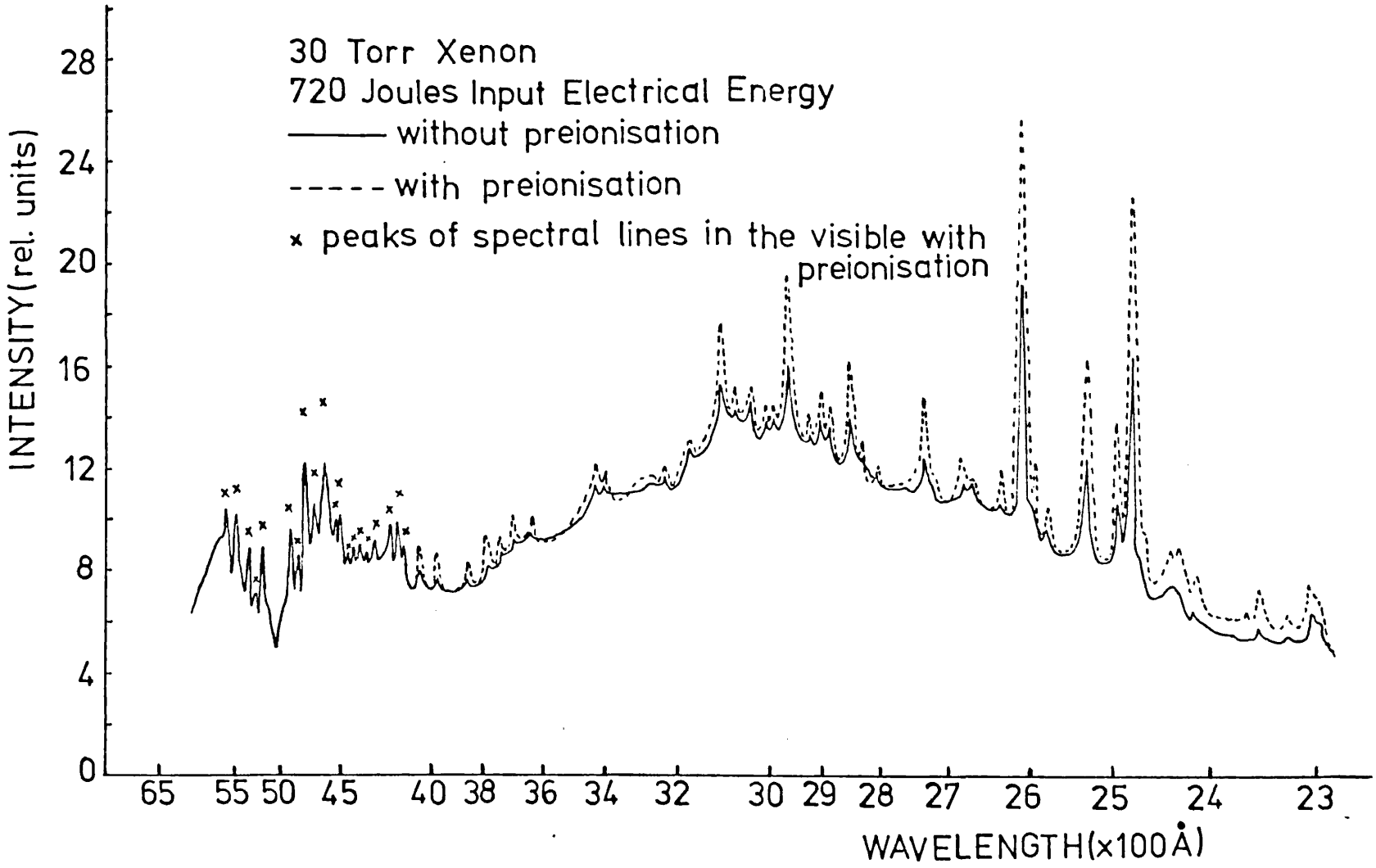

Fig. 6.5: Emission spectrum of a Xenon filled coaxial flashtube with and without preionisation.

line spectrum is predominant during the early stages of such pulsed discharges. This conclusion is in accordance with the theoretical prediction that the thermal radiation continuum - which constitutes most of the overall continuum emitted from high current density discharges - is weak during the early stages of such pulsed discharges, but it becomes stronger as thermal equilibrium is approached (see section 3.4).

6.4.2 Dependence of the enhancement on the delay between main and preionising pulses

As was mentioned in previous sections, the enhancement of the output optical power was found to be dependent on the delay between main and preionising pulses. Figure 6.3b shows a number of oscilloscope traces of the optical output corresponding to successive flashes and various delays between the two pulses. These traces were initiated by the preionising pulse, except for the one on the left - corresponding to a flash without preionisation - which was initiated by the input signal itself. In this way, the delay between the two pulses could be measured.

Figure 6.4b shows a graph which gives the variation of the enhancement of the output peak power with the delay between main and preionising pulses. From this graph it is found that the enhancement is high for delays between 3 and 6 μsecs. It seems that, for delays shorter than 3μsecs, the number of initiatory electrons cumulated in the discharge volume as a result of the AC discharge is not high enough to increase substantially the speed of processes in the main discharge. The observed decreasing enhancement with increasing delay, for delays longer than 6 μsecs, can be explained on the grounds of the population decay of initiatory electrons which takes effect once the preionising pulse has ceased ($\sim$ 6 μsecs) and is due to diffusion and electron-ion recombination processes.

6.4.3 Other observations

Although no significant increase of the flashtube output power - due to preionisation - was observed when the pressure was increased above 100 Torr, there was evidence that, even at higher pressures, the radio-frequency preionisation system produced enough electrons (evenly distributed over the discharge volume) to prevent an early shattering of the flashtube and to improve the discharge pattern. First, the sound produced by the shock-waves in the flashtube discharges was much softer and reduced with regard to the sound produced in discharges without preionisation. Secondly, it was possible to operate the flashtube at pressures above 200 Torr (E/p values as low as 10 Volts/cm.Torr) without any sign of destruction.

Observations of the near field pattern of iodine laser beam in a pumping arrangement involving MARK 1 (see Fig. 7.2 in the next chapter), offered enough evidence that uniform flashtube discharges were achieved at pressures above 200 Torr when preionisation was used.

6.5 COMMENTS

In this investigation, it has been established that the use of pulsed radio-frequency preionisation in a fast, high energy coaxial flashtube system results in the improvement of the system performance. The main aspects of the improved system performance are

a) the enhancement of the output power and luminous efficiency of the flashtube at low gas pressures,

b) the possibility of operating the system at gas pressures in excess of 200 Torr, without being restricted by localised (non-uniform)

discharges, and

c) the protection of the flashtube from strong shock-waves which are produced by such localised discharges at high pressures.

As was mentioned in sub-section 6.4.1, no significant increase of the optical output was observed at pressures in the flashtube above 100 Torr when the radio-frequency preionising pulse was applied. It seems that, at higher pressures, the number of initiatory electrons produced by such a pulse is not high enough to speed up processes in the main discharge; this is the case, because the amplitude of electron oscillations in the gas, which is inversely proportional to the square of the radio-frequency of the oscillation (see section 6.2), does not match the shorter mean free paths of electrons at higher pressures. As a future reference, it is expected that the use of VHF or microwave preionisation will result in the enhancement of the output power of coaxial flashtubes at pressures higher than 100 Torr.

CHAPTER 7

OUTPUT MEASUREMENTS FROM A COAXIAL FLASHTUBE PUMPED IODINE PHOTODISSOCIATION LASER

7.1 EXPERIMENTAL DETAILS

Since the discovery of the iodine photodissociation laser[22], several optical pumping systems equipped with linear flashtubes have been constructed to excite various active alkyl and fluoroalkyl-iodides (see sections 2.1 and 2.3). It is believed that a coaxial flashtube arrangement for pumping such active materials was used for the first time during the course of this investigation; some iodine laser output results from this investigation were reported in a recent paper[143]. In this chapter, a complete account of the iodine laser output measurements is given, together with details about the coaxial flashtube pumping arrangement.

In this experimental session, a triaxial pumping arrangement was employed consisting of MARK 1 and a 0.65 cm inside radius laser cell; according to equation 5.3, the coupling efficiency of this pumping arrangement was ∿28%. A three-stage Marx generator was constructed for this experiment; it was equipped with capacitors and spark gaps identical to those of the five-stage system. In most flashes, the flashtube was subjected to a low energy (∿150 mJoules) radio-frequency preionisation. The preionising pulse was applied ∿6 μsecs prior to the arrival of the main pulse.

The active photodissociative iodide in the laser cell was 1 - C_3F_7I vapour. The vapour pressure in the cell could be varied by a regulator and several valves installed along the vacuum line (PTFE), which connected the laser cell and the glass bottle containing 1 - C_3F_7I in liquid phase.

After each flash, the laser cell was evacuated through a vacuum line which started from the other end of the cell and, then, fresh vapour (free of molecular iodine) was flown into it.

Finally, the effective length of the laser cavity was 35 cm and the reflectivity of the output mirror was 60%.

7.2 RESULTS AND DISCUSSION

The results obtained during this experimental session consist of energy measurements of the iodine laser output and observations of the near field pattern of the laser beam. The parameters varied in this session are the gas type and pressure in the flashtube, the input electrical energy and the pressure of the active vapour in the laser cell. In addition, output energy measurements were made with and without preionisation. These experiments provided a good opportunity to evaluate the potentiality of such coaxial flashtube systems as pump sources for iodine photodissociation lasers and to ascertain the ultraviolet output of the flashtube in the region between 2200Å and 3000Å. Moreover, the near field patterns of the laser beam offered useful information about the discharge pattern in the flashtube.

Figure 7.1 shows the efficiency of the iodine laser output at various E/p values and input electrical energies, but for a fixed vapour pressure of 100 Torr in the laser cell. As expected, the laser efficiency increases with decreasing E/p value as a consequence of the higher luminous efficiencies and faster optical pulses (see sub-section 2.3.4) provided by the flashtube at lower E/p values. The laser efficiency increases also with increasing input electrical energy applied to the flashtube; this is due to the fact that the fraction of pump energy spent in order to reach thresh-

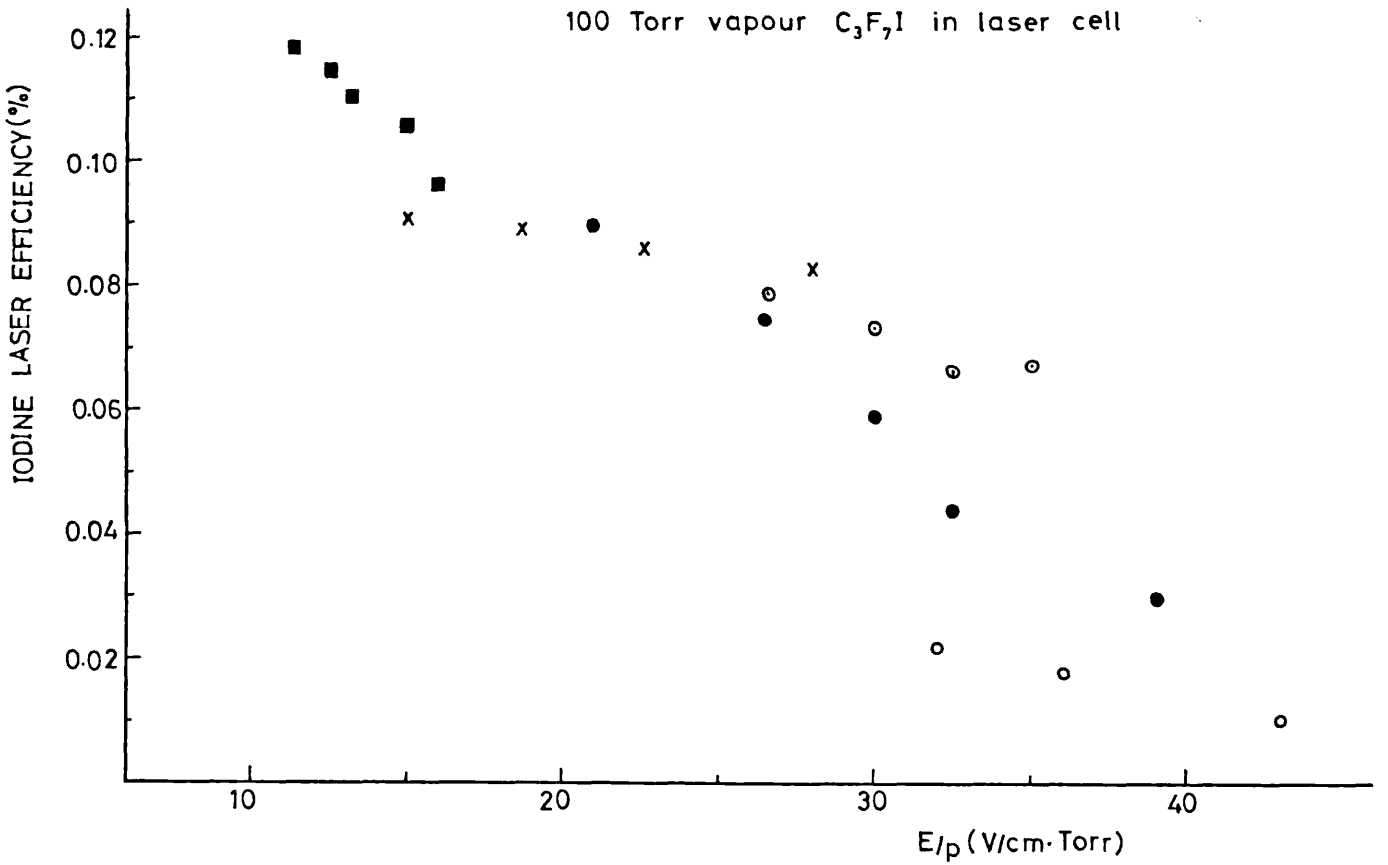

Fig. 7.1 : Iodine laser output characteristics.

old for laser oscillation is smaller when higher input electrical energies are used. From Fig. 7.1, it is also noticed that at higher E/p values (low gas pressures), the laser efficiency is substantially increased when the flashtube is subjected to preionisation; but, at low E/p values, no significant change of the laser efficiency, due to preionisation, has been observed.

It was confirmed that the iodine laser output was most efficient when the pressure of 1 - C_3F_7I vapour in the laser cell was 100 Torr. In Table 7.1, the energy of the laser output at various vapour pressures is given for a fixed input electrical energy and gas pressure in the flashtube.

TABLE 7.1

Input El. Energy (Joules)	Pressure in F.T. (Torr)	Vapour Pressure (Torr)	Laser output Energy (mJoules)
600	80	50	350
600	80	80	420
600	80	100	530
600	80	150	340

Iodine laser outputs around 1 Joule were achieved for an input electrical energy of 800 Joules when the vapour pressure was 100 Torr and the flashtube was filled with Xenon at pressures ∿200 Torr; the laser efficiency corresponding to these conditions was ∿0.12%. This efficiency is quite satisfactory considering that the coupling efficiency of the pumping arrangement used is only 28%. In this session, the flashtube was not fired at input energies higher than 800 Joules, because there was a feeling that it could not withstand higher energy densities. It is reminded that the construction of MARK 1 is based on the adhesive sealing technique (see section 4.1) in which the ends of the quartz tubes are rigidly attached to the electrodes of

the flashtube; besides, amongst the four flashtubes studied, MARK 1 has the smallest discharge volume. It is expected that the use of a biaxial flashtube pumping system like that of MARK 4 (which is based on the 'O' ring sealing technique and has a coupling efficiency of 40% and a discharge volume of 74 cc) instead of MARK 1 would result in increased laser efficiencies; in such a case, the flashtube system could be fired at much higher input electrical energies and laser efficiencies above 0.3% should be expected.

Figure 7.2 shows four burnmark patterns of the iodine laser beam on developed unexposed polaroid film for various system parameters. The dependence of the laser output on the gas pressure in the flashtube, the vapour pressure in the laser cell and the input electrical energy can be easily observed from Fig. 7.2 when individual burnmarks are compared.

These burnmarks provide information about the absorption of pump light by the active medium and the discharge pattern in the coaxial flashtube. From the variation of brightness in the cross-section of the burnmarks it is implied that the fraction of pump light absorbed by the peripheral parts of the active medium is much higher than the fraction absorbed by the central parts; this feature is, to a great extent, due to the geometry of coaxial flashtube pumping systems. When the intensity of the pump light is not high enough, the central parts of the active medium do not reach threshold conditions for laser oscillation and, as a result, a ring shaped output laser beam is obtained (Fig. 7.2c) . But when the intensity of the pump light is high, laser action is achieved over the entire cross-section of the active medium (Fig. 7.2d).

Finally, these burnmarks provide enough evidence that the discharge pattern in the flashtube is uniform, even at pressures as high as 210 Torr

a) 42 KV pulse
(590 Joules inp.Elec.Energy)
60 Torr Xenon in flashtube
75 Torr C_3F_7I vapour in laser cell.

(b) 42 KV pulse
(590 Joules inp.Elec.Energy)
80 Torr Xenon in flashtube
40 Torr C_3F_7I vapour in laser cell.

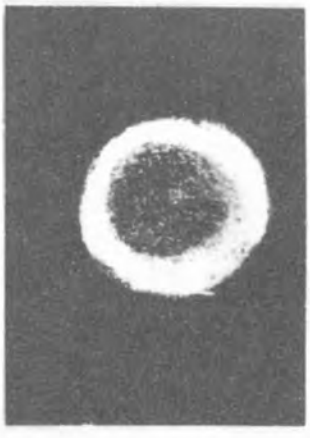

c) 42 KV pulse
(590 Joules inp.Elec.Energy)
80 Torr Xenon in flashtube
100 Torr C_3F_7I vapour in laser cell.

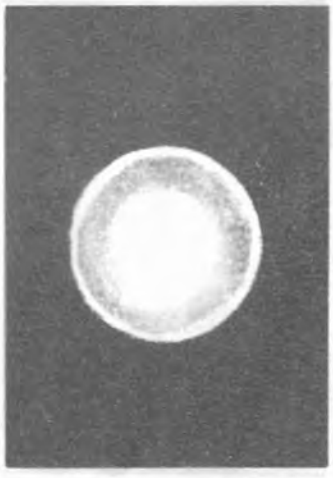

(d) 48 KV pulse
(770 Joules inp.Elec.Energy)
210 Torr Xenon in flashtube
100 Torr C_3F_7I vapour in laser cell.

Fig.7.2: Iodine laser beam burnmark patterns on developed unexposed polaroid film placed close to the output mirror.

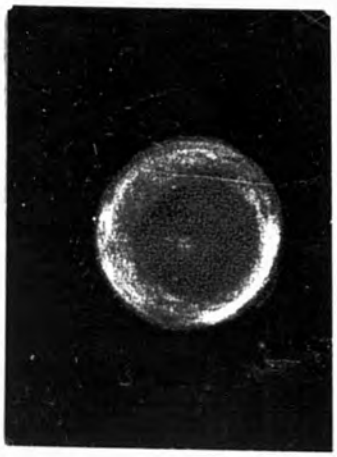

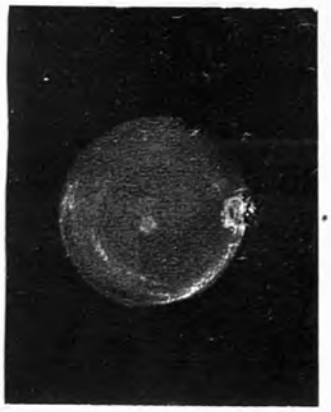

(E/p values ∿10 Volts/cm.Torr). The uniform discharge pattern at high pressures is partly attributed to preionisation and partly to the sharp electrode tips of the particular flashtube used (see section 4.1); such electrode tips favour the cold emission of electrons[79] from a cathode within a high electric field.

7.3 FURTHER ANALYSIS ON THE DEPOPULATION OF THE UPPER LASER LEVEL DUE TO RECOMBINATION AND DEACTIVATION OF ATOMIC IODINE IN THE PRESENCE OF MOLECULAR IODINE

In this section, the proof of equations (2.8), (2.10) and (2.11) is given. First, the expression (2.8), giving the recombination half-time of an atomic iodine sample in the presence of molecular iodine, is derived from the rate equation (2.4a) by taking into account the variation of molecular iodine concentration with time. In the second part of this section, the expressions (2.10) and (2.11), giving the population decay of a sample of iodine atoms in the excited $^2P_{\frac{1}{2}}$ state due to deactivation collisions with iodine molecules, are derived from equation (2.5a); again a variable concentration of molecular iodine is considered.

A) Recombination of atomic iodine in the presence of molecular iodine

The rate equation (2.4a) can be written:

$$-\frac{dI}{dt} = K_1 I^2 \left[I_2 + I_2(t)\right] \qquad (7.1)$$

For simplicity, the concentrations of compounds are symbolised without the brackets. In this way, I represents the concentration of atomic iodine at time t, I_2 represents the concentration of molecular iodine at time $t = 0$ and $I_2(t)$ is the concentration of molecular iodine formed during the time interval t; the quantity $I_2 + I_2(t)$ represents the total concentration of molecular iodine at time t.

The concentration of molecular iodine formed during the time interval t is related to the concentration of atomic iodine by the simple equation:

$$I_2(t) = \tfrac{1}{2}\,[I_o - I] \qquad (7.2)$$

where I_o is the concentration of atomic iodine at $t = 0$.

Substitution of $I_2(t)$ in equation (7.1) gives:

$$-\frac{dI}{dt} = \tfrac{1}{2}K_1 I^2 [2I_2 + I_o - I] \qquad (7.3)$$

Separation of the variables and integration of differential equation (7.3) gives:

$$-\int \frac{dI}{I^2\,[I_o + 2I_2 - I]} = \tfrac{1}{2}K_1 \int dt + c \qquad (7.4)$$

and

$$\frac{1}{[I_o + 2I_2]I} + \frac{1}{[I_o + 2I_2]^2} \ln \frac{I_o + 2I_2 - I}{I} = \tfrac{1}{2}K_1 t + c \qquad (7.5)$$

For $t = 0$, $I = I_o$ and it is found that

$$c = \frac{1}{[I_o + 2I_2]I_o} + \frac{1}{[I_o + 2I_2]^2} \ln \frac{2I_2}{I_o} \qquad (7.6)$$

Substitution of c in equation (7.5) gives:

$$\frac{I_o - I}{I_o[I_o + 2I_2]I} + \frac{1}{[I_o + 2I_2]^2} \ln \frac{[I_o + 2I_2 - I]I_o}{2I_2 I} = \tfrac{1}{2}K_1 t \qquad (7.7)$$

There is no analytical solution of equation (7.7) giving the variation of atomic iodine concentration with time. However, for $I = I_o/2$, the recombination half-time can be found:

$$T_r = \frac{2}{K_1 I_o [I_o + 2I_2]} + \frac{2 \ell n \left[2 + \frac{I_o}{2I_2}\right]}{K_1 [I_o + 2I_2]^2} \qquad (7.8)$$

Equation (7.8) is identical with equation (2.8).

B) Deactivation of excited atomic iodine by collisions with molecular iodine

The rate equation (2.5a) can be written:

$$-\frac{dI^*}{dt} = K_2 I^* [I_2 + I_2(t)] \qquad (7.9)$$

where I^* represents the concentration of excited iodine atoms. From equation (7.9) it is deduced that

$$-\int \frac{dI^*}{I^*} = K_2 I_2 \int dt + K_2 \int I_2(t)dt + c_1 \qquad (7.10)$$

and

$$\ell n I^* = K_2 I_2 t + K_2 \int I_2(t)dt + c_1 \qquad (7.11)$$

In order to find an analytical expression giving the variation of $I_2(t)$ with time, the rate equation for the product of atomic iodine recombination is considered.

$$\frac{dI_2(t)}{dt} = K_1 I^2 [I_2 + I_2(t)] \qquad (7.12)$$

From equation (7.2) it is obtained that

$$I = I_o - 2I_2(t) \tag{7.13}$$

Substitution of I in equation (7.12) gives a differential equation of two variables which can be separated and integrated

$$\int \frac{dI_2(t)}{[I_o - 2I_2(t)]^2[I_2 + I_2(t)]} = K_1 \int dt + c_2 \tag{7.14}$$

$$\frac{1}{[I_o + 2I_2][I_o - 2I_2(t)]} + \frac{1}{[I_o + 2I_2]^2} \ln \frac{I_2 + I_2(t)}{I_o - 2I_2(t)} = K_1 t + c_2 \tag{7.15}$$

For $t = 0$, $I_2(t) = 0$ and thus

$$c_2 = \frac{1}{[I_o + 2I_2]I_o} + \frac{1}{[I_o + 2I_2]^2} \ln \frac{I_2}{I_o} \tag{7.16}$$

Substitution of c_2 in equation (7.15) gives eventually

$$\frac{2I_2(t)}{[I_o + 2I_2][I_o - 2I_2(t)]I_o} + \frac{1}{[I_o + 2I_2]^2} \ln \frac{[I_2 + I_2(t)]I_o}{[I_o - 2I_2(t)]I_2} = K_1 t \tag{7.17}$$

From this equation it is apparent that $I_2(t)$ cannot be expressed in an analytical form as a function of time. However, approximate solutions of $I_2(t)$ can be obtained from equation (7.17), if the relative values of parameters I_o and I_2 are taken into account. In this way, one can distinguish two cases

(a) when I_2 is comparable to or higher than I_o ($I_2 \sim I_o$ or $I_2 > I_o$) and

(b) when I_2 is much smaller than I_o ($I_2 << I_o$).

In the former case, it can be readily proved that the second term in the left hand side of equation (7.17) is much smaller than the first term for any value of $I_2(t)$ in the interval between 0 and $\frac{I_o}{2}$. (It must be pointed out that $I_2(t)$ can take on values which satisfy the condition $0 \leq I_2(t) \leq \frac{I_o}{2}$.) Therefore, if the second term in the left hand side of equation (7.17) is omitted, an approximate analytical solution of $I_2(t)$ can be obtained.

$$I_2(t) = \tfrac{1}{2} \frac{I_o A t}{1 + At} \tag{7.18}$$

where

$$A = K_1 I_o [I_o + 2I_2]. \tag{7.19}$$

From equations (7.11) and (7.18) it is obtained

$$-\ell n I^* = K_2 I_2 t + \frac{K_2 A I_o}{2} \int \frac{t\, dt}{1 + At} + c_1 \tag{7.20}$$

and

$$-\ell n I^* = K_2 I_2 t + \frac{K_2 A I_o}{2} \left[\frac{t}{A} - \frac{1}{A^2} \ell n [1 + At] \right] + c_1 \tag{7.21}$$

For $t = 0$, $I^* = I_o^*$ and therefore

$$c_1 = -\ell n\, I_o^* \tag{7.22}$$

Finally, it is found that the decay of population of excited atomic iodine is given by

$$I^* = I_o^* [1 + At]^B e^{-Ct} \tag{7.23}$$

where

$$B = \frac{K_2}{2K_1[I_o + 2I_2]} \tag{7.24}$$

$$C = \frac{K_2[I_o + 2I_2]}{2} \tag{7.25}$$

In the case that $I_2 << I_o$, the first term in the left hand side of equation (7.17) becomes very small compared to the second term for any value of $I_2(t)$ in the interval between 0 and $\frac{I_o}{2}$. Under these circumstances it is found that

$$I_2(t) = \frac{I_o I_2[e^{Dt} - 1]}{I_o + 2I_2 e^{Dt}} \tag{7.26}$$

where

$$D = K_1[I_o + 2I_2]^2 \tag{7.27}$$

Substitution of $I_2(t)$ in equation (7.11) gives

$$-\ell nI^* = K_2 I_2 t + K_2 I_o I_2 \int \frac{e^{Dt}}{I_o + 2I_2 e^{Dt}}\, dt - K_2 I_o I_2 \int \frac{1}{I_o + 2I_2 e^{Dt}}\, dt + c_1 \tag{7.28}$$

and

$$-\ell nI^* = \frac{K_2[I_o + 2I_2]}{2D} \ell n\,[I_o + 2I_2 e^{Dt}] + c_1 \tag{7.29}$$

or

$$-\ell nI^* = B\ \ell n[I_o + 2I_2 e^{Dt}] + c_1 \tag{7.30}$$

For $t = 0$, $I^* = I_o^*$ and thus

$$c_1 = -\ell nI_o^* - \ell n[I_o + 2I_2]^B \tag{7.31}$$

Finally, from equations (7.30) and (7.31) it is found that

$$I^* = I_o^* \left[\frac{I_o + 2I_2}{I_o + 2I_2 e^{Dt}} \right]^B \qquad (7.32)$$

CONCLUSIONS

In this work it has been my intention to provide, in a comprehensive and systematic manner, the fundamental principles and important data concerning the design and operation of high energy coaxial flashtube systems for the excitation of fluid laser materials. I have also tried to investigate the conditions which should be satisfied by such coaxial flashtube systems and by active materials, such as organic dye solutions and photodissociative alkyl- or fluoroalkyl-iodides, in order to achieve effective pumping of the materials and generation of efficient laser outputs.

The experimental study of output characteristics of coaxial flashtubes, although not original in its conception, has revealed some new information and confirmed previous observations and theories concerning the discharge mechanism and emission of light by such flashtubes, two areas about which little has been known. The experiments involving the excitation or organic dye solutions and 1 - C_3F_7I vapour have determined the terms under which the coaxial flashtube systems used in this work can be employed as potential pump sources for high power dye and iodine lasers. The work on the radio-frequency preionisation of coaxial flashtubes is entirely original. In several occasions, attempts have been made to tackle some theoretical topics in a qualitative and sometimes quantitative way; such topics include the overall luminous efficiency of flashtubes, the coupling efficiency of coaxial systems, the nature of light emitted from rare gas discharges, the quenching effects of atomic iodine recombination and deactivation processes on the iodine laser output, etc.

With the exception of the pioneering work of a few groups in the USA and the Soviet Union, research on coaxial flashtubes (in both experimental and theoretical respects) has been limited in comparison to that on linear

flashtubes. This is natural up to a certain point, since linear flashtubes have been widely used in several research fields and have successfully excited most optically pumped laser materials, while the applications of coaxial flashtubes have been fewer. Hence, coaxial flashtubes have not been commercially exploited in a large scale. The unavailability of commercial coaxial flashtube systems meant that they had to be devised and constructed in the laboratory during the course of the investigation. Likewise, most of the apparatus used were constructed in the laboratory; for this reason, they have been described in detail, together with the experimental techniques used.

Throughout this thesis, it is repeatedly stressed that a high energy coaxial flashtube, and generally any flashtube system used as a pump source for lasers, should (i) display a high luminous efficiency, (ii) withstand high input electrical energies, and (iii) have as long a life as possible. It has been shown that high luminous efficiency can be achieved through a proper selection of flashtube parameters (gas type and pressure, voltage, etc.). On the other hand, the life of the flashtubes has been extended by using the 'O' ring construction technique. As far as the aspects of operation mentioned in this paragraph are concerned, an improved coaxial flashtube performance has been observed by applying radio-frequency preionisation in the flashtube.

The main results and achievements of this investigation are summarised below:

(a) For the first time, uniform discharges and high optical outputs have been achieved in Xenon filled coaxial flashtubes at E/p values as low as 10 Volts/cm.Torr. It has been confirmed that the luminous efficiency and the output optical power of such flashtubes increase with decreasing E/p value.

(b) Flashtubes of special construction ('O' ring sealing technique) have been fired 10^5 times each at input electrical energy densities up to 18 Joules/cc and input power levels up to 500 MWatts without any sign of damage.

(c) It has been proved that photoionisation constitutes an important process in the electrical breakdown of rare gases and in coaxial flashtube discharges.

(d) It has been found that most of the light emitted from these flashtubes lies in the near UV and visible spectral regions (in fact, their emission spectrum is more intense in the near UV, rather than the visible). This feature makes them suitable pump sources for dyes, with absorption bands in the UV (mainly) and visible regions, and alkyl- or fluoroalkyl-iodides.

(e) Xenon filled coaxial flashtubes have displayed the highest luminous efficiency and output optical power.

(f) The usefulness of pulsed radio-frequency preionisation in improving the overall performance of coaxial flashtubes has been established. It has been possible to extend the range of operation of such flashtubes towards the direction of low E/p values (down to 10 Volts/cm.Torr) without having to be restricted by non-uniform discharges. An enhancement of the optical output from the flashtubes has been observed for gas pressures in the flashtube below 100 Torr.

(g) Considering the electrical powers involved, the discharge system, as a whole, has exhibited good synchronisability when coupled with the preionisation device.

(h) Efficient output from the iodine photodissociation laser has been achieved by using a coaxial flashtube pumping system. The measurements of

fluorescent outputs from dye solutions have indicated that such systems can be used as pump sources for dye lasers.

(i) The quantitative analysis on the recombination and deactivation of excited atomic iodine in the presence of molecular iodine has explained the iodine laser termination prior to the flash termination observed in previous works. The need for fast, powerful optical pulses for pumping iodine photodissociation lasers has been established.

REFERENCES

1. T.H. Maiman, Nature 187 (1960), 493.

2. A.L. Schawlow, C.H. Townes, Phys. Rev. 112 (1958), 1940.

3. A. Yariv, J.P. Gordon, Proc. I.E.E.E. 51 (1963), 4.

4. A. Javan, W.R. Bennett Jr., D.R. Herriott, Phys. Rev. Lett. 6 (1961), 106.

5. R.N. Hall, G.E. Fenner, J.D. Kingsley, T.J. Soltys, R.O. Carlson, Phys. Rev. Lett. 9 (1962), 366.

   M.I. Natham, G. Burns, W.P. Dumke, F.H. Dill Jr., G. Lasher, Appl. Phys. Lett. 1 (1962), 62.

6. S. Jacobs, G. Gould, P. Rabinowitz, Phys. Rev. Lett. 7 (1961), 415.

7. C.K.N. Patel: Gas Lasers in LASERS Vol. 2 (Edited by A.K. Levine), Marcel Dekker, New York 1968, pp. 12-14 and 36-39.

8. J.F. Holzrichter, A.L. Schawlow, Annals New York Academy of Sciences 168 (1969-70), 703.

9. D. Röss; Lasers, Light Amplifiers and Oscillators, Academic Press, London and New York, 1969, pp. 383-384.

10. H. Winston, R.A. Gudmundsen, Appl. Opt. 3 (1964), 143.

11. A. Lempicki, H. Samelson, Phys. Letters 4 (1963), 133.

12. P.P. Sorokin, J.R. Lankard, IBM Jour. Research and Development 10 (1966), 162.

13. A. Heller, Appl. Phys. Lett. 9 (1966), 106.

14. F.P. Schäfer, W. Schmidt, J. Volze, Appl. Phys. Lett. 9 (1966), 306.

15. P.P. Sorokin, J.R. Lankard, IBM Jour. Research and Develop. 11 (1967), 148.

16. W. Schmidt, F.P. Schäfer, Z. Naturforsch. 22a (1967), 1563.

17. B.H. Soffer, B.B. McFarland, Appl. Phys. Lett. 10 (1967), 266.

18. O.G. Peterson, S.A. Tuccio, B.B. Snavely, Appl. Phys. Lett. 17 (1970), 245.

19. L.F. Johnson, K. Nassau, Proc. IRE 49 (1961), 1704.

    J.E. Geusic, H.M. Marcos, L.G. van Vitert, Appl. Phys. Lett. 4 (1964), 182.

20. E. Snitzer, J. Opt. Soc. Am. 52 (1962), 602.

21. F.N. Baltakov, B.A. Barikhin, L.V. Sukhanov, JETP Lett. (Sov. Physics) 19 (1974), 174.

22. J.V.V. Kasper, G.C. Pimentel, Appl. Phys. Lett. 5 (1964), 231.

23. J.V.V. Kasper, J.H. Parker, G.V. Pimentel, J. Chem. Phys. 43 (1965), 1827.

24. M.A. Pollack, Appl. Phys. Lett. 8 (1966), 36.

25. A.J. DeMaria, C.J. Ultee, Appl. Phys. Lett. 9 (1966), 67.

26. K. Hohla, K.L. Kompa, Appl. Phys. Lett. 22 (1973), 77.

K. Hohla, G. Brederlow, W. Fuss, K.L. Kompa, J. Raeder, R. Volk, S. Witkowski, K.J. Witte, J. Appl. Phys. 46 (1975), 808.

27. V.A. Gaidash, G.A. Kirillov, S.B. Kormer, S.G. Lapin, V.I. Shemyakin and V.K. Shurygin, JETP Lett. 20 (1974), 107.

N.G. Basov, L.E. Golubev, V.S. Zuev, V.A. Katulin, V.N. Netemin, V. Yu. Nosach, O. Yu. Nosach and A.L. Petrov, Sov. J. Quant. Electron. 3 (1974), 524.

28. M.A. Pollack, Appl. Phys. Lett. 9 (1966), 44 and 230.

29. R.L. Byer, R.L. Herbst, H. Kildal, M.D. Levenson, Appl. Phys. Lett. 20 (1972), 463.

30. F.P. Schäfer: Principles of Dye Laser Operation in DYE LASERS, Springer-Verlag, 1973.

31. M. Bass, T.F. Deutsch, M.J. Weber: Dye Lasers in LASERS Vol. 3 (Edited by A.K. Levine and A.J. DeMaria), Marcel Dekker, New York 1971, pp. 269-345.

32. M.J. Weber, M. Bass, IEEE J. Quantum Electron. 5 (1969), 175.

33. A. Jablonski, Z. Physik, 94 (1935), 38.

34. J. Franck, Trans. Faraday Soc. 21 (1926), 536.

E. U. Condon, Phys. Rev. 32 (1928), 858.

35. P.M. Rentzepis, Chem. Phys. Letters 2 (1968), 117.

36. B.B. Snavely, F.P. Schäfer, Phys. Letters 28A (1969), 728.

37. P. Pringsheim: Fluorescence and Phosphorescence, Wiley, New York, 1949, p.316.

38. B.B. Snavely, O.G. Peterson, IEEE J. Quant. Electron. 4 (1968), 540.

39. P.P. Sorokin, J.R. Lankard, V.L. Moruzzi, E.C. Hammond, J. Chem. Phys. 48 (1968), 4726.

40. B.I. Stepanov, A.N. Rubinov, Soviet Physics - Usp. 11 (1968), 304.

41. M. Bass, T.F. Deutsch, M.J. Weber, Appl. Phys. Lett. 13 (1968), 120.

42. A.V. Aristov, Yu. S. Maslyukov, Optics and Spectros. 24 (1968), 450.

43. H.W. Furumoto, H.L. Ceccon, Appl. Optics 8 (1969), 1613.

44. J.M. Drake, E.M. Tam, R.I. Morse, IEEE J. Quant. Electron. 8 (1972), 92.

45. D. Porret, C.F. Goodeve, Proc. Roy. Soc. (London), A165 (1938), 31.

46. M.I. Christie, A.J. Harrison, R.G.W. Norrish, G. Porter. Proc. Roy. Soc. (London) A231 (1955), 446.

47. V. Yu. Zalesskii, Soviet Physics JETP 34 (1972), 474.

48. M.A. Gusinow, Optics Communic. 15 (1975), 190.

49. D.L. Bunker, N. Davidson, J. Amer. Chem. Soc., 80 (1958), 5085.

50. R.J. Donovan, D. Husain, Nature 206 (1965), 171.

51. V. Yu. Zalesskii, T.I. Krupenikova, Optics and Spectr. 30 (1971), 439.

52. P.B. Ayscough, J. Chem. Physics, 24 (1956), 944.

53. F.T. Aldridge, Appl. Phys. Letters 22 (1973), 180.

F.T. Aldridge, IEEE, J. of Quant. Electr. 11 (1975), 215.

54. H.E. Edgerton, K.J. Germehausen, Electronics 4 and 5 (1932), 220.

55. J.M. Meek, J.D. Craggs: Electrical breakdown of gases, Clarendon Press, Oxford (1953), p.403.

56. J.B. Hasted: Physics of Atomic Collisions. 2nd Edition, Butterworth, London (1972).

57. A.A. Kruithof, Physica, 7 (1940), 519.

58. M.J. Druyvesteyn, F.M. Penning, Rev. Mod. Phys. 12 (1940), 87.

59. M.A. Biondi, S.C. Brown, Phys. Rev. 75 (1949), 1700.

60. W.L. Granowski: Der electrishe Strom in Gas I, Akad. Verlag, Berlin (1955).

61. G.L. Weissler, Phys. Rev. 63 (1943), 96.

62. F. Llewellyn-Jones: Ionisation and breakdown in gases, Methuen, London (1957), p.19.

63. A.M. Cravath, Phys. Rev., 36 (1930), 248.

64. C. Ramsauer, R. Kollath, Ann. der Physik, 3 (1929), 536.

65. R.B. Brode, Rev. Mod. Phys. 5 (1933), 257.

66. A. von Engel: Ionised Gases, Clarendon Press, Oxford (1965), pp. 42-50.

67. J.B. Hasted: Physics of Atomic Collisions, 2nd Edition. Butterworth, London (1972), p. 344.

68. S.J.B. Corrigan, A. von Engel, Proc. Phys. Soc. London 72 (1958), 786.

69. J.D. Craggs, J.M. Meek, Proc. Roy. Soc. (London), A186 (1946), 241.

J.D. Craggs, W. Hopwood, J.M. Meek, J. Appl. Phys. 18 (1947), 919.

70. M.A. Biondi, Phys. Rev. 82 (1951), 543.

71. J.B. Hasted: Physics of Atomic Collisions, 2nd Edition, Butterworth, London (1972), p. 672.

72. A.V. Phelps, Phys. Rev. 99 (1955), 1307.

73. A.A. Kruithof, F.M. Penning, Physica, 4 (1937), 430.

A.A. Kruithof, M.J. Druyvesteyn, Physica 4 (1937), 450.

74. M.A. Biondi, Phys. Rev. 88 (1952), 660.

E.E. Benton, E.E. Ferguson, F.A. Matson, W.W. Robertson, Phys. Rev. 128 (1962), 206.

75. A. von Engel: Ionised Gases, Clarendon Press, Oxford (1965), p.63.

76. A.C.G. Mitchell, M.W. Zemansky: Resonance Radiation, Cambridge Univ. Press (1934).

77. J.A.R. Samson, F.L. Kelly, GCA Tech. Report No. 64-63-N (1964).

J.A.R. Samson, J. Optic Soc. Am. 54 (1964), 420.

Cross-section results from these references are given in 'Photoionisation processes in gases' by G.V. Marr, Acad. Press. New York, London, (1967).

78. S.C. Haydon, Survey of Phenomena in Ionised Gases (invited papers), 8th Intern. Confer. on Phenomena in Ion. Gases, Vienna (1967), pp. 495-518.

79. F. Llewellyn-Jones: Ionisation and breakdown in gases, Methuen, London (1957), pp. 105-112.

80. G.A. Kachickas, L.M. Fisher, Phys. Rev. 88 (1952), 878.

L.H. Fisher, B. Bederson, Phys. Rev. 81 (1951), 109.

81. J.S. Townsend: Electricity in Gases, Oxford Univ. Press (1915)

J.S. Townsend: Electrons in Gases, Hutchinson, London (1947).

82. L.B. Loeb: Fundamental Processes of Electrical Discharges in Gases, J. Wiley (1939).

83. J.M. Meek, Phys. Rev., 57 (1940), 57.

84. H. Raether, Zeitschrift f. Physik, 112 (1939), 464.

85. F. Llewellyn-Jones, A.B. Parker, Nature, 165 (1950), 960.

F. Llewellyn-Jones, A.B. Parker, Proc. Roy. Soc. (London) A213 (1952), 185.

86. P.M. Davidson, Brit. J. Appl. Phys. 4 (1953), 170.

87. W. Körmann, Zeit. f. Naturforschung, 19a (1964), 926.

88. W. Rogowski, Archiv. f. Electrotechnik, 20 (1928), 99.

89. R. Schade, Zeit. f. Physik, 104 (1937), 487.

90. W. Hopwood, Proc. Phys. Soc. 62B (1949), 657.

91. F. Llewellyn-Jones: Ionisation and Breakdown in Gases, Methuen, London (1957), pp. 90-97.

92. A. von Engel: Ionised Gases, Clarendon Press, Oxford (1965), p. 202.

93. S.I. Drabkina, J. Exp. and Theor. Physics (USSR), 21 (1951), 473.

94. S.I. Braginskii, Sov. Phys. JETP, 7 (1958), 1068.

95. J. Zeleny, J. Appl. Phys. 13 (1942), 103 and 444.

96. M.N. Saha, Phil. Mag. 40 (1920), 472 and 809.

97. M. Garbuny: Optical Physics, Academic Press, New York (1965), pp. 50-55.

98. W. Finkelnberg, J. Opt. Soc. Amer. 39 (1949), 185.

99. J.F. Prince, W.W. Robertson, J. Chem. Phys. 45 (1966), 2577.

J.F. Prince, W.W. Robertson, J. Chem. Phys. 46 (1967), 3309.

100. W. Wieme, Proc. of the 11th Intern. Confer. on Phenomena in Ionis. Gases (Contrib. Papers), Prague (1973), 407.

101. C. Kenty, J. Chem. Phys. 47 (1967), 2545.

102. I.A. Vasileva, Yu. Z. Zhdanova, A.K. Muatsakanyan, Optics and Spectros. 29 (1970), 345.

103. R. Boucique, P. Moerman, Proc. of the 12th Inter. Confer. on Phenomena in Ion. Gases (Contrib. Papers), Eidhoven (1975), 13.

104. A. Rutscher, S. Pfau, Physica 81C (1976), 395.

105. S.C. Brown: Introduction to Electrical Discharges in Gases, Wiley, New York, London (1966), pp. 150-156.

106. J. Meyer, Brit. J. Appl. Phys. 18 (1967), 801.

107. J.L. Emmett, A.L. Schawlow, E.H. Weinberg, J. Appl. Phys. 35 (1964), 2601.

J.L. Emmett, A.L. Schawlow, Appl. Phys. Lett. 2 (1963), 11.

108. I.S. Marshak, Soviet Phys. Usp. 5 (1962), 478.

109. J.H. Goncz, J. Appl. Phys. 36 (1965), 742.

110. J.P. Markiewicz, J.L. Emmett, IEEE J. Quant. Electronics 2 (1966), 707.

111. J.F. Holzrichter, J.L. Emmett, Appl. Optics, 8 (1969), 1459.

112. M. Ciftan, C.F. Luck, C.G. Shafer, H. Statz, Proc. IRE 49 (1961), 960.

113. S.B. Schuldt, R.L. Aagard, Appl. Optics 2 (1963), 509.

114. D. Röss, Appl. Optics, 3 (1964), 259.

115. C. Bowness, D. Missio, T. Rogala, Proc. IRE, 50 (1962), 1704.

116. D.L. Fried, P. Eltgroth, Proc. IRE, 50 (1962), 2489.

117. S. Claesson, L. Lindqvist, Arkiv. f. Kemi, 12 (1957), 1.

118. C.H. Church, D. Ryan, J.P. Lesnick, J. Opt. Soc. Am., 53 (1963), 514.

119. J.P. Lesnick, C.H. Church, IEEE J. Quant. Electron. 2 (1966), 16.

120. T.F. Ewanizky, R.H. Wright Jr., Appl. Optics, 12 (1973), 120.

121. J.B. Marling, J.G. Hawley, E.M. Liston, W.B. Grant, Appl. Optics, 13 (1974), 2317.

122. KODAK Publication No. JJ-32.

F. Grum, G.W. Luckey, Appl. Optics 7 (1968), 2289.

123. J.D. Craggs, J.M. Meek: High Voltage Laboratory Technique, Butterworths, London (1954).

124. R.N. Lewis, E.A. Jung, G.L. Chapman, L.S. Van Loon, T.A. Romanowski, IEEE Transac. on Nucl. Science 13 (1966), 84.

125. G.J. Dezenberg, E.L. Roy. W.B. McKhight, IEEE J. Quant. Electron. 8 (1972), 58.

126. J.J. Ramirez, J. Appl. Phys. 47 (1976), 1925.

127. ILFORD Technical Information Sheet B12-8.

128. Yu. N. Gorokhovskii: Spectral studies of the photographic process (English translation). The Focal Press, London and New York (1965), p. 51.

129. Eastman Organic Chemical Bulletin,KODAK Publication No. JJ60-743.

130. DYES FOR LASERS, KODAK Publication No. JJ-169.

131. J.A. Myer, C.L. Johnson, E. Kierstead, R.D. Sharma, I. Itzkan, Appl. Phys. Lett. 16 (1970), 3.

132. B.B. Snavely, O.G. Peterson, R.F. Reithel, Appl. Phys. Lett. 11 (1967), 275.

133. M.A. Gusinow, IEEE J. Quant. Electron., 11 (1975), 929.

134. A.R. Striganov, N.S. Sventitskii, Tables of Spectral Lines of Neutral and Ionised Atoms, Plenum, New York-Washington (1968), p. 44.

135. C. Raptis, unpublished.

136. J.D. Clarke, P.J. Hutton, Proc. of the 6th Intern. Confer. on Phenomena in Ion. Gases, Paris (1963).

137. N.G. Basov, E.M. Belenov, Y.A. Danilychev, A.F. Suckhov, Sov. J. Quant. Electronics, 1 (1971), 306.

138. O.P. Judd, Appl. Phys. Lett.,22 (1973), 95.

139. J.L. Emmett, A.L. Schawlow, Appl. Phys. Lett. 2 (1963), 204.

140. H.W. Gandy, A.C. Kolb, W.H. Lupton, J.F. Weller, Appl. Phys. Lett. 4 (1964), 11.

141. M.H. Ornstein, V.E. Derr, Appl. Optics, 13 (1974), 2100.

142. A. Papayoanou, R.G. Buser, IEEE J. Quant. Electron. 3 (1967), 227.

143. C. Raptis, V.I. Little, S. Majumdar, Proceedings of the 12th Intern. Congress on High Speed Photography (Photonics), Toronto 1976, SPIE Vol. 97, Washington (1977), pp. 462-467.

144. D.B. Nichols, W.M. Brandenberg, IEEE, J. Quant. Electron. 8 (1972), 718.

145. J.M. Meek, J.D. Craggs: Electrical Breakdown of Gases, Clarendon Press, Oxford (1953), p. 374.

146. G. Francis: Ionisation Phenomena in Gases, Butterworths, London (1960), p. 83.

ENHANCEMENT OF LUMINOUS EFFICIENCY OF HIGH ENERGY FLASH TUBES USING HIGH POWER PRE-IONISATION

C. Raptis, V. I. Little, S. Majumdar
Department of Physics, Royal Holloway College, University of London
Egham Hill, Egham, Surrey, TW20 OEX, England

Abstract

Several kilojoule co-axial flash tubes and their 5-stage Marx generator are described. The maximum peak power input to the flash tubes is around 500 MWatts. Systematic time resolved measurements of flash tube characteristics for gas pressures from 20 to 210 Torr and for electrical pulses up to 80 KV are reported. Optimum E/p values have been obtained. Radio frequency pre-ionisation was used, for the first time successfully in a flash tube, which resulted in the enhancement of the peak power output by up to a factor of at least 2 and the improvement of the flash tube operation. The dependence of the enhancement on the delay between pre-ionising pulse and main pulse is analysed. Uniform discharges for E/p values as low as 10 volts/Torr.cm have been achieved for the first time in co-axial flash tubes using this technique. Advantages of this technique compared to previous pre-ionization techniques are considered. The system reported here appears to be superior in the following aspects: 1) Enhancement of peak output power, 2) Improvement of amplitude jitter of the flash tube output, 3) Life of the flash tube. Advantages of using such a system for high power lasers are discussed and comparisons with previous fast rise time co-axial flash tube systems are considered. The use of these flash tubes to pump iodine photodissociation laser and dye solutions is described.

Introduction

The advantages of co-axial flash tubes for the generation of high power optical pulses have, in the last decade, attracted the attention of many workers in this field (1,2,3,4). One of the main problems encountered in the development of high power and high energy flash tubes of any type (linear, helical or co-axial) has been the non-linear impedance of gaseous discharges (5). The ionisation of gas under the influence of a high electrical field, as is experienced in flash tubes, depends on the arc formation time in the gas. The non-linear dynamic impedance of a flash tube is caused by this ionisation mechanism and is such that rapid deposition of electrical energy in the gas becomes very difficult when one arc channel is utilised. In the usual co-axial flash tubes, normally used in low energy (around 100 Joules) dye laser systems, a very rapidly rising electrical impulse is used for creating a large multiplicity of arcs in the annular discharge space (2,3).

However, such a system can only operate for low pressures (E/p values higher than 30 Volts/Torr.cm). At higher pressures (i.e. lower E/p values) single channeling occurs causing the flash tube to shatter (2).

In the system reported here we describe a method which enabled us to operate co-axial flash tubes at input energies up to 1.5 KJoules and at high pressures (E/p values as low as 10 Volts/Torr.cm). This was achieved by using a radio frequency pre-ionising pulse to generate 'seed' electrons over the whole discharge volume. Nichols and Brandenberg (6) used a similar radio frequency pulse successfully in their attempt to achieve uniform discharge in a transverse flow electrical-discharge CO_2 laser at high pressures.

The electrical discharge system was a 5-stage Marx generator equipped with medium inductance capacitors. Each stage could be charged up to 20 KV giving an overall electrical energy up to 2 KJoules.

An enhancement of the luminous output was observed, consistent with pre-ionisation in this system, implying a better rate of deposition of electrical energy in the gas.

System Details

The main objectives of the experiment reported have been:
1) The evaluation of flash tube output with pre-ionisation at high energies
2) Optimisation of flash tube E/p values without having to be limited by localised arc formation

The Marx generator was chosen for its fast and high voltage pulse characteristics. Fig.1 shows the schematic diagram of the Marx generator used. The output impedance of the generator was about 2 Ohms. Pressurised spark gaps were used as commutators.

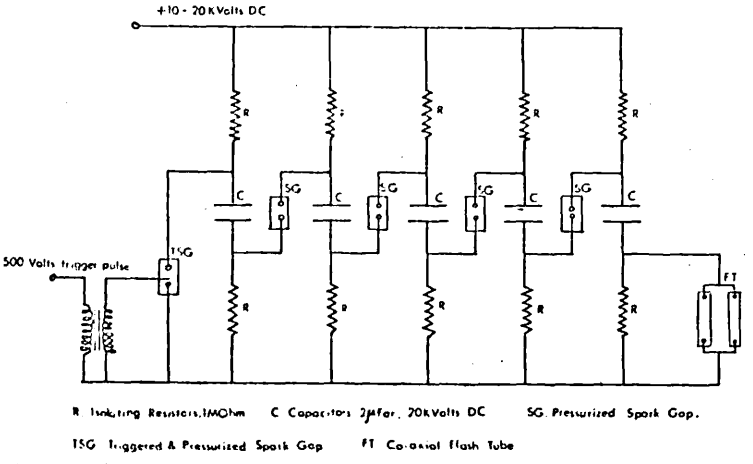

Fig.1. Schematic diagram of the Marx-generator used

The flash tubes were made of silicon tubes and were completely demountable (Fig.2). eir length was 20cm and their gas volume varied between 47cc and 108cc. The outside lls of the flash tubes were coated (just before operation) with KODAK white reflecting int. A coat as thick as 1mm was necessary for 99% reflectivity. The optical pulse was tected through a narrow strip (1cm) in the middle of the flash tube. Reflection of the ght on the outside wall caused further ionisation of the gas (photo-ionisation).

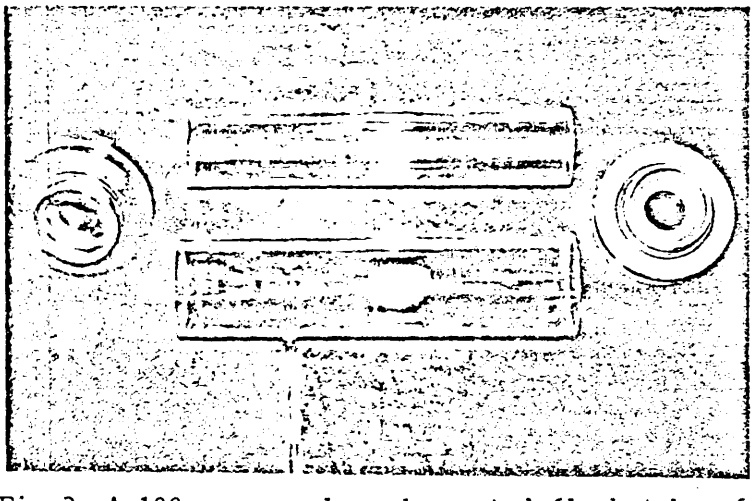

Fig.2. A 100cc gas volume demounted flash tube after use

Fig.3 shows a schematic diagram of the experimental arrangement. The output of the sh tubes was measured using an I.T.L. photodiode type HD 125 UV which had a sapphire dow for ultraviolet sensitivity. TECTRONIX oscilloscopes type 551 and 554 were emp- ed in order to detect the signal from the photodiode.

The radio frequency pre-ionising pulse was applied to the system through a suitably ulated wire around the outer wall of the flash tube in such a way that a coil of 15-20 ns was formed. The peak amplitude and the frequency of the pre-ionising pulse were V and 10MHz respectively. This frequency was not high enough for efficient pre- isation of the gas above 65Torr. As a result, there was no substantial enhancement of inous peak power above that pressure. However, even at higher pressures the pre- ising system produced enough 'seed' electrons to prevent any shattering of the flash e. The electrical power in the radio frequency excitor was 1MWatt.

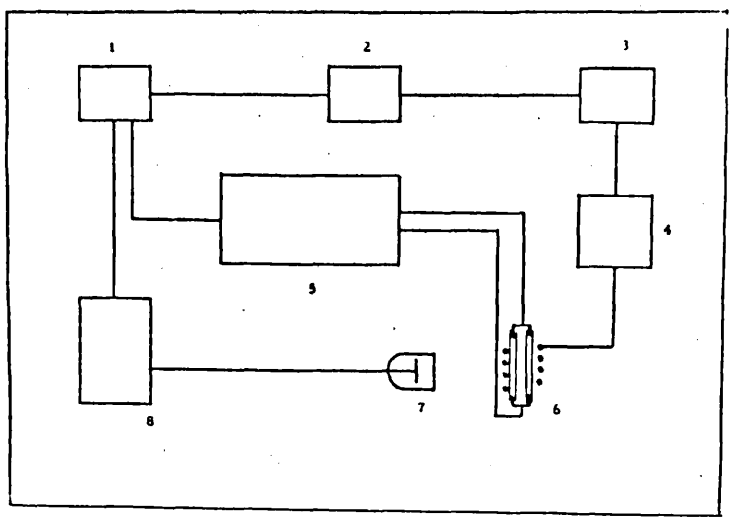

Fig.3. Experimental arrangement for measuring the optical output of the flash tube with pre-ionisation. The oscilloscope traces are triggered by the master trigger of the system.

Results

a) Enhancement of luminous output

Fig.4 shows the enhancement of luminous output of a 50cc gas volume flash tube between 2000 Å and 7000 Å as a function of gas fill up to 100Torr of Xenon. It will be noticed that at lower gas fills the enhancement is better due to better pre-ionisation. No significant increase of output, due to pre-ionisation, was observed when the pressure was

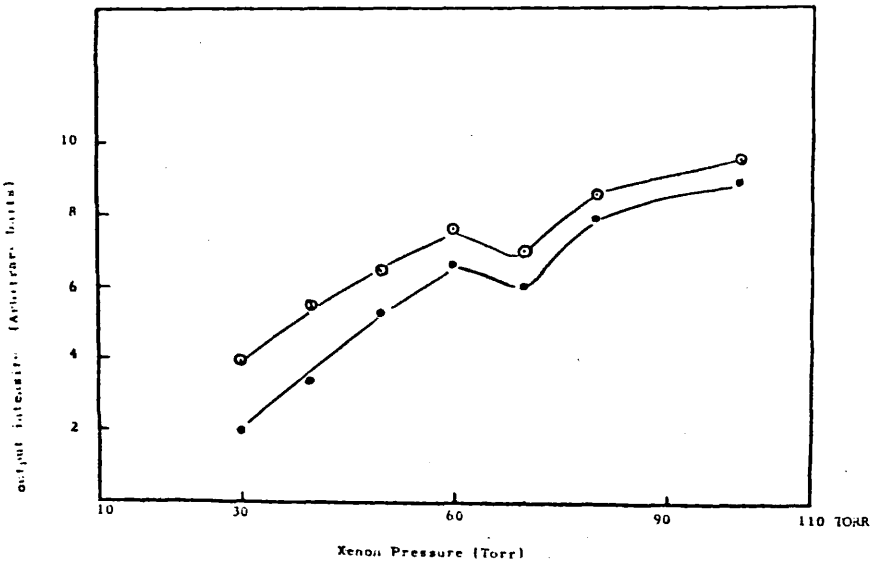

Fig.4. Luminous peak power of a 50cc gas volume co-axial flash tube as a function of the gas pressure. Top curve with radio frequency pre-ionisation of 70KV peak amplitude and 10MHz frequency. Bottom curve without pre-ionisation.

increased above 110Torr. At still higher pressures, the breakdown of the gas became less uniform. Fig.5(a) shows two oscilloscope traces of the photodiode signal from the flash tube, showing a higher output when radio frequency pre-ionisation was used. However, when electrodes with sharp edges were employed in the flash tubes the output was found to

ıcrease almost linearly up to a pressure of 210Torr. This further enhancement was thought ıe to field emission of electrons from the electrodes, causing a further pre-ionisation f the gas.

) Time behaviour of output with the pre-ionising pulse

The enhancement of output power was crucially dependent on the delay between the pre-ınising pulse and the main discharge pulse. A delay of approximately 4μsecs in the rrival of the main pulse was found to be optimum. Fig.5(b) shows the output of a number f successive shots when this delay was varied between 3μsecs and 14μsecs. The trace

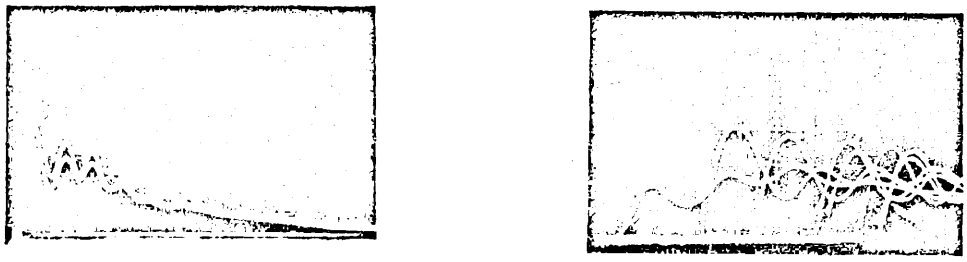

(a) (b)

Fig.5. (a) Enhancement of the optical output with pre-ionisation. Both traces were taken at 30Torr Xenon pressure and 750Joules input electrical energy. Horizontal scale 5μsecs/cm. (b) Output of a number of flashes at various delays between pre-ionising and main discharge pulse. The traces were triggered by the master trigger, except the one in the extreme left (no pre-ionisation) which was triggered by the scope. Horizontal scale 2μsecs/cm. 30Torr pressure in the flash tube.

tarting at the extreme left was obtained when no pre-ionisation was used; this trace was nternally triggered by the scope, while the rest on the right were initiated by the aster trigger as is illustrated in Fig.3. Fig.6 shows a graph correlating the enhancement f luminous output as a function of the delay between pre-ionising and main discharge ulses. An interesting feature of this system was its extremely low jitter in delay etween the triggering of the system and the output optical pulse: this was less than 0 nanosecs when the system was functioning at its best optical output.

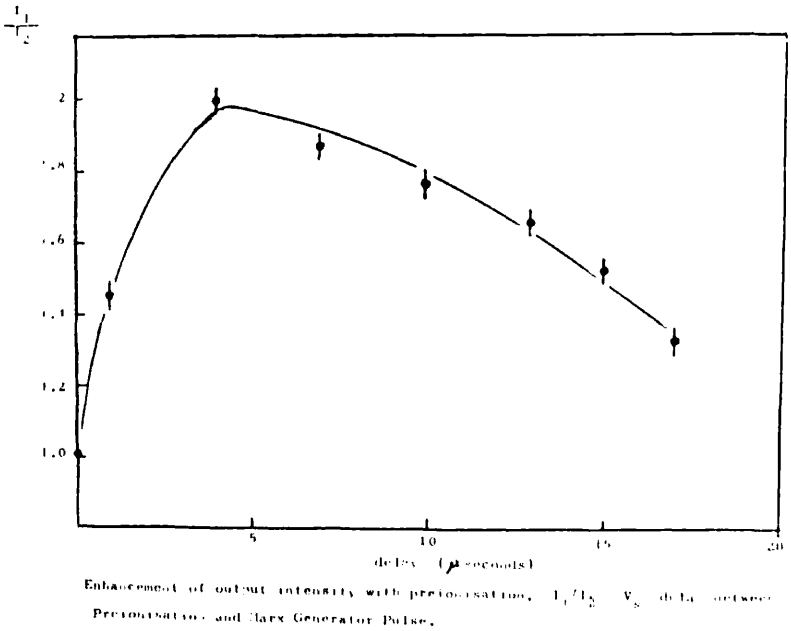

Enhancement of output intensity with preionisation. I_1/I_2 vs delay between Preionisation and Marx Generator Pulse.

Fig.6. Enhancement of the optical output from a 50cc flash tube with pre-ionisation, as a function of the delay between pre-ionising and main discharge pulses.

c) Fluorescence of Rhodamine 6G and photodissociation of C_3F_7I

So far, we have used these flash tubes to optically excite C_3F_7I and Rhodamine 6G. C_3F_7I photodissociates and generates atomic iodine at the excited $^2P_{1/2}$ state which transits to the less populated lower $^2P_{3/2}$ state giving light at 1.33u. Kasper and Pimentel (7) were the first to report photodissociation laser emission in this line. For this laser, the optical output from the flash tube requires to be peaked around 2700 Å. Therefore this was a good test to ascertain the ultraviolet output of our co-axial flash tubes. Fig.7 shows the iodine laser output when C_3F_7I vapour at 100Torr was pumped by a 47cc flash tube at various E/p values and input energies with and without pre-ionisation*. The coupling of the flash tube and the laser cell was only about 45% and the output mirror was of 60% reflectivity. Yet efficiencies in excess of 0.15% were achieved at Xenon pressures of 210Torr. In this experiment a 3-stage Marx generator was used.

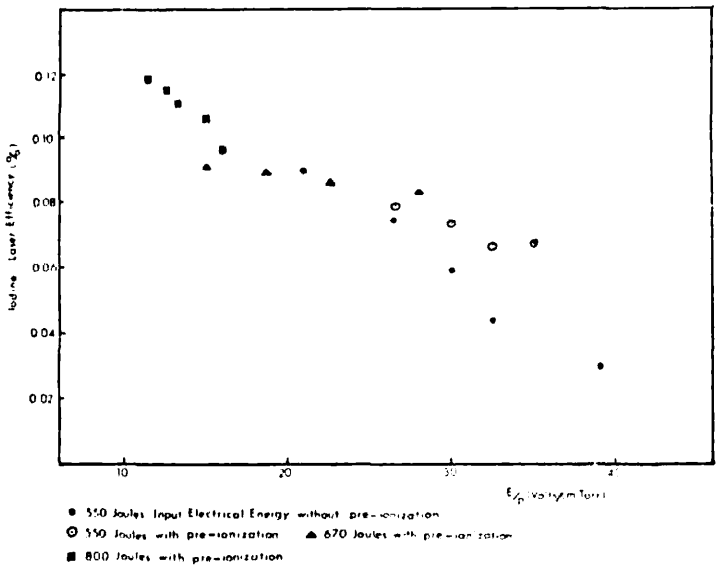

Fig.7. Iodine laser output pumped by a 47cc co-axial flash tube at various gas fills, input energies, with and without pre-ionisation. C_3F_7I vapour at 100Torr in the laser cell. 60% reflectivity output mirror.

Fig.8 shows the fluorescence output of Rhodamine 6G in Ethanol ($5x10^{-5}M$) using a 100cc flash tube at various input energies and gas fills. The excitation wavelength of Rhodamine 6G peaks around 5500Å, although there is substantial absorption at shorter wavelengths. The fluorescence energy output was measured at the end of the dye cell. The efficiency of this output was around 0.07%, for flash tube-dye cell coupling of 40%. There was no pre-ionisation applied to the system in this experiment.

d) Life

The three flash tubes used so far have been operated for more than 10^5 flashes each without any obvious signs of damage or oblation. The energy density in these flash tubes has varied between 3 and 15 Joules/cc and input electrical power levels have been up to 500 MWatts.

Conclusions

The usefulness of high power radio frequency pre-ionisation in extending the range of operation of co-axial flash tubes has been established. The output of these flash tubes between 2000Å and 7000Å was very intense and was higher than that obtained without pre-ionisation.

Emmett and Schawlow (8) reported enhancement of the output from double-pulsed linear flash tubes. The first pulse was much slower than the second (main) and caused enough pre-ionisation to prevent the shattering of the tubes. Ornstein and Derr (9) recently reported a method of increasing the optical output using a prepulse. In these systems, the rather slow pre-ionising pulse did not create multiple arcs as happens in our case. As a result, the main discharge follows a single arc channel which precludes the use of this type of pre-ionisation in co-axial flash tubes at high pressures.

* This work was done at Manchester University in collaboration with Dr.King and Dr.Baker to whom we are grateful for the facilities offered.

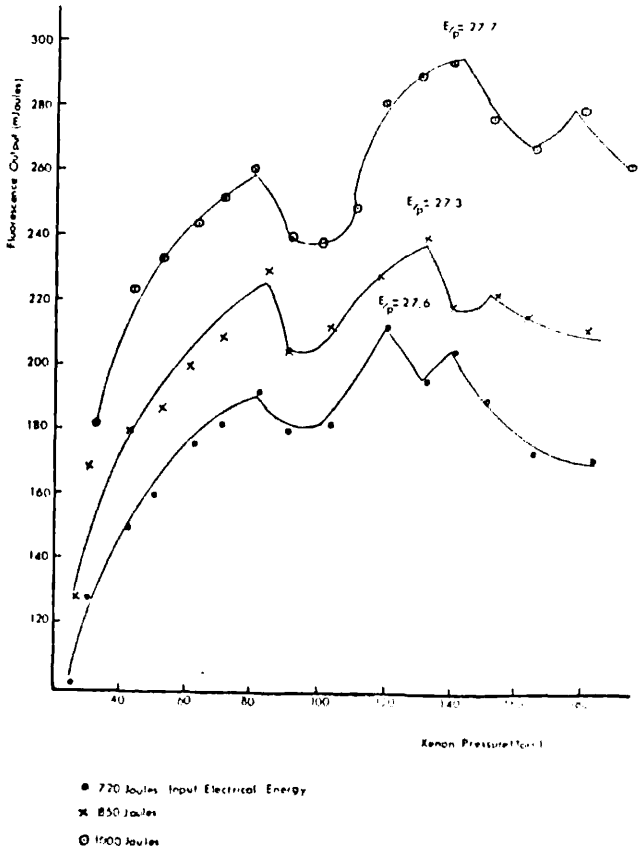

Fig.8. Fluorescence energy output from a 5×10^{-5}M Rhodamine 6G in Ethanol solution pumped by a 100cc co-axial flash tube at various gas pressures and input electrical energies. This output was measured at the end of the dye cell.

Other workers (10) reported satisfactory results when very fast Blumlein drive ystem was employed for both pre-ionising and main discharge pulses. Here, however, the re-ionising pulse timing and power was inadequate for the operation of the flash tubes t high pressures.

We observed that even with relatively low frequencies of pre-ionisation, very low /p values could be obtained in our flash tubes at pressures in excess of 200Torr. The se of V.H.F. or microwave pre-ionisation would improve the efficiency further. We hope o explore this area in future. Work with iodine photodissociation laser and with the luorescent output of Rhodamine 6G dye proved the efficiency of the system at 2700Å and n the visible. This was also confirmed by spectroscopic studies of the luminous output.

Fast synchronisability of the system is yet another added advantage for the use of hese flash tubes for high power laser amplifiers.

Finally the very long life of the flash tubes is unique, operating in Kilojoule, ultimegawatt energy and power ranges respectively.

References

. Claesson, S., Lindqvist, L., Arkiv Kemi, Vol.2, p.1, 1957.
. Sorokin,P.P., Lankard,J.R., Moruzzi,V.L., Hammond,E.C., J.Chem.Phys.,48,p.4726,1968.
. Furumoto,H.W., Ceccon,H.L., Appl.Optics, Vol.8, p.1613, 1969.
. Ewanizky,T.F., Wright Jr.,R.H., Appl.Optics, Vol.12, p.120, 1973.
. Markiewicz,J.P., Emmett,J.L., IEEE J.of Quan.Electronics,Vol.QE-2,p.707, 1966.
. Nichols,D.B., Brandenberg,W.M., IEEE J.of Quant.Electronics,Vol.QE-8, p.718, 1972.
. Kasper,J.V.V., Pimentel,G.C., Appl.Phys.Letters, Vol.5, p.231, 1964.
. Emmett,J.L., Schawlow,A.L., Appl.Phys.Letters, Vol.2, p.204, 1963.
. Ornstein,M.H., Derr,V.E., Appl.Optics, Vol.13, p.2100, 1974.
0. Allingam,C.O., Dooley,P.J., Little,V.I., French,S.,Majumdar,S., Proceedings of the 1th International Congress on High Speed Photography, London, 1974, p.236. Pergamon ress, 1975.